NANOFABRICATION OF BIOINSPIRED ARCHITECTURES WITH LIGHT HARVESTING PROTEINS

Maryana Escalante

Thesis committee members:

Prof. dr.	G. van der Steenhoven	University of Twente (chairman)
Prof. dr.	V. Subramaniam	University of Twente (thesis advisor)
Dr. ir.	C. Otto	University of Twente (assistant advisor)
Prof. dr.	C. N. Hunter	University of Sheffield
Prof. dr.	T. J. Aarstma	University of Leiden
Prof. dr.	J. L. Herek	University of Twente
Prof. dr.	J. Huskens	University of Twente
Prof. dr.	M.C. Elwenspoek	University of Twente

The research described in this thesis was carried out at the Biophysical Engineering Group, MESA+ Institute for Nanotechnology and Faculty of Science and Technology, University of Twente. P.O. Box 217, 7500 AE Enschede, The Netherlands.

This research has been financially supported by NanoNed, the nanotechnology program of the Dutch Ministery of Economic Affairs. (Nanofabrication cluster, project number 7124)

Cover design: Boudewijn de Jong, Maryana Escalante
Printed by: Wöhrmann Print Service

ISBN 978-90-365-2919-8
doi: 10.3990/1.9789036529198

NANOFABRICATION OF BIOINSPIRED ARCHITECTURES WITH LIGHT HARVESTING PROTEINS

PROEFSCHRIFT

ter verkrijging van
de graad van doctor aan de Universiteit Twente,
op gezag van de rector magnificus,
prof. dr. H. Brinksma,
volgens besluit van het College voor Promoties,
in het openbaar te verdedigen
op vrijdag 11 december 2009 om 13:15 uur

door

Maryana Escalante Marun

geboren op 11 augustus 1980
te Barcelona, Venezuela

Dit proefschrift is goedgekeurd door:

Prof. dr. V. Subramaniam (promotor) en
Dr. C. Otto (assistent-promotor)

To my family and Boudewijn

Table of Contents

Chapter 1

Introduction*

This chapter presents a broad overview of the concepts associated with bionanofabrication in general. This overview includes the most common chemical approaches for the adsorption of biomolecules on surfaces. Also a survey of unconventional nanofabrication for low cost and fast prototyping of bionanostructures at the micro- and nanometer scale is presented and their respective advantages and open challenges are discussed. The survey includes: microcontact printing (μCP), nanoimprint lithography (NIL), optical lithography and dip-pen nanolithography. Many examples of the fabrication of periodic and functional nanostructures are given in this chapter, with a preference of nanostructures with biomolecules. Furthermore, we introduce the photosynthetic unit (PSU) from purple bacteria. In this research we use purified components from the PSU and assemble them on different surfaces in order to study adsorption, organization, functional properties and energy migration in these ubiquitous photosynthetic systems. To evaluate how these properties correlate with their performance in native photosynthetic membranes based on previous work, we use state-of-the-art characterization techniques combining atomic force microscope and fluorescence microscopy.

* Part of this chapter has been submitted as a book chapter: Cees Otto, Maryana Escalante, Chien-Ching Wu, Vinod Subramaniam, "Biologically Inspired Nanopatterning" in Comprehensive Nanoscience and Technology (Edited by David Andrews, Greg Scholes and Gary Wiederrecht), Elsevier B.V

1.1 INTRODUCTION

Biology is a major source of inspiration for nanoscience. The cell is an exquisite example of engineering where a collection of sophisticated nanomachines work in unison. Having been developed and refined over billions of years, these nanomachines perform complicated tasks very efficiently. They control biological systems with unprecedented precision and selectivity. They include catalysts, functional systems (enzyme, ribosomes, proteins, protein aggregates), lipid bilayers, ion channels, cytoskeletal elements, nucleic acids, motor proteins, etc.[1]

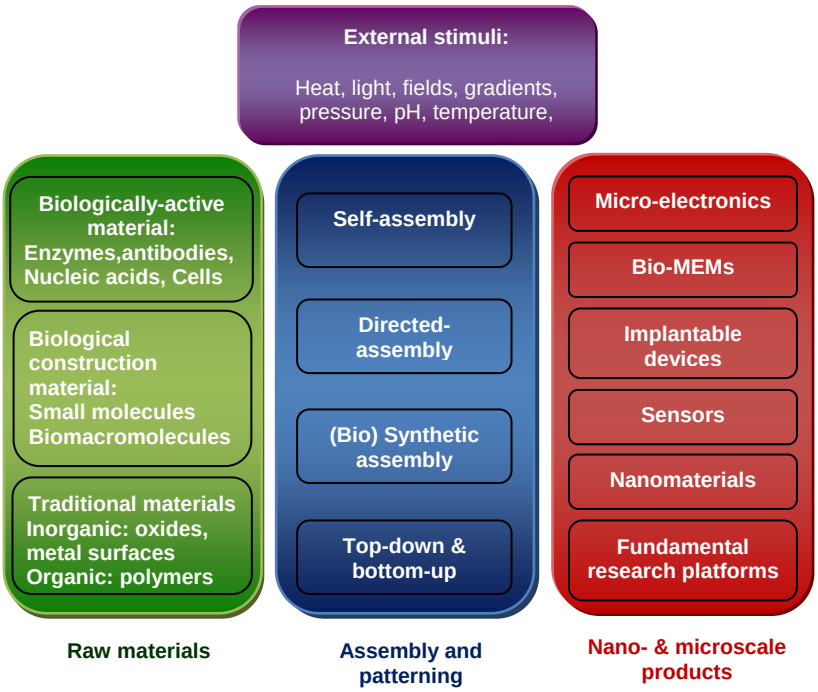

Figure 1.1. *Biomolecules can be used in the fabrication of functional devices. The assembly can be achieved by exploiting the intrinsic physicochemical properties of the molecules, by directing the assembly through external stimuli or by bioengineering specific recognition sites that promote the selective assembly either on biological or non-biological surfaces.*

Biomolecules constitute a unique toolbox with systems that provide exceptional properties that can be incorporated into nanofabrication platforms presenting both opportunities and challenges for the development of functional hybrid devices. One key requirement is the ability to selectively organize multiple biomolecules on surfaces from the micrometer to the nanometer scale in a two- or three- dimensional

space. Moreover, control over orientation is critically important in the development, for example, of immunodiagnostics, as the optimum orientation of an antibody can greatly increase the surface binding ability and therefore the sensitivity for biosensing applications.[2] Developments in this area include selective orientation of antibodies and antibody fragments.[3-4] Other important parameters to fine-tune are binding strength, binding dynamics, packing density and arrangement, and reversibility of the assembly process. As is indicated in Figure 1.1 there is a growing list of examples where biomolecules are contributing to a broad range of activities besides conventional recognition and detection. These include the use of biological material as construction elements where new material properties can be explored.

In general biomolecules have a precisely controlled structure and size, and present a variety of physicochemical properties. For example, lipids are amphiphilic, DNA is anionic, while proteins, depending on their aminoacid sequence, show a range of solubility, hydrophobicity and charge distribution. These properties in some cases can promote self-assembly and can also be manipulated by external stimuli to direct the assembly into hierarchical molecular assemblies (Figure 1.1). Biomolecules are able to perform their native tasks very efficiently under physiological conditions and their processing is usually environmental friendly. The precise structure of natural material in combination with the ability to control their structure (e.g. to alter sequence) allows properties to be engineered for specific functions.

Biological systems offer many examples of nanostructures interacting in a complex manner. Several biomolecules, including nucleic acids, proteins, lipids and oligosaccharides react with other biological components by molecular recognition,[5] which suggest new strategies that can be exploited to build artificial nanosystems from the “bottom up”.

Different interactions can be used to control the biomolecular-substrate interface. The simplest method is physical adsorption where mutual attraction between the solid surface and the biomolecules (e.g. proteins) results in coverage of the surface. In this case protein adsorption results from attractive forces such as ionic, hydrophobic, or van der Waals forces. Even though physisorption or chemisorption do offer some reversibility in binding and therefore the potential of dense packing

with high order, the predictability of binding stoichiometry and thermodynamic binding parameters is small, and thus the practical control is limited.

A more stable way is to use covalent interactions, where the protein is linked to the surface through chemical bonds. This is based upon residues typically present on the exterior of the protein. It is a random process and can occur simultaneously through many residues which increases the heterogeneity of the distribution of immobilized proteins. The functional groups listed in Table 1 can be used to direct chemical coupling with suitable types of derivatized substrates.[6]

Table 1. *Commonly available functional groups in proteins and functionalities of the required surfaces.*[7]

Side groups	Amino acids	Surfaces
-NH2	Lys, hydroxyl-Lys	carboxylic acid
		active ester (NHS)
		Epoxy
		Aldehyde
-SH	Cys	Maleimide
		pyrydyil disulfide
		vinyl sulfone
-COOH	Asp, Glu	Amine
-OH	Ser, Thr	Epoxy

Amine-reactive: is the most common method for the immobilization of proteins, makes use of the amine groups of the lysine amino acid. The abundance of lysine residues might create multipoint attachment of the proteins. N-Hydroxysuccinimide (NHS)-activated carboxylic acid is generally used for coupling with protein amine groups forming stable peptide bonds.[8-9]

Carboxy-reactive: mild coupling methods (e.g. carbodiimide activation)[10] can be used to immobilize proteins via carboxylic groups through the aspartic and glutamic acid which are abundant on the surface of proteins.

Thiol chemistry: through the cysteine groups which contain a thiol functionality able to create internal disulfide bonds.[11] Cysteines are less abundant that Lysines (< 1%), therefore oriented immobilization of the protein is possible.

Epoxy chemistry: though covalent interaction between proteins and epoxy groups are known to be slow, previously adsorbed proteins have been shown to

react at a high rate.[12] Multifunctional groups with two moieties have been designed, one containing groups able to promote physical adsorption and the other having epoxy groups in sufficient amounts to enable covalent immobilization.[13]

Photoactive chemistry: photochemical reactions can be performed under mild conditions and the most commonly used photoreagents, i.e. arylazides, diazirines, benzophenones and nitrobenziles[14] are activated at λ = 350 nm, to which biomolecules are usually transparent. After light activation, the reagent undergoes chemical transformations which lead to the formation of bonds between the photo-generated products and the proteins.

Strategies adopted from established capture reagent/fusion protein pairs have been employed to uniformly orient proteins on surfaces through noncovalent interactions. Some examples are listed below.

High affinity ligand pairs: such as lectins, avidin-biotin, streptavidin-biotin, provide stable immobilization, similar to covalent interactions.[15-16] However in this approach there is no control and flexibility over the strength of the interaction, and therefore the packing density in some cases could be compromised.

Nickel Nitrilotriacetic Acid: this is regularly used to purify proteins in immobilized metal affinity chromatography (IMAC) for example in N-nitrilotriacetic acid (NTA) columns. NTA is a tetradentate ligand and its complex with a divalent metal ion (Ni^{II}, Co^{II}, Cu^{II}, and Zn^{II}) has two binding sites available for binding to a His_6 sequence. Dissociation of the proteins attached by means of (metal ion)NTA-His-tag interactions can be induced by releasing the chelate complex using EDTA or by using a competitive agent such as histidine or imidazole. This approach was introduced by Tampé *et al* on gold substrates,[17] and recently this approach has been expanded to different surfaces to pattern a wide range of biomolecules.[18-22]

DNA-directed immobilization: oligonucleotide-directed immobilization contributes with the high stability of DNA oligomers and the unique site-selectivity of the specific Watson-Crick base paring. Biomolecules of interest need to be coupled with ssDNA, providing specific recognition sites for complementary oligonucleotides.[23] Currently the incorporation into larger molecules is still a challenge.

Supramolecular interactions: has been applied for the immobilization of proteins to surfaces[24] since they represent an elegant solution to control binding stoichiometry, strength and dynamics.[25-29] In order to enhance binding affinities, multivalent supramolecular interactions may be employed. Multivalency is described as the simultaneous binding of multiple functionalities on one entity with multiple complementary functions on another entity.[30] Recent studies include designed host-guest systems or receptor-ligand types.[31]

Many other chemical strategies have been used for the immobilization of biomolecules and have been reviewed by Rusimi *et al*[7] and Johkheijm *et al*.[32]

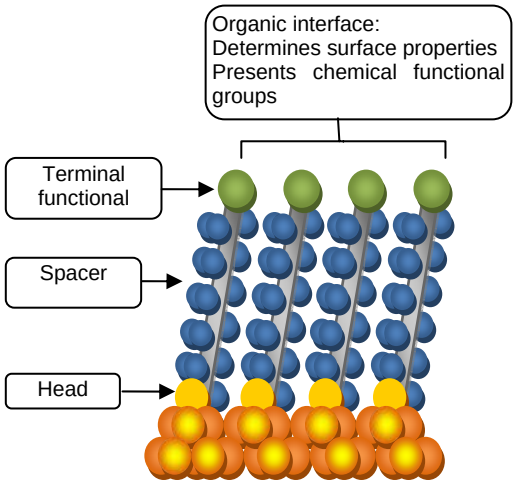

Figure 1.2. *Example of a schematic of an ideal single-crystalline SAM of alkanethiolates supported on gold surface with a (111) orientation. General characteristics of the SAM are indicated. Adapted from* [36].

To induce the assembly of the biological material in a controlled way, different external stimuli can be used (light,[33] fields,[34] gradients[35]), usually in combination with surface modification of the substrate upon which the assembly is performed. Self-assembled monolayers (SAMs) provide a convenient way to tailor the interfacial properties of different substrates (e.g. oxides, metals, metals-oxides, semiconductors, polymers). They are organic assemblies formed by the adsorption of molecules from gas or liquid phase. The adsorbates organize spontaneously onto the structure of the surfaces. SAMs are themselves structured with a number of useful properties (Figure 1.2). The molecules that form the SAMs have a "head group", with a specific affinity for the substrate, an intermediate alkyl chain and a

diversity of terminal groups (e.g. acids, alcohols, amines, esters, fluorocarbons, nitriles). The terminal groups have highly modifiable chemical functionalities which can be tuned to control the directed assembly of biomolecules on surfaces.

1.1.1 Functional groups on activated surfaces

Surface modification with a spacer/linker (crosslinkers) allows the attachment of virtually any desired reactive group. The spacer/linker also has the function of separating the biomolecules from the surfaces in order to prevent steric constraints induced by close contact to the substrate. The crosslinkers can be of a variety of lengths and physico-chemical characteristics; they can be rigid, flexible, hydrophobic, hydrophilic, charged or neutral.[37] Crosslinking reagents contain two or more reactive ends that are capable of attaching to specific functional groups (primary amines, sulfhydryls) on proteins or other molecules. Homobifunctional linker reagents have identical reactive groups at either end. Heterobifunctional linkers are reagents with different reactive groups at either end. For a complete list of crosslinkers refer to Pierce.[38]

1.1.2 Protein repellant surfaces

Effective reduction of non-specific adsorption of proteins is a requirement for the controlled and directional deposition of proteins. Various surfaces/chemical functionalization has been used for this purpose: for example agarose,[39] bovine serum albumin (BSA),[40] cellulose acetate,[41] elastin-like polypeptides,[42] sarcosine[43] and polysaccharides[44] are naturally occurring surfaces. Synthetic polymers have also been used such as: fluorocarbon polymers and molecules,[45-46] polyvinyl alcohol[47] and the most commonly used and studied is based on surfaces modified with oligo(ethylene glycol derivatives).[48-49] A thorough characterization of these surfaces has been conducted by Whitesides and coworkers.[50]

1.2 Patterning strategies in bionanofabrication: controlling size and shape of the assembly

Natural processes rely on self-assembly. It is so far not completely clear how this actually gives rise to the dynamic and transient structures in living systems. However, self-assembly is a generally known molecular organization principle in

chemistry and as such also very attractive to pattern biomolecules into functional biostructures. In the formation of nanopatterns, control over the size, the precise shape as well as the spacing between repetitive elements of a pattern is of essential importance for functional micro- and nano-scale devices. Biomolecular patterns can be fabricated either by the formation of templates where the target molecules will subsequently adsorb (SAMs) or by the direct deposition of molecules. For this purpose, successful fabrication techniques exist, which originally emerged from developments in microelectronics. Photolithography, electron-beam lithography, and still other techniques are potentially well suited to pattern bio-organic molecules. The tasks for which these techniques were originally designed, were to form patterns in radiation-sensitive materials, like e.g. photoresist or electron-beam resist, on ultra-flat glass or semiconductor surfaces. Still, the requirements for the patterning biological matter with strong structure dependent functionalities poses significant challenges in adapting existing lithographic techniques for applications in this field.

The demands of biotechnology to handle soft matter, with unusual molecular systems properties, which are often embedded in a more complex hierarchy of molecular interactions, requires precise control of interconnected structures with nanometer dimensions. As a result, some of the oldest and conceptually simplest forms of lithography –embossing, molding, stamping and writing– are now being widely used for their potential to serve as the basis for nanofabrication techniques.[51] These techniques encompass two basic approaches: the top-down approach, where a bulk material is directly patterned using irradiation or molding, and the bottom-up approach using self-assembly of molecules or compounds on a surface to enable selective anchoring of biomolecules. Often the choice of the nanofabrication method is a compromise between the effectiveness, cost and technology available.

In the following section, the most widely used bionanofabrication techniques are briefly introduced by a technical description of the original method, evolution of the process, and then some state-of-the-art applications. We conclude with summary remarks with respect to the advantages and challenges in our progress to fuse the fundamental fields of science with nanopatterning strategies for functional biomolecules.

1.2.1 Soft-lithography

These techniques are based on the preparation of a soft mold or stamp by casting a liquid polymer precursor on usually a topographically patterned hard substrate. A number of polymers can be used for this purpose. The most common elastomeric polymer used is poly(dimethylsiloxane) (PDMS). PDMS is a durable material, unreactive towards a wide range of patterned materials and chemically resistant. Commercial kits are available of this polymer,[52-54] which makes the process inherently inexpensive and gives the possibility of parallel production of stamps. Microcontact printing (*μCP*) is the most popular soft-lithography bionanofabrication technique where the elastomeric stamp can be used to directly pattern biomolecules or to template areas for their subsequent adsorption. Other soft lithography techniques used for the patterning of biomolecular assemblies include micro- and nanomolding in capillaries (MIMIC).[55-56]

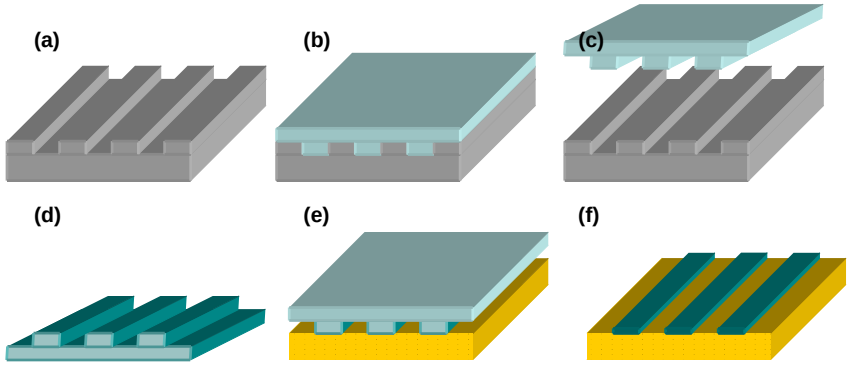

Figure 1.3. *Schematic illustration of the fabrication of topographically patterned elastomeric stamps (e.g. PDMS) (top) and their use for the fabrication of chemically patterned Au substrates (bottom). (a) Fabrication and silanization of the silicon master; (b) pour PDMS prepolymer over master and cure (over night, 60 °C); (c) peel off PDMS, (d) ink and dry stamp; (e) printing on the substrate; (f) removal of the stamp results in patterning of the underlying substrate with the ink molecules.*

Microcontact printing was introduced by Whitesides and coworkers[36] who envisioned an alternative fabrication technique that moves away from conventional photolithography. In this approach PDMS structures were prepared by casting the silicon rubber onto the desired pattern. The stamps were coated with alkanethiol molecules as ink and were used to create self-assembled monolayers on gold substrates through conformal contact in a massively parallel fashion (Figure 1.3). In the context of this chapter, *μCP* was initially used for the direct printing of proteins

in 1998.[57] Chicken immunoglobulin's (IgGs) were directed patterned onto glass and polystyrene surfaces at the nanoscale for protein recognition,[57] and on polymers using biotin-streptavidin linkages.[58-59]

Due to the hydrophobic surface properties of PDMS, water soluble inks do not wet the surface of the elastomer and do not permeate the bulk, restricting the usage of, for example, inorganic complexes and biomolecules.[60] The oxidation of the PDMS surface (e.g. by oxygen plasma) allows the printing of such polar inks since a thin silica-like surface layer is formed upon oxidation.[61]

In *μCP* issues such as the stamp deformation during the removal from the template and during the contact with the substrate limit the resolution.[62-65] However, with *μCP* conventional patterns with dimensions of few hundreds of nanometers are still possible.[66-67] When the aspect ratio is high, buckling and lateral collapse of the PDMS features can occur, while at low aspect ratios roof collapse is possible.[65,67] To overcome these issues, soon after the introduction of *μCP,* a tendency could be seen towards an increasing number of process variations, either by changing the printing procedure itself or by varying the properties of the ink or the stamp. Other elastomers besides PDMS such as block copolymer thermoplastics,[68] and fluorocarbon-modified siloxanes[69] have been used.

For an accurate and uniform transfer of the ink from the stamp to the substrate, in general two contradictory characteristics are needed: high mechanical stability of the micro- and nanostructures and good capability to achieve conformal contact down to the nanometer scale despite potential substrate roughness or contamination. A high mechanical stability requires a high Young's modulus, while efficient conformal contact is facilitated by increased elasticity. To improve the stamp stability, a composite stamp structure, a thin PDMS stamp built on a rigid back support, has been used to pattern proteins on solid substrates.[70] Increased strength of the stamp allows printing of features < 100 nm, nanocontact printing (*nCP*), for example with the use of polyolefin plastomers (POPs).[71] Poly(ether-ester) were used as stamp materials to accurately pattern proteins on surfaces using lower ink concentrations and inking times compared to PDMS stamps.[72] Other hydrophilic stamp materials were developed for the printing of proteins and biomolecules. Hydrogel copolymers of 6-acryloyl-b-O-methylgalactopyranoside and ethylene glycol dimethacrylate on solid supports were used as stamps for *μCP*.[73] Composite

stamps produced from two UV-curable materials,[72] and poly(ethylene glycol) diacrylate, were used to perform μCP of polar biomolecules.[74]

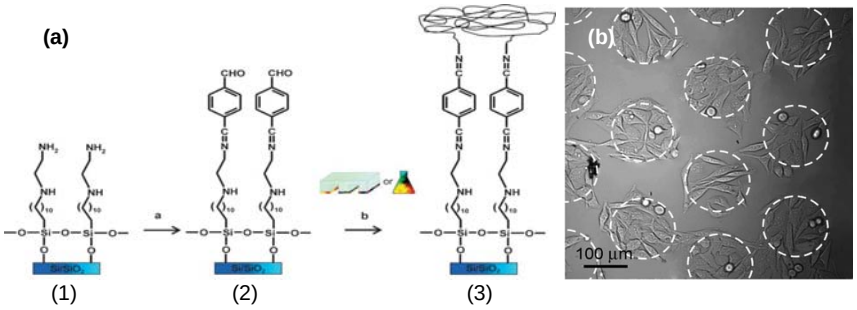

Figure 1.4. *(a) Route to covalent immobilization of protein Col3a1 on silicon oxide surface. (1) aminoterminated substrate, (2) aldehyde terminated substrate, (3) substrates with Col3a1 protein patterned by μCP. (b) Patterns of HeLa cells obtained by microcontact printing 100 μm dots of protein Col3a1.*[78]

μCP has been used to direct the adsorption of cells on surfaces.[75-77] For example HeLa cells were patterned using the interaction with patterned Col3a1 protein.[78] Silicon oxide substrates were modified with amino-terminated SAMs and then the amino groups were converted into aldehyde groups by the reaction with terephthaldialdehyde.[79] Substrates modified in this manner can be directly patterned with collagen-like proteins by microcontact printing using a PDMS stamp (Figure 1.4a). Free amine residues in the protein form imine bonds with the aldehyde SAM. The remaining areas of the aldehyde SAM can subsequently be blocked with amino-PEG forming areas resistant to cell adhesion. HeLa cells were seeded and incubated on the patterned substrates. The cells adhere and spread selectively on the protein islands (Figure 1.4b).

Efforts are carried out to make of *μCP* a multiplexing technique (patterning of many different molecules in one substrate). Intuitively, there are two ways to print different proteins onto a single substrate using soft lithographic techniques: i) sequential inking and printing, and ii) parallel inking of a stamp followed by a single printing. The sequential method is conceptually straightforward. Different stamps (stamps having different patterns and/or various inks) can be printed many times onto the same substrate.

An interesting parallel strategy can make use of flat stamps (stamps lacking of a surface relief).[80] In this approach the stamp serves merely as a vehicle for

transferring proteins patterned on the planar stamp to the target surface. With a flat stamp no buckling or side and roof collapse can occur. The main technical requirement to perform such parallel printing is to ink locally the stamp with different proteins. Any patterning-by-adsorption method can be used. For example, flat stamps have been inked in an area-selective manner using a robotic spotting system, and then used to fabricate a multiprobe array of amino-modified oligonucleotide spots.[81] The resolution of this approach is limited by the resolution of the spotting system. A different method is based on physically limiting the area exposed to the solution of proteins during inking, for example, with microfluidic networks.[82-83]

Figure 1.5a illustrates this approach. 16 different proteins were transferred to a plastic substrate from a previously inked flat stamp using a multi-channel microfluidic network. Unlike for other inks (e.g., thiols or metal ions),[84] this strategy is not compromised by the diffusion of proteins on the flat stamp before ultimately printing them on the substrate. Also, sub-100-nm resolution in protein patterning was achieved in the work of Delamarche and coworkers by exploiting the differences in adhesion of proteins to PDMS and silicon.[85] A flat PDMS stamp with a homogeneous protein layer was placed on a patterned silicon nanotemplate. With the removal of the stamp, due to the less hydrophobic character of silicon compared to PDMS, proteins were subtracted from the stamp leaving a patterned protein layer on the noncontacted areas. These protein patterns could subsequently be transferred onto another substrate.[85] A step further in the patterning of multiple biomolecules in one step makes use of a microstructured PDMS macrostamp, recently introduced by Vieu and coworkers.[86] The macrostamp is constituted of several pads (made of PDMS) linked together by a PDMS foil. These millimetric size pads match perfectly the 1536 wells of a titration plate (Figure 1.5b). By simply dipping the macrostamp inside a filled titration plate, a large number of different inks can be adsorbed at one time and later transferred by a printing step. The accuracy and spatial resolution of μCP is combined with a multiplexing process with hundreds of different inks by fabricating a molding system that allows molding of each pad in front of a silicon master covered with micro- or nanometer size features.

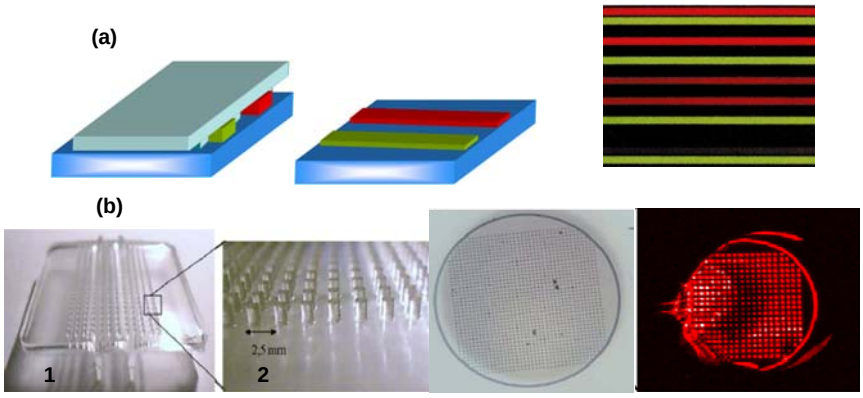

Figure 1.5. *(a) A microstructured PDMS layer is used as a microfluidic network for the patterning of flat surfaces. The channels can be filled with solutions of different molecules. After removal of the PDMS structure, the biomolecules pattern remains on the surface. (b) Use of a microstructured macrostamp for the patterning of different biomolecules.*[86] *The stamp has the macrostructure of the microwell plate. Each macro pillar is patterned with micro (and potentially submicron) structures.*

To increase the printing capability of the stamps, the use of porous stamps have been recently introduced, where the porous structure acts as an ink reservoir to be able to use the same stamp to print the same pattern reproducibly several times. This approach has been used for the direct printing of macro(bio)molecules.[87]

The combination of *μCP* with supramolecular host–guest interactions led to various improvements in nanopatterning of (bio)molecules. Proteins were selectively picked up from crude biological solutions and then printed on substrates by Delamarche *et al*.[88] Stamps functionalized with reactive groups bound the proteins from complex mixtures and aided the transfer of these biomolecules onto the target substrates. Other groups immobilized ssDNA on a stamp and immersed it in a solution containing the complementary DNA previously end functionalized with chemical motifs able to interact with the targeted substrate. During printing, the preformed dsDNA is dissociated, and after the removal of the stamp the complementary copy of the master pattern is created.[89]

μCP has progressed rapidly since its introduction. While the general concept remains the same, a pattern is transferred to a substrate by conformal contact between the stamp and the substrate; marked variations in the process and materials have helped to overcome the initial limitations inherent to the technique. Polar and apolar (bio)molecular inks, composite stamps, chemically and/or physically tailored

stamp-surfaces and/or substrates and featureless stamps are currently used such that sub-100 nm features can be reliably reproduced. Motivated by applications in bio(sensing), but also by fundamental research, efforts have been driven towards the fabrication of research platforms for functional chemical, supramolecular and biological interactions. The fabrication of high density multiple biomolecules (e.g. proteins) all in the micron- and submicron regime is still an open challenge, not only for the nanofabrication community but for the scientific community in general since in this regime the detection and analysis tools become more demanding.

1.2.2 Nanoimprint lithography (NIL)

Nanoimprint lithography (NIL) is a parallel nanofabrication embossing technique known for high-throughput patterning of polymers nanostructures at great precision and low cost. Thermal NIL was first introduced by Chou and coworkers in 1995[90] followed by UV-NIL developed at Philips Research Laboratories.[91] There have been variations in NIL processes, which are mostly variants of the initially introduced thermal and UV-NIL. The success of this method has enabled it to pass the technology transfer barrier from a laboratory scale process to industrial preproduction. NIL has been included in the International Technology Roadmap for Semiconductors as a candidate technology for IC production.[92] Moreover, much interest in NIL originates from the search for low-cost methods for the fabrication of high numbers of identical devices (e.g. for a research project) particularly in the area of sensors, biochips and templates for tissue engineering.[93]

In this section the presentation of NIL will be limited to an introduction to thermal NIL. The principle of a thermal nano-imprint lithography process is shown in Figure 1.6. Thermal NIL relies entirely on the concept of a direct contact between the stamp and the polymer-coated substrate. A hard stamp or mold with the desired micrometer or nanometer range features is needed. The stamp can be fabricated by optical lithography and/or electron beam lithography and combined dry etching or metal lift-off. Nevertheless, new approaches propose for example modified hardened patterned polymers which can also be used as stamps,[94] and alternative methods such as interference lithography,[95] edge lithography[96] and non conventional materials such as cicada wings.[97] The stamp with nanostructures on its surface is used to deform a thin film deposited on a substrate. To transfer the pattern to the

underlying film, an etching process, such as reactive ion etching (RIE), is used to remove the residual compressed areas (Figure 1.6c).

Figure 1.6. *Schematic diagram of the nanoimprint lithography process. (a) Imprinting with a stamp creates a thickness contrast into a deformable polymer layer. (b) Removal of the stamp retains the pattern. (c) Pattern transfer into the polymer using anisotropic etching to remove the residual polymer layer in the compressed areas.*

The patterned film can be either a thermoplastic, UV (or thermally)-curable polymer or other deformable material. The optimal process parameters are a trade-off between structure height of the stamp, polymer thickness, pressure, the required temperature and imprinting time. Thermal NIL benefits from the availability of polymers such as poly(methyl methacrylate) (PMMA) and polystyrene (PS) with a wide range of molecular weights, M_w. For a thermoplastic polymer, the glass transition temperature (T_g) is the reference point to determine $T_{imprint}$ and T_{demold}. $T_{imprint}$ is usually 50-70 ˚C higher than the T_g, at which the resist will become more fluidic and the mold can be pressed into the resist with relative ease. T_{demold} is chosen below T_g to take advantage of the internal consistency of the material while lifting of the stamp. A compliance layer is necessary to distribute the pressure uniformingly over the substrate. This prevents damage to both the stamp and the substrate, while at the same time improving the embossing results. During imprint (also called molding, embossing, forming or shaping), the polymer is displaced by squeeze flow (pressure applied to the system) and capillary forces (the surface energy controls the spreading of the viscous material) until it replicates the surface profile of the stamp. Next, the system is cooled down below its T_g before being separated from the mold. During demolding (also called detachment, separation or de-embossing) adhesion and friction forces are exerted on the stamp features. To aid the demolding process it is customary to have a low adhesion between the polymer and the stamp. This is achieved by surface modification either of the stamp or the polymer layer. Different solutions have been proposed for stamp release: non-

sticking stamp materials[98-100] antiadhesive coating,[101-102] non-sticking resist materials,[103] and dissolvable stamps.[104]

After demolding the substrate results in a continuous layer of polymer with a surface topography. The local patterning, which results in a geometrical contrast, can be improved by removing the residual thin polymer layer, e.g. by reactive ion etching (RIE), until the thin intermediate areas become open "windows" to the substrate. Both the surface shaping and the polymer thinning are global processes. Particularly for the latter highly anisotropic RIE has been developed to preserve the dimensions in the lateral directions while only the height is decreased during etching.[105]

NIL has become very attractive and is becoming a widely used technology, because it is a robust approach that can be combined with a very high resolution as was demonstrated soon after its introduction.[106] Figure 1.7 shows scanning electron microscope (SEM) images of a mold with pillar arrays with diameter of 10 nm (a), the imprinted 10 nm hole array in PMMA (b) and the corresponding Ti/Au dot pattern on a silicon substrate after a lift-off process in panel (c). Such dimensions are very exciting as they are clearly within the range of sizes of biomolecules

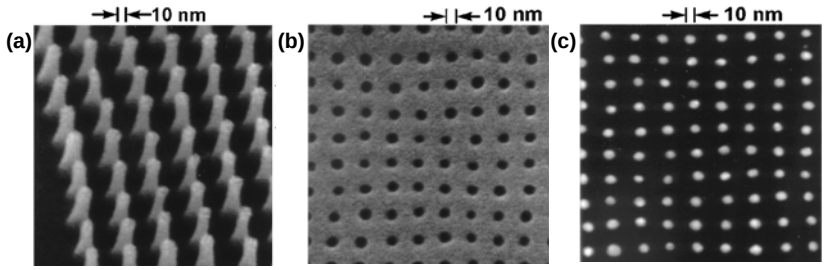

Figure 1.7. *(a) Scanning electron microscope (SEM) image of a fabricated mold with a 10 nm diameter array. (b) SEM image of holes arrays imprinted in PMMA. (c) SEM image of Ti/Au dot pattern on a silicon substrate fabricated by NIL and lift-off process. Reproduced from*[106]

The advantages of NIL make this technique attractive for numerous applications in organic electronics,[107] photonics e.g. organic lasers,[108] and high resolution OLEDs[109], high density patterned magnetic media,[110] nanoscale control of polymer crystallization,[111] as well as for organic solar cells.[112] Recently NIL has been used in biological applications for instance to manipulate DNA in nanofluidic channels,[113-114] to investigate the effect of imprinted nanostructures on cell culture[115] and fabrication nanoscale protein patterns.[18, 116-118] In general for the latter purpose

NIL is used to create templates which serve as masks for chemical functionalization with the anchor points of the biomolecules to the substrate. This approach was followed by Hoff and coworkers[118] who were among the first groups to use NIL for patterning proteins (Figure 1.8).

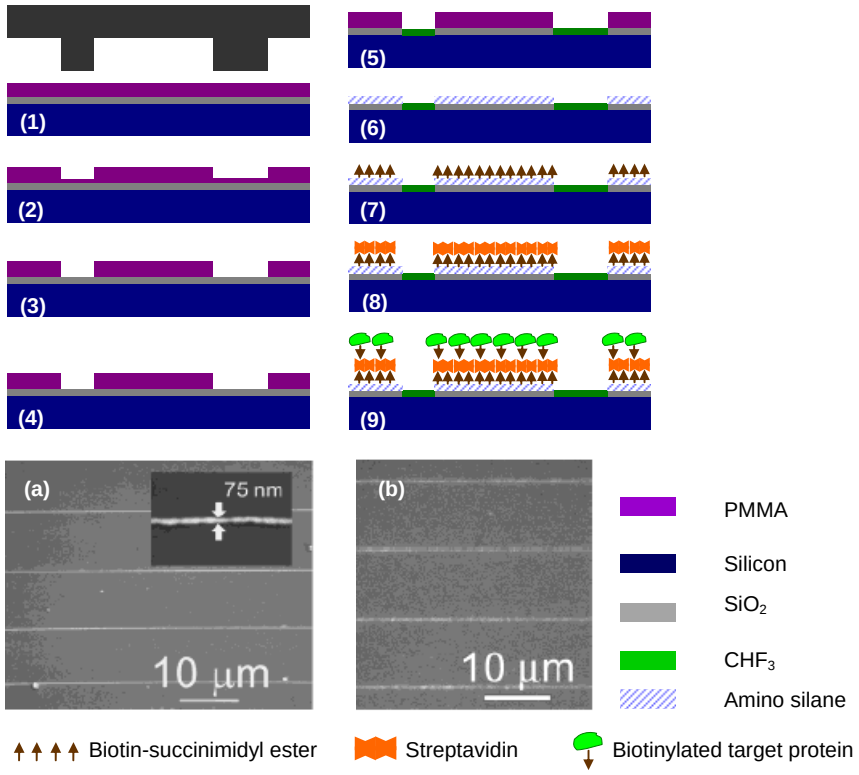

Figure 1.8. *Process flow diagram of substrate patterning and protein immobilization. Spin-coated PMMA polymer is patterned by NIL. Exposed SiO_2 regions are etched and passivated via CHF_3 RIE. Residual PMMA is stripped away with acetone. An aminosilane monolayer is covalently attached to the exposed "patterned regions". Biotin-succinimidyl ester is then covalently linked. Streptavidin is bound to the biotin layer. Finally, the biotinylated target protein is bound to the streptavidin layer. Proteins patterned onto sub-100 nm features. (a) SEM image of oxide nanolines formed on a Si substrate by NIL and RIE. (Inset) Close-up SEM of oxide nanoline, showing a line width of less than 100 nm. (b) Fluorescence micrograph of nanolines after patterning with biotinylated BSA and binding rhodamine-labeled streptavidin. Figure adapted from [118].*

Hoff and coworkers used a silicon mold fabricated by standard e-beam lithography and dry etching with sub < 100 nm features. The mold was coated with perfluorochlorosilane to facilitate mold separation after imprinting. PMMA was

spun onto a substrate of 60 nm thick silicon dioxide on silicon. The PMMA was patterned by NIL. O_2 reactive ion etching (RIE) was used to remove the residual PMMA layer in the patterned regions. CHF_3 RIE was used to etch the newly exposed oxide, transferring the patterns to the oxide layer. In addition, this etching process deposits a thin passivating (hydrophobic) layer of CF_x polymer residue on the newly exposed Si surface. The remaining PMMA was then removed by sonication in acetone. The exposed oxide pattern selectively reacts with an aminosilane to form a covalently bound monolayer. The substrate was placed in a flow cell which allows sequential introduction of various buffers to the substrate. Biotin is covalently bound to the exposed primary amine tail group of the patterned surface by filling the flow cell with a biotin-succinimidyl ester solution. Similarly, a streptavidin layer is deposited. The resultant streptavidin monolayer serves as a base for the specific adsorption of any biotinylated target protein, in this case biotinylated BSA. In order to visualize the pattern with fluorescent imaging, the substrate was later exposed to a rhodamine-labeled streptavidin solution. The spatial dimensions in the patterns were reported to be about 75 nm.

Other biological systems that have been patterned using NIL are integral and membrane proteins.[18, 116] Since NIL is not a direct deposition technique, NIL does not involve a direct manipulation of the biological material, but provides a way to create chemical patterns at high resolution onto which the proteins can later self-assemble due to biochemical interactions. This advantage of NIL helps to avoid that external pressure is exerted on the target molecules. Furthermore, this makes the technique particularly suited for the preparation of patterns of delicate biological material for which structural integrity is intimately linked to functionality. It also has the advantage that the assembly process on the surface and further characterization can be conducted in near-physiological in liquid environment. Moreover because the chemical areas are well defined and of high contrast, one can think of active vs. passivated areas, the ability of molecules to diffuse is much less likely to reduce spatial resolution after patterning.

NIL is one of the most promising alternative nanofabrication techniques and constitutes a major example of the combination of top-down and bottom-up methods within the different nanofabrication approaches. It provides an unprecedented parallel capacity for the patterning of sub-100 nm structures in areas up to square

centimeters; however, for optimum results the designs are restricted to geometries usually on the same scale because the stamp filling depends on the structure aspect ratio and density.[119] Challenges still promise to keep scientists busy in order to meet mass production standards, zero residual layer, near room temperature imprinting for decreasing the imprinting time (heating and cooling down curve), among other general issues like dewetting, air inclusion and the possibility for multilayer NIL alignment. Still open is the issue of multi-biomolecules patterning using NIL. However, a promising alternative is the combination of NIL for the patterning of small arrays of active areas, with for example, microfluidics assisted techniques such as micromolding in capillaries [55-56] (MIMIC) or nanomolding in capillaries[120] where different inks can be injected to the micro- or nanochannels and bind specifically to the pre-patterned areas with NIL.

1.2.3 Optical lithography

Light offers convenient methods to introduce surface patterns. Multiple methods are available to exploit the various mechanisms of light interaction with molecular surface layers.[121] Optical lithography, in a broader sense, uses light to transfer a pattern to a light-sensitive chemical resist. Commercial standards have been developed to create ~10 nm features and sub-100 nm features are commonly used in microelectronic devices. In this "run for miniaturization" the development of photosensitive resists is in constant progress. Optical lithography has found its way into the fabrication of biological arrays on surfaces in micro- and nanometer dimensions.[122]

The size of the individual polymers (typically 5-10 nm radius, when they are considered as random coils), the extent of the dimension of illumination and the diffusion of radicals in the film determine the minimum resolution that can be achieved using polymer resists. As a result, self-assembled monolayers (SAMs) become attractive as photoresists, because the individual molecules that make up these layers occupy areas smaller than 0.25 nm^2 and because the layers are very thin, < 3 nm. Strategies to implement optical lithography for patterning include the irradiation at very short wavelengths (<250 nm, high energy UV) in the presence of oxygen. This can lead to the chemical degradation of a whole molecular layer as has been shown for aryl- and alkylsilanes at 193 nm.[123]

At longer wavelengths, light initiates photoconversion of the anchor group in SAMs of alkanethiolates. The oxidized species can be removed from the substrate during rinsing with a polar solvent such as water or ethanol. Also, light induced attachment on a silicon oxide layer has been demonstrated with aldehydes and 1-alkenes. Photoactivation of a surface layer can be achieved if the monolayer-forming molecules are functionalized with a photosensitive group. This is a particularly interesting approach, since a large variety of photosensitive and reactive molecules are known that can be combined with many different functional groups.[124]

This procedure usually involves two steps: first, the surface active molecules with unprotected groups are deposited on the substrate, and second, the photosensitive groups are introduced into the monolayer by reaction with the surface. An improvement of the former procedure is the synthesis of surface-active molecules (thiols and silanes) with the photosensitive moieties directly attached to the functional groups prior to the formation of the monolayer.[125-126]

Jonas *et al*[121] reported photosensitive silanes for direct monolayer lithography, and it was also shown that functional surface groups were introduced, which is not possible directly by silanation (-OH and –COOH groups are incompatible with the triethoxysilane anchor group). Complex combinations of different functional and protecting groups can thus be achieved by simultaneous coadsorption of the corresponding silane mixtures and orthogonal activation. Orthogonal activation is defined as the possibility to selectively remove one type of protecting group in the presence of others in any chronological sequence. Although this represents a major challenge, it is also an important virtue of "protecting-group" chemistry. In the case of photosensitive protecting groups, individual addressing requires specific differences in sensitivity to selected wavelengths and intensities. Among the reported photoprotecting groups, 3,5-dimethoxybenzoin esters are known to be effectively cleaved by low intensity irradiation at wavelengths below 300 nm, while nitroveratryl (Nvoc) derivatives, being less reactive, are cleaved at longer wavelengths (420 nm).

Whitesides and coworkers[126] introduced a method that uses polyfunctional alkanethiols to form SAMs on a gold substrate presenting two types of photocleavable bonds: an *o*-nitrobenzyl amine-protecting group that cleaves the

amine-protecting group on exposure to light with a wavelength of 365 nm and a thiolate bond (Au-S) that cleaves on exposure to light with a wavelength of 220 nm. Actually, light at 220 nm removes the entire SAM, regardless of functionality, from the surface and produces a region of unprotected gold. A different SAM can be formed in those regions that were previously exposed to light of the appropriate wavelength upon incubation with a solution of a different alkanethiol. The first experiments used a conventional lithography approach to expose the photosensitive SAMs through a mask with micrometer dimensions.

The limitation of conventional lithography to achieve diffraction-limited dimensions has motivated the development of alternative ingenious techniques that exploit optical methods for the fabrication of structures with dimensions in the nanometer scale. One such technique is Near-Field Scanning Optical Lithography that uses a nanoscale aperture of a near-field scanning optical microscope (NSOM) probe to selectively expose an underlying photosensitive material leading to the formation of defined structures. The evanescent field at the sub-wavelength sized tip of the probe is essential to obtain a high resolution. The rapid decay of the evanescent field with distance (< 100 nm) requires that the distance between the sample and tip should be maintained within close proximity.

NSOM lithography owes its origin to the visionary work of Synge.[127] He proposed to use a non-transparent screen with a small aperture through which photons were collected with the spatial resolution of the size of the aperture. The success of this approach was hindered by the experimental problem to approach the near field of the emitting object and to maintain this distance between the aperture and the object. The emergence of scanning probe microscopy techniques in the 1980s[128-129] provided the means to realize the ideas of Synge. By 1992 Betzig and Trautman developed a near-field scanning optical microscope which used an optical fiber formed into a sharp tip[130] in conjunction with shear-force modulation to monitor the distance between the tip and the surface.[131-132] Near field images were acquired with an asperity at the apex of a sharp, metal coated glass fiber.[133] Betzig and Trautman used a NSOM to expose regions of a thin film magneto-optic material. Illumination led to the formation of areas of the order of 70 nm, which possessed a magnetization in the opposite direction than the surrounding material.[130]

Subsequent attempts to scale down conventional photolithography for the manufacture of gratings and other structures,[134-135] have generated reproducible structures of the order of ~100 nm. Other contributions to this field include the ablation of dye molecules,[136] thermal modification,[137-138] and selective modification of polymers.[139-140] Riehn *et al* fabricated structures in poly(p-phenylene vinylene), and concluded that only when the film thickness is smaller than the aperture radius can the excitation be effectively confined and therefore the feature size depends mainly on the tip-aperture radius and the tip-sample separation. Based on such considerations, self-assembled monolayers, which are a few nanometers thick, became highly attractive materials to perform NSOM lithography.

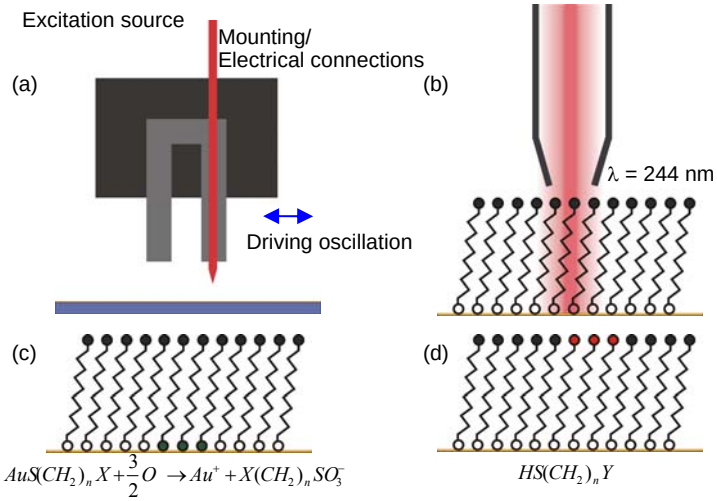

Figure 1.9. *Schematic diagram illustrating the basic principle of NSOM lithography. (a) A shear-force mode near-field scanning optical microscope, in which the probe is an etched optical fiber, aluminum coated with a nanometer aperture at the apex. (b) A self-assembled monolayer is exposed to the evanescent field associated with an NSOM probe coupled to an UV laser. (c) Photochemical conversion of the alkylthiolate adsorbates to alkylsulfonates. (d) Immersion of the sample in a solution of a different thiol, results in the formation of a chemical pattern.*

Particularly self-assembled monolayers of alkanethiols have been explored for their potential in near-field lithography for nanopatterning. Exposure of alkanethiols SAMs to UV light (λ ~ 250 nm) in air leads to a conversion of the gold thiolate complex to a weakly bound alkylsulfonate.[141-143]

$$AuSR + \frac{3}{2}O_2 + e^- \rightarrow Au + RSO_3^-$$

The immersion of the sample in a solution containing a different thiol replaces the oxidation products by the new thiol functionality through adsorbtion to the surface.[142,143]

The former approach was scaled down by Leggett and coworkers for scanning near-field photolithography (SNP). The basic principle is illustrated in Figure 1.9 in which selective photo-oxidation of the adsorbate head group is achieved by exposure to an evanescent field associated with an optical fiber NSOM probe.

Figure 1.10 shows friction force microscopy (FFM) images of patterns fabricated in carboxylic-terminated SAMs by first exposing the sample to the NSOM tip and subsequently immersing the sample in a solution of a methyl-terminated thiol. Figure 1.10a shows a parallel array of lines with a FWHM of 20 nm. 9 nm lines are possible, although at lower reproducibility rate (Figure 10b), which is equivalent to a resolution of λ/30. In the context of biotechnology this corresponds to the size of many proteins.

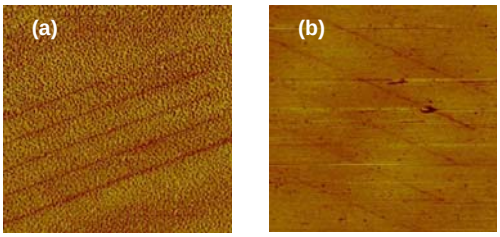

Figure 1.10. *Friction force microscopy of structures formed in SAMs by SNP. (a) FWHM 20 nm, 4.5 x 4.5 μm², (b) FWHM 9 nm, 3.0 x 3.0 μm². Reproduced from* [144].

In the same line of work, SNP has been used for the creation of submicron structures of biological material. Upon exposure of oligo(ethylene glycol) OEG-terminated SAM, which exhibit high resistance to the adsorption of proteins,[43, 50] to UV light, the sample was immersed in a solution of mercaptohexadecanoic acid. The surface was then activated by exposure to a solution of 1-ethyl-3,3-dimethyl carbodiimide (EDC) and N-hydroxysuccinimide (NHS).[8, 144] This resulted in active ester functionalities that react with amine groups of the proteins. SNP has also been used to create biomolecular arrays on oxide surfaces. The exposure of benzyl chloride to UV light in the presence of oxygen resulted in the formation of benzaldehyde. On further exposure the aldehyde may be converted to benzoic

acid.[145-146] With this procedure an array of spots of carboxylic acid groups was created, to which calf thymus DNA was later coupled (Figure 1.11b).

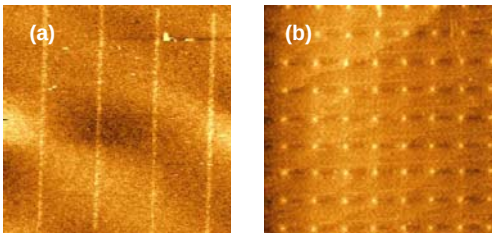

Figure 1.11. *Topographical image of nanometer-scale patterns fabricated by SNP, Image size 2.8 x 2.8 μm². (a) IgG on EDC/NHS activated carboxylic acid. (b) OEG- and carboxylic acid- terminated SAMs following incubation with calf thymus DNA. Reproduced from [146].*

In the context of nanolithography, optical methods provide a great chemical selectivity for photosensitive monolayers. Based on its intrinsic serial characteristic, which can be considered as a drawback for mass production, however, can be exploited in order to sequentially initiate chemical reactions with nanometer scale precision. This opens the possibility for the fabrication of multiple biomolecules arrays by the sequential activation-deposition of molecules. The feedback system of the NSOM instrument allows the placement of the excitation probe in close vicinity to the prior patterned areas. Whether the placement can be made at molecular dimensions is still an open question.

1.2.4 Atomic force microscope assisted nanolithography: Dip-pen nanolithography

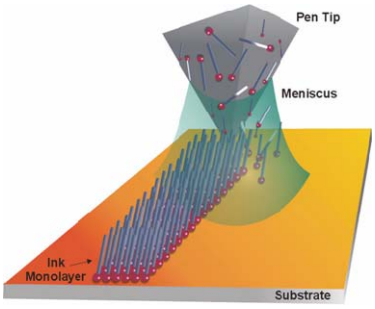

Figure 1.12*. Schematic representation of molecular transport in the dip-pen nanolithography (DPN) process. Figure from reference [147].*

Dip-pen nanolithography (DPN) is a scanning probe based technique that generally involves the coating of an atomic-force microscope cantilever tip with the molecules to be transferred to a substrate (Figure 1.12). Once the tip is in contact with the substrates, the molecules assemble on the surface by capillary transport; and by translation of the tip across the surface, arbitrary patterns can be produced, which makes DPN an excellent prototyping approach.

DPN was first introduced by Mirkin and coworkers,[148] demonstrating the feasibility of DPN by depositing simple alkanethiols onto a gold surface. Soon after its introduction the sophistication of the experiments quickly ramped up, exemplified by the depositing a great collection of inks onto a variety of substrates and conditions. There are many factors such as humidity, set-point, tip modification, the chemistry involved in binding between ink and the substrates, chemical purity of ink, tip and the substrate, tip shape and size, properties of the ink and the substrate that play an important role in successful pattern formation by DPN.

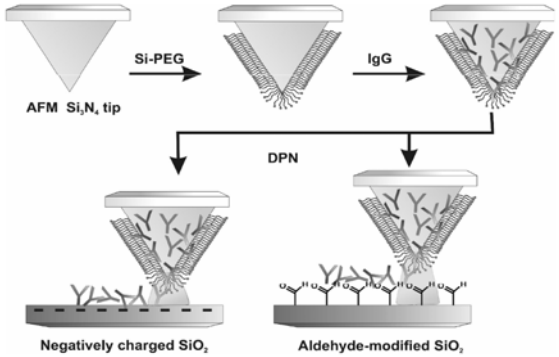

Figure 1.13. *Diagram of proof-of-concept experiments, in which proteins were absorbed on preformed MHA patterns [149].*

Depositions performed in a controlled environment where humidity levels could be adjusted to optimize transport revealed the technique's applicability to a wide range of systems. A general initial approach was the nanopatterning of a mercaptohexadecanoic acid (MHA) on Au surfaces to serve as a template for nanopatterning of biomolecules. MHA reacts with biomolecules by reaction with amine groups, which avoids the need for empirical optimization for each combination of substrate and ink. For example, with this approach ~ 100 nm patterns of Immunoglobulin G (Figure 1.13),[149] lysozyme,[149]biotin-streptavidin,[58]

elastine-like polypeptides (ELPs),[150] alkylamine-modified DNA,[151] and viruses[152] have been fabricated.

Although the method offers potential advantages, initially the DPN system had three major restrictions for patterning biomolecules: (i) slow patterning speed due to its serial characteristic and also due to a low diffusion rate of high-molecular-weight molecules; (ii) short operating time due to a limited ink volume on the tip; and (iii) depending on the biomolecules, it might be difficult to retain biological activity on the tip surface upon drying. Several variations of the technique have emerged to contribute to solve these issues. Some examples are given below.

For nanotechnology applications, it is desirable to perform a rich variety of lithography and microscopy operations in a sequential manner (i.e patterning and in situ inspection). For this purpose a multifunctional probe is one alternative.[153] Also the combination of atomic force microscopy and fluorescence microscopy has proven its capabilities.[154-156] In the field of multifunctional probes many approaches can be found in literature. Wang[153] presents a multipurpose probe that consists of multiple tips, each of them capable of performing a dedicated function, shown in Figure 1.14a. The array consists of sharp chemically coated probes used for DPN, a cantilever probe with an elastomeric tip (PDMS) to print chemical patterns and conventional imaging probes (scanning probe contact printing, SPCP). Each probe is able to engage independently from the others by means of thermal actuation. The newest technology from NanoInk Inc. introduced fifty-five thousand tips working in parallel which can create 88 million features on a 1 cm^2 area (Figure 14b).[157] The biggest challenge still remains in this field: to introduce additional fifty-five thousand different inks to the array.

To increase the ink reservoir the AFM tip for nanolithography has been the object of several modifications. For example, Deladi et al.[158] presented an approach that consists of an AFM probe with integrated fluidic channels running over the cantilever beams; Figure 1.14c. Fountain-pens with controlled dispensing of ink have also been designed.[159] Sponge-like tips have been fabricated in order to generate nanoarrays of large molecular weight biomolecules by a physical stamping mechanism when the tip makes contact with the substrate surface.[160] Lee and coworkers have developed a nano-porous polymer coated AFM tip by ring opening polymerization of 2-methyl-2-oxazoline. The tip's surface, modified with the nano-

porous polyoxazoline has pore sizes ranging from 30 nm to 100 nm. This tip can easily absorb large-molecular-weight biomolecules and generate protein nanostructures 60 times faster than with the conventional silicon tip. Proof of concept experiments show rabbit IgG protein nanostructures on MHA modified gold surfaces[160] and visible fluorescent proteins on silicon oxide surfaces.[161]

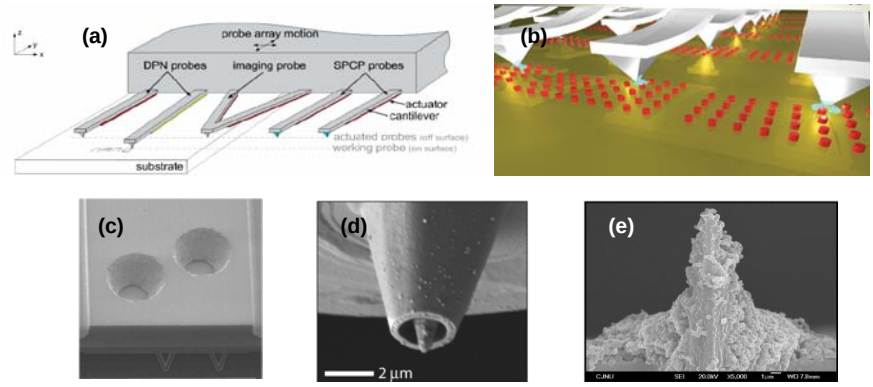

Figure 1.14. *(a) Schematic diagram showing sequential operations of lithography and microscopy using an active multifunctional probe array consisting of different functional probes,[153] (b) Tip pens working in parallel,[157] (c) Modified AFM probe with integrated fluidic channels,[158] (d)Fountain pen with electric field controlled ink release,[159] (e) Nano-porous polyoxazoline-coated stamp tip.[160]*

Dip-pen nanolithography has demonstrated to be a versatile nanofabrication approach for the fabrication of biofunctional patterns. Efforts have been put towards increasing the patterning capabilities, in terms of parallel production with the fabrication of multiprobe arrays, and the increase of ink reservoir either by the implementation of nanochannels in the AFM cantilever or by modification of the tip surface. One of the strengths of the technique in comparison with the approaches based on micro- or nanomolding in general is that any pattern-shape can be fabricated in situ which is optimal for prototyping purposes.

1.2.5 Nanopatterning techniques outlook

Currently, many nanopatterning techniques have proven to be useful for the fabrication of functional biomolecular assemblies on surfaces with controlled size and shape. However the bionanofabrication field in general remains fragmented, focusing primarily on individual processes. A compromise is usually made between the resolution, scalability, cost and availability. There are common major

challenges: (i) the controlled deposition of different biomolecular materials through controlled-reversible specific interactions in defined areas with nanometer precision; (ii) the integration and development of state-of-the-art characterization techniques, able to resolve functional activity and structural properties of the biological materials. For example the development of a combined atomic force fluorescent microscope[154] allows the characterization of the physical attributes such as height, width, friction and mechanical stress simultaneously with optical response. This optical response can be used to address functionality of the biomolecules by monitoring molecular recognition through dye labeled molecules, spectral characteristics of fluorescent molecules, etc. Finally (iii) the integration among the fabrication steps that operates at different length scales ranging from the molecular to the macromolecular world remains a challenge.

1.3 Combined Atomic Force Fluorescence Microscope

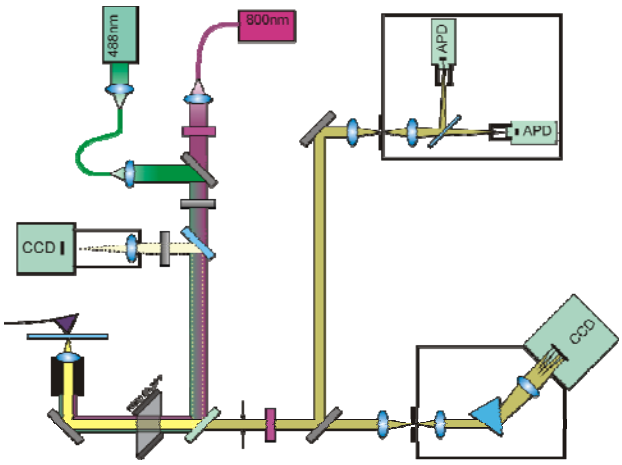

Figure 1.15. *Schematic of the AFFM. A laser diode with a wavelength of 1050 nm was installed in the AFM head in combination with a narrow band interference filter. This prevents undesired excitation of the chromophores and allows the effective suppression of this laser light in the detection path of the fluuorescence microscope. The layout of the confocal-fluorescence microscope shows the two excitations available: 488 nm and 800 nm and the two different detection paths for photon counting (APD) and spectral discrimination by a prism based spectrograph.*[154]

The integration of atomic force microscopy (AFM) and confocal fluorescence microscopy (CFM), Figure 1.15, combines the high resolution topographical

imaging of AFM with the reliable (bio)chemical identification capability of optical methods. The atomic force fluorescence microscope (AFFM) is capable of performing simultaneous optical and topographic measurements with single molecule sensitivity throughout the whole visible to near-infrared spectral region. The instrument is equipped with a spectrograph/CCD camera combination, enabling combined topographic and fluorescence spectral imaging, which significantly enhances discrimination of spectroscopically distinct objects. The modular design allows easy switching between different modes of operation such as tip-scanning, sample-scanning or mechanical manipulation, all of which are combined with synchronous optical detection.

1.4 Photosynthetic proteins from purple bacteria

Photosynthesis is a fundamental process in nature in which solar energy is converted into chemical energy for living organisms. Photosynthesis occurs in plants, algae and some species of bacteria. Although a large variety of photosynthetic organisms exist, which can be distinguished by their typical light harvesting antennas and electron transport system, they all have in common basic principles of energy transport. Solar energy is collected by the photosynthetic antenna-protein complexes which are formed by pigment molecules (carotenoids and chlorophylls in plants and bacteriochlorophylls in bacteria). The pigment molecules are non-covalently bound to the protein matrix. After the solar energy is collected by the antennas, the excitation is transferred to the photosynthetic reaction center (RC) where charge separation occurs.[162] For example, the photosynthetic systems of purple bacteria are organized in several peripheral antenna complexes (LH2) surrounding the core antennae (LH1), each of which encloses a reaction center. Together they form a photosynthetic unit (PSU). The photosynthetic units are interconnected in larger domains, where excitation transfer can take place.

Images at submolecular resolution of native membranes have shed light on the architecture of the photosynthetic apparatus in different photosynthetic bacteria, i.e., *Blastochloris (Blc.) viridis*,[163] *Rhodospirillum (Rsp.) photometricum*,[164-165] *Rhodobacter (Rb.) sphaeroides* [166-167] and *Rb.blasticus*.[168] Frese *et al*[169] provided detailed information about long-range organization mechanisms of photosynthetic pigment-protein complexes in the photosynthetic purple bacteria. Other highly

ordered arrangements of photosynthetic systems, as revealed by negative-stain-aided electron microscopy, have also been reported.[170-171] For photosynthesis to remain efficient, the composition of the photosynthetic apparatus varies under different light conditions. In many purple photosynthetic bacteria, this chromatic adaptation involves modulation of the quantity of peripheral and core light-harvesting (LH) complexes and, in some species, involves the expression of LH complexes with modified absorption.[172] The emerging understanding of the organization mechanisms of the LH complexes gradually opens the field to their application to directed ensemble formation of photoactive complexes in vitro.

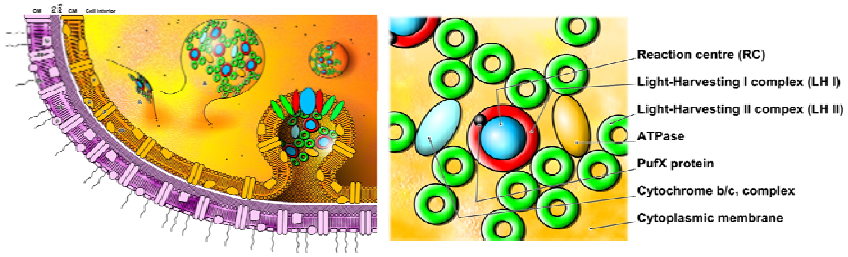

Figure 1.16. *A model of the intracytoplasmic membranes of Rb. Sphaeroides. The model shows fully formed invaginations and sites of initiation of membrane growth. Blue represents RCs, LH1 complexes are in red and LH2 complexes are in green. Reproduced from* [175].

Rb. sphaeroides has been an invaluable model and the object of many studies for diverse aspects of biophysics, biochemistry and molecular biology. Such studies span a wide range of topics, including bacteriochlorophyll (Bchl) biosynthesis, membrane assembly, secondary electron transfer, molecular genetics, reaction center structure and photochemistry and light harvesting structure, mutagenesis and spectroscopy.[173] *Rb. sphaeroides* contains three main complexes: the reaction centre (RC), which is the site of primary photochemistry, and the light-harvesting (LH) antenna complexes LH1 and LH2, which capture light energy and funnel excitation energy towards the RC. These complexes together form the PSU and are localised within the highly invaginated intracytoplasmic membrane (ICM) (Figure 1.16). LH2, the peripheral light-harvesting complex, is present in variable amounts according to the incident light intensity. In contrast, the core light-harvesting complex, LH1, is present in a fixed stoichiometry to the RC.[174] In *Rb. sphaeroides* the light-harvesting complexes are usually referred to by their in vivo absorption maxima, B875 (LH1) and B800-850 (LH2).

1.4.1 The antennas

As discussed above, *Rb. sphaeroides* contains a light-harvesting system composed of two antenna complexes, LH1 and LH2. Other photosynthetic bacteria differ in their light-harvesting composition; for example, *Rs. rubrum* and *Rps. viridis* possess a single core antenna complex.[176] In *Rps. acidophila* however, there exists a third type of light-harvesting complex, LH3, which has absorbance peaks at 800 and 820 nm.[177]

The antenna complexes of all purple bacteria studied to date contain two small hydrophobic polypeptides which are known as α and β, which occur in a 1:1 ratio and consist of 50-60 amino acids that contain a single membrane-spanning helix.[178] The function of these proteins is to determine the position, orientation and environment for the light-harvesting pigments, which are Bchl*a* and carotenoids. The carotenoids are found in abundance in photosynthetic organisms and have two major functions in photosynthesis. First, as accessory light-harvesting pigments, they absorb light energy in the 450-600 nm range, and transfer it to neighboring Bchl molecules, thereby increasing the spectral range over which light energy can be absorbed beyond the limitations of Bchl absorption. Second, as photoprotective agents, carotenoids play a vital role in preventing photooxidative damage[179-180]since they can quench singlet oxygen directly, or they quench the triplet excited Bchl (^{3}Bchl*a**) sensitizer, preventing the production of singlet oxygen.[181]

1.4.1.1 The peripheral light-harvesting LH2 complex

The LH2 complex has two absorbance maxima, arising from Bchls which absorb maximally at 800 nm and 850 nm; therefore they are known as B800 and B850 respectively.[182] Each αβ-heterodimer in LH2 is non-covalently associated with three molecules of Bchl, two of which absorb at 850 nm and a third at 800 nm. The structures of LH2 from *Rps. acidophila* (Figure 1.17) and *Rhodovulum sulfidophilum* were determined by X-ray crystallography[183] and electron microscopy[184] to be nonamers of the αβ-heterodimers. A more refined structure of *Rps. acidophila* LH2 at 2.0 Å is available.[185] The atomic resolution images show that the *Rps. acidophila* LH2 complex consists of a ring of nine αβ-heterodimers, forming a hollow cylinder that spans the membrane. The B850 Bchls form an

eighteen-member ring of overlapping molecules coordinated to alternate α- and β-polypeptides by a histidine ligand. These Bchls are positioned vertically with respect to the membrane plane and are situated toward the periplasmic face of the membrane. In contrast, the nine-member ring of B800 Bchls are relatively well separated, and positioned between the helices of the β-polypeptides in the outer ring. They lie toward the cytoplasmic face of the membrane and are almost parallel to it. The nine membrane-spanning carotenoids are not associated with the polypeptides but are in close contact with both the B800 and B850 Bchls.[186] A second ring of carotenoids is present, the heads of which are located below the B850 Bchls.

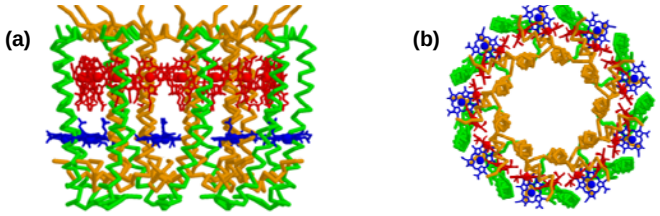

Figure 1.17. *The structure of the Rps. acidophila LH2 complex. (a) shows a side-view of the complex, the concentric rings of polypeptides and Bchls can be seen. The α-polypeptides (brown), β-polypeptides (green), B800 (blue) and B850 (red). (b) shows the projection view of the same structure. From this angle the circular shape of the complex can be observed. From reference* [183].

1.4.1.2 The core LH1 complex

The LH1 core antenna has a single absorbance maximum at 875 nm, imparted by the two B875 Bchls non-covalently associated to each αβ-heterodimer.[187] Several models exist based on LH2 structures and LH1 projection maps which show that the LH1 complex is similar in architecture to LH2, although it is twice as large in ring diameter, 12 nm vs. 6 nm.[188] The ring hole size is sufficient (8 nm) to accommodate one RC. Two-dimensional crystal from *R. rubrum* RC-LH1 were analyzed by electron cryomicroscopy, and the projection maps (8.5 Å) revealed that it the LH1 unit is composed of 16 αβ-heterodimers surrounding a single RC.[189]

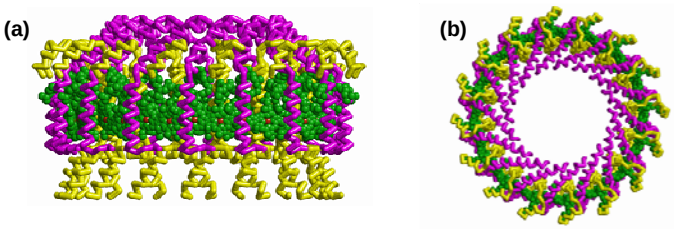

Figure 1.18. *Model of LH1 from Rb. sphaeroides. (a) shows a side view in which model α-polypeptides are shown in yellow, β-polypeptides (magenta), Bchl molecules (green) with the central magnesium atom (red). (b) shows a projection view of the same model. The N-terminal helix of LH1 β-polypeptide is directed towards the RC and is predicted to make contact with the RC-H subunit* [190].

1.4.1.3 The reaction centre

The RC from *Rb. sphaeroides* contains three protein subunits (Figure 1.19) known as L (light), M (medium) and H (heavy).[191] The L and M subunits are homologous and are related by a pseudo-twofold circular symmetry. Multiple pigment molecules (cofactors) are bound to the L and M subunits and are arranged accordingly in two symmetric branches, commonly referred to as A branch and B branch: two Bchls which form a strongly interacting dimer and are known as the "special pair" (P_A, P_B), two accessory Bchls in close proximity to the "special pair" (B_A, B_B), two bacteriopheophytins (H_A, H_B) and a pair of quinones (Q_A, Q_B).[192-193] Only the branch more closely associated with L-subunit is used in the light-driven electron transfer process and is accordingly termed the "active" branch.[194] There is a carotenoid molecule that disrupts the two-fold symmetry of the complex and is within van der Waals contact with the accessory Bchl of the inactive branch. The H-subunit has a single membrane spanning polypeptide, the majority of the protein is forming a globular region at the cytoplasmic surface of the membrane. The RC-LH1 together are known as the core complex.

Figure 1.19*. The three-dimensional structure of the photosynthetic RC from Rhodobacter Sphaeroides, (front view) shows the protein subunits L, M, H of the RC in light blue, green and dark blue respectively. The chromophores are shown in the center. Figure from* [195].

1.4.2 Biomimicry with Photosynthetic Proteins

The purified components of the PSU are interesting candidates for applications in synthetic light converting circuits due to their well defined optical properties, such as a broad spectral range, high absorption cross section, efficient energy transfer[8] and high photo-stability. Although these biomolecules are membrane proteins and their functional activity is strongly dependent on the surrounding lipid environment, recent research has focused on extracting them from their native environment in order to integrate them in different substrates. This allows one to investigate its single molecule and collective behavior and potential applications in hybrid functional materials.

1.5 Thesis overview

The preceding sections gave a broad overview of state-of-the-art nanofabrication techniques with specific examples in the fabrication of functional nanostructures with biomolecules. Different interactions between the surfaces and target molecules were also introduced. In this thesis we seek to create bionanoassemblies in order to explore the unique energy transfer properties of light harvesting complexes by producing biomolecular photonic wires. We seek answers to the following questions: Can purified components of the photosynthetic system be assembled on different surfaces while retaining their optical properties? Can structures of light harvesting complexes with controlled size and shape be fabricated? Can we achieve assemblies of closely packed LHC that enable energy migration? How does energy

migration in fabricated arrays of light harvesting complexes compare to the natural arrays in photosynthetic membranes?

In the following chapters we use diverse nanofabrication techniques in order to direct the assembly on micro- and nanostructured surfaces of purified units from the photosynthetic purple bacteria. Other biological systems used were visible fluorescent proteins and α-synuclein, an intrinsically unfolded protein associated with Parkinson's disease. In order to characterize the biological assemblies on the surfaces AFM imaging in combination with optical imaging (spectral fluorescence microscopy and lifetime measurements) were performed in liquid conditions.

In Chapter 2 NIL is used to create chemical patterns of several millimeters in length and widths in the micro- and submicrometer scale to direct the assembly of LH2 complexes through electrostatic interactions. Influence of the patterning procedure on the optical response of the complexes is discussed. In Chapter 3, high resolution LH2 complexes arrays of sub-100 nm width are fabricated by the combination of host-guest interaction and NIL. The use of host-guest interactions provide the advantage of using an interaction which is in principle tunable and reversible, and provided that the target molecules, in this case LH2 complexes have appropriate binding sites engineered in strategic positions, the protein complexes could be adsorbed in an oriented fashion on a surface. Chapter 4 discusses spatial energy migration experiments on the engineered arrays of LH2 complexes. Chapter 5 makes use of printing techniques for the fabrication of biological structures that exhibit fluorescent resonance energy transfer (FRET) in the lateral and axial directions. For this purpose we used the visible fluorescent proteins EGFP and DsRed-FT as donor and acceptor molecules respectively.

In Chapter 6 we describe the fabrication of 2D and 3D structures of the core complex dimers LH1-RC. We use fluorescence microscopy to investigate the spectral response of the confined structures. In Chapter 7 we create micro- and nanometer patterns of LH1 and LH2 complexes on different substrates (SiO_2, flat gold, gold-nanoparticles and CaF_2) prepared either by μCP or NIL in combination with self-assembly techniques. Fluorescence microscopy, Raman spectroscopy (RM) and Surface-enhanced Raman spectroscopy (SERS) were used as characterization methods.

Chapter 8 suggests future directions and preliminary experiments for the fabrication of mixed protein complexes arrays. Also α-synuclein super-fibrils are assembled on patterned substrates fabricated by NIL. Fluorescence microscopy and Raman spectroscopy reveals the formation of β-sheets on the super-fibril structures. Potential experiments are suggested that will help to discover properties of controlled assemblies of LH complexes onto nanostructures surfaces. Further developments to manipulate optical properties of the LH complexes on artificial assemblies are also briefly introduced.

1.6 REFERENCES

1. Lodish, H.; Baltimore, D.; Berk, A.; Zipursky, S. L.; Matsudaira, P.; Darnell, J., *Molecular Cell Biology*. American Scientific Books, Inc: New York, 1995.
2. Alarie, J. P.; Sepaniak, M. J.; Vodinh, T., Evaluation of Antibody Immobilization Techniques for Fiber Optic-Based Fluoroimmunosensing. *Analytica Chimica Acta* **1990,** 229, (2), 169-176.
3. Borrebaeck, C. A. K., Antibodies in diagnostics - from immunoassays to protein chips. *Immunology Today* **2000,** 21, (8), 379-382.
4. Lueking, A.; Cahill, D. J.; Mullner, S., Protein biochips: a new and versatile platform technology for molecular medicine. *Drug Discovery Today* **2005,** 10, (11), 789-794.
5. Philp, D.; Stoddart, J. F., Self-assembly in natural and unnatural systems. *Angewandte Chemie-International Edition* **1996,** 35, (11), 1155-1196.
6. Hermanson, G. T., *Bioconjugated Techniques*. Academic Press: San Diego, CA, 1996.
7. Rusmini, F.; Zhong, Z. Y.; Feijen, J., Protein immobilization strategies for protein biochips. *Biomacromolecules* **2007,** 8, (6), 1775-1789.
8. Patel, N.; Davies, M. C.; Hartshorne, M.; Heaton, R. J.; Roberts, C. J.; Tendler, S. J. B.; Williams, P. M., Immobilization of protein molecules onto homogeneous and mixed carboxylate-terminated self-assembled monolayers. *Langmuir* **1997,** 13, (24), 6485-6490.
9. Rao, S. V.; Anderson, K. W.; Bachas, L. G., Controlled layer-by-layer immobilization of horseradish peroxidase. *Biotechnology And Bioengineering* **1999,** 65, (4), 389-396.
10. Fernandezlafuente, R.; Rosell, C. M.; Rodriguez, V.; Santana, C.; Soler, G.; Bastida, A.; Guisan, J. M., Preparation Of Activated Supports Containing Low Pk Amino-Groups - A New Tool For Protein Immobilization Via The Carboxyl Coupling Method. *Enzyme And Microbial Technology* **1993,** 15, (7), 546-550.
11. Jongsma, M. A.; Litjens, R., Self-assembling protein arrays on DNA chips by auto-labeling fusion proteins with a single DNA address. *Proteomics* **2006,** 6, (9), 2650-2655.
12. Mateo, C.; Abian, O.; Fernandez-Lorente, G.; Pedroche, J.; Fernandez-Lafuente, R.; Guisan, J. M., Epoxy sepabeads: A novel epoxy support for stabilization of industrial enzymes via very intense multipoint covalent attachment. *Biotechnology Progress* **2002,** 18, (3), 629-634.
13. Grazu, V.; Abian, O.; Mateo, C.; Batista-Viera, F.; Fernandez-Lafuente, R.; Guisan, J. M., Novel bifunctional epoxy/thiol-reactive support to immobilize thiol containing proteins by the epoxy chemistry. *Biomacromolecules* **2003,** 4, (6), 1495-1501.
14. Fleming, S. A., Chemical Reagents In Photoaffinity-Labeling. *Tetrahedron* **1995,** 51, (46), 12479-12520.

15. Nguyen, G. H.; Milea, J. S.; Rai, A.; Smith, C. L., Mild conditions for releasing mono and bis-biotinylated macromolecules from immobilized streptavidin. *Biomolecular Engineering* **2005,** 22, (4), 147-150.
16. Smith, C. L.; Milea, J. S.; Nguyen, G. H., Immobilization of nucleic acids using biotin-strept(avidin) systems. In *Immobilisation Of Dna On Chips Ii*, 2005; Vol. 261, pp 63-90.
17. Tinazli, A.; Tang, J. L.; Valiokas, R.; Picuric, S.; Lata, S.; Piehler, J.; Liedberg, B.; Tampe, R., High-affinity chelator thiols for switchable and oriented immobilization of histidine-tagged proteins: A generic platform for protein chip technologies. *Chemistry-a European Journal* **2005,** 11, (18), 5249-5259.
18. Maury, P.; Escalante, M.; Peter, M.; Reinhoudt, D. N.; Subramaniam, V.; Huskens, J., Creating nanopatterns of his-tagged proteins on surfaces by nanoimprint lithography using specific NiNTA-Histidine interactions. *Small* **2007,** 3, (9), 1584-1592.
19. Reynolds, N. P.; Tucker, J. D.; Davison, P. A.; Timney, J. A.; Hunter, C. N.; Leggett, G. J., Site-specific immobilization and micrometer and nanometer scale photopatterning of yellow fluorescent protein on glass surfaces. *Journal of the American Chemical Society* **2009,** 131, (3), 896-897.
20. Aravinda, C. L.; Cosnier, S.; Chen, W.; Myung, N. V.; Mulchandani, A., Label-free detection of cupric ions and histidine-tagged proteins using single poly(pyrrole)-NTA chelator conducting polymer nanotube chemiresistive sensor. *Biosensors and Bioelectronics* **2009,** 24, (5), 1451-1455.
21. Kim, K. H.; Kim, J. D.; Kim, Y. J.; Kang, S. H.; Jung, S. Y.; Jung, H., Protein immobilization without purification via dip-pen nanolithography. *Small* **2008,** 4, (8), 1089-1094.
22. Klenkar, G.; Valiokas, R.; Lundström, I.; Tinazli, A.; Tampé, R.; Piehler, J.; Liedberg, B., Piezo dispensed microarray of multivalent chelating thiols for dissecting complex protein-protein interactions. *Analytical Chemistry* **2006,** 78, (11), 3643-3650.
23. Schweitzer, B.; Wiltshire, S.; Lambert, J.; O'Malley, S.; Kukanskis, K.; Zhu, Z. R.; Kingsmore, S. F.; Lizardi, P. M.; Ward, D. C., Immunoassays with rolling circle DNA amplification: A versatile platform for ultrasensitive antigen detection. *Proceedings Of The National Academy Of Sciences Of The United States Of America* **2000,** 97, (18), 10113-10119.
24. Mammen, M.; Choi, S. K.; Whitesides, G. M., Polyvalent interactions in biological systems: Implications for design and use of multivalent ligands and inhibitors. *Angewandte Chemie - International Edition* **1998,** 37, (20), 2755-2794.
25. Ludden, M. L. W.; Mulder, A.; Schulze, K.; Subramaniam, V.; Tampe, R.; Huskens, J., Anchoring of histidine-tagged proteins to molecular printboards: Self-assembly, thermodynamic modeling, and patterning. *Chemistry-a European Journal* **2008,** 14, (7), 2044-2051.
26. Turchanin, A.; Tinazli, A.; El-Desawy, M.; Grossann, H.; Schnietz, M.; Solak, H. H.; Tampe, R.; Golzhauser, A., Molecular self-assembly, chemical lithography, and biochemical tweezers: A path for the fabrication of functional nanometer-scale protein arrays. *Advanced Materials* **2008,** 20, (3), 471-+.
27. Dankers, P. Y. W.; Harmsen, M. C.; Brouwer, L. A.; Van Luyn, M. J. A.; Meijer, E. W., A modular and supramolecular approach to bioactive scaffolds for tissue engineering. *Nature Materials* **2005,** 4, (7), 568.
28. Zhang, L.; Wu, Y.; Brunsveld, L., A synthetic supramolecular construct modulating protein assembly in cells. *Angewandte Chemie - International Edition* **2007,** 46, (11), 1798.
29. Martos, V.; Castreño, P.; Valero, J.; de Mendoza, J., Binding to protein surfaces by supramolecular multivalent scaffolds. *Current Opinion in Chemical Biology* **2008,** 12, (6), 698.
30. Glick, G. D.; Toogood, P. L.; Wiley, D. C.; Skehel, J. J.; Knowles, J. R., Ligand recognition by influenza virus: The binding of bivalent sialosides. *Journal of Biological Chemistry* **1991,** 266, (35), 23660-23669.

31. Huskens, J., Multivalent interactions at interfaces. *Current Opinion in Chemical Biology* **2006,** 10, (6), 537-543.
32. Jonkheijm, P.; Weinrich, D.; Schroder, H.; Niemeyer, C. M.; Waldmann, H., Chemical Strategies for Generating Protein Biochips. *Angewandte Chemie-International Edition* **2008,** 47, (50), 9618-9647.
33. Caelen, I.; Gao, H.; Sigrist, H., Protein density gradients on surfaces. *Langmuir* **2002,** 18, (7), 2463-2467.
34. Brusatori, M. A.; Tie, Y.; Van Tassel, P. R., Protein adsorption kinetics under an applied electric field: An optical waveguide lightmode spectroscopy study. *Langmuir* **2003,** 19, (12), 5089-5097.
35. Ekblad, T.; Andersson, O.; Tai, F. I.; Ederth, T.; Liedberg, B., Lateral Control of Protein Adsorption on Charged Polymer Gradients. *Langmuir* **2009,** 25, (6), 3755-3762.
36. Love, J. C.; Estroff, L. A.; Kriebel, J. K.; Nuzzo, R. G.; Whitesides, G. M., Self-assembled monolayers of thiolates on metals as a form of nanotechnology. *Chemical Reviews* **2005,** 105, (4), 1103-1169.
37. Rusin, K. M.; Fare, T. L.; Stemple, J. Z., Immobilization Of Flavoproteins On Silicon - Effect Of Cross-Linker Chain-Length On Enzyme-Activity. *Biosensors & Bioelectronics* **1992,** 7, (5), 367-373.
38. http://www.piercenet.com/products
39. Ponten, J.; Stolt, L., Proliferation Control In Cloned Normal And Malignant Human-Cells. *Experimental Cell Research* **1980,** 129, (2), 367-375.
40. Bernard, A.; Renault, J. P.; Michel, B.; Bosshard, H. R.; Delamarche, E., Microcontact printing of proteins. *Advanced Materials* **2000,** 12, (14), 1067-1070.
41. Carter, S. B., Principles Of Cell Motility - Direction Of Cell Movement And Cancer Invasion. *Nature* **1965,** 208, (5016), 1183-&.
42. Nath, N.; Hyun, J.; Ma, H.; Chilkoti, A., Surface engineering strategies for control of protein and cell interactions. *Surface Science* **2004,** 570, (1-2), 98-110.
43. Ostuni, E.; Chapman, R. G.; Holmlin, R. E.; Takayama, S.; Whitesides, G. M., A survey of structure-property relationships of surfaces that resist the adsorption of protein. *Langmuir* **2001,** 17, (18), 5605-5620.
44. Luk, Y. Y.; Kato, M.; Mrksich, M., Self-assembled monolayers of alkanethiolates presenting mannitol groups are inert to protein adsorption and cell attachment. *Langmuir* **2000,** 16, (24), 9604-9608.
45. Ko, K. S.; Jaipuri, F. A.; Pohl, N. L., Fluorous-based carbohydrate microarrays. *Journal Of The American Chemical Society* **2005,** 127, (38), 13162-13163.
46. Vargo, T. G.; Bekos, E. J.; Kim, Y. S.; Ranieri, J. P.; Bellamkonda, R.; Aebischer, P.; Margevich, D. E.; Thompson, P. M.; Bright, F. V.; Gardella, J. A., Synthesis And Characterization Of Fluoropolymeric Substrata With Immobilized Minimal Peptide Sequences For Cell-Adhesion Studies .1. *Journal Of Biomedical Materials Research* **1995,** 29, (6), 767-778.
47. Sugawara, T.; Matsuda, T., Photochemical Surface Derivatization Of A Peptide-Containing Arg-Gly-Asp (Rgd). *Journal Of Biomedical Materials Research* **1995,** 29, (9), 1047-1052.
48. Hoffmann, J.; Groll, J.; Heuts, J.; Rong, H. T.; Klee, D.; Ziemer, G.; Moeller, M.; Wendel, H. P., Blood cell and plasma protein repellent properties of Star-PEG-modified surfaces. *Journal Of Biomaterials Science-Polymer Edition* **2006,** 17, (9), 985-996.
49. Mrksich, M.; Sigal, G. B.; Whitesides, G. M., Surface-Plasmon Resonance Permits in-Situ Measurement of Protein Adsorption on Self-Assembled Monolayers of Alkanethiolates on Gold. *Langmuir* **1995,** 11, (11), 4383-4385.
50. Prime, K. L.; Whitesides, G. M., Self-Assembled Organic Monolayers - Model Systems for Studying Adsorption of Proteins at Surfaces. *Science* **1991,** 252, (5009), 1164-1167.
51. Rogers, J.; Nuzzo, R., Recent progress in soft lithography. *Materials Today* **2005**, 50-56.

52. Lee, J. N.; Park, C.; Whitesides, G. M., Solvent compatibility of poly(dimethylsiloxane)-based microfluidic devices. *Analytical Chemistry* **2003,** 75, (23), 6544-6554.
53. Dow Corning www.dowcorning.com/.
54. Gelest www.gelest.com.
55. Lee, J. H.; Kim, H. E.; Im, J. H.; Bae, Y. M.; Choi, J. S.; Huh, K. M.; Lee, C. S., Preparation of orthogonally functionalized surface using micromolding in capillaries technique for the control of cellular adhesion. *Colloids and Surfaces B: Biointerfaces* **2008,** 64, (1), 126-134.
56. Shim, H. W.; Lee, J. H.; Hwang, T. S.; Rhee, Y. W.; Bae, Y. M.; Choi, J. S.; Han, J.; Lee, C. S., Patterning of proteins and cells on functionalized surfaces prepared by polyelectrolyte multilayers and micromolding in capillaries. *Biosensors and Bioelectronics* **2007,** 22, (12), 3188-3195.
57. Bernard, A.; Delamarche, E.; Schmid, H.; Michel, B.; Bosshard, H. R.; Biebuyck, H., Printing patterns of proteins. *Langmuir* **1998,** 14, (9), 2225-2229.
58. Hyun, J.; Ahn, S. J.; Lee, W. K.; Chilkoti, A.; Zauscher, S., Molecular recognition-mediated fabrication of protein nanostructures by dip-pen lithography. *Nano Letters* **2002,** 2, (11), 1203-1207.
59. Yang, Z. P.; Chilkoti, A., Microstamping of a biological ligand onto an activated polymer surface. *Advanced Materials* **2000,** 12, (6), 413-+.
60. Gates, B. D.; Xu, Q. B.; Stewart, M.; Ryan, D.; Willson, C. G.; Whitesides, G. M., New approaches to nanofabrication: Molding, printing, and other techniques. *Chemical Reviews* **2005,** 105, (4), 1171-1196.
61. Ferguson, G. S.; Chaudhury, M. K.; Biebuyck, H. A.; Whitesides, G. M., Monolayers on Disordered Substrates - Self-Assembly of Alkyltrichlorosilanes on Surface-Modified Polyethylene and Poly(Dimethylsiloxane). *Macromolecules* **1993,** 26, (22), 5870-5875.
62. Bietsch, A.; Michel, B., Conformal contact and pattern stability of stamps used for soft lithography. *Journal of Applied Physics* **2000,** 88, (7), 4310-4318.
63. Delamarche, E.; Schmid, H.; Michel, B.; Biebuyck, H., Stability of molded polydimethylsiloxane microstructures. *Advanced Materials* **1997,** 9, (9), 741-746.
64. Hui, C. Y.; Jagota, A.; Lin, Y. Y.; Kramer, E. J., Constraints on microcontact printing imposed by stamp deformation. *Langmuir* **2002,** 18, (4), 1394-1407.
65. Sharp, K. G.; Blackman, G. S.; Glassmaker, N. J.; Jagota, A.; Hui, C. Y., Effect of stamp deformation on the quality of microcontact printing: Theory and experiment. *Langmuir* **2004,** 20, (15), 6430-6438.
66. Sotomayor Torres, C. M., Alternative Lithography: Unleashing the Potentials of Nanotechnology. **2003**.
67. Roca-Cusachs, P.; Rico, F.; Martinez, E.; Toset, J.; Farre, R.; Navajas, D., Stability of microfabricated high aspect ratio structures in poly(dimethylsiloxane). *Langmuir* **2005,** 21, (12), 5542-5548.
68. Fichet, G.; Stutzmann, N.; Muir, B. V. O.; Huck, W. T. S., Microembossing of elastomeric triblock copolymers. *Advanced Materials* **2002,** 14, (1), 47-51.
69. Tsibouklis, J.; Nevell, T. G., Ultra-low surface energy polymers: The molecular design requirements. *Advanced Materials* **2003,** 15, (7-8), 647-650.
70. James, C. D.; Davis, R. C.; Kam, L.; Craighead, H. G.; Isaacson, M.; Turner, J. N.; Shain, W., Patterned protein layers on solid substrates by thin stamp microcontact printing. *Langmuir* **1998,** 14, (4), 741-744.
71. Csucs, G.; Kunzler, T.; Feldman, K.; Robin, F.; Spencer, N. D., Microcontact printing of macromolecules with submicrometer resolution by means of polyolefin stamps. *Langmuir* **2003,** 19, (15), 6104-6109.
72. Trimbach, D. C.; Stapert, H.; Van Orselen, J.; Jandt, K. D.; Bastioansen, C. W. M.; Broer, D. J., Improved microcontact printing of proteins using hydrophilic thermoplastic elastomers as stamp materials. *Advanced Engineering Materials* **2007,** 9, (12), 1123-1128.

73. Martin, B. D.; Brandow, S. L.; Dressick, W. J.; Schull, T. L., Fabrication and application of hydrogel stampers for physisorptive microcontact printing. *Langmuir* **2000,** 16, (25), 9944-9946.
74. Lee, N. Y.; Lim, J. R.; Lee, M. J.; Kim, J. B.; Jo, S. J.; Baik, H. K.; Kim, Y. S., Hydrophilic composite elastomeric mold for high-resolution soft lithography. *Langmuir* **2006,** 22, (21), 9018-9022.
75. Cheng, Q.; Li, S.; Komvopoulos, K., Plasma-assisted surface chemical patterning for single-cell culture. *Biomaterials* **2009,** 30, (25), 4203-4210.
76. Hook, A. L.; Voelcker, N. H.; Thissen, H., Patterned and switchable surfaces for biomolecular manipulation. *Acta Biomaterialia* **2009,** 5, (7), 2350-2370.
77. Jenik, M.; Seifner, A.; Krassnig, S.; Seidler, K.; Lieberzeit, P. A.; Dickert, F. L.; Jungbauer, C., Sensors for bioanalytes by imprinting-Polymers mimicking both biological receptors and the corresponding bioparticles. *Biosensors and Bioelectronics* **2009,** 25, (1), 9-14.
78. Rozkiewicz, D. I.; Kraan, Y.; Werten, M. W. T.; de Wolf, F. A.; Subramaniam, V.; Ravoo, B. J.; Reinhoudt, D. N., Covalent microcontact printing of proteins for cell patterning. *Chemistry-a European Journal* **2006,** 12, (24), 6290-6297.
79. Rozkiewicz, D. I.; Ravoo, B. J.; Reinhoudt, D. N., Reversible covalent patterning of self-assembled monolayers on gold and silicon oxide surfaces. *Langmuir* **2005,** 21, (14), 6337-6343.
80. Perl, A.; Reinhoudt, D. N.; Huskens, J., Microcontact printing: Limitations and achievements. *Advanced Materials* **2009,** 21, (22), 2257.
81. Rozkiewicz, D. I.; Brugman, W.; Kerkhoven, R. M.; Ravoo, B. J.; Reinhoudt, D. N., Dendrimer-mediated transfer printing of DNA and RNA microarrays. *Journal of the American Chemical Society* **2007,** 129, (37), 11593-11599.
82. Foley, J.; Schmid, H.; Stutz, R.; Delamarche, E., Microcontact printing of proteins inside microstructures. *Langmuir* **2005,** 21, (24), 11296-11303.
83. Juncker, D.; Schmid, H.; Bernard, A.; Caelen, I.; Michel, B.; de Rooij, N.; Delamarche, E., Soft and rigid two-level microfluidic networks for patterning surfaces. *Journal of Micromechanics and Microengineering* **2001,** 11, (5), 532-541.
84. Balmer, T. E.; Schmid, H.; Stutz, R.; Delamarche, E.; Michel, B.; Spencer, N. D.; Wolf, H., Diffusion of alkanethiols in PDMS and its implications on microcontact printing (mu CP). *Langmuir* **2005,** 21, (2), 622-632.
85. Coyer, S. R.; Garcia, A. J.; Delamarche, E., Facile preparation of complex protein architectures with sub-100-nm resolution on surfaces. *Angewandte Chemie-International Edition* **2007,** 46, (36), 6837-6840.
86. Lalo, H.; Cau, J. C.; Thibault, C.; Marsaud, N.; Severac, C.; Vieu, C., Microscale multiple biomolecules printing in one step using a PDMS macrostamp. *Microelectronic Engineering* **2009,** 86, (4-6), 1428-1430.
87. Xu, H.; Ling, X. Y.; van Bennekom, J.; Duan, X.; Ludden, M. J. W.; Reinhoudt, D. N.; Wessling, M.; Lammertink, R. G. H.; Huskens, J., Microcontact Printing of Dendrimers, Proteins, and Nanoparticles by Porous Stamps. *Journal of the American Chemical Society* **2009,** 131, (2), 797-803.
88. Renault, J. P.; Bernard, A.; Juncker, D.; Michel, B.; Bosshard, H. R.; Delamarche, E., Fabricating microarrays of functional proteins using affinity contact printing. *Angewandte Chemie-International Edition* **2002,** 41, (13), 2320-2323.
89. Yu, A. A.; Savas, T.; Cabrini, S.; diFabrizio, E.; Smith, H. I.; Stellacci, F., High resolution printing of DNA feature on poly(methyl methacrylate) substrates using supramolecular nano-stamping. *Journal of the American Chemical Society* **2005,** 127, (48), 16774-16775.
90. Chou, S. Y.; Krauss, P. R.; Renstrom, P. J., Imprint of Sub-25 Nm Vias and Trenches in Polymers. *Applied Physics Letters* **1995,** 67, (21), 3114-3116.

91. Haisma, J.; Verheijen, M.; vandenHeuvel, K.; vandenBerg, J., Mold-assisted nanolithography: A process for reliable pattern replication. *Journal of Vacuum Science & Technology B* **1996,** 14, (6), 4124-4128.
92. International Technology Roadmap for Semiconductors (ITRS) 2006.
93. Truskett, V. N.; Watts, M. P. C., Trends in imprint lithography for biological applications. *Trends in Biotechnology* **2006,** 24, (7), 312-317.
94. Bruinink, C. M.; Peter, M.; Maury, P. A.; De Boer, M.; Kuipers, L.; Huskens, J.; Reinhoudt, D. N., Capillary force lithography: Fabrication of functional polymer templates as versatile tools for nanolithography. *Advanced Functional Materials* **2006,** 16, (12), 1555-1565.
95. Park, S.; Schift, H.; Solak, H. H.; Gobrecht, J., Stamps for nanoimprint lithography by extreme ultraviolet interference lithography. *Journal of Vacuum Science & Technology B* **2004,** 22, (6), 3246-3250.
96. Zhao, Y.; Berenschot, E.; de Boer, M.; Jansen, H.; Tas, N.; Huskens, J.; Elwenspoek, M., Fabrication of a silicon oxide stamp by edge lithography reinforced with silicon nitride for nanoimprint lithography. *Journal of Micromechanics and Microengineering* **2008,** 18, (6), -.
97. Zhang, G. M.; Zhang, J.; Xie, G. Y.; Liu, Z. F.; Shao, H. B., Cicada wings: A stamp from nature for nanoimprint lithography. *Small* **2006,** 2, (12), 1440-1443.
98. Altun, A. O.; Jeong, J. H.; Rha, J. J.; Choi, D. G.; Kim, K. D.; Lee, E. S., Fabrication of fluorine-doped diamond-like carbon stamps for UV nanoimprint lithography. *Nanotechnology* **2006,** 17, (18), 4659-4663.
99. Barbero, D. R.; Saifullah, M. S. M.; Hoffmann, P.; Mathieu, H. J.; Anderson, D.; Jones, G. A. C.; Welland, M. E.; Steiner, U., High resolution nanoimprinting with a robust and reusable polymer mold. *Advanced Functional Materials* **2007,** 17, (14), 2419-2425.
100. Hirai, Y.; Yoshida, S.; Takagi, N.; Tanaka, Y.; Yabe, H.; Sasaki, K.; Sumitani, H.; Yamamoto, K., High aspect pattern fabrication by nano imprint lithography using fine diamond mold. *Japanese Journal of Applied Physics Part 1-Regular Papers Short Notes & Review Papers* **2003,** 42, (6B), 3863-3866.
101. Beck, M.; Graczyk, M.; Maximov, I.; Sarwe, E. L.; Ling, T. G. I.; Keil, M.; Montelius, L., Improving stamps for 10 nm level wafer scale nanoimprint lithography. *Microelectronic Engineering* **2002,** 61-2, 441-448.
102. Schift, H.; Saxer, S.; Park, S.; Padeste, C.; Pieles, U.; Gobrecht, J., Controlled co-evaporation of silanes for nanoimprint stamps. *Nanotechnology* **2005,** 16, (5), S171-S175.
103. Choi, P.; Fu, P. F.; Guo, L. J., Siloxane copolymers for nanoimprint lithography. *Advanced Functional Materials* **2007,** 17, (1), 65-70.
104. Schaper, C. D.; Miahnahri, A., Polyvinyl alcohol templates for low cost, high resolution, complex printing. *Journal of Vacuum Science & Technology B* **2004,** 22, (6), 3323-3326.
105. Li, M. T.; Chen, L.; Zhang, W.; Chou, S. Y., Pattern transfer fidelity of nanoimprint lithography on six-inch wafers. *Nanotechnology* **2003,** 14, (1), 33-36.
106. Chou, S. Y.; Krauss, P. R.; Zhang, W.; Guo, L. J.; Zhuang, L., Sub-10 nm imprint lithography and applications. *Journal of Vacuum Science & Technology B* **1997,** 15, (6), 2897-2904.
107. Cedeno, C. C.; Seekamp, J.; Kam, A. P.; Hoffmann, T.; Zankovych, S.; Torres, C. M. S.; Menozzi, C.; Cavallini, M.; Murgia, M.; Ruani, G.; Biscarini, F.; Behl, M.; Zentel, R.; Ahopelto, J., Nanoimprint lithography for organic electronics. *Microelectronic Engineering* **2002,** 61-2, 25-31.
108. Pisignano, D.; Persano, L.; Mele, E.; Visconti, P.; Anni, M.; Gigli, G.; Cingolani, R.; Favaretto, L.; Barbarella, G., First-order imprinted organic distributed feedback lasers. *Synthetic Metals* **2005,** 153, (1-3), 237-240.
109. Kao, P. C.; Chu, S. Y.; Chen, T. Y.; Zhan, C. Y.; Hong, F. C.; Chang, C. Y.; Hsu, L. C.; Liao, W. C.; Hon, M. H., Fabrication of large-scaled organic light emitting devices on

the flexible substrates using low-pressure imprinting lithography. *Ieee Transactions on Electron Devices* **2005,** 52, (8), 1722-1726.
110. Martin, J. I.; Nogues, J.; Liu, K.; Vicent, J. L.; Schuller, I. K., Ordered magnetic nanostructures: fabrication and properties. *Journal of Magnetism and Magnetic Materials* **2003,** 256, (1-3), 449-501.
111. Hu, Z. J.; Baralia, G.; Bayot, V.; Gohy, J. F.; Jonas, A. M., Nanoscale control of polymer crystallization by nanoimprint lithography. *Nano Letters* **2005,** 5, (9), 1738-1743.
112. Aryal, M.; Buyukserin, F.; Mielczarek, K.; Zhao, X. M.; Gao, J. M.; Zakhidov, A.; Hu, W. C., Imprinted large-scale high density polymer nanopillars for organic solar cells. *Journal of Vacuum Science & Technology B* **2008,** 26, (6), 2562-2566.
113. Cao, H.; Tegenfeldt, J. O.; Austin, R. H.; Chou, S. Y., Gradient nanostructures for interfacing microfluidics and nanofluidics. *Applied Physics Letters* **2002,** 81, (16), 3058-3060.
114. Guo, L. J.; Cheng, X.; Chou, C. F., Fabrication of size-controllable nanofluidic channels by nanoimprinting and its application for DNA stretching. *Nano Letters* **2004,** 4, (1), 69-73.
115. Fredin, N. J.; Broderick, A. H.; Buck, M. E.; Lynn, D. M., Nanoimprinted Thin Films of Reactive, Azlactone-Containing Polymers: Combining Methods for the Topographic Patterning of Cell Substrates with Opportunities for Facile Post-Fabrication Chemical Functionalization. *Biomacromolecules* **2009,** 10, (4), 994-1003.
116. Escalante, M.; Zhao, Y. P.; Ludden, M. J. W.; Vermeij, R.; Olsen, J. D.; Berenschot, E.; Hunter, C. N.; Huskens, J.; Subramaniam, V.; Otto, C., Nanometer arrays of functional light harvesting antenna complexes by nanoimprint lithography and host-guest interactions. *Journal of the American Chemical Society* **2008,** 130, (28), 8892-+.
117. Falconnet, D.; Pasqui, D.; Park, S.; Eckert, R.; Schift, H.; Gobrecht, J.; Barbucci, R.; Textor, M., A novel approach to produce protein nanopatterns by combining nanoimprint lithography and molecular self-assembly. *Nano Letters* **2004,** 4, (10), 1909-1914.
118. Hoff, J. D.; Cheng, L. J.; Meyhofer, E.; Guo, L. J.; Hunt, A. J., Nanoscale protein patterning by imprint lithography. *Nano Letters* **2004,** 4, (5), 853-857.
119. Heyderman, L. J.; Schift, H.; David, C.; Gobrecht, J.; Schweizer, T., Flow behaviour of thin polymer films used for hot embossing lithography. *Microelectronic Engineering* **2000,** 54, (3-4), 229-245.
120. Kumar, G.; Tang, H. X.; Schroers, J., Nanomoulding with amorphous metals. *Nature* **2009,** 457, (7231), 868-872.
121. del Campo, A.; Boos, D.; Spiess, H. W.; Jonas, U., Surface modification with orthogonal photosensitive silanes for sequential chemical lithography and site-selective particle deposition. *Angewandte Chemie-International Edition* **2005,** 44, (30), 4707-4712.
122. Chrisey, L. A.; OFerrall, C. E.; Spargo, B. J.; Dulcey, C. S.; Calvert, J. M., Fabrication of patterned DNA surfaces. *Nucleic Acids Research* **1996,** 24, (15), 3040-3047.
123. Dulcey, C. S.; Georger, J. H.; Krauthamer, V.; Stenger, D. A.; Fare, T. L.; Calvert, J. M., Deep Uv Photochemistry of Chemisorbed Monolayers - Patterned Coplanar Molecular Assemblies. *Science* **1991,** 252, (5005), 551-554.
124. Blawas, A. S.; Reichert, W. M., Protein patterning. *Biomaterials* **1998,** 19, (7-9), 595-609.
125. Jonas, U.; del Campo, A.; Kruger, C.; Glasser, G.; Boos, D., Colloidal assemblies on patterned silane layers. *Proceedings of the National Academy of Sciences of the United States of America* **2002,** 99, (8), 5034-5039.
126. Ryan, D.; Parviz, B. A.; Linder, V.; Semetey, V.; Sia, S. K.; Su, J.; Mrksich, M.; Whitesides, G. M., Patterning multiple aligned self-assembled monolayers using light. *Langmuir* **2004,** 20, (21), 9080-9088.
127. Synge, E. H., A suggested method for extending microscopic resolution into untra-microscopic region. *Philos. Mag.* **1928,** 6, 356.
128. Binnig, G.; Rohrer, H., Scanning Tunneling Microscopy. *Helvetica Physica Acta* **1982,** 55, (6), 726-735.

129. Binnig, G.; Rohrer, H.; Gerber, C.; Weibel, E., Tunneling through a Controllable Vacuum Gap. *Applied Physics Letters* **1982,** 40, (2), 178-180.
130. Betzig, E.; Trautman, J. K., Near-Field Optics - Microscopy, Spectroscopy, and Surface Modification Beyond the Diffraction Limit. *Science* **1992,** 257, (5067), 189-195.
131. Betzig, E.; Finn, P. L.; Weiner, J. S., Combined Shear Force and near-Field Scanning Optical Microscopy. *Applied Physics Letters* **1992,** 60, (20), 2484-2486.
132. Toledocrow, R.; Yang, P. C.; Chen, Y.; Vaeziravani, M., Near-Field Differential Scanning Optical Microscope with Atomic Force Regulation. *Applied Physics Letters* **1992,** 60, (24), 2957-2959.
133. Karrai, K.; Grober, R. D., Piezoelectric Tip-Sample Distance Control for near-Field Optical Microscopes. *Applied Physics Letters* **1995,** 66, (14), 1842-1844.
134. Krausch, G.; Wegscheider, S.; Kirsch, A.; Bielefeldt, H.; Meiners, J. C.; Mlynek, J., Near-Field Microscopy and Lithography with Uncoated Fiber Tips - a Comparison. *Optics Communications* **1995,** 119, (3-4), 283-288.
135. Smolyaninov, I. I.; Mazzoni, D. L.; Davis, C. C., Near-field direct-write ultraviolet lithography and shear force microscopic studies of the lithographic process. *Applied Physics Letters* **1995,** 67, (26), 3859-3861.
136. Zeisel, D.; Nettesheim, S.; Dutoit, B.; Zenobi, R., Pulsed laser-induced desorption and optical imaging on a nanometer scale with scanning near-field microscopy using chemically etched fiber tips. *Applied Physics Letters* **1996,** 68, (18), 2491-2492.
137. Hosaka, S.; Kikukawa, A.; Koyanagi, H.; Shintani, T.; Miyamoto, M.; Nakamura, K.; Etoh, K., SPM-based data storage for ultrahigh density recording. *Nanotechnology* **1997,** 8, A58-a62.
138. Imura, R.; Shintani, T.; Nakamura, K.; Hosaka, S., Nanoscale modification of phase change materials with near-field light. *Microelectronic Engineering* **1996,** 30, (1-4), 387-390.
139. Credo, G. M.; Lowman, G. M.; DeAro, J. A.; Carson, P. J.; Winn, D. L.; Buratto, S. K., Probing nanoscale photo-oxidation in organic films using spatial hole burning near-field scanning optical microscopy. *Journal of Chemical Physics* **2000,** 112, (18), 7864-7872.
140. Wei, P. K.; Hsu, J. H.; Fann, W. S., Study of conjugated polymer blend films by a near field scanning optical microscopy. *Synthetic Metals* **1999,** 102, (1-3), 1209-1210.
141. Brewer, N. J.; Rawsterne, R. E.; Kothari, S.; Leggett, G. J., Oxidation of self-assembled monolayers by UV light with a wavelength of 254 nm. *Journal of the American Chemical Society* **2001,** 123, (17), 4089-4090.
142. Huang, J. Y.; Hemminger, J. C., Photooxidation of Thiols in Self-Assembled Monolayers on Gold. *Journal of the American Chemical Society* **1993,** 115, (8), 3342-3343.
143. Tarlov, M. J.; Burgess, D. R. F.; Gillen, G., Uv Photopatterning of Alkanethiolate Monolayers Self-Assembled on Gold and Silver. *Journal of the American Chemical Society* **1993,** 115, (12), 5305-5306.
144. Montague, M.; Ducker, R. E.; Chong, K. S. L.; Manning, R. J.; Rutten, F. J. M.; Davies, M. C.; Leggett, G. J., Fabrication of biomolecular nanostructures by scanning near-field photolithography of oligo(ethylene glycol)-terminated self-assembled monolayers. *Langmuir* **2007,** 23, (13), 7328-7337.
145. Miranda, M. A.; Perez-Prieto, J.; Font-Sanchis, E.; Scaiano, J. C., One- vs two-photon processes in the photochemistry of 1,n-dihaloalkanes. *Accounts of Chemical Research* **2001,** 34, (9), 717-726.
146. Sun, S. Q.; Montague, M.; Critchley, K.; Chen, M. S.; Dressick, W. J.; Evans, S. D.; Leggett, G. J., Fabrication of biological nanostructures by scanning near-field photolithography of chloromethylphenyisiloxane monolayers. *Nano Letters* **2006,** 6, (1), 29-33.
147. Haaheim, J.; Eby, R.; Nelson, M.; Fragala, J.; Rosner, B.; Zhang, H.; Athas, G., Dip Pen Nanolithography (DPN): Process and instrument performance with NanoInk's NSCRIPTOR system. *Ultramicroscopy* **2005,** 103, (2), 117-132.
148. Piner, R. D.; Zhu, J.; Xu, F.; Hong, S. H.; Mirkin, C. A., "Dip-pen" nanolithography. *Science* **1999,** 283, (5402), 661-663.

149. Lee, K. B.; Park, S. J.; Mirkin, C. A., Protein nanoarrays generated by Dip-Pen Nanolithography. *Abstracts of Papers of the American Chemical Society* **2002,** 223, C94-C94.
150. Hyun, J.; Lee, W. K.; Nath, N.; Chilkoti, A.; Zauscher, S., Capture and release of proteins on the nanoscale by stimuli-responsive elastin-like polypeptide "switches". *Journal of the American Chemical Society* **2004,** 126, (23), 7330-7335.
151. Demers, L. M.; Mirkin, C. A., Combinatorial templates generated by dip-pen nanolithography for the formation of two-dimensional particle arrays. *Angewandte Chemie-International Edition* **2001,** 40, (16), 3069-3071.
152. Vega, R. A.; Shen, C. K. F.; Maspoch, D.; Robach, J. G.; Lamb, R. A.; Mirkin, C. A., Monitoring single-cell infectivity from virus-particle nanoarrays fabricated by parallel dip-pen nanotithography. *Small* **2007,** 3, (9), 1482-1485.
153. Wang, X. F.; Liu, C., Multifunctional probe array for nano patterning and imaging. *Nano Letters* **2005,** 5, (10), 1867-1872.
154. Kassies, R.; Van der Werf, K. O.; Lenferink, A.; Hunter, C. N.; Olsen, J. D.; Subramaniam, V.; Otto, C., Combined AFM and confocal fluorescence microscope for applications in bio-nanotechnology. *Journal of Microscopy-Oxford* **2005,** 217, 109-116.
155. Basabe-Desmonts, L.; Wu, C. C.; Van Der Werf, K. O.; Peter, M.; Bennink, M.; Otto, C.; Velders, A. H.; Reinhoudt, D. N.; Subramaniam, V.; Crego-Calama, M., Fabrication and visualization of metal-ion patterns on glass by dip-pen nanolithography. *ChemPhysChem* **2008,** 9, (12), 1680-1687.
156. Madl, J.; Rhode, S.; Stangl, H.; Stockinger, H.; Hinterdorfer, P.; Schütz, G. J.; Kada, G., A combined optical and atomic force microscope for live cell investigations. *Ultramicroscopy* **2006,** 106, (8-9), 645-651.
157. Salaita, K.; Wang, Y. H.; Fragala, J.; Vega, R. A.; Liu, C.; Mirkin, C. A., Massively parallel dip-pen nanolithography with 55000-pen two-dimensional arrays. *Angewandte Chemie-International Edition* **2006,** 45, (43), 7220-7223.
158. Deladi, S.; Tas, N. R.; Berenschot, J. W.; Krijnen, G. J. M.; de Boer, M. J.; de Boer, J. H.; Peter, M.; Elwenspoek, M. C., Micromachined fountain pen for atomic force microscope-based nanopatterning. *Applied Physics Letters* **2004,** 85, (22), 5361-5363.
159. Loh, O. Y.; Ho, A. M.; Rim, J. E.; Kohli, P.; Patankar, N. A.; Espinosa, H. D., Electric field-induced direct delivery of proteins by a nanofountain probe. *Proceedings of the National Academy of Sciences of the United States of America* **2008,** 105, (43), 16438-16443.
160. Lee, J.-H.; An, Y.-C.; Choi, D.-S.; Lee, M.-J.; Kim, K.-M.; Lim, J.-H., Fabrication of a Nano-Porous Polyoxazoline-Coated Tip for Scanning Probe Nanolithography. *Macromolecular Symposia* **2007,** 249-250 (1), 307–311.
161. Wu, C. C.; Xu, H.; Otto, C.; Reinhoudt, D. N.; Lammertink, R. G. H.; Huskens, J.; Subramaniam, V.; Velders, A. H., Porous multilayer-coated AFM tips for dip-pen nanolithography of proteins. *Journal of the American Chemical Society* **2009,** 131, (22), 7526-7527.
162. Vangrondelle, R.; Dekker, J. P.; Gillbro, T.; Sundstrom, V., Energy-Transfer and Trapping in Photosynthesis. *Biochimica Et Biophysica Acta-Bioenergetics* **1994,** 1187, (1), 1-65.
163. Scheuring, S.; Seguin, J.; Marco, S.; Levy, D.; Robert, B.; Rigaud, J. L., Nanodissection and high-resolution imaging of the Rhodopseudomonas viridis photosynthetic core complex in native membranes by AFM. *Proceedings of the National Academy of Sciences of the United States of America* **2003,** 100, (4), 1690-1693.
164. Scheuring, S.; Rigaud, J. L.; Sturgis, J. N., Variable LH2 stoichiometry and core clustering in native membranes of Rhodospirillum photometricum. *Embo Journal* **2004,** 23, (21), 4127-4133.
165. Scheuring, S.; Sturgis, J. N.; Prima, V.; Bernadac, A.; Levy, D.; Rigaud, J. L., Watching the photosynthetic apparatus in native membranes. *Proceedings of the National Academy of Sciences of the United States of America* **2004,** 101, (31), 11293-11297.

166. Bahatyrova, S.; Frese, R. N.; Siebert, C. A.; Olsen, J. D.; van der Werf, K. O.; van Grondelle, R.; Niederman, R. A.; Bullough, P. A.; Otto, C.; Hunter, C. N., The native architecture of a photosynthetic membrane. *Nature* **2004,** 430, (7003), 1058-1062.
167. Olsen, J. D.; Tucker, J. D.; Timney, J. A.; Qian, P.; Vassilev, C.; Hunter, C. N., The Organization of LH2 Complexes in Membranes from Rhodobacter sphaeroides. *Journal of Biological Chemistry* **2008,** 283, (45), 30772-30779.
168. Scheuring, S.; Busselez, J.; Levy, D., Structure of the dimeric PufX-containing core complex of Rhodobacter blasticus by in situ atomic force microscopy. *Journal of Biological Chemistry* **2005,** 280, (2), 1426-1431.
169. Frese, R. N.; Siebert, C. A.; Niederman, R. A.; Hunter, C. N.; Otto, C.; van Grondelle, R., The long-range organization of a native photosynthetic membrane. *Proceedings of the National Academy of Sciences of the United States of America* **2004,** 101, (52), 17994-17999.
170. Bibby, T. S.; Nield, J.; Barber, J., Three-dimensional model and characterization of the iron stress-induced CP43 '-photosystem I supercomplex isolated from the cyanobacterium Synechocystis PCC 6803. *Journal of Biological Chemistry* **2001,** 276, (46), 43246-43252.
171. Jungas, C.; Ranck, J. L.; Rigaud, J. L.; Joliot, P.; Vermeglio, A., Supramolecular organization of the photosynthetic apparatus of Rhodobacter sphaeroides. *Embo Journal* **1999,** 18, (3), 534-542.
172. Hartigan, N.; Tharia, H. A.; Sweeney, F.; Lawless, A. M.; Papiz, M. Z., The 7.5-A electron density and spectroscopic properties of a novel low-light B800 LH2 from Rhodopseudomonas palustris. *Biophysical Journal* **2002,** 82, (2), 963-977.
173. Hunter, C. N.; Tucker, J. D.; Niederman, R. A., The assembly and organisation of photosynthetic membranes in Rhodobacter sphaeroides. *Photochemical & Photobiological Sciences* **2005,** 4, (12), 1023-1027.
174. Aagaard, J.; Sistrom, W. R., Control of Synthesis of Reaction Center Bacteriochlorophyll in Photosynthetic Bacteria. *Photochemistry and Photobiology* **1972,** 15, (2), 209-&.
175. Naylor, G. W.; Addlesee, H. A.; Gibson, L. C. D.; Hunter, C. N., The photosynthesis gene cluster of Rhodobacter sphaeroides. *Photosynthesis Research* **1999,** 62, (2-3), 121.
176. Aust, V.; Angerhofer, A.; Ullrich, J.; von SchÃ¼tz, J. U.; Wolf, H. C.; Cogdell, R. J., ADMR of carotenoid triplet states in bacterial photosynthetic antenna and reaction center complexes. *Chemical Physics Letters* **1991,** 181, (2-3), 213.
177. Hu, X. C.; Ritz, T.; Damjanovic, A.; Autenrieth, F.; Schulten, K., Photosynthetic apparatus of purple bacteria. *Quarterly Reviews of Biophysics* **2002,** 35, (1), 1-62.
178. Brunisholz, R. A.; Zuber, H., Structure, Function and Organization of Antenna Polypeptides and Antenna Complexes from the 3 Families of Rhodospirillaneae. *Journal of Photochemistry and Photobiology B-Biology* **1992,** 15, (1-2), 113-140.
179. Cogdell, R. J.; Howard, T. D.; Bittl, R.; Schlodder, E.; Geisenheimer, I.; Lubitz, W., How carotenoids protect bacterial photosynthesis. *Philosophical Transactions of the Royal Society of London Series B-Biological Sciences* **2000,** 355, (1402), 1345-1349.
180. Frank, H. A.; Chadwick, B. W.; Oh, J. J.; Gust, D.; Moore, T. A.; Liddell, P. A.; Moore, A. L.; Makings, L. R.; Cogdell, R. J., Triplet Triplet Energy-Transfer in B800-850 Light-Harvesting Complexes of Photosynthetic Bacteria and Synthetic Carotenoporphyrin Molecules Investigated by Electron-Spin-Resonance. *Biochimica Et Biophysica Acta* **1987,** 892, (3), 253-263.
181. Guiraud, H. J.; Foote, C. S., Chemistry of Superoxide Ion .3. Quenching of Singlet Oxygen. *Journal of the American Chemical Society* **1976,** 98, (7), 1984-1986.
182. Cogdell, R. J., Carotenoids in Photosynthesis. *Pure and Applied Chemistry* **1985,** 57, (5), 723-728.
183. Mcdermott, G.; Prince, S. M.; Freer, A. A.; Hawthornthwaitelawless, A. M.; Papiz, M. Z.; Cogdell, R. J.; Isaacs, N. W., Crystal-Structure of an Integral Membrane Light-Harvesting Complex from Photosynthetic Bacteria. *Nature* **1995,** 374, (6522), 517-521.

184. Savage, H.; Cyrklaff, M.; Montoya, G.; Kuhlbrandt, W.; Sinning, I., Two-dimensional structure of light harvesting complex II (LHII) from the purple bacterium Rhodovulum sulfidophilum and comparison with LHII from Rhodopseudomonas acidophila. *Structure* **1996,** 4, (3), 243-252.
185. Papiz, M. Z.; Prince, S. M.; Howard, T.; Cogdell, R. J.; Isaacs, N. W., The structure and thermal motion of the B800-850 LH2 complex from Rps. acidophila at 2.0 (A)over-circle resolution and 100 K: New structural features and functionally relevant motions. *Journal of Molecular Biology* **2003,** 326, (5), 1523-1538.
186. Freer, A.; Prince, S.; Sauer, K.; Papiz, M.; HawthornthwaiteLawless, A.; McDermott, G.; Cogdell, R.; Isaacs, N. W., Pigment-pigment interactions and energy transfer in the antenna complex of the photosynthetic bacterium Rhodopseudomonas acidophile. *Structure* **1996,** 4, (4), 449-462.
187. Broglie, R. M.; Hunter, C. N.; Delepelaire, P.; Niederman, R. A.; Chua, N. H.; Clayton, R. K., Isolation and Characterization of the Pigment-Protein Complexes of Rhodopseudomonas-Sphaeroides by Lithium Dodecyl Sulfate-Polyacrylamide Gel-Electrophoresis. *Proceedings of the National Academy of Sciences of the United States of America-Biological Sciences* **1980,** 77, (1), 87-91.
188. Walz, T.; Jamieson, S. J.; Bowers, C. M.; Bullough, P. A.; Hunter, C. N., Projection structures of three photosynthetic complexes from Rhodobacter sphaeroides: LH2 at 6 angstrom LH1 and RC-LH1 at 25 angstrom. *Journal of Molecular Biology* **1998,** 282, (4), 833-845.
189. Jamieson, S. J.; Wang, P. Y.; Qian, P.; Kirkland, J. Y.; Conroy, M. J.; Hunter, C. N.; Bullough, P. A., Projection structure of the photosynthetic reaction centre-antenna complex of Rhodospirillum rubrum at 8.5 angstrom resolution. *Embo Journal* **2002,** 21, (15), 3927-3935.
190. Conroy, M. J.; Westerhuis, W. H. J.; Parkes-Loach, P. S.; Loach, P. A.; Hunter, C. N.; Williamson, M. P., The solution structure of Rhodobacter sphaeroides LH1 beta reveals two helical domains separated by a more flexible region: Structural consequences for the LH1 complex. *Journal of Molecular Biology* **2000,** 298, (1), 83-94.
191. Okamura, M. Y.; Steiner, L. A.; Feher, G., Characterization of Reaction Centers from Photosynthetic Bacteria .1. Subunit Structure of Protein Mediating Primary Photochemistry in Rhodopseudomonas-Spheroides R-26. *Biochemistry* **1974,** 13, (7), 1394-1402.
192. Ermler, U.; Fritzsch, G.; Buchanan, S. K.; Michel, H., Structure of the Photosynthetic Reaction-Center from Rhodobacter-Sphaeroides at 2.65-Angstrom Resolution - Cofactors and Protein-Cofactor Interactions. *Structure* **1994,** 2, (10), 925-936.
193. Ermler, U.; Michel, H.; Schiffer, M., Structure and Function of the Photosynthetic Reaction-Center from Rhodobacter-Sphaeroides. *Journal of Bioenergetics and Biomembranes* **1994,** 26, (1), 5-15.
194. Michel, H.; Epp, O.; Deisenhofer, J., Pigment Protein Interactions in the Photosynthetic Reaction Center from Rhodopseudomonas-Viridis. *Embo Journal* **1986,** 5, (10), 2445-2451.
195.www.gla.ac.uk/departments/biochemistrycellbiology/researchinterests/academicstaff/richardcogdell.

Chapter 2

Directed Assembly of Functional Light Harvesting Antenna Complexes onto Chemically Patterned Substrates*

In this chapter we report the directed assembly of the photosynthetic membrane proteins LH1 and LH2 isolated from the purple bacterium Rhodobacter sphaeroides onto chemically patterned substrates. Nanoimprint lithography was used to pattern discrete regions of amino- and fluoro-terminated or poly(ethylene glycol) self-assembled monolayers onto a glass substrate. Densely packed layers of assembled protein complexes were observed with atomic force microscopy. The protein complexes attached selectively to the amino-terminated regions by electrostatic interactions. Spectral images generated with a hybrid scanning probe and fluorescence microscope confirmed that the patterned proteins retained their native optical signatures.

---

* This chapter has been published in: Escalante, M.; Maury, P.; Bruinink, C. M.; van der Werf, K.; Olsen, J. D.; Timney, J. A.; Huskens, J.; Hunter, C. N.; Subramaniam, V.; Otto, C., Directed assembly of functional light harvesting antenna complexes onto chemically patterned surfaces. *Nanotechnology* 2008, 19, (2) 025101

2.1 INTRODUCTION

Nature has evolved elegant schemes that use nano-scale architectures to produce striking optical effects.[1-2] For example, in photosynthesis, the harvesting of solar energy and its subsequent conversion into stable products depends on an interconnected macromolecular network of membrane-associated chlorophyll-protein complexes. Although much has been speculated about the native organization of this network,[3] the native architecture of the complex in purple bacterial membranes was only recently revealed using atomic force microscopy (AFM).[4-5]

In most purple bacteria, the photosynthetic membranes contain two types of light harvesting antenna complexes LH2 and LH1. The peripheral LH2 complexes absorb photons and transfer the energy from one complex to another in a series of radiationless transfers (hopping) until the excitation reaches the inner antenna, LH1, which encloses the reaction center RC.[6-7] Both complexes are comprised of roughly circularly arranged αβ helices with bound carotenoid and bacteriochlorophyll (Bchl) pigments that allow the absorption of light in a broad band.[8-10] The LH2 complex is built of 9 identical subunits, each consisting of an α and a β polypeptide. The LH2 α polypeptides form an inner ring surrounded by the β ring; in all, 27 bacteriochlorophyll (Bchl) molecules are bound to this structure (18 Bchl B850 molecules and the remaining B800). The LH1 complex surrounds the RC in an arrangement of 16 αβ protomers and 32 Bchls (B875).[11] These integral proteins have become archetypal molecular electronic devices due to their high excitation transfer rate (LH2→LH1→RC ~100 ps) and high efficiency (~95 %).[12] Thus, if integrated with solid state electronics they might offer an example for future generation of devices organized by a macromolecular scaffold.

In the last decade, major efforts have been focused on the design and synthesis of supramolecular structures with precise dimensions and chemical compositions because of their potential to be integrated in hybrid systems for molecular electronics and photonics. Particularly challenging is the fabrication of molecular wires that guide light by near field interaction of molecules in close proximity to each other, because success depends on the accurate control of the chromophore arrangement. Some efforts towards achieving this goal include the synthesis of arrays of porphyrin,[13] DNA-based molecular wires,[2, 14] and molecular photonic

wires for sensing applications.[15] In parallel, the integration of photosynthetic protein complexes with conducting surfaces has also attracted much attention. RCs have been mainly used because of their possible applications in chemo- and biosensors and in current generation[16-19] To our knowledge however, no previous reports have been presented on the immobilization of the antenna protein complexes (LH1 & LH2) onto patterned surfaces and their spectral response. Furthermore, we present conclusive evidence from hyperspectral fluorescence imaging that the optical functionality of LH1 and LH2 in the patterns is retained.

Several immobilization procedures have been used for the attachment of biomolecules on a surface while retaining biological activity. These include: electrostatic interactions,[20] covalent bonds,[21] biospecific interactions[22] and supramolecular interactions.[23-24] Moreover, many fabrication techniques have been employed for the creation of micro- and nanometer scale molecular assemblies such as conventional photolithography,[25] dip pen nanolithography (DPN)[26] microcontact printing (μCP),[27] scanning near field photolithography (SNP)[28] and nanoimprint lithography (NIL).[29] NIL is a general approach to chemical patterning amenable to the most common substrates, affords high resolution, small features[30-31] where ~ 6 nm has been reported, and a prospect for high throughput. NIL has the potential to be directly used for application purposes and is considered in the international technology roadmap for semiconductors (ITRS).[32]

The efficient and robust molecular aggregates of different light harvesting systems in nature inspired us to use purified components as molecular photonic structures in nanotechnology. To verify and understand the properties of such bio-inspired assemblies onto chemically functionalized surfaces, we make use of a combination of top-down and bottom-up approaches. We direct the assembly of light harvesting antenna complexes LH1 and LH2 onto chemically modified glass substrates through electrostatic interactions between the surface and the protein complexes as the anchoring mechanism. Combining biomolecular self-assembly with NIL for cost-effective patterning at high resolution and high throughput can lead to the large-scale fabrication of molecular photonic wires of unprecedented efficiency. We make use of AFM and fluorescence spectral microscopy to determine the assembly behaviour and spectral response of the patterned complexes to establish if the morphology and optical signatures resemble their native properties.

2.2 MATERIALS AND METHODS

Materials: N-3-(trimethoxysilyl)propylethylenediamine (Aldrich), 1H,1H,2H,2H-perfluorodecyltrichlorosilane (ABCR), 2-Methoxy(polyethyleneoxy) propyl trimethoxysilane (ABCR) and PMMA (molecular weight 350 kD, Aldrich) were used as received.

Protein purification: LH1 complexes were purified as described previously.[11] The LH2 complex was solubilized from membranes from photosynthetically grown wild-type Rhodobacter sphaeroides using 4% N,N-Dimethyldodecylamine-N-oxide (LDAO), and purified on DEAE (Sigma) and Resource Q (GE Healthcare) columns, then size fractionated on a Superdex 200 gel filtration column (GE Healthcare).

Substrate functionalization: The general procedure for the fabrication of chemically patterned substrates with NIL has been reported before.[33] In short, for the micrometer size structures the stamps for NIL were made by photolithography followed by reactive ion etching (RIE, Elektrotech Twin system PF 340). 1H,1H,2H,2H-Perfluorodecyltrichlorosilane was used as an anti-adhesion layer to facilitate the stamp–imprint separation. Substrates (microscope coverslips, Menzel-glaser # 1,5) were cleaned by immersion in piranha solution (3:1 concentrated H_2SO_4 / 33% aqueous H_2O_2) for 15 min, rinsed copiously with water and dried with N2. Then they were coated with a 300 nm thick layer of PMMA (40 g/L) by spin coating (110 nm thick for the nanometer structures). Stamp and substrate were put in contact; a pressure of 40 bars was applied at a temperature of 180 °C using a hydraulic press (Specac). The residual layer was removed by dipping the substrates in acetone for 40 s. Subsequently, SAM formation was performed by gas-phase evaporation of 1H,1H,2H,2H-Perfluorodecyltrichlorosilane in a desiccator under vacuum. Next the polymer template was removed using acetone in an ultrasonic bath for 2 hours and the substrate was dried with N_2. A second silanization with N-3-(trimethoxysilyl)propyl-ethylenediamine followed. The substrates were later rinsed with acetone and ethanol and dried with a stream of N_2. The aminoalkyl SAM yielded positively charged areas while the perfluorinated SAM constituted neutral areas, which resisted the adsorption of proteins. The stamps used for the nanometer size features were fabricated by capillary force lithography onto a commercially available UV photocurable polymer mrl-6000.[34-35] After imprinting, the residual layer was removed by physical etching during approximately 20 seconds in oxygen

plasma (RIE-Elektrotech, 10 W, 10 mT, 10 sccm O_2). Subsequently, activation of the surface took place by deposition of the aminoalkyl SAM from the gas phase. The remaining PMMA was stripped and the complementary areas were passivated with 2-Methoxy(polyethyleneoxy)propyl trimethoxysilane (referred as PEG silane) in distilled toluene for 2 hours. The substrates were later copiously rinsed with toluene followed with acetone, ethanol and dried with a stream of N_2.

Protein immobilization: We deposited a 25 μl drop of ~ 0.2 μM protein aggregates in an aqueous buffered solution of 20 mM HEPES, pH 8.0, containing 0.03 wt % β-DDM (n-dodecyl-β-D-maltoside) detergent, onto the substrate. A 20 minute incubation of the protein solution was done in a humid environment. The concentration of protein was optimized in a dilution experiment. The selected protein concentration in the drop volume is sufficient to cover the active area below the hemispherical drop. The sample was then copiously rinsed with a 20 mM solution of Hepes buffer.

Characterization: Atomic Force Microscopy, Fluorescent Spectral Microscopy and Image Processing

A custom-built stand-alone AFM combined with a confocal fluorescence (spectral) microscope was used for morphological and optical characterization.[36] For AFM imaging standard silicon nitride cantilevers with a length of 85 μm, force constant of 0.5 N/m, and operating frequencies of 25–35 kHz (in liquid) (ThermoMicroscopes, Sunnyvale, CA) were used. AFM images were obtained using tapping mode in liquid (10 mM TRIS-HCl, 150mM KCl). Images contained 256 x 256 pixels and were recorded at a line scanning frequency of 2–4 Hz. Topographical images were quantitatively analyzed using the Scanning Probe Image Processor (SPIP) software (Image Metrology ApS, Lyngby, Denmark). We performed AFM imaging using extremely low tapping amplitudes (directly related to the tapping force) to minimize any mechanical deformations as reported elsewhere.[4, 11]

Fluorescence spectral microscopy was performed using 800 nm excitation provided by a diode laser (Roithner Laser Technik, RLT80010MG). The laser beam is reflected by a dichroic beam splitter (Chroma, Q850LPXXR) towards an oil-immersion objective (Nikon, Plan Fluor 100x NA 1.3), which focuses the light onto the sample. The fluorescence light is collected by the same objective and passes through the dichroic beam splitter. By switching a flip mirror, the fluorescence light

can be directed either towards a single photon counting avalanche photodiode (APD) (SPCM-AQR-14, Perkin Elmer Optoelectronics) or towards a custom designed prism-based spectrograph with single molecule sensitivity equipped with a liquid nitrogen-cooled CCD camera (Spec-10:100B, Princeton Instruments). The spectrograph–CCD camera combination is used for conventional spectral imaging where a complete spectrum is recorded for each image pixel. The spectral images reported have 64 x 64 pixels with an integration time of 100 ms per pixel. The excitation power was ~ 4 μW measured at the back aperture of the objective.

2.3 RESULTS AND DISCUSSION

2.3.1 Micrometer arrays of LH1 and LH2 complexes on chemically patterned glass substrates.

The suitability of NIL for the creation of chemically functionalized substrates [29] and immobilization of biological samples has been addressed before.[33] The schematic procedure is depicted in Figure 2.1**.** Polymer templates were created by NIL on PMMA/Glass substrates followed by residual layer removal (1). For the micrometer size structures a fluoroalkyl SAM that acts as a protein resistant layer was deposited on the polymer free areas (2). Subsequently, the remaining polymer was removed (3) and the polymer-free areas were functionalized with an amino-terminated silane. Line patterns with a width of 4 μm were created. The resolution of this technique is dictated by the dimensions of the stamp. These structures could be made in areas of 1x1 cm^2 on microscope coverslips. The hybrid microscope used for characterization requires optically transparent samples at the wavelength used (excitation 800 nm, emission 850 - 920 nm) for simultaneous measurements.

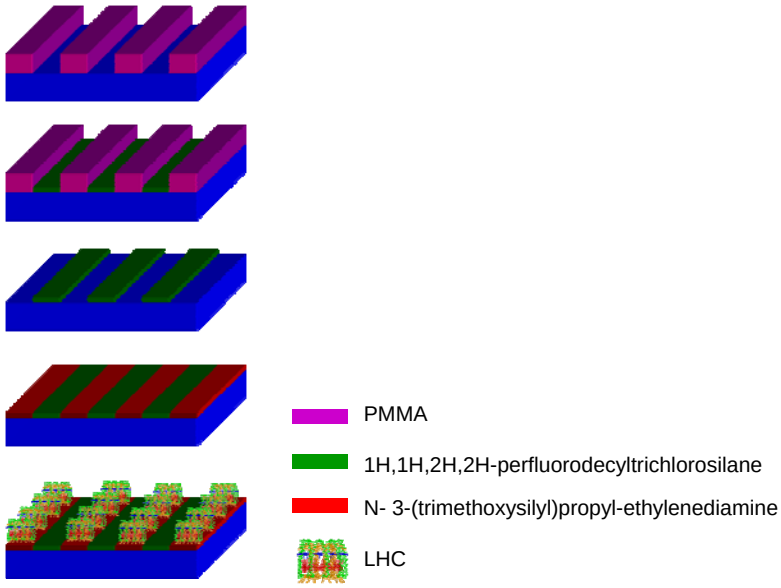

Figure 2.1. *Process flow schematics of substrate patterning and protein immobilization. 1: Spin coated PMMA is patterned by NIL and the residual polymer layer is removed. 2: The polymer free areas are passivated with a fluoroalkyl SAM. 3: The remaining PMMA is stripped. 4: An aminosilane SAM is formed on the complementary areas. 5: Protein solution is incubated on the chemically patterned substrates.*

Figure 2.2a shows a friction image of the chemically patterned substrate (amino/fluoroalkyl SAM). The higher friction areas (brighter areas) correspond to the aminoalkyl SAM.

The subsequent exposure of the patterns to a dilute solution of single protein complexes (either LH1 or LH2) resulted in a selective assembly of the biological material to the amino-terminated areas. The selective assembly is primarily driven by the electrostatic interaction between the protein complex and the terminal amino groups of the SAM which are positively charged at the pH used.[20] Figure 2.2b shows an AFM image of LH2 complexes attached onto the chemically patterned substrates. The image was recorded in tapping mode in liquid. The height measured on the patterns is around 4 nm (Figure 2.2d), which when added to the ~1.8 nm in difference between the amino and fluoroalkyl layers gives a total height of ~5.8 nm, which is in accordance with the expected dimensions of this protein complex of around 6 nm in height and 7 nm in diameter.

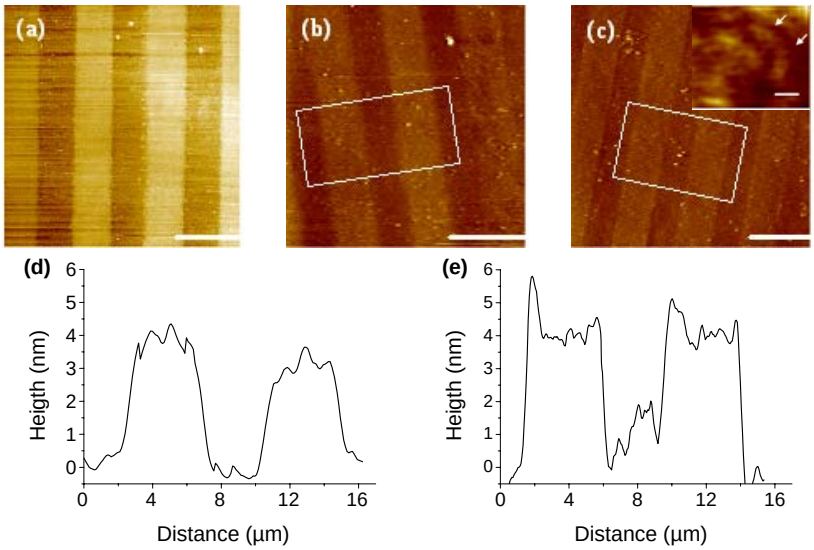

Figure 2.2. *(a) Friction force image of chemically patterned substrate (amino/fluoroalkyl). AFM topographies (liquid) of the protein complexes immobilized onto the chemically patterned substrate. Images acquired in tapping mode under physiological conditions and their respective cross section, z-scale 30 nm (b) , (d) LH2 complexes, (c), (e) LH1 complexes. Scale bar 8µm. Images 256 x 256 pixels. The inset in panel (c) shows close packed arrangement of single LH1 complexes, z-scale 3 nm, and scale bar 20 nm.*

Similarly, LH1 complexes without reaction centers were immobilized on the patterned surfaces. The corresponding AFM image is shown in Figure 2.2c. The measured height along the patterned protein line is approximately 4 nm. This gives a protein height of ~ 6 nm. The expected dimensions of this protein complex are ~ 6 nm in height and 12 nm in diameter. Both height data indicate that a monolayer of LHCs was adsorbed onto the activated surface.

The inset in Figure 2.2c shows a 300 nm area of the patterned regions of LH1 complexes. Despite the lack of resolution, a high density arrangement of proteins was observed without significant height differences in this region. This image suggests that during the self-assembly process the protein complexes are arranged in a quasi-oriented fashion on the surface with the αβ apoprotein perpendicular to the surface as found in native membranes. The measured height on the patterns of LH1 complexes is ~ 6 nm. No significantly higher values were found, which would be expected if the proteins were assembled in a random fashion. This result also indicates that the protein complexes self-orient on the surface. This observation is

further supported by the structure of the membrane protein which has two well separated (~4 nm) hydrophilic charged regions. Based on a consideration of the nature of the charged residues, the periplasmic face of LH2 and the cytoplasmic face of LH1 are likely to be negatively charged.

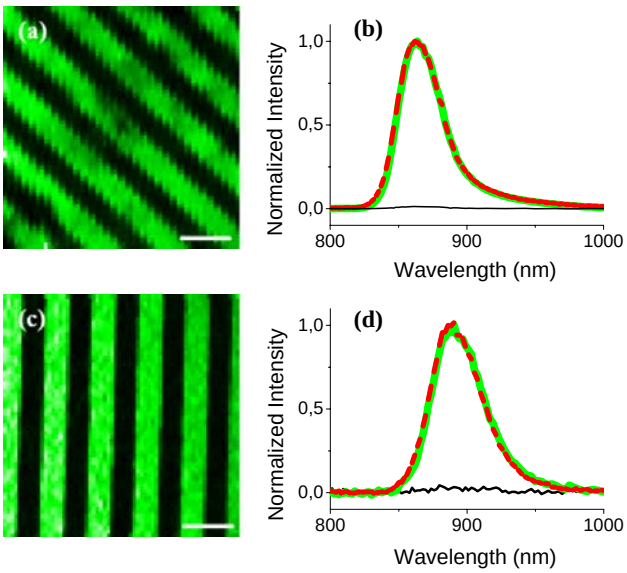

Figure 2.3. *(False colour) Spectral images of single light harvesting antenna complexes immobilized onto chemically patterned glass substrates (amino/fluoroalkyl) demonstrating the retained biological activity. (a) LH2 complexes. (c) LH1 complexes. An 800 nm laser-diode is used as excitation source. 64 x 64 pixels, 100 ms integration time, scale bar 8 μm. Comparison of the normalized spectral response of the patterned protein complexes (solid-green) with the emission spectra of the respective bulk signal (dashed-red) for (b) LH2 complexes and (d) LH1 complexes. Spectra recorded on the passivated areas are plotted in black. Each curve is the average of 10 spectra on the area of interest.*

Spectral images of the patterned complexes were acquired to address their functionality. Similar to the AFM images, the optical characterization was carried out in a liquid environment. 800 nm excitation was used to efficiently excite the LH2 complexes via the bacteriochlorophyll (Bchl a) B800. The patterns of the LH1 complex were excited at the same wavelength. Although this wavelength is not optimized for the B875 bacteriochlorophyll pigments, a high signal to noise ratio could still be registered. Our set-up has single molecule sensitivity, which is favourable also for the detection of protein non-specifically bound onto the passivated areas. Figure 2.3a and c show respectively the spectral images for LH2

and LH1 complexes immobilized on the substrates. A complete spectrum was recorded at each pixel of the image. For display purposes, the spectral image consists of data integrated over the respective emission bands of LH1 and LH2 protein complexes. The green areas correspond to those where the protein complexes were immobilized. The passivated areas are shown in black. The high contrast between both areas is evident. Some pixelation can be observed due to the number of pixels acquired per images (64 x 64); this effect is more pronounced in Figure 2.3a because the sample is oriented at a 45° angle with respect to the scanning direction. This is purely a function of the large pixel size and the orientation of the figure and has no further influence on the quality of the spectral information of the images.

Figure 2.3b shows a comparison between the emission spectra of the LH2 protein complexes in solution before immobilization (dashed-red) and after patterning on the surface (solid-green). The spectral data from the patterns are average spectra from 10 individual image pixels. The LH2 fluorescence emission maximum is found at ~865 nm, and no spectral shift is detected between the protein complex in solution and the assembled complex on the surface. This agreement strongly indicates that the immobilization procedure did not affect the conformational and optical properties of the complex. Similar results are obtained for the immobilization of the LH1 complexes. In this case, the emission maximum is around ~892 nm which is typical of LH1 emission. The fluorescence intensity ratio between the amino- and fluoroalkyl- functionalized areas is in excess of 100, confirming that nonspecific binding of the antenna complexes to the fluoroalkyl layer is negligible, (Figure 2.3b and d).

2.3.2 Submicrometer arrays of LH2 complexes

The fabrication of structures in arrays of functional LHCs of nanometer-scale widths was also addressed. Capillary force lithography was used to create nanometer sized features onto an UV curable polymer which later served as hard stamps for the NIL procedure. In this way, after removal of the residual PMMA layer, activation of the surface by the formation of the aminoalkyl SAM took place. The polymer mask was removed and the remaining areas were passivated with PEG-silane which is known to be highly resistant to protein adsorption.[37] The stamps

were designed to separate nano-scale features with micrometer distances. This combines favorably with the sub-micrometer resolution of far field optical microscopy as we have used here.

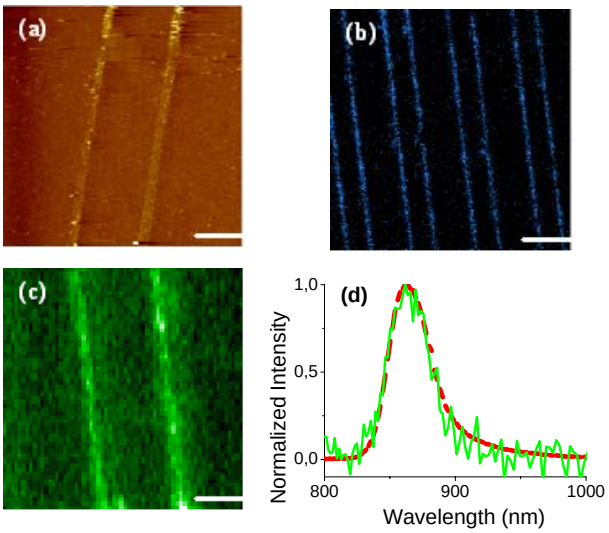

Figure 2.4. *LH2 complexes immobilized onto chemically patterned substrate amino/PEG. (a) AFM height image tapping mode in liquid, scale bar 2 µm, z-scale 25 nm. FWHM of the patterned lines 350 nm with 3 µm separation (b) (False colour) Fluorescent image of LH2 complexes captured by APD, scale bar 6 µm, 128x128 pixel, separation between the patterned lines either 3 or 5µm. (c) (False colour) Spectral image, scale bar 1.6 µm, 64x64 pixels, 50 ms integration time (d) Comparison of the normalized spectral response of the patterned LH2 complexes (solid-green) with the emission spectral of the respective bulk signal (dashed-red).*

Figure 2.4a shows the AFM topography of the adsorbed LH2 complexes onto the amino/PEG patterns of approximately 350 nm in width. The activity of the patterned protein complexes is confirmed by the fluorescent image of the regular array (Figure 2.4b) and also by the spectral image (Figure 2.4c) that shows full integrity of the complex on the surface.

The fabrication of complex micro- and nano-patterned assemblies of light harvesting antenna complexes combined with structural and functional studies using innovative hybrid microscopy can contribute to the creation of biophotonic-waveguides of high efficiency which will inspire synthetic chemists to create supramolecular structures capable of mimicking the natural antennas.

2.4 CONCLUSIONS

We have successfully immobilized light harvesting protein complexes LH2 and LH1 from *Rhodobacter sphaeroides* onto glass substrates. The assemblies exhibit native-like optical spectra indicating no loss of conformational integrity that would be reflected in modified optical properties. Since NIL allows features as small as 6 nm[30-31] we anticipate that organization of individual protein complexes in nanometer-scale patterns will be possible. Alternative assembly strategies to immobilize light harvesting antenna complexes on chemically patterned surfaces are currently under study. This work points towards the possibility to create biophotonic devices in a controlled manner with nanometer spatial resolution.

2.5 ACKNOWLEGEMENTS

We are grateful to the Nanotechnology Network in The Netherlands (NanoNed), project 7124 for financial support. Also we are grateful for financial support from the Council for Chemical Sciences of the Netherlands Organization for Scientific Research (NWO-CW) (P.M.; Vidi Vernieuwingsimpuls grant 700.52.423 to J.H.). C.M.B MESA+ Institute for Nanotechnology (Strategic Research Orientation Advanced Photonic Structures). C.N.H. and J.D.O. gratefully acknowledge the funding of the BBSRC UK. R. Vermeij is acknowledged for fruitful discussions.

2.6 REFERENCES

1. Vukusic, P.; Sambles, J. R., Photonic structures in biology. *Nature* **2003,** 424, (6950), 852-855.
2. Tinnefeld, P.; Heilemann, M.; Sauer, M., Design of molecular photonic wires based on multistep electronic excitation transfer. *ChemPhysChem* **2005,** 6, (2), 217-222.
3. Ritz, T.; Park, S.; Schulten, K., Kinetics of excitation migration and trapping in the photosynthetic unit of purple bacteria. *Journal of Physical Chemistry B* **2001,** 105, (34), 8259-8267.
4. Bahatyrova, S.; Frese, R. N.; Siebert, C. A.; Olsen, J. D.; Van Der Werf, K. O.; Van Grondelle, R.; Nlederman, R. A.; Bullough, P. A.; Otto, C.; Hunter, C. N., The native architecture of a photosynthetic membrane. *Nature* **2004,** 430, (7003), 1058-1062.
5. Scheuring, S.; Sturgis, J. N.; Prima, V.; Bernadac, A.; Lévy, D.; Rigaud, J. L., Watching the photosynthetic apparatus in native membranes. *Proceedings of the National Academy of Sciences of the United States of America* **2004,** 101, (31), 11293-11297.
6. Van Grondelle, R.; Dekker, J. P.; Gillbro, T.; Sundstrom, V., Energy transfer and trapping in photosynthesis. *Biochimica et Biophysica Acta - Bioenergetics* **1994,** 1187, (1), 1-65.
7. Schubert, A.; Stenstam, A.; Beenken, W. J. D.; Herek, J. L.; Cogdell, R.; Pullerits, T.; Sundström, V., In Vitro Self-Assembly of the Light Harvesting Pigment-Protein LH2

Revealed by Ultrafast Spectroscopy and Electron Microscopy. *Biophysical Journal* **2004,** 86, (4), 2363-2373.
8. McDermott, G.; Prince, S. M.; Freer, A. A.; Hawthornthwaite-Lawless, A. M.; Papiz, M. Z.; Cogdell, R. J.; Isaacs, N. W., Crystal structure of an integral membrane light-harvesting complex from photosynthetic bacteria. *Nature* **1995,** 374, (6522), 517-521.
9. Roszak, A. W.; Howard, T. D.; Southall, J.; Gardiner, A. T.; Law, C. J.; Isaacs, N. W.; Cogdell, R. J., Crystal Structure of the RC-LH1 Core Complex from Rhodopseudomonas palustris. *Science* **2003,** 302, (5652), 1969-1972.
10. Walz, T.; Jamieson, S. J.; Bowers, C. M.; Bullough, P. A.; Hunter, C. N., Projection structures of three photosynthetic complexes from Rhodobacter sphaeroides: LH2 at 6 Å, LH1 and RC-LH1 at 25 Å. *Journal of Molecular Biology* **1998,** 282, (4), 833-845.
11. Bahatyrova, S.; Frese, R. N.; Van Der Werf, K. O.; Otto, C.; Hunter, C. N.; Olsen, J. D., Flexibility and size heterogeneity of the LH1 light harvesting complex revealed by atomic force microscopy: Functional significance for bacterial photosynthesis. *Journal of Biological Chemistry* **2004,** 279, (20), 21327-21333.
12. Pullerits, T.; Sundström, V., Photosynthetic Light-Harvesting Pigment-Protein Complexes: Toward Understanding How and Why. *Accounts of Chemical Research* **1996,** 29, (8), 381-389.
13. Choi, M. S.; Yamazaki, T.; Yamazaki, I.; Aida, T., Bioinspired molecular design of light-harvesting multiporphyrin arrays. *Angew. Chem., Int. Ed.* **2004,** 43, 150-158.
14. Sánchez-Mosteiro, G.; Van Dijk, E. M. H. P.; Hernando, J.; Heilemann, M.; Tinnefeid, P.; Sauer, M.; Koberlin, F.; Patting, M.; Wahl, M.; Erdmann, R.; Van Hulst, N. F.; García-Parajó, M. F., DNA-based molecular wires: Multiple emission pathways of individual constructs. *Journal of Physical Chemistry B* **2006,** 110, (51), 26349-26353.
15. Wosnick, J. H.; Swager, T. M., Molecular photonic and electronic circuitry for ultra-sensitive chemical sensors. *Current Opinion in Chemical Biology* **2000,** 4, (6), 715-720.
16. Das, R.; Kiley, P. J.; Segal, M.; Norville, J.; Yu, A. A.; Wang, L.; Trammell, S. A.; Reddick, L. E.; Kumar, R.; Stellacci, F.; Lebedev, N.; Schnur, J.; Bruce, B. D.; Zhang, S.; Baldo, M., Integration of photosynthetic protein molecular complexes in solid-state electronic devices. *Nano Letters* **2004,** 4, (6), 1079-1083.
17. Trammell, S. A.; Wang, L.; Zullo, J. M.; Shashidhar, R.; Lebedev, N., Orientated binding of photosynthetic reaction centers on gold using Ni-NTA self-assembled monolayers. *Biosensors and Bioelectronics* **2004,** 19, (12), 1649-1655.
18. Nakamura, C.; Hasegawa, M.; Nakamura, N.; Miyake, J., Rapid and specific detection of herbicides using a self-assembled photosynthetic reaction center from purple bacterium on an SPR chip. *Biosensors and Bioelectronics* **2003,** 18, (5-6), 599-603.
19. Ciobanu, M.; Kincaid, H. A.; Jennings, G. K.; Cliffel, D. E., Photosystem I patterning imaged by scanning electrochemical microscopy. *Langmuir* **2005,** 21, (2), 692-698.
20. Zhou, D.; Wang, X.; Birch, L.; Rayment, T.; Abell, C., AFM study on protein immobilization on charged surfaces at the nanoscale: Toward the fabrication of three-dimensional protein nanostructures. *Langmuir* **2003,** 19, (25), 10557-10562.
21. Zhang, F.; Fath, M.; Marks, R.; Linhardt, R. J., A highly stable covalent conjugated heparin biochip for heparin-protein interaction studies. *Analytical Biochemistry* **2002,** 304, (2), 271-273.
22. Liu, G. Y.; Amro, N. A., Positioning protein molecules on surfaces: A nanoengineering approach to supramolecular chemistry. *Proceedings of the National Academy of Sciences of the United States of America* **2002,** 99, (8), 5165-5170.
23. Ludden, M. J. W.; Péter, M.; Reinhoudt, D. N.; Huskens, J., Attachment of streptavidin to β-cyclodextrin molecular printboards via orthogonal host-guest and protein-ligand interactions. *Small* **2006,** 2, (10), 1192-1202.
24. Ludden, M. J. W.; Mulder, A.; Tampé, R.; Reinhoudt, D. N.; Huskens, J., Molecular printboards as a general platform for protein immobilization: A supramolecular

solution to nonspecific adsorption. *Angewandte Chemie - International Edition* **2007,** 46, (22), 4104-4107.
25. Sorribas, H.; Padeste, C.; Tiefenauer, L., Photolithographic generation of protein micropatterns for neuron culture applications. *Biomaterials* **2002,** 23, (3), 893-900.
26. Lee, S. W.; Oh, B. K.; Sanedrin, R. G.; Salaita, K.; Fujigaya, T.; Mirkin, C. A., Biologically active protein nanoarrays generated using parallel dip-pen nanolithography. *Advanced Materials* **2006,** 18, (9), 1133-1136.
27. Rozkiewicz, D. I.; Kraan, Y.; Werten, M. W. T.; De Wolf, F. A.; Subramaniam, V.; Ravoo, B. J.; Reinhoudt, D. N., Covalent microcontact printing of proteins for cell patterning. *Chemistry - A European Journal* **2006,** 12, (24), 6290-6297.
28. Sun, S.; Montague, M.; Critchley, K.; Chen, M. S.; Dressick, W. J.; Evans, S. D.; Leggett, G. J., Fabrication of biological nanostructures by scanning near-field photolithography of chloromethylphenylsiloxane monolayers. *Nano Letters* **2006,** 6, (1), 29-33.
29. Hoff, J. D.; Cheng, L. J.; Meyhöfer, E.; Guo, L. J.; Hunt, A. J., Nanoscale protein patterning by imprint lithography. *Nano Letters* **2004,** 4, (5), 853-857.
30. Chou, S. Y.; Krauss, P. R.; Zhang, W.; Guo, L.; Zhuang, L., Sub-10 nm imprint lithography and applications. *Journal of Vacuum Science and Technology B: Microelectronics and Nanometer Structures* **1997,** 15, (6), 2897-2904.
31. Austin, M. D.; Ge, H.; Wu, W.; Li, M.; Yu, Z.; Wasserman, D.; Lyon, S. A.; Chou, S. Y., Fabrication of 5 nm linewidth and 14 nm pitch features by nanoimprint lithography. *Applied Physics Letters* **2004,** 84, (26), 5299-5301.
32. International Technology Roadmap for Semiconductors (ITRS) 2006 http://www.itrs.net. **2006**.
33. Maury, P.; Péter, M.; Mahalingam, V.; Reinhoudt, D. N.; Huskens, J., Patterned self-assembled monolayers on silicon oxide prepared by nanoimprint lithography and their applications in nanofabrication. *Advanced Functional Materials* **2005,** 15, (3), 451-457.
34. Bruinink, C. M.; Péter, M.; De Boer, M.; Kuipers, L.; Huskens, J.; Reinhoudt, D. N., Stamps for submicrometer soft lithography fabricated by capillary force lithography. *Advanced Materials* **2004,** 16, (13), 1086-1090.
35. Bruinink, C. M.; Péter, M.; Maury, P. A.; De Boer, M.; Kuipers, L.; Huskens, J.; Reinhoudt, D. N., Capillary force lithography: Fabrication of functional polymer templates as versatile tools for nanolithography. *Advanced Functional Materials* **2006,** 16, (12), 1555-1565.
36. Kassies, R.; Van Der Werf, K. O.; Lenferink, A.; Hunter, C. N.; Olsen, J. D.; Subramaniam, V.; Otto, C., Combined AFM and confocal fluorescence microscope for applications in bio-nanotechnology. *Journal of Microscopy* **2005,** 217, (1), 109-116.
37. Kannan, B.; Castelino, K.; Chen, F. F.; Majumdar, A., Lithographic techniques and surface chemistries for the fabrication of PEG-passivated protein microarrays. *Biosensors and Bioelectronics* **2006,** 21, (10), 1960-1967.

Chapter 3

Nanometer arrays of functional light harvesting antenna complexes by nanoimprint lithography and host-guest interactions*

In this chapter we show an approach based on the combination of site-directed mutagenesis, nanoimprint lithography and multivalent host-guest interactions for the realization of engineered ordered functional arrays of purified components of the photosynthetic system, the membrane-bound LH2 complex. In addition to micrometer-scale patterned structures, we demonstrated the use of nanometer-scale hard NIL stamps to generate functional protein arrays approaching molecular dimensions.

* This chapter has been published in: Escalante, M.; Zhao, Y. P.; Ludden, M. J. W.; Vermeij, R.; Olsen, J. D.; Berenschot, E.; Hunter, C. N.; Huskens, J.; Subramaniam, V.; Otto, C., Nanometer arrays of functional light harvesting antenna complexes by nanoimprint lithography and host-guest interactions. *Journal of the American Chemical Society* **2008,** 130, (28), 8892

3.1 INTRODUCTION

Supramolecular interactions play a key role in the functional architecture of nature. On patterned surfaces, interactions can be adjusted in strength and further modulated by the orientation of target molecules.[1-2] Here, we have engineered functional ordered arrays of purified components of the photosynthetic system. We relied on multivalent interactions to drive the selective assembly of light harvesting LH2 antenna complexes onto nanometer structured β-cyclodextrin (β-CD) monolayers[2] patterned by nanoimprint lithography (NIL).

Reindhoudt, Huskens and coworkers have developed the so-called molecular printboard that consists of self-assembled cyclodextrin monolayers on different surfaces such as gold and glass.[3] β-CD is a water soluble cyclic oligosaccharide made of seven glucose units linked through α-1,4 bonds, block 1, Figure 3.2. On account of this specific geometrical shape and chemical anisotropy, β-CD molecules may form inclusion complexes in aqueous media with a wide range of molecules or macromolecules containing hydrophobic moieties.[4] Provided that they are functionalized with the appropriate guest molecule, e.g. an adamantyl moiety, fluorescent molecules,[1] dendrimers[5] and proteins[2] can be positioned on the molecular printboard.

The nanomachinery of the photosynthetic bacterium *Rhodobacter sphaeroides* has been an invaluable model for the study of biophysics, biochemistry and molecular biology of photosynthesis.[6] The membrane-bound LH2 complex is built of 9 identical subunits each consisting of an α and a β polypeptide. A total of 27 bacteriochlorophyll (BChl) molecules (18 BChl B850 and 9 B800) are bound to this structure having dimensions of ~7 nm in height and ~7 nm in diameter.[7-8] LH2 are interesting candidates for applications in synthetic light converting circuits because of their well defined optical properties, such as a broad spectral range, high absorption cross section, efficient energy transfer[9] and high photo-stability. Photosynthetic antenna systems have been used in studies exploiting covalent[10] and electrostatic interactions[11] to promote attachment to a chemically defined surface. A major challenge remains in the control of the interfacial properties and the associated multiple weak interactions to produce and optimize organized molecular structures with controlled directional energy migration.

3.2 MATERIALS AND METHODS

Materials: All chemicals were used as received: *N*-[3-(trimethoxysilyl)propyl]-ethylenediamine] (Aldrich), 1H,1H,2H,2H-perfluorodecyltrichlorosilane (ABCR), 2-[Methoxy(polyethyleneoxy)propyl]trimethoxysilane (ABCR), PMMA (molecular weight 350 kD, Aldrich), 2-[Methoxy(polyethyleneoxy)propyl]trimethoxysilane (ABCR), 1,4-phenylenediisothiocyanate (Acros). βCD-heptamine and hexa(ethyleneglycol)mono(adamantyl ether) were synthesized as reported.[12-13]

Scheme 1. *Synthesis*

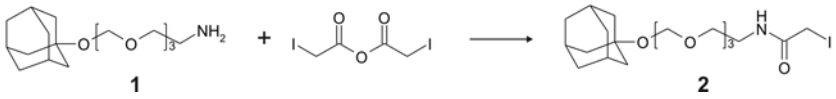

Iodoacetyl-tri(ethyleneglycol))mono(adamantyl ether) was prepared by dissolving compound **1**[14] (163 mg, 0.50 mmol) and iodoacetic anhydride (200 mg, 0.56 mmol) in DMF. To this mixture diisopropylethylamine (129 mg, 1 mmol) was added. The reaction was performed in the dark in an icebath at 0 °C for 1 hour. Subsequently, THF was removed by rotary evaporation under vacuum, giving a brown colored oil as the product (yield 172 mg. 64 %).

^{1}H NMR (300 MHz, $CDCl_3$): δ: 7.75-3.50 (m, 16H, O*CH*$_2$*CH*$_2$O + O*CH*$_2$CH$_2$NH), 2,85 (m, 4H, *CH*$_2$NH + *CH*$_2$I), 2.15 (m, 3H, CH$_2$*CH*CH$_2$Ad), 1.76-1.75 (m, 16H, CH*CH*$_2$CAd), 1.64-1.58 (m, 6H, CH*CH*$_2$CHAd); MS (FAB-MS): *m/z* calculated for [M+H$^+$] 596.4, found 597.5.

Protein purification: The LH2 complex was solubilized from membranes from photosynthetically grown *Rhodobacter sphaeroides* using 4% *N*,*N*-Dimethyldodecylamine-*N*-oxide (LDAO), and purified on DEAE (Sigma) and Resource Q (GE Healthcare) columns, then size fractionated on a Superdex 200 gel filtration column (GE Healthcare). The mutagenesis protocol has been described before.[15]

Protein labeling: Protein aggregates in an aqueous buffered solution (20 mM HEPES, pH 8.0, 0.03 % β-DDM (n-dodecyl-β-D-maltoside) were mixed at 1:20 molar equivalent with the AdI in DMSO. The total concentration of DSMO in the solution is < 1,3 % to prevent disruption of the complexes. The mixture was

incubated overnight at +4°C under rotation at 2 rpm. Labeled protein was purified by desalting and was collected in the initial buffer.

β-CD layer formation onto non-patterned substrates: Substrates (microscope coverslips, Menzel-glaser # 1,5) were cleaned by immersion in piranha solution (3:1 concentrated H_2SO_4 / 33% aqueous H_2O_2) for 15 min, rinsed copiously with water and dried with N_2. *Warning: Piranha solution should be handled with care.* *N*-[3-(trimethoxysilyl)propyl]ethylenediamine] SAM formation was performed by gas-phase evaporation in a desiccator under vacuum overnight, rinsed with ethanol and dried with N_2. Transformation of the amine-terminated SAMs to isothiocyanate-terminated layers was accomplished by exposure to a 0.1 M solution of 1,4-phenylenediisothiocyanate in toluene at 50 °C for 2 h under N_2, followed by rinsing with toluene and drying with N_2. β-CD-terminated SAMs were obtained by reaction of the isothiocyanate-terminated monolayers with a 1mM solution of β-CD heptamine in Millipore water (pH 8.5) at 50 °C for 2 h. The substrates were briefly sonicated in Millipore water, rinsed with Millipore water, and gently dried in a stream of N_2.

Patterned surfaces of β-CD-Fluoralkyl/PEG: Chemically patterned amino-terminated/PEG surfaces were prepared as before.[11] We used silicon ridges of ~40 nm width with a period of 4 μm as a hard stamp (similar to reference[16]). These dimensions are compatible with the sub-micrometer resolution of far field optical microscopy used for optical characterization.

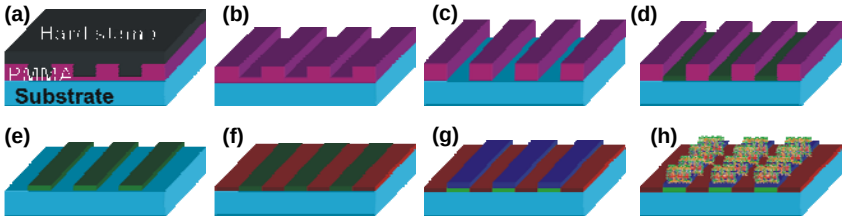

Figure 3.1. *Representation of the different steps for the fabrication of the chemically patterned surfaces (β-CD/PEG) by nanoimprint lithography and subsequent immobilization of the protein complexes. (a) Thermal NIL in PMMA, (b) demolding of the silicon stamp, (c) removal of the polymer residual layer, (d) chemical functionalization of the polymer-free areas, (e) removal of the polymer mask, (f) chemical passivation of the complementary areas, (g) self-assembly of β-CD host-molecules monolayer, (h) assembly of the LH2$_n$Ad protein complexes on the β-CD monolayer*

In short, (Figure 3.1), substrates (microscope coverslips, Menzel-glaser # 1,5) were cleaned as described before. Then they were coated with a 90 nm thick layer of PMMA (20 g/L) by spin coating. Stamp and substrate were put in contact; a pressure of 40 bars was applied at a temperature of 180 °C using a hydraulic press (Specac), and separation was performed at 110 °C. After imprinting, the residual layer was removed by physical etching during approximately 20 seconds in oxygen plasma (RIE-Elektrotech, 20 W, 10 mT, 10 sccm O_2). In this step, the lateral dimensions of the polymer-free areas are increased relative to that of the NIL stamp, since in the process the side walls of the polymer barrier are also slightly etched away. Subsequently, activation of the surface took place by deposition of the aminoalkyl SAM from the gas phase.[17] The remaining PMMA was stripped and the complementary areas were passivated with 2-[Methoxy(polyethyleneoxy)propyl] trimethoxysilane (referred as PEG silane) in distilled toluene for 2 hours, Figure 3.1f. The substrates were later copiously rinsed with toluene followed with ethanol and dried with a stream of N_2. Then the β-CD SAM was assembled as described in the previous section.

Protein immobilization on patterned surfaces: We deposited a drop of adamantyl modified protein aggregates (25 μl, ~ 0.4μM) in an aqueous buffered solution (20 mM HEPES, pH 8.0, 0.03 wt % β-DDM (n-dodecyl-β-D-maltoside), 1mM AdHEG) onto the substrate which was previously treated with AdHEG (25 μl, 1 mM) for 10 minutes. A 20 minute incubation of the protein solution was done in a chamber with wet paper to assure a humid environment (Figure 3.1h). The sample was then rinsed with buffer. The concentration of protein was optimized in a dilution experiment.

Atomic force characterization: A custom-built stand-alone AFM combined with a confocal fluorescence (spectral) microscope was used for morphological and optical characterization.[18] For AFM imaging standard silicon nitride cantilevers with a length of 85 μm, force constant of 0.5 N/m, and operating frequencies of 25–35 kHz (in liquid) (ThermoMicroscopes, Sunnyvale, CA) were used. AFM images were obtained using tapping mode in liquid (10 mM TRIS-HCl, 150mM KCl). Images contained 256x256 or 512x512 pixels and were recorded at a line scanning frequency of 2–4 Hz. Topographical images were quantitatively analyzed using the Scanning Probe Image Processor (SPIP) software (Image Metrology ApS, Lyngby,

Denmark). We performed AFM imaging using extremely low tapping amplitudes (directly related to the tapping force) to minimize any mechanical deformations.[8]

Fluorescence spectral microscopy: Fluorescence spectral microscopy was performed using 800 nm excitation from a diode laser (Roithner Laser Technik, RLT80010MG). The laser beam is reflected via a dichroic beam splitter (Chroma, Q850LPXXR) towards an oil-immersion objective (Nikon, Plan Fluor 100 ×NA 1.3), which focuses the light onto the sample. The fluorescence light is collected by the same objective and passes through the dichroic beam splitter. By switching a foldable mirror, the fluorescence light can be directed either towards a single photon counting avalanche photodiode (APD) (SPCM-AQR-14, Perkin Elmer Optoelectronics) or towards a custom designed prism-based spectrograph with single molecule sensitivity equipped with a liquid nitrogen-cooled CCD camera (Spec-10:100B, Princeton Instruments).

3.3 RESULTS AND DISCUSSION

3.3.1 Micrometer arrays of LH1 and LH2 complexes on chemically patterned glass substrates.

LH2 complexes were engineered with cysteine residues at the penultimate position of the C-terminus of the alpha polypeptide chain. These strategic positions at the periplasmic face ensured the orientation of all of the protein complexes upon binding to the surface. The cysteine residues were modified with iodoacetyl-tri(ethylene glycol)mono(adamantyl ether), AdI, block 3, Figure 3.2. Protein aggregates in an aqueous buffered solution of 20 mM HEPES, pH 8.0, 0.03% n-dodecyl-β-D-maltoside (β-DDM) were mixed in 1:20 molar equivalent with the AdI in 1.3% dimethyl sulfoxide (DSMO) to yield an average of three adamantyl molecules linked to each protein complex, hereafter referred to as Ad_nLH2.[19]

When adsorbing Ad_nLH2 onto a βCD-coated glass substrate (Figure 3.2, block 1), hexa(ethyleneglycol)mono(adamantylether) AdHEG, block 2, served as a temporary blocking agent for the β-CD cavities, preventing non-specific adsorption by shielding the surface with the HEG chain.[12] The monovalent AdHEG is later effectively displaced through competition by exploiting the higher affinity of the ultivalent Ad_nLH2.[1312] The assembly on the patterned surface is depicted in block 4.

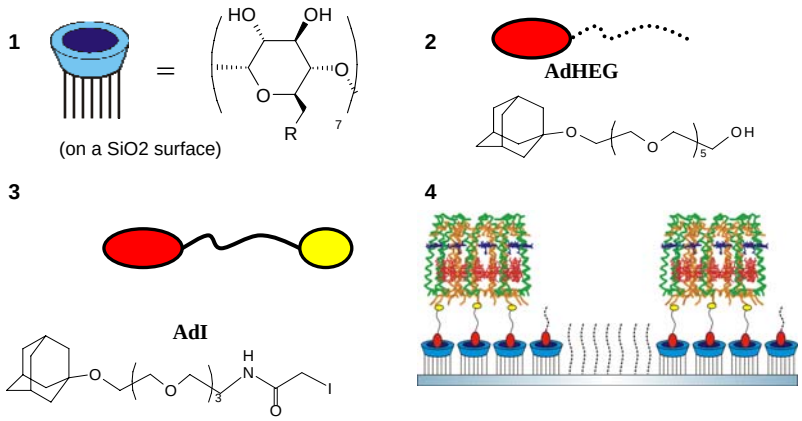

Figure 3.2. *Representation of host, guest and target molecules. 1. β-CD heptamine, host molecule. 2 Hexa(ethylene glycol)mono(adamantyl ether) (AdHEG), 3 iodoacetyl-tri(ethylene glycol)mono(adamantyl ether), (AdI), 4 Ad_nLH2 on the β-CD monolayer.*

We used a custom-built hybrid high resolution scanning probe-spectral microscope[18] to characterize the patterned proteins in liquid conditions. A fluorescence titration allowed us to simultaneously address the optical properties after modification of the LH2 complex and the specificity of the binding on non-patterned β-CD surfaces. Upon excitation of the LH2 complexes via the B800 BChl (donor), the energy is then transferred within the complex to the B850 (acceptor) and ultimately emitted as fluorescence. A dilute solution of non-modified LH2 complexes was incubated onto the β-CD monolayer and rinsed with buffer. The average emission spectra (blue box trace ■, Figure 3.3a), indicates a high contribution of non-specific adsorption. Subsequently, after pre-treating the surface with 1mM solution of AdHEG, a solution of non-modified LH2 complexes in 1 mM AdHEG was incubated onto the substrate. The non-specific adsorption was reduced by 94% (open box trace □). The previous experiment was repeated with Ad_nLH2 complexes. The increase in intensity of the emission signal (green star trace *) reveals that the protein complexes specifically bind to the surface by replacement of the monovalent AdHEG with the multivalent Ad_nLH2. This replacement[13] and the observed stability against rinsing with a βCD solution[2] are evidence for the formation of stable multivalent complexes via at least 3 Ad linkers. Quantitatively, the spectral response from the immobilized Ad_nLH2 complexes showed no visible shift at the emission maximum, ~868 nm, with respect to bulk measurements of non-

modified LH2 complexes (red triangle trace ▼). This observation is compelling evidence that the complete procedure of labeling and surface adsorption has maintained the structural integrity of the LH2 membrane protein.

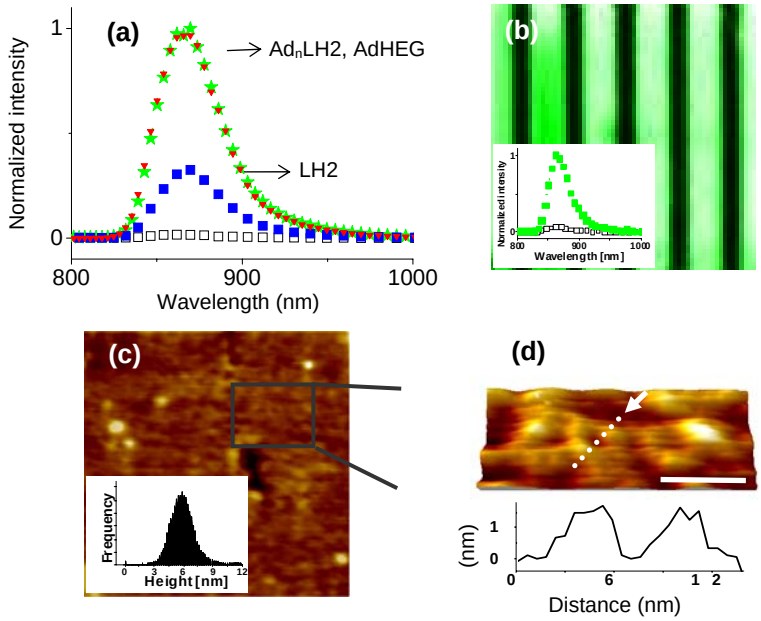

Figure 3.3. *(a) Fluorescence titration: Non-labeled LH2 (blue, ■). Non-labeled LH2, 1 mM AdHEG (open, □). Ad$_n$LH2, 1mM AdHEG (green, *). Reference spectrum of non-labeled LH2 in solution (red ▼). (b) False color, fluorescent-spectral image of Ad$_n$LH2 patterns (β-CD/PEG), 40x40μm, 64x64 pixels; inset emission spectra active area (green, ■), passivated (open, □). (c). AFM topography in liquid, 150x150 nm area, 256x256 pixels, inset histogram height distribution. (d) Section across a LH2 complex showing a profile along the dotted line, scale bar 10 nm.*

We combined the advantages of NIL as a top-down technique to control the lateral dimensions on the nanometer scale and host guest interactions as a bottom-up approach to drive the specific positioning of the biomolecules onto the desired active areas. Figure 3.3b shows a representative spectral image for the patterned Ad$_n$LH2 complexes. On each pixel, a full spectrum was recorded, and integrated over the respective emission band of the LH2 complexes. The exposure of patterns of β-CD SAMs surrounded by a protein resistant PEG SAM[20] to the solution of Ad$_n$LH2, 1mM AdHEG resulted in the selective assembly of the protein onto the β-CD regions (green) in a ratio of 16:1 as indicated by the averaged emission spectra

(inset Figure 3.3b) from active (■) and passivated (□) areas. A monolayer coverage was suggested by quantitative spectral images, which revealed only minor variations (<5%) in intensity over the patterned area.

We performed AFM imaging at low tapping amplitudes to assess the density of the putative monolayer; Figure 3.3c shows an AFM height image of the patterned LH2 complexes; analysis of the surface indicates a uniform height of ~6nm (inset) with reference to the defect (black region), suggesting monolayer coverage of the protein. In the AFM image (Figure 3.3d) ring-shaped LH2 proteins could be observed, which are attributed to the exposed face of the complexes. The height histogram (inset Figure 3.3c) indicated less than 1% multilayer stacked aggregates of proteins in agreement with the fluorescence images.

3.3.2 Nanometer arrays of LH2 complexes

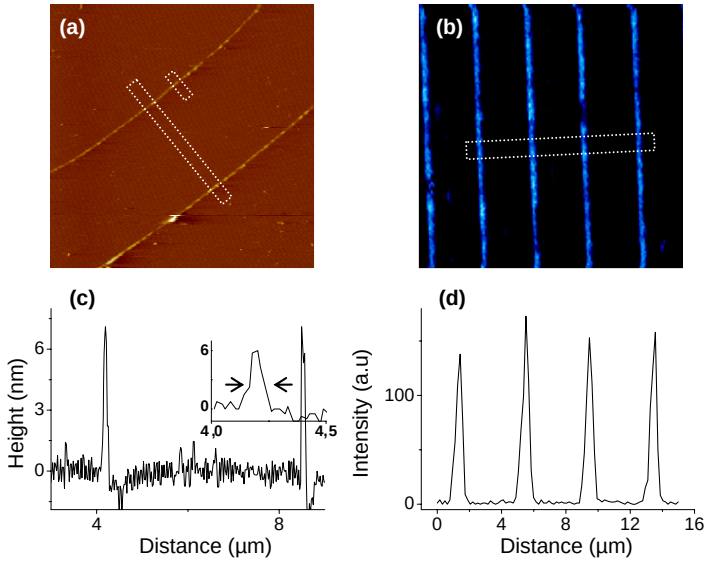

Figure 3.4. *(a) AFM topography in liquid of Ad_nLH2 β-CD/PEG SAM, 10x10µm, z-scale 30 nm, and respective cross section (c), fwhm of 80 nm (inset). (b) False color fluorescent image. (d) Cross section of (b).*

In an attempt to prepare structures approaching molecular dimensions with a view towards building new light harvesting and guiding devices, NIL was performed using stamps with silicon ridges as small as 40 nm with a 4 µm period. Figure 3.4a shows an AFM height image in liquid of Ad_nLH2 complexes on a β-CD SAM. The mean FWHM of the lines after processing is 80 ± 5 nm with a height of

~ 6 ± 1 nm consistent with the assembly of a monolayer of LH2 complexes, Figure 3.4c. The increase in width, relative to that of the NIL stamp, is attributed to the process of removal of the residual layer in the imprinting process. Figure 3.4b shows a fluorescence image acquired with a single photon counting avalanche photodiode, with intensity variations of ±14% along the lines.

3.4 CONCLUSIONS

We have achieved exquisite spatial control at different length scales of functional specifically-bound LH2 complexes in a high throughput manner by exploiting host-guest interactions and NIL. Features as small as 80 nm where the LH2 complexes specifically bind were created. Multivalent binding of the membrane protein is demonstrated by displacement of the monovalent AdHEG as was shown in the fluorescent titration measurements. Moreover, we presented clear spectral evidence that the fluorescence emission of the LH2 complexes remains unaltered upon chemical modification and patterning on the surface, which clearly indicated the preserved biological activity of the complex. In situ characterization of the formation of these assemblies at molecular dimensions and the fabrication of mixed protein arrays will be the subject of future research.

3.5 ACKNOWLEGEMENTS

We are grateful to the Nanotechnology Network in The Netherlands (NanoNed), project 7124 for financial support. Also we are grateful for financial support from the Council for Chemical Sciences of the Netherlands Organization for Scientific Research (NWO-CW) (P.M.; Vidi Vernieuwingsimpuls grant 700.52.423 to J.H.). C.N.H. and J.D.O. gratefully acknowledge the funding of the BBSRC UK. R.

3.6 REFERENCES

1. Mulder, A.; Onclin, S.; Péter, M.; Hoogenboom, J. P.; Beijleveld, H.; Maat, J. T.; García-Parajó, M. F.; Ravoo, B. J.; Huskens, J.; Van Hulst, N. F.; Reinhoudt, D. N., Molecular printboards on silicon oxide: Lithographic patterning of cyclodextrin monolayers with multivalent, fluorescent guest molecules. *Small* **2005,** 1, (2), 242-253.
2. Ludden, M. J. W.; Reinhoudt, D. N.; Huskens, J., Molecular printboards: Versatile platforms for the creation and positioning of supramolecular assemblies and materials. *Chemical Society Reviews* **2006,** 35, (11), 1122-1134.
3. Huskens, J., Multivalent interactions at interfaces. *Current Opinion in Chemical Biology* **2006,** 10, (6), 537-543.

4. Kham, K.; Guerrouache, M.; Carbonnier, B.; Lazerges, M.; Perrot, H.; Millot, M. C., Supramolecular interactions between β-cyclodextrin and hydrophobically end-capped poly(ethylene glycol)s: A quartz crystal microbalance study. *Journal of Colloid and Interface Science* **2007,** 315, (2), 800-804.
5. Nijhuis, C. A.; Huskens, J.; Reinhoudt, D. N., Binding control and stoichiometry of ferrocenyl dendrimers at a molecular printboard. *Journal of the American Chemical Society* **2004,** 126, (39), 12266-12267.
6. Hunter, C. N.; Tucker, J. D.; Niederman, R. A., The assembly and organisation of photosynthetic membranes in Rhodobacter sphaeroides. *Photochemical and Photobiological Sciences* **2005,** 4, (12), 1023-1027.
7. Scheuring, S.; Seguin, J.; Marco, S.; Lévy, D.; Breyton, C.; Robert, B.; Rigaud, J. L., AFM characterization of tilt and intrinsic flexibility of Rhodobacter sphaeroides light harvesting complex 2 (LH2). *Journal of Molecular Biology* **2003,** 325, (3), 569-580.
8. Bahatyrova, S.; Frese, R. N.; Van Der Werf, K. O.; Otto, C.; Hunter, C. N.; Olsen, J. D., Flexibility and size heterogeneity of the LH1 light harvesting complex revealed by atomic force microscopy: Functional significance for bacterial photosynthesis. *Journal of Biological Chemistry* **2004,** 279, (20), 21327-21333.
9. Sundström, V.; Pullerits, T.; Van Grondelle, R., Photosynthetic light-harvesting: Reconciling dynamics and structure of purple bacterial LH2 reveals function of photosynthetic unit. *Journal of Physical Chemistry B* **1999,** 103, (13), 2327-2346.
10. Reynolds, N. P.; Janusz, S.; Escalante-Marun, M.; Timney, J.; Ducker, R. E.; Olsen, J. D.; Otto, C.; Subramaniam, V.; Leggett, G. J.; Hunter, C. N., Directed formation of micro- and nanoscale patterns of functional light-harvesting LH2 complexes. *Journal of the American Chemical Society* **2007,** 129, (47), 14625-14631.
11. Escalante, M.; Maury, P.; Bruinink, C. M.; van der Werf, K.; Olsen, J. D.; Timney, J. A.; Huskens, J.; Hunter, C. N.; Subramaniam, V.; Otto, C., *Nanotechnology* **2008,** 19, 025101.
12. Onclin, S.; Mulder, A.; Huskens, J.; Ravoo, B. J.; Reinhoudt, D. N., Molecular printboards: Monolayers β-cyclodextrins on silicon oxide surfaces. *Langmuir* **2004,** 20, (13), 5460-5466.
13. Ludden, M. J. W.; Mulder, A.; Tampé, R.; Reinhoudt, D. N.; Huskens, J., Molecular printboards as a general platform for protein immobilization: A supramolecular solution to nonspecific adsorption. *Angewandte Chemie - International Edition* **2007,** 46, (22), 4104-4107.
14. Ludden, M. J. W.; Péter, M.; Reinhoudt, D. N.; Huskens, J., Attachment of streptavidin to β-cyclodextrin molecular printboards via orthogonal host-guest and protein-ligand interactions. *Small* **2006,** 2, (10), 1192-1202.
15. Olsen, J. D.; Robert, B.; Siebert, C. A.; Bullough, P. A.; Hunter, C. N., Role of the C-Terminal Extrinsic Region of the α Polypeptide of the Light-Harvesting 2 Complex of Rhodobacter sphaeroides: A Domain Swap Study. *Biochemistry* **2003,** 42, (51), 15114-15123.
16. Haneveld, J.; Berenschot, E.; Maury, P.; Jansen, H., Nano-ridge fabrication by local oxidation of silicon edges with silicon nitride as a mask. *Journal of Micromechanics and Microengineering* **2006,** 16, (6), S24-S28.
17. Maury, P.; Péter, M.; Mahalingam, V.; Reinhoudt, D. N.; Huskens, J., Patterned self-assembled monolayers on silicon oxide prepared by nanoimprint lithography and their applications in nanofabrication. *Advanced Functional Materials* **2005,** 15, (3), 451-457.
18. Kassies, R.; Van Der Werf, K. O.; Lenferink, A.; Hunter, C. N.; Olsen, J. D.; Subramaniam, V.; Otto, C., Combined AFM and confocal fluorescence microscope for applications in bio-nanotechnology. *Journal of Microscopy* **2005,** 217, (1), 109-116.
19. Molecular Probes, Invitrogen Corporation, Carlsbad, CA.
20. Kannan, B.; Castelino, K.; Chen, F. F.; Majumdar, A., Lithographic techniques and surface chemistries for the fabrication of PEG-passivated protein microarrays. *Biosensors and Bioelectronics* **2006,** 21, (10), 1960-1967.

Chapter 4

Long-Range Energy Propagation in Nanometer Arrays of Light Harvesting Antenna Complexes*

In this chapter we report the first observation of long-range transport of excitation energy within a bio-mimetic molecular light-guide constructed from LH2 antenna complexes from Rhodobacter sphaeroides, organized vectorially into functional nanoarrays. Fluorescence microscopy of the emission of light after local excitation with a diffraction-limited light beam reveals long-range transport of excitation energy over micrometer distances, which is much larger than required in the parent bacterial system. The transport was established from the influence of active energy-guiding layers on the observed fluorescence emission. We speculate that such an extent of energy migration occurs as a result of efficient coupling between many hundreds of LH2 molecules. These results demonstrate the potential for long-range energy propagation in hybrid systems composed of natural light harvesting antenna molecules from photosynthetic organisms.

* This chapter has been submitted for publication as: Maryana Escalante, Aufried Lenferink, Yiping Zhao, Niels Tas, Jurriaan Huskens, C. Neil Hunter, Vinod Subramaniam and Cees Otto. Long-Range Energy Propagation in Nanometer Arrays of Light Harvesting Antenna Complexes.

4.1 INTRODUCTION

The capability to manipulate bio-molecules with nanometer precision on surfaces in a massively parallel fashion is an important strategy to create complex novel hybrid structures with physical and chemical[1] properties and performance beyond those currently envisioned in, for example, energy storage and optical applications. In this context, purified components of photosynthetic organisms have been proposed as molecules for integration in solid-state electronic devices,[2] for the creation of patterned fluorescent nanoarrays,[3-4] and for application in sensing devices.[2, 5-6] The nanomachinery of the photosynthetic bacterium *Rhodobacter (Rb.) sphaeroides* has been a valuable model and object of many studies for diverse aspects of biophysics, biochemistry and molecular biology. Such studies span a wide range of topics, including bacteriochlorophyll (BChl) biosynthesis, membrane assembly, secondary electron transfer, molecular genetics, reaction center structure and photochemistry, and light harvesting structure, mutagenesis and spectroscopy.[7] Although a large variety of photosynthetic organisms exist, which can be distinguished by their typical light harvesting antennas and electron transport system, they have in common basic principles of energy transport. The photosynthetic antenna-protein complexes collect solar energy and transfer electronic excitation energy to the photosynthetic reaction center (RC), where charge separation occurs.[8] In *Rb. sphaeroides* the antenna LH2 complex is built of 9 identical subunits each consisting of an α and a β polypeptide. The LH2 α polypeptides form an inner ring surrounded by the β ring. In total 27 BChl molecules are bound to this structure of which 18 BChl make up the B850 system and 9 BChl interact to form the B800 system.[9] The LH2 complex has dimensions of ~7 nm in height and ~7 nm in diameter.[10] In *Rb. sphaeroides* LH2 transfers energy to the RC via the LH1 complex, which surrounds the RC. The $(RC\text{-}LH1\text{-}PufX)_2$ dimer complex consists of 28 αβ protomers and 56 B875 Bchls, the dimensions of which are ~11.5 x 23 nm and ~9.4 nm in height.[11-12] The purified components of the photosynthetic unit are interesting candidates for the fabrication of photonic structures in nanotechnology which might find applications in synthetic light converting constructs because of their well defined optical properties, such as a broad spectral range, high absorption cross section, efficient energy transfer and high photo-stability.[13-14]

The unique capability of light harvesting molecules to efficiently guide energy to the reaction center has been extensively investigated.[14-16] In particular the very early events in energy transfer from carotenoids to the B800 and B850 ring systems has been well established.[17] It has been proposed that typically within ~100 picoseconds[18-19] an excitation arrives at the special pair in the reaction center.

The actual organization of bacterial photosynthetic membranes has been revealed by AFM.[20-22] Although significant variation in organization occurs, it was observed that close connections between LH2 and LH1 occur most frequently.[20] It can therefore be concluded from the high resolution AFM data that the distances for excitons to travel are generally small and of the order of 4 nm for nearest neighbor complexes and up to 50 nm for extended systems, e.g. such as bacterial photosynthetic vesicles.[19] So, although LH2 and LH1 have exquisite properties for light transport, it is by no means obvious that these systems are suitable for long-range energy transport.

In this work, we report for the first time the direct observation of long-range transport in synthetic nanometer arrays of natural light harvesting antenna LH2 from *Rb. sphaeroides*. The arrays are ~80 nm wide and several microns in length. We emphasize in particular the extremely long-range energy transport that we observe in a significant fraction of photonic events. We used two different LH2 assemblies for energy propagation experiments: LH2-only lipid reconstituted 2D crystals and engineered quasi-1D nanometer arrays of LH2 fabricated on chemically functionalized substrates. Our experimental far-field optical results with an excitation wavelength of 800 nm show that energy is transported away from the excitation point "guided" by the ordered natural antennas. The analysis examines the influence of active energy-guiding layers on the observed Point Spread Function (PSF_{obs}) of fluorescence emission (Figure 4.1). In the absence of light transport, a narrow diffraction limited PSF_{obs} results, while in the presence of transport the PSF_{obs} is broadened by molecular transport of excitons, which causes the emission of light at a distance away from the excitation point. We selected LH2 crystals of sufficient size (> 4 μm), much larger than the size of the point spread function (PSF_{ill}) of the focused laser beam (0.45 μm). Such crystals can be considered as two-dimensional light-harvesting arrays. The PSF_{obs} appears as a circular profile due to this 2D arrangement. In engineered 80 nanometer wide line-arrays the PSF_{obs}

follows the geometry of the lines. For measurements under ambient oxygen concentration a decrease was observed in the extent of energy transport compared to the extent of transport in the absence of oxygen.

4.2 MATERIALS AND METHODS

LH2 nanometer arrays: For the fabrication of nanometer arrays of LH2 complexes we used a recently reported approach based on a combination of site-directed mutagenesis, nanoimprint lithography (NIL) and multivalent host-guest interactions.[23] Materials, Protein purification and labeling, substrate patterning and functionalization were performed as described in chapter 4. A representation of the host, guest and targets molecules is shown in Chart 4.1.

Chart 4.1. *Representation of host, guest and target molecules.*

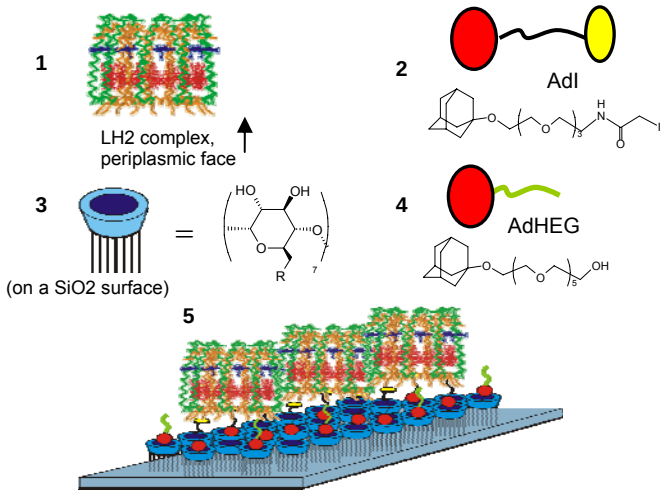

1 Representation of LH2 complex with the periplasmic face pointing down. 2(AdHEG), 3 iodoacetyl-tri(ethylene glycol)) mono(adamantyl ether), (AdI), 3 β-CD heptamine, host molecule, 4 Hexa(ethylene glycol)mono(adamantyl ether), 5 Ad_nLH2 on the β-CD monolayer.

LH2 crystals*:* The LH2 complexes were solubilized from membranes from photosynthetically grown *Rb. sphaeroides* using 4% *N*,*N*-Dimethyldodecylamine-*N*-oxide (LDAO), and purified on DEAE (Sigma) and Resource Q (GE Healthcare) columns, then size fractionated on a Superdex 200 gel filtration column (GE Healthcare). The mutagenesis protocol has been described before.[24] LH2 complexes were crystallized as described in Walz et al.[25]

NIL was used to chemically pattern substrates with active β-CD monolayers to specifically bind Ad_nLH2. The complementary areas have been passivated with polyethylene glycol.[26] NIL was performed using stamps with silicon ridges as small as 40 nm and a 4 μm period.[27] The assembly on the patterned surface is depicted in block 5, Chart 4.1.

Characterization: We used a custom-built hybrid scanning probe-spectral microscope (Atomic Force Fluorescence Microscope, AFFM)[28] to characterize the antenna arrays in liquid conditions. For AFM imaging standard silicon nitride cantilevers with a length of 85 μm, force constant of 0.5 N/m, and resonance frequency between 25–35 kHz in liquid (ThermoMicroscopes, Sunnyvale, CA) were used. AFM images were obtained using tapping mode. Images contained 512x512 pixels and were recorded at a line scanning frequency of 2–4 Hz. Topographical images were quantitatively analyzed using the Scanning Probe Image Processor (SPIP) software (Image Metrology ApS, Lyngby, Denmark). Fluorescence spectral microscopy was performed using 800 nm light from a diode laser (Roithner Laser Technik, RLT80010MG), at excitation powers below the threshold for annihilation.[29] The laser beam is reflected from the dichroic beam splitter (Chroma, Q850LPXXR) towards an oil-immersion objective (Nikon, Plan Fluor 100 ×, NA=1.3), which focuses the light onto the sample. The fluorescence light is collected by the same objective and passes through the dichroic beam splitter. Two foldable mirrors direct the fluorescence light either towards a single photon counting avalanche photodiode (APD) (SPCM-AQR-14, Perkin Elmer Optoelectronics), or towards a custom designed prism-based spectrograph with single molecule sensitivity equipped with a liquid nitrogen-cooled CCD camera (Spec-10:100B, Princeton Instruments), or to a direct-imaging branch to record the image of the photoemission on a CCD camera (Pixis 400, Princeton Instruments). The imaging optics was designed such that ~50 nm in object space (x- and y-direction) corresponded with one pixel (20 x 20 μm) on the camera.

The concept of the experiment for direct observation of energy propagation on the LH2 structures is depicted in Figure 4.1. The pattern of the fluorescent emission, represented by the orange area, is collected on the CCD camera of the imaging branch, and compared with the PSF_{obs} of the laser beam reflected from a passive surface, represented by the blue colored area. For a 2D structure such as the LH2-

only 2D crystal (Figure 4.1a) it is expected that energy will propagate radially away from the excitation area as indicated by the green arrows. In geometrically confined structures, such as line-arrays of LH2 complexes, with a width much smaller than the PSF_{ill} of the laser beam as shown in Figure 4.1b, excitonic transport will be confined by the specific geometry of the array. The accuracy of far field fluorescence microscopy in determining the point-spread function is only dependent on the signal-to-noise ratio of the acquired PSF_{obs} and is therefore perfectly able to detect and determine the extent of excitation transfer.

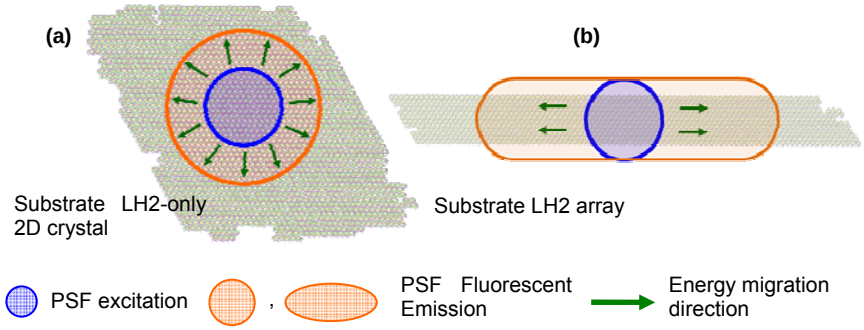

Figure 4.1. *Schematic representation of different LH2 substrates used for energy migration experiments: (a) LH2-only 2D crystal, (b) nanometer array of LH2 complexes. The figure depicts how upon local excitation (PSF_{ill}: blue area, not to scale with respect to LH2 molecules), the PSF_{obs} of the fluorescent emission (orange area) varies depending on the geometry of an active guiding layer. For crystals the fluorescent emission spreads isotropically along the surface; however on the nanometer line-arrays the propagation follows the structure of the molecular organization.*

4.3 RESULTS AND DISCUSSION

Figure 4.2a, 4.2b show AFM height images in liquid of Ad_nLH2 complexes on a β-CD SAM. The mean FWHM of the lines after processing is 80 ± 5 nm with a height of ~ 7 ± 1 nm, (Figure 4.2e), consistent with the assembly of a monolayer of LH2 complexes. Figure 4.2c shows a fluorescence image of the engineered nano-line-arrays with a uniform intensity distribution along the lines (standard deviation of 4%). The sample was spectrally characterized in each pixel. Quantitatively, the spectral response from the immobilized Ad_nLH2 complexes, Figure 4.2f, showed no visible shift of the emission maximum at ~868 nm (filled black squares), with respect to bulk measurements of non-modified LH2 complexes indicated by the gray

filled area. We conclude that the structural integrity of the LH2 membrane proteins is preserved by this method of patterning. We also selected LH2 2D crystals for energy transport experiments. Figure 4.2d shows an AFM topography image of 2D LH2 acquired under physiological conditions, while a higher resolution image of the crystal shows the periodic arrangement of the LH2 complexes (Figure 4.2g).

4.3.1 LH2 nanoarrays and 2D crystals

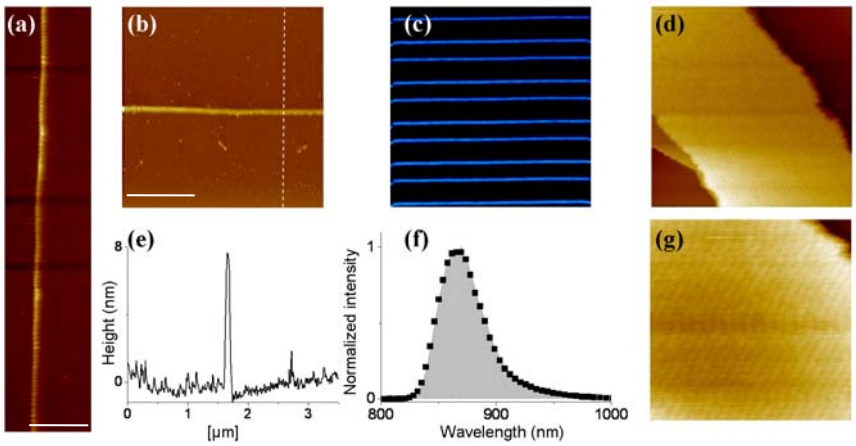

Figure 4.2. *(a), (b) AFM topography in liquid of patterned Ad_nLH2 on β-CD/PEG SAM (scale bar 1 µm), and the respective cross section (e) indicated by the white dotted line in panel (b). (c) False color fluorescent image of patterned Ad_nLH2 β-CD/PEG SAM, frame size 39 x 39 µm. (f) Fluorescence emission spectrum from patterned Ad_nLH2 (black squares) compared to LH2 in solution, filled gray area (d) Example of LH2-only 2D crystal, frame size 624 x 624 nm, (g) zoom-in from panel (d) (120 x 120 nm) that shows the packing of LH2 proteins in the crystal.*

4.3.2 Imaging energy propagation by fluorescence microscopy

To detect energy migration in the LH2 assemblies we proceeded to image the fluorescence emission after resonant excitation with laser light of 800 nm. Similar to the situation in the photosynthetic bacterial membrane these molecular antennas are able to transfer energy to neighboring molecules. Figure 4.3 shows false color confocal fluorescence images of the different LH2 structures and the corresponding image of the PSF_{obs} acquired with the direct imaging camera. LH2 crystal substrates were prepared by adsorbing 1 µl of sample solution onto the surface of amino functionalized glass coverslips for ~ 2 minutes, followed by rinsing with MilliQ

water in order to remove weakly bound crystal patches. The sample was immediately placed onto the AFFM stage and kept in liquid condition for imaging. A confocal fluorescence image of the 2D-LH2 crystals was acquired in order to locate their position on the glass support (Figure 4.3a). Subsequently, the laser beam was parked on a crystal and the fluorescence emission was imaged on the global imaging CCD-camera (Figure 4.3b) As a reference, we also measured the PSF_{ill} of the laser beam from an inactive substrate, such as bare glass or a bleached LH2 crystal. For bleaching a section of the LH2 crystal the laser beam was parked on the crystal until no LH2 fluorescence emission was detected in the spectrograph. A confocal image of the latter structure is presented in Figure 4.3c. The laser PSF_{obs} is displayed in Figure 4.3d. No difference was observed between the PSF_{obs} of the laser beam on a bleached LH2 crystal with respect to the PSF_{obs} on a glass-only area (FWHM 400 ± 50 nm). This observation indicates that the difference in dimensions and shape of the PSF_{obs} measured on an active light-guiding layer is evidence of energy migration on the layer, ruling out contributions from scattering of the monolayers and LH2 molecules. Global imaging of the PSF_{obs} was also performed on nanometer arrays of Ad_nLH2 complexes, (Figure 4.3e, 4.3f). From Figure 4.3f, it can be observed that the fluorescence emission upon local excitation of the array becomes elongated and follows the architecture of the patterned protein nanoarray.

Figure 4.3g shows the intensity profiles of the PSF_{obs} measured along the y-direction on the different substrates. The blue circles ○ indicate the laser beam PSF_{obs}, the red squares □ the PSF_{obs} on a 2D-LH2 crystal, and the green diamond ◊ the intensity profile corresponding to the PSF_{obs} on a nanometer array of LH2 complexes. These graphs were acquired at a laser intensity of 370 nW (measured at the back aperture of the objective). The measured diffraction limited spot size of the laser beam has a FWHM of 400 nm ± 50 nm (Figure 4.2d). Since the dimension of the LH2 line-array is approximately 80 nm in the y-direction, Figure 4.2f, it is observed with the same diffraction limited width of 400 nm ± 50 nm. For the case of the 2D-LH2-crystal the fluorescence emission has a FWHM of ~ 900 nm ± 50 nm. The PSF_{obs} in the x-direction for the 2D crystals and the laser beam is similar to that in the y-direction as can be observed in Figure 4.3h. We conclude that energy migration results in a considerable broadening of the PSF_{obs} in the 2D-LH2 crystals.

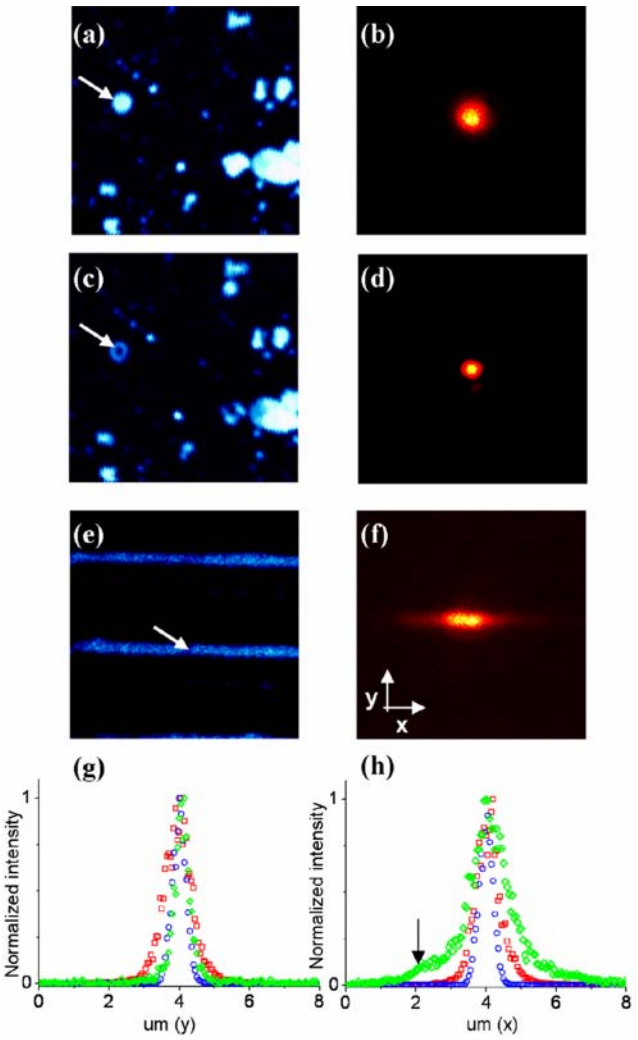

Figure 4.3. *False color fluorescence confocal images of different LH2 substrates, left, 128 x 128 pixels, P=1.8 μW (a, c) 40 x 40 μm, (e) 9 x 9 μm. PSF_{obs} of the fluorescence emission, right, (b, d, f frame size 160 x 160 pixel, 8 x 8 μm) upon local excitation and their respective profile in y and x-directions (g, h). (a, b) LH2-only 2D crystals. (c, d) Reference PSF_{obs} laser beam upon prolonged exposure of the previous crystal. (e, f) bioengineered LH2-only nanoarray. (g) Profile of the fluorescence emission in y- and (h) in x-direction, the arrow indicates events 2μm away from the center of the excitation point, LH2-only 2D crystals, red squares □; laser, blue circles ○; LH2 nanometer arrays, green diamond ◊.*

A higher degree of energy transport is evident in the nanopatterned line-array of LH2 complexes. The intensity profile in the x-direction is depicted in Figure 4.3h.

The FWHM of the PSF_{obs} of the nanometer arrays of LH2 upon local excitation increases to 1200 nm. Closer inspection of the emission profile reveals emission beyond 2 μm, indicated by the arrow in Figure 4.3h, from the average excitation point. If excitonic transport can be described as diffusional transport[a] in the quasi-one dimensional line-array with a stepsize of ~ 6.8 nm, which is the diameter of an LH2 antenna protein, this would suggest that approximately $(2000/6.8)^2 \sim 8.6 \times 10^4$ steps are made before the excitation is spontaneously emitted from the assembly. The fluorescence lifetime, τ_{fl}, of the emission of single LH2 complexes is approximately 1 to 1.5 ns.[29-30] If this lifetime also holds for the whole assembly we have to assume that the transfer time of the excitation between individual pairs of LH2 molecules is of the order of 15 femtoseconds in a considerable fraction of all transfer events. It has been difficult to determine LH2-LH2 transfer times directly, however a recent 3-photon echo experiment reported a transfer time of ~ 5 ps[31] which is within the range of existing theoretical estimates.[32] This contradictory result may indicate that not only diffusional transport plays a role, but also that more unidirectional transport events are prominent, for instance by coherent transport processes.

Moment analysis of the intensity distribution along the LH2 assemblies was performed to facilitate a quantitative comparison of the extent of the energy migration in relation to the intensity distribution of the laser excitation beam. First, second and third central moments were calculated according to equation 1 to compare the extent of transport in different experiments.

$$\mu_n(a) = \sum_i (x_i - a)^n P(x_i)$$

equation 1

where $\mu_n(a)$ is the n[th] order moment around the maximum intensity centered in pixel a, x_i is the displacements in pixels from a, and $P(x_i)$ is the respective intensity value in the pixel x_i. We used the normalized ratio $\mu_n(a)_{LH2assemblies}/\mu_n(a)_{Laser}$. The higher order moments in the moment analysis of the intensity profile are most

[a] $\left\langle X^2(n) \right\rangle = dn\varepsilon^2$, with d the dimension (1, 2..,), n the number of steps, ε the step size (6.8 nm for LH2).

prominent when the extent of the energy transport increases. The central moments ratios are presented in Table 1.

Table 1. Ratio $_n(a)_{LH2assemblies}$ / $\mu_n(a)_{Laser}$ in x- and y-direction (x, y)

	$\mu_n(a)_{LH2assemblies}$ / $\mu_n(a)_{Laser}$		
	$\mu_1(x,y)$	$\mu_2(x,y)$	$\mu_3(x,y)$
LH2-only 2D crystal	1.8, 1.7	2.3, 2.0	1.3, 1.2
LH2 nanometer array	3.4, 1.0	6.1, 1.0	5.8, 1.0

n = 1, 2, 3.

In the x-direction, for the 2D-LH2 crystals, $\mu_2 > \mu_1$, and are 2.30 and 1.80 respectively. The deviation from "one" indicates a broadening of the emission-PSF upon illumination of the 2D-crystals. Although the third moment μ_3 has a lower value than the 2nd- and 1st-moment, the clear difference from "one" indicates significant long-range energy transport. A more dramatic effect is observed for the nanometer line-arrays. The magnitudes of the first 3 moments are much larger for nanometer line-arrays of LH2 than for 2D-LH2 crystals, as displayed in Table 1. This apparent broadening of the PSF in the nanometer array of LH2 complexes with respect to that on the LH2-only 2D crystal can be attributed to the differences in arrangements of the individual LH2 complexes in the structures. Previously AFM has revealed differences in packing of the LH2 structures (zig-zag and up-down orientation and empty lipid regions)[33] which would influence the efficiency of the energy transfer process. The energy propagation results on the 1D nanometer LH2 complex arrays can serve as evidence that the host-guest patterning approach leads to tight packing of protein complexes, since this is a requirement for efficient energy propagation.

4.3.3 Oxygen influence on extent of energy transport.

It is well known[34-35] that the presence of oxygen affects the integrity of BChl molecules either through triplet state formation and subsequent oxidation by singlet oxygen or through direct oxidation of excited state BChl.[36-37] We have investigated the extent of energy transport in the presence of ambient concentrations of oxygen with the expectation that this would significantly reduce exciton transport in arrays

of light harvesting complexes. The oxygen level was reduced by nitrogen flushing to a level not detectable with an electrolytic oxygen meter (0,01 mg/L, Cyberscan 110, Eutech Instruments, Nijkerk, The Netherlands).

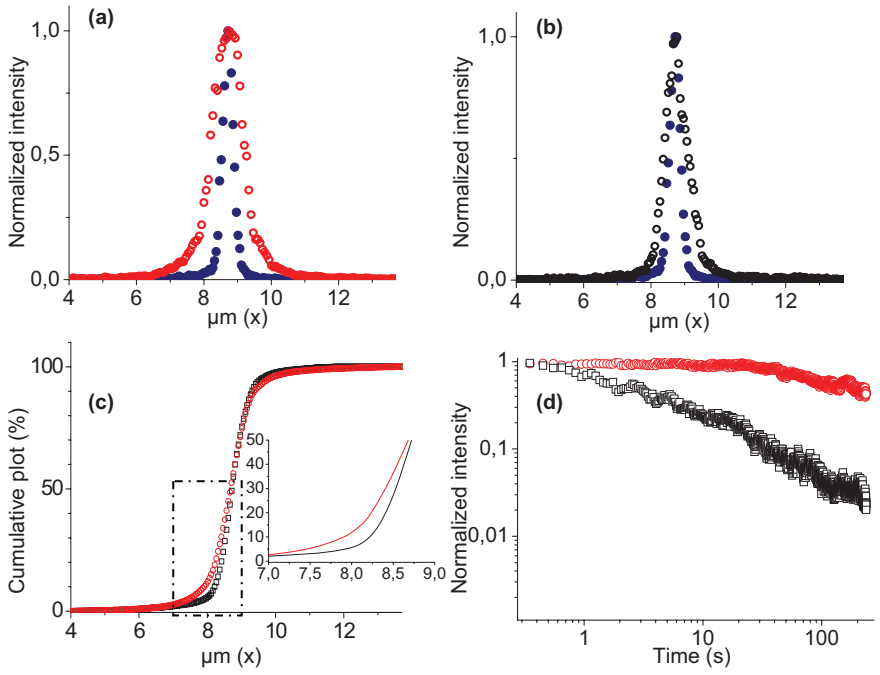

Figure 4.4. *PSF_{obs} on nanometer arrays of Ad_nLH2 compared with the PSF_{ill}, excitation power (•) 80 nW. (a) Oxygen reduced ○, (b) Ambient oxygen concentration o. (c) Cumulative intensity plot of the intensity of the PSF_{obs}, the inset indicates the significant shortening in distance by the presence of oxygen in the buffer. (d) Fluorescence time trace on the nanometer arrays of Ad_nLH2, in oxygen (empty black squares, □) and oxygen reduced (empty red circles, ○)*

Figure 4.4 a,b show the result of the broadening of the fluorescence emission on nanometer arrays of LH2. The measurements were performed in both ambient concentration of dissolved oxygen in the buffer and in de-oxygenated buffer respectively. The FWHM measured on the nanometer arrays of LH2 complexes is 1.1 ± 0.1 µm when measured in de-oxygenated buffer (Figure 4.4a, red circles, •) as compared to 0.4 µm for a reflected beam (blue circles, •). In ambient dissolved oxygen conditions, the FWHM of PSF_{obs} is 0.7 ± 0.1 µm (Figure 4.4b, black circles, •). A cumulative intensity plot of the PSF_{obs}, Figure 4.4c, indicates that

approximately 10 % of the energy propagation events occur at a distance up to 1260 nm from the center of the excitation beam in the absence of oxygen. In the presence of oxygen this distance shortens to 700 nm. The effect of oxygen is further exemplified in Figure 4.4d, which shows fluorescence timetraces on nanometer line arrays in the absence (red) and presence (black) of oxygen at low excitation power. From the curve it can be observed that photobleaching in the absence of oxygen is absent up to about 20 s. It can be concluded that bleaching does not affect the fluorescence images (Figure 4.3), which are acquired in 100 ms.

4.3.4 Controlling direction of energy propagation by introducing defects in the arrays.

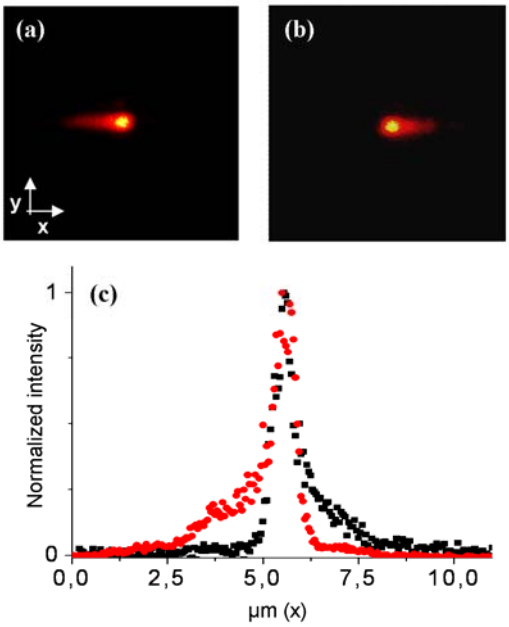

Figure 4.5. *The effect of defect areas on energy propagation. PSF_{obs} of the fluorescence emission when the excitation laser beam is positioned at the (a) left or (b) right of defect area (created by photobleaching), energy migration follows the direction of the line. (c) Intensity distribution from panel (a) filled red circles ●, left and (b), filled black squares ■, right.*

By selectively creating optical interruptions for the excitonic transport on the patterned nanoarrays, we could observe directionality in the propagation direction. The laser line was parked on an array of LH2 and defects (dimensions of few

hundred nanometers corresponding to the size of the confocal spot) were created by prolonged exposure to the laser beam in order to hamper the energy migration process through those areas. We then proceeded to excite the nanometer array by placing the beam slightly to the left and to the right of the induced defect with the scan stage. The images of the fluorescence emission PSF_{obs} on the arrays are shown in Figure 4.5a and 4.5b respectively. Figure 4.5c shows the intensity profile along the patterned arrays. From the profiles a directional propagation of energy can be clearly observed, as light does not propagate through the defect area. Transport in either direction can be observed just depending on which side of the defect area the antenna array is excited. The red circles • show the case of illumination on the left and propagation to the left and the opposite direction is observed when the laser beam is placed towards the right of the defect, as is illustrated by the filled black square curve ■ in Figure 4.5(c).

4.4 CONCLUSIONS

In summary, we report the direct observation of long-range energy migration in bioengineered, closely packed arrays of LH2 antenna complexes. The spatial extent of transport was determined by an analysis of the PSF of the fluorescence emission and comparison with the PSF of the excitation laser beam. Experimental data showed evidence of excitonic transport in 2D-LH2 crystals and on nanometer line-arrays of LH2 complexes. In comparison with the natural arrangement of the antenna complexes in photosynthetic organisms,[38] which does not require long-distance transport, we have observed unprecedented energy propagation distances on the bioengineered nanometer arrays. These results demonstrate the potential of using natural antennas from photosynthetic organisms in hybrid systems for long-range energy propagation. In a wider context, these results may have a profound impact on strategies to harvest and transport solar energy in devices for sustainable energy production. These concepts will be further explored in experiments which include more complex architectures and time-resolved optical measurements.

4.5 ACKNOWLEDGEMENTS

We thank the Nanotechnology Network in The Netherlands (NANONED), for financial support, project number 7124. M.E. thanks Dr. M. Ludden for the synthesis of the adamantyl compounds and Dr. J. Olsen for continued support.

4.6 REFERENCES

1. Govorov, A. O.; Carmeli, I., Hybrid structures composed of photosynthetic system and metal nanoparticles: Plasmon enhancement effect. *Nano Letters* **2007,** 7, (3), 620-625.
2. Das, R.; Kiley, P. J.; Segal, M.; Norville, J.; Yu, A. A.; Wang, L.; Trammell, S. A.; Reddick, L. E.; Kumar, R.; Stellacci, F.; Lebedev, N.; Schnur, J.; Bruce, B. D.; Zhang, S.; Baldo, M., Integration of photosynthetic protein molecular complexes in solid-state electronic devices. *Nano Letters* **2004,** 4, (6), 1079-1083.
3. Escalante, M.; Maury, P.; Bruinink, C. M.; van der Werf, K.; Olsen, J. D.; Timney, J. A.; Huskens, J.; Hunter, C. N.; Subramaniam, V.; Otto, C., Directed assembly of functional light harvesting antenna complexes onto chemically patterned surfaces. *Nanotechnology* **2008,** 19, (2), -.
4. Reynolds, N. P.; Janusz, S.; Escalante-Marun, M.; Timney, J.; Ducker, R. E.; Olsen, J. D.; Otto, C.; Subramaniam, V.; Leggett, G. J.; Hunter, C. N., Directed formation of micro- and nanoscale patterns of functional light-harvesting LH2 complexes. *Journal of the American Chemical Society* **2007,** 129, (47), 14625-14631.
5. Trammell, S. A.; Wang, L.; Zullo, J. M.; Shashidhar, R.; Lebedev, N., Orientated binding of photosynthetic reaction centers on gold using Ni-NTA self-assembled monolayers. *Biosensors and Bioelectronics* **2004,** 19, (12), 1649-1655.
6. Nakamura, C.; Hasegawa, M.; Nakamura, N.; Miyake, J., Rapid and specific detection of herbicides using a self-assembled photosynthetic reaction center from purple bacterium on an SPR chip. *Biosensors and Bioelectronics* **2003,** 18, (5-6), 599-603.
7. Hunter, C. N.; Daldal, F.; Thurnauer, M. C.; Beatty, J. T., *The Purple Phototropic Bacteria.* . Springer: Dordrecht, 2008; Vol. 28.
8. Vangrondelle, R.; Dekker, J. P.; Gillbro, T.; Sundstrom, V., Energy-Transfer and Trapping in Photosynthesis. *Biochimica Et Biophysica Acta-Bioenergetics* **1994,** 1187, (1), 1-65.
9. McDermott, G.; Prince, S. M.; Freer, A. A.; Hawthornthwaite-Lawless, A. M.; Papiz, M. Z.; Cogdell, R. J.; Isaacs, N. W., Crystal structure of an integral membrane light-harvesting complex from photosynthetic bacteria. *Nature* **1995,** 374, (6522), 517-521.
10. Scheuring, S.; Seguin, J.; Marco, S.; Lévy, D.; Breyton, C.; Robert, B.; Rigaud, J. L., AFM characterization of tilt and intrinsic flexibility of Rhodobacter sphaeroides light harvesting complex 2 (LH2). *Journal of Molecular Biology* **2003,** 325, (3), 569-580.
11. Fotiadis, D.; Qian, P.; Philippsen, A.; Bullough, P. A.; Engel, A.; Hunter, C. N., Structural Analysis of the Reaction Center Light-harvesting Complex I Photosynthetic Core Complex of Rhodospirillum rubrum Using Atomic Force Microscopy. *Journal of Biological Chemistry* **2004,** 279, (3), 2063-2068.
12. Qian, P.; Hunter, C. N.; Bullough, P. A., The 8.5 Å projection structure of the core RC-LH1-PufX dimer of Rhodobacter sphaeroides. *Journal of Molecular Biology* **2005,** 349, (5), 948-960.
13. Sundström, V.; Pullerits, T.; Van Grondelle, R., Photosynthetic light-harvesting: Reconciling dynamics and structure of purple bacterial LH2 reveals function of photosynthetic unit. *Journal of Physical Chemistry B* **1999,** 103, (13), 2327-2346.

14. Van Grondelle, R.; Novoderezhkin, V. I., Energy transfer in photosynthesis: Experimental insights and quantitative models. *Physical Chemistry Chemical Physics* **2006,** 8, (7), 793-807.
15. Pullerits, T.; Sundstrom, V., Photosynthetic light-harvesting pigment-protein complexes: Toward understanding how and why. *Accounts of Chemical Research* **1996,** 29, (8), 381-389.
16. Cogdell, R. J.; Gardiner, A. T.; Roszak, A. W.; Law, C. J.; Southall, J.; Isaacs, N. W., Rings, ellipses and horseshoes: how purple bacteria harvest solar energy. *Photosynthesis Research* **2004,** 81, (3), 207-214.
17. Herek, J. L.; Wohlleben, W.; Cogdell, R. J.; Zeidler, D.; Motzkus, M., Quantum control of energy flow in light harvesting. *Nature* **2002,** 417, (6888), 533-535.
18. Cogdell, R. J.; Gall, A.; Kohler, J., The architecture and function of the light-harvesting apparatus of purple bacteria: from single molecules to in vivo membranes. *Quarterly Reviews of Biophysics* **2006,** 39, (3), 227-324.
19. Şener, M. K.; Olsen, J. D.; Hunter, C. N.; Schulten, K., Atomic-level structural and functional model of a bacterial photosynthetic membrane vesicle. *Proceedings of the National Academy of Sciences of the United States of America* **2007,** 104, (40), 15723-15728.
20. Scheuring, S.; Sturgis, J. N.; Prima, V.; Bernadac, A.; Levy, D.; Rigaud, J. L., Watching the photosynthetic apparatus in native membranes. *Proceedings of the National Academy of Sciences of the United States of America* **2004,** 101, (31), 11293-11297.
21. Bahatyrova, S.; Frese, R. N.; Siebert, C. A.; Olsen, J. D.; van der Werf, K. O.; van Grondelle, R.; Niederman, R. A.; Bullough, P. A.; Otto, C.; Hunter, C. N., The native architecture of a photosynthetic membrane. *Nature* **2004,** 430, (7003), 1058-1062.
22. Scheuring, S.; Sturgis, J. N., Chromatic adaptation of photosynthetic membranes. *Science* **2005,** 309, (5733), 484-487.
23. Escalante, M.; Zhao, Y. P.; Ludden, M. J. W.; Vermeij, R.; Olsen, J. D.; Berenschot, E.; Hunter, C. N.; Huskens, J.; Subramaniam, V.; Otto, C., Nanometer arrays of functional light harvesting antenna complexes by nanoimprint lithography and host-guest interactions. *Journal of the American Chemical Society* **2008,** 130, (28), 8892-+.
24. Olsen, J. D.; Robert, B.; Siebert, C. A.; Bullough, P. A.; Hunter, C. N., Role of the C-Terminal Extrinsic Region of the α Polypeptide of the Light-Harvesting 2 Complex of Rhodobacter sphaeroides: A Domain Swap Study. *Biochemistry* **2003,** 42, (51), 15114-15123.
25. Walz, T.; Jamieson, S. J.; Bowers, C. M.; Bullough, P. A.; Hunter, C. N., Projection structures of three photosynthetic complexes from Rhodobacter sphaeroides: LH2 at 6 Å, LH1 and RC-LH1 at 25 Å. *Journal of Molecular Biology* **1998,** 282, (4), 833-845.
26. Kannan, B.; Castelino, K.; Chen, F. F.; Majumdar, A., Lithographic techniques and surface chemistries for the fabrication of PEG-passivated protein microarrays. *Biosensors and Bioelectronics* **2006,** 21, (10), 1960-1967.
27. Zhao, Y.; Berenschot, E.; Jansen, H.; Tas, N.; Huskens, J.; Elwenspoek, M., Sub-10 nm silicon ridge nanofabrication by advanced edge lithography for NIL applications. *Microelectronic Engineering* **2009,** 86, (4-6), 832-835.
28. Kassies, R.; Van der Werf, K. O.; Lenferink, A.; Hunter, C. N.; Olsen, J. D.; Subramaniam, V.; Otto, C., Combined AFM and confocal fluorescence microscope for applications in bio-nanotechnology. *Journal of Microscopy-Oxford* **2005,** 217, 109-116.
29. Pflock, T.; Dezi, M.; Venturoli, G.; Cogdell, R. J.; Kohler, J.; Oellerich, S., Comparison of the fluorescence kinetics of detergent-solubilized and membrane-reconstituted LH2 complexes from Rps. acidophila and Rb. sphaeroides. *Photosynthesis Research* **2008,** 95, (2-3), 291-298.
30. Chen, X. H.; Zhang, L.; Weng, Y. X.; Du, L. C.; Ye, M. P.; Yang, G. Z.; Fujii, R.; Rondonuwu, F. S.; Koyama, Y.; Wu, Y. S.; Zhang, J. P., Protein structural deformation induced lifetime shortening of photosynthetic bacteria light-harvesting complex LH2 excited state. *Biophysical Journal* **2005,** 88, (6), 4262-4273.
31. Agarwal, R.; Rizvi, A. H.; Prall, B. S.; Olsen, J. D.; Hunter, C. N.; Fleming, G. R., Nature of disorder and inter-complex energy transfer in LH2 at room temperature: A three

pulse photon echo peak shift study. *Journal of Physical Chemistry A* **2002,** 106, (33), 7573-7578.
32. Ritz, T.; Damjanovic, A.; Schulten, K., The quantum physics of photosynthesis. *Chemphyschem* **2002,** 3, (3), 243-248.
33. Bahatyrova, S.; Frese, R. N.; van der Werf, K. O.; Otto, C.; Hunter, C. N.; Olsen, J. D., Flexibility and size heterogeneity of the LH1 light harvesting complex revealed by atomic force microscopy - Functional significance for bacterial photosynthesis. *Journal of Biological Chemistry* **2004,** 279, (20), 21327-21333.
34. Rutkauskas, D.; Novoderezkhin, V.; Cogdell, R. J.; van Grondelle, R., Fluorescence spectral fluctuations of single LH2 complexes from Rhodopseudomonas acidophila strain 10050. *Biochemistry* **2004,** 43, (15), 4431-4438.
35. Rutkauskas, D.; Novoderezhkin, V.; Cogdell, R. J.; van Grondelle, R., Fluorescence spectroscopy of conformational changes of single LH2 complexes. *Biophysical Journal* **2005,** 88, (1), 422-435.
36. Law, C. J.; Cogdell, R. J., The effect of chemical oxidation on the fluorescence of the LH1 (B880) complex from the purple bacterium Rhodobium marimum. *Febs Letters* **1998,** 432, (1-2), 27-30.
37. Bopp, M. A.; Sytnik, A.; Howard, T. D.; Cogdell, R. J.; Hochstrasser, R. M., The dynamics of structural deformations of immobilized single light-harvesting complexes. *Proceedings of the National Academy of Sciences of the United States of America* **1999,** 96, (20), 11271-11276.
38. Olsen, J. D.; Tucker, J. D.; Timney, J. A.; Qian, P.; Vassilev, C.; Hunter, C. N., The Organization of LH2 Complexes in Membranes from Rhodobacter sphaeroides. *Journal of Biological Chemistry* **2008,** 283, (45), 30772-30779.

Chapter 5

FRET Pair Printing of Fluorescent Proteins*

We report for the first time the directed assembly and characterization of FRET pairs on micrometer dimension patterned surfaces. We used visible fluorescent proteins expressing a hexahistidine affinity tag as component molecules for the construction of the FRET constructs, where His_6-EGFP served as donor fluorophore and His_6-DsRed-FT as the acceptor. We created 2D and 3D structures that exhibit Fluorescence Resonance Energy Transfer at the interfaces between the donor and acceptor patterns in the lateral or axial directions respectively. We quantitatively visualized the energy transfer by multiparameter optical microscopy.

* This chapter has been published in: Escalante, M.; Blum, C.; Cesa, Y.; Otto, C.; Subramaniam, V., FRET pair printing of fluorescent proteins. *Langmuir* **2009,** 25, (12), 7019

5.1 INTRODUCTION

The precipitous advances in micro- and nano-fabrication in parallel with biotechnology have given rise to a complex and exciting combined field, *bionanofabrication*, which enables innovative ways of building complex structures with biological functionality. Current research efforts are aimed at exploiting the intrinsic functionality of biomolecules to create new hybrid systems.[1] In this context, ordered arrays of protein molecules that can serve as donors and acceptors in an energy transfer pair are of clear interest for the fabrication of functional devices. Such complex arrays can open up possibilities to fabricate structures of energy transfer coupled systems that might prove useful in fundamental studies as well as in artificial light harvesting systems. While visible fluorescent (VFP) protein FRET (Förster *or* Fluorescence Resonance Energy Transfer) pairs have been exploited for studying dynamic biological processes, these proteins have largely been unexplored in the context of devices and micro- and nanostructured surfaces. Recent steps towards this goal have shown repeated photochromicity cycles in GFP mutants[2] which opens a door for including these molecules into high-density optical memories and switches,[3] demonstrating the potential of VFPs beyond their classical use in cellular biology, biochemistry and biotechnology.[4]

VFPs are well-suited for exploratory studies of surface immobilization and patterning, due to their structural robustness and intrinsic fluorescence that is characteristic of the structural integrity of the protein. All VFPs share a common cylindrical β-barrel monomer structure with diameter of 2.4 nm and height of 4.2 nm.[5-6] The fluorescent chromophore forms in the center of the protein in an autocatalytic process after transcription and folding of the protein.[7-8] The closely-packed structure is responsible for the protein's structural stability and high fluorescence efficiency because of the physical sequestration of the chromophore.[5-6, 9] Moreover, VFPs can be tailored by protein engineering to obtain mutants with enhanced photophysical properties[10-11] and to introduce binding sites for their directional assembly on chemically functionalized surfaces.

Previous research has shown different ways to pattern VFPs: Benedetto *et al*[12] used soft molding techniques to pattern GFP and EGFP entrapped in the microstructures of poly(acrylamide) gel (PAAG). Direct microcontact printing (μCP) of GFPs on non-functionalized surface has also been shown.[13] Control over

the immobilization has been achieved through supramolecular chemistry in combination with protein engineering, for example by the insertion of a hexahistidine (His_6) tag. The His tag binds to a nickel nitrilotriacetate (NiNTA) self-assembled monolayer.[14-15]

A prerequisite for the inclusion of biomolecules in hybrid structures is the preservation of their functional properties upon immobilization on the surface. In the case of photoactive molecules, such as in the case of VFPs, the corresponding optical signatures (spectra and lifetime information) should be studied and be quantified. As a complementary technique to conventional surface characterization techniques such as surface plasmons resonance (SPR),[16] x-ray microscopy,[17] and atomic force microscopy (AFM),[18] for fluorescent systems the availability of pulsed lasers and fast detection electronics for fluorescent lifetime imaging (FLIM) have given rise to new spectroscopic techniques that enrich the optical characterization toolbox (usually based on intensity and emission spectra). FLIM provides information about the fluorescence mechanism and the interaction with the local environment of the fluorophore.[19-20]

The robustness and efficient optical properties of VFPs[21] inspired us to use these protein building blocks in combination with microcontact printing techniques to go one step further and to pattern Förster energy transfer systems of VFPs. We demonstrate the potential of this approach by patterning the biological emitters EGFP (Förster donor) and DsRed-FT (Förster acceptor) engineered with a hexahistidine (His_6) tag on chemically functionalized NiNTA substrates. We use multiparameter imaging spectroscopy to show energy transfer in the lateral direction at the interface of the micro-patterned structures. We also show energy transfer in the axial direction by printing the Förster acceptor molecules directly on a Förster donor modified surface.

5.2 MATERIALS AND METHODS

***Materials**:* All chemicals were used as received. *N*-[3-(trimethoxysilyl)propyl]-ethylenediamine] (Aldrich), 1H,1H,2H,2H perfluoredecyltrichlroro silane (ABCR), N-[3-(trimethoxysilyl)propyl]-ethylenediamine (Aldrich), 1,4-phenylene diisothio-cyanate (Acros), N,N-bis(carboxymethyl)-lysine (Aldrich), $NiCl_2$ (Aldrich).

***Protein purification**:* Plasmids encoding for the His-tagged DsRed-FT and EGFP were transformed into Escherichia coli bacteria. Expression of the proteins was induced by 1 mM IPTG and the collected cells were lysed. Proteins were purified by binding on a nickel-NTA agarose resin and elution by 250 mM imidazole. The eluted fractions were dialyzed against 100 mM Tris-HCl, pH 8.0, 100 mM NaCl overnight.

***Substrate preparation**:* Substrates (microscope coverslips, Menzel-glaser # 1,5) were cleaned by immersion in piranha solution (3:1 concentrated H_2SO_4 / 33% aqueous H_2O_2) for 15 min, rinsed copiously with water and dried with a stream of N_2. *Warning: Piranha solution should be handled with care.* NiNTA monolayers were obtained similar as described elsewhere.[14] *N*-[3-(trimethoxysilyl)propyl] ethylenediamine] monolayer formation was performed by gas-phase evaporation in a desiccator under vacuum overnight, rinsed and sonicated with ethanol and dried with N_2. Transformation of the amine-terminated monolayer to isothiocyanate-terminated layers was accomplished by exposure to a 0.1 M solution of 1,4-phenylenediisothiocyanate in toluene at 50 °C for 2 h under N_2, followed by rinsing with toluene and drying with N_2. NTA monolayers were obtained by reaction of the isothiocyanate-terminated monolayers with a 2.5mM aqueous solution of N,N-bis(carboxymethyl)-l-lysine solution (10mM TRIS buffer, pH 8) at 50 °C for 4 h. The substrates were rinsed with Millipore water and gently dried in a stream of N_2. Samples were immersed in a 0.1M solution of $NiCl_2$ (10mM TRIS buffer, pH 8), to allow absorption of Ni^{2+} on the NTA SAM, during 10 min, rinsed with buffer and dried in a N_2 flow. Regeneration and reuse of the substrates was possible by rinsing with 1M imidazole, 250 mM EDTA, recharging with nickel ions, and subsequently attaching a second VFP.

Microcontact printing: PDMS stamps were prepared by casting a manually mixed 10:1 (v/v) of poly(dimethylsiloxane) and curing agent (Sylgard 184, Dow Corning) against a patterned silicon master. The stamps were cured overnight at 60 °C. Silicon masters fabricated by photolithography contained micrometer-sized features (hexagonally oriented 10 μm circular features separated by 5 μm) and treated with 1H,1H,2H,2H perfluoredecyltrichlorosilane to facilitate separation of the PDMS from the master.

The protein solution 1 μM was incubated on the PDMS stamp for 30 minutes at room temperature. Before printing, the stamps were blown dry in a stream of N_2. The stamp was brought into conformal contact with the substrate for 10 min onto the glass and then carefully removed. The substrates were rinsed with 10mM TRIS buffer, pH8 and kept in liquid environment for optical characterization.

Sample characterization: To characterize the spectral and lifetime of the emission of the patterned fluorescent proteins, we used a custom-built setup capable of wide-field fluorescence imaging as well as scanning-stage confocal microscopy for fluorescent lifetime and spectral imaging. The light sources used were a mercury lamp for wide-field fluorescence imaging, and a laser diode emitting at 469 nm modulated at 20 MHz (BDL475, Becker & Hickl, Germany) for local excitation when recording emission spectra and lifetime traces. The sample was illuminated using a 60x objective (60x, 1.2 numerical aperture, water immersion, Olympus), the emission from the sample was collected by the same objective. Wide-field images were recorded with a color camera (AxioCam HRc, Zeiss). For the emission images, a standard blue filter cube (U-MWB2, Olympus) was used. White balance was optimized for a halogen light temperature of 3200 K, in accordance with the manufacturer's recommendation for fluorescence imaging. We verified the consistency between the color camera image and the coloring visible in the eyepiece of the microscope. Contrast, brightness, and gamma were globally optimized for whole images, and no digital color-changing filters were applied. To record local emission spectra, a glass plate was used as beam splitter. The emitted light was imaged by a prism spectrometer onto a cooled CCD camera (Newton EMCCD DU970N-BV, Andor). Wavelength calibration was achieved using a calibrated light source (Cal-2000 Mercury Argon Calibration source, Ocean Optics). All pictures and spectra were recorded in epi-illumination. For fluorescence lifetime imaging a time correlated single photon counting (TCSPC) module (SPC-830, Becker & Hickl, Germany) attached to a single photon avalanche diode detector (PDM Series, MPD, Italy) was used. For recording the lifetime traces, in order to avoid crosstalk, a removable 510 nm bandpass filter (FF01-510/10-25, Semrock) was inserted in the detection path for the emission of the EGFP protein; a removable 590 nm longpass filter was inserted instead for the lifetime of the DsRed-FT. The lifetime data was analyzed using the Becker & Hickl SPCImage software package. No binning was

used in all cases to maximize resolution. The spectral and lifetime images were built by a matrix of 64 x 64 pixels with a step size of 700 nm.

***Bleaching experiments**:* For the axial FRET pair printing experiments, the red chromophore of DsRed-FT was selectively bleached by prolonged exposure of the sample through a standard green cube (G-2A, Nikon, λ = 510 – 560 nm). The sample was exposed until no red emission was detected with the imaging camera and with the spectrograph.

5.3 RESULTS AND DISCUSSION

5.3.1 EGFP (donor) and DsRed-FT (acceptor) molecules in an energy transfer pair

To explore the interaction between VFPs and their properties while immobilized onto chemically patterned substrates, we used purified EGFP and DsRed-FT as donors and acceptors in a FRET pair. The monomeric enhanced green fluorescent protein, EGFP (Figure 5.1, left), an optimized variant of the *Aequoria* GFP, emits in the green visible region (λ_{max} = 508 nm). DsRed-FT is a red emitting (λ_{max} = 590 nm) tetrameric reef coral fluorescent protein in which four cylindrical monomers form a dimer of dimers (Figure 5.1, right).[22] DsRed-FT is derived from DsRed by introducing the mutations Val105Ala, Ser197Thr, and is commercially available as Fluorescent Timer (DsRed-FT). The spectral overlap between the emission spectrum of EGFP and the absorption spectrum of DsRed-FT is good, yet the emission of the two proteins is spectrally well separated.

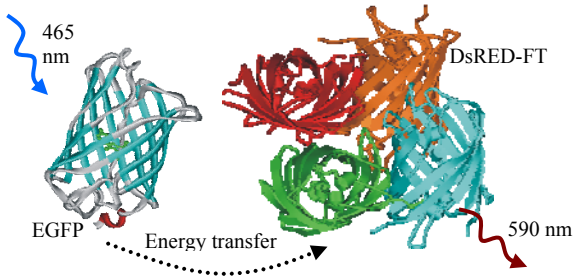

***Figure 5.1.** Structures of EGFP, a monomeric protein in which the chromophore forms in the center of a cylindrical barrel (left), and DsRed, a tetrameric protein in which four cylindrical monomers form a dimer of dimers (right).*

5.3.2 FRET at the interface of 2D structures

Microcontact printing was used for the patterning of micrometer-sized circular features of EGFP in a hexagonal arrangement. The diagram of the fabrication process is shown in Scheme 5.1. First the elastomeric PDMS stamp was incubated with 1 µM solution of EGFP in Tris buffer (pH8). After inking, the stamps were dried and put into conformal contact with the NiNTA modified glass substrate (Scheme 5.1b) and removed after 10 minutes (Scheme 5.1c). Subsequently, the exposure of the substrate to a 0.1 µM solution of DsRed-FT resulted in the selective assembly of the DsRed-FT on the EGFP-free areas. At the interface between the EGFP pattern and the backfilled DsRed-FT we expect that energy transfer will occur due to the molecular proximity of a suitable Förster donor and acceptor (Scheme 5.1d). This phenomenon is visible with lifetime resolution. The samples were kept in liquid environment for further characterization.

Scheme 5.1. *Representation of the patterning of EGFP and DsRed-FT on a NiNTA surface by µCP*

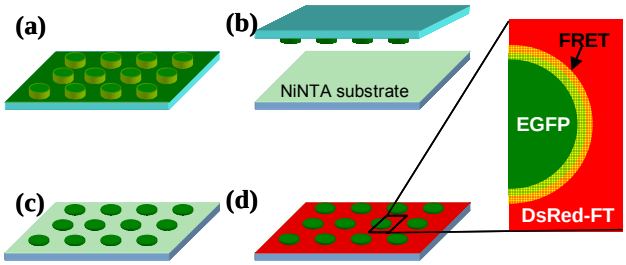

(a) PDMS stamp was inked with a protein solution of EGFP. (b) The PDMS stamp was brought into conformal contact with the substrate. (c) PDMS stamp is removed from the substrate, micrometer features in hexagonal arrays remain bound on the surface. (d) A solution of a second fluorescent protein, DsRed-FT is used to backfill the remaining areas. At the interfaces where the EGFP and DsRed-FT are in molecular proximity, energy transfer (FRET) can occur (inset).

To characterize the substrates, we used a custom-built setup capable of wide-field fluorescence imaging as well as scanning-stage confocal microscopy for fluorescent lifetime and spectral imaging. First, the patterned substrates were investigated with epifluorescence microscopy using a standard filter cube (λ = 460 - 490 nm) for true color imaging above 510 nm (Figure 5.2a). The patterned substrate showed a uniform and distinctive green emission of the EGFP on the dots array and the red emission of the DsRed-FT in the complementary areas. Moreover, spectral and

lifetime images of the patterned biological emitters were acquired to address their functionality and interaction with the surrounding medium. Therefore the sample was imaged three times: once for recording the decay curves of EGFP, a second time to record the decay curves of the DsRed-FT, and a last time to record the emission spectra over the whole sampled area. To separate the contributions from EGFP and DsRed-FT in the lifetime measurements, a bandpass filter centered at 510 nm was inserted in the detection path while recording the decay curves for the EGFP, and a longpass filter with a cut-on at 590 nm was inserted instead for the DsRed-FT decay curves.

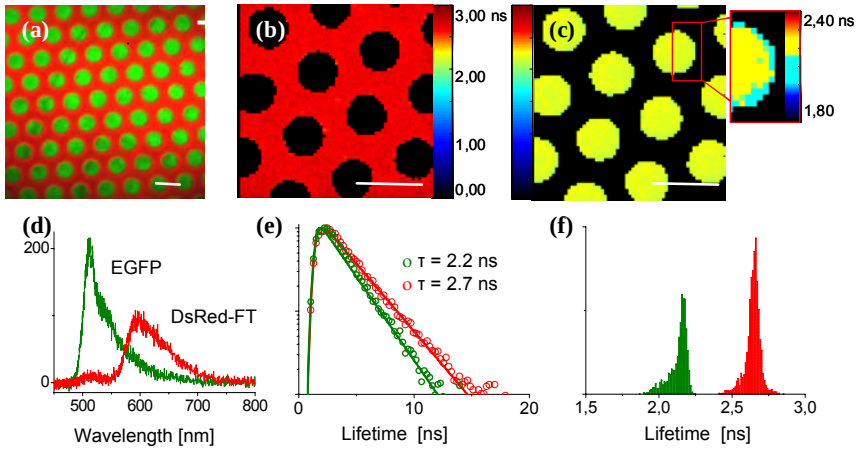

Figure 5.2. *Dual patterning of EGFP and DsRed-FT on NiNTA functionalized substrates. (a) True color widefield imaging of the VFPs micropatterned substrates, scale bar 15 µm. Lifetime imaging shows the distinctive areas and functionality of the two proteins, 45 x 45 µm, lifetime colorbar [ns] (b) Lifetime image DsRed-FT, 590 nm long pass filter, (c) Lifetime image EGFP, 510 nm bandpass filter, the inset shows the decrease in lifetime at the edges of the patterned areas that is at the interface between both fluorescent proteins. (Förster radius convolved with point spread function, PSF). (d) Typical emission spectra of EGFP maximum at ~ 509 nm, and DsRed-FT maximum at ~ 590 nm. (e), (f) typical decay curves and composite lifetime histograms of EGFP 2.20 ns (left), DsRed-FT 2.70 ns (right) as extracted from the images.*

For the spectral characterization, a glass plate was used as beam splitter in order to collect all the spectral information from the surface upon excitation with the 469 nm laser diode. Figure 5.3d shows representative spectra of the different areas corresponding to the EGFP (green curve) and DsRed-FT (red curve) respectively. The spectral response from the immobilized emitters showed neither cross

contamination nor visible shifts of their emission maxima with respect to bulk measurements in solution, ~ 509 nm for EGFP and ~ 590 nm for DsRed-FT. This observation provides strong evidence that the structural integrity of the protein has been preserved upon processing. The patterned proteins proved to be stable during the characterization of each sample (~ hours), consistent at different points of the sample at different time intervals, as expected in the absence of a competitive agent at high concentration.[15, 23] In the emission spectrum of the DsRed-FT, apart from the strong red emission band, a weak band is present around 508 nm, in the green region. This weak green emission is also observed in solution and originates from non-mature green emitting chromophores. The minor contribution of the green emitting chromophore of DsRed-FT to the total signal is neglected in the further analysis.

Lifetime images of the patterned EGFP and DsRed-FT are depicted in Figure 5.2 (b) and (c) respectively. The typical decay curves are shown in Figure 5.2e, and the lifetime distributions from the respective images in Figure 5.2f. Decay characteristics fitted well to a monoexponential decay function. Biexponential fits neither improved the χ^2 nor provided significant new lifetime components within the sampled areas. The histogram for EGFP shows a lifetime distribution centered around 2.20 ns and for DsRed-FT on 2.70 ns. No significant shift is observed in the main peak of the lifetime distribution, which also indicates that the cross-contamination between the different proteins is minimal. As expected, the lifetimes recorded for all proteins immobilized to glass surfaces were consistently shifted to lower values compared to lifetimes recorded in aqueous solution (in solution: EGFP 2.9 ns, DsRed-FT 3,7 ns). The decrease in lifetime is caused by the presence of the high refractive index material glass that we use as substrate for our samples. For fluorescent proteins the decrease of lifetime with increasing refractive index has been shown[24-25] while recently this effect has been used to sense the refractive index inside living cells.[26] The quantification of the reduction of the lifetime of the emitter due to FRET with its acceptor pair but also because of its interaction with the substrate is important for the design of hybrid energy migration systems because it provides insights, for example, in the relevant spatial length scales for energy propagation.

For DsRed-FT we find a monomodal distribution of lifetimes. In contrast to this observation, the distribution of lifetimes for the EGFP on the patterned substrates is clearly asymmetric with a decided tail on the short side of the lifetime axis. This asymmetry is absent for EGFP alone patterned on a surface, where the distribution can be approximated by a Gaussian. A decrease in lifetime of the FRET donor molecule EGFP in the presence of the acceptor is a clear sign for energy transfer, since energy transfer is a process competing with radiative deactivation. Thus lifetime imaging to detect FRET is a direct and robust method not suffering from complications like direct acceptor excitation and crosstalk between channels, as is often the case in traditional intensity-based measurements. We point out, however, that FRET could also be detected by detecting the sensitized acceptor emission accompanied by commensurate decrease in donor intensity. The decrease in lifetime (tail of the histogram, EGFP) is expected at the interface of the patterned structures where the two VFPs meet. In the inset of Figure 5.2b, by expanding the color scale, we can see that the lifetime is shorter at the edges of the patterned EGFP than at the center of the patterned region. This is a strong indication of FRET.

The energy transfer efficiency, *E*, is estimated to be around 7 % based on equation 1.

$$E = 1 - \frac{\tau_{DA}}{\tau_D} \qquad (1)$$

where τ_D is the lifetime of the donor and τ_{DA} is the lifetime of the donor in the presence of the acceptor. Although we expect high energy transfer efficiency at the meeting point between both proteins (few nanometers), we are sampling a confocal spot of around 500 nm, therefore we report an average lifetime of efficiently FRET coupled EGFP in direct contact with DsRed-FT and EGFP with no direct contact to a FRET acceptor resulting in no, or less efficient, coupling.

5.3.3 FRET pairs at the interface of 3D structures

Microcontact printing was used for patterning micrometer circular features of DsRed-FT in a hexagonal arrangement on top of an EGFP coated substrate. The diagram of the fabrication process is shown in Scheme 5.2. The NiNTA modified substrate was exposed to a dilute solution of the donor molecule EGFP (0.1 μM,

Tris buffer, pH 8.0), rinsed with buffer solution, and carefully dried in a stream of nitrogen, resulting in an surface functionalized with EGFP (Scheme 5.2a). Subsequently, the elastomeric PDMS stamp was incubated with a solution of DsRed-FT (1 µM, Tris buffer, pH 8.0), the stamp was dried and put into conformal contact with the EGFP modified substrates (Scheme 5.2b). The removal of the stamp resulted in the physical adsorption of DsRed-FT on EGFP, and due to the close proximity of the different proteins in the two layers, in the formation of a FRET pair (Scheme 5.2c). The sample was kept in liquid for the duration of the measurements. For initial characterization, spectral and lifetime images of the patterned structures were acquired to address FRET between the biological emitters. Later the red-emitter chromophore (acceptor molecule) was photobleached, thus destroying the FRET pair, and a new complete characterization was carried out on the same area of the sample.

Scheme 5.2. *Schematic representation of the printing of DsRed-FT onto an EGFP modified surface and subsequent bleaching of the red chromophore of DsRed-FT.*

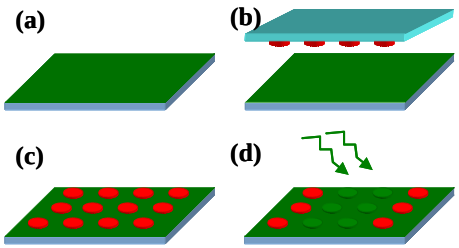

(a) EGFP is adsorbed via NiNTA-His_6 on the surface from solution. (b) PDMS stamp was inked with a protein solution of DsRed-FT and brought into conformal contact with the substrate to produce hexagonal microarrays of DsRed-FT onto EGFP. (c) After recording spectral and lifetime images the sample was exposed for several minutes to intense green light (510 - 560 nm) to selectively photobleach the red chromophore of the DsRed-FT (d).

Widefield images and spectral imaging (Figure 5.3a) confirm the patterning of the DsRed-FT on the EGFP substrates. A complete spectrum was recorded at each pixel of the image. For display purposes, the spectral image consists of data integrated over the respective emission band of the DsRed-FT. Representative emission spectra of the areas indicated by the arrows clearly shows the presence of EGFP, 509nm, and DsRed-FT, 590 nm, (red curve, Figure 5.3c) on the dot arrays, and in the surrounding areas only the presence of EGFP (green curve, Figure 5.3c).

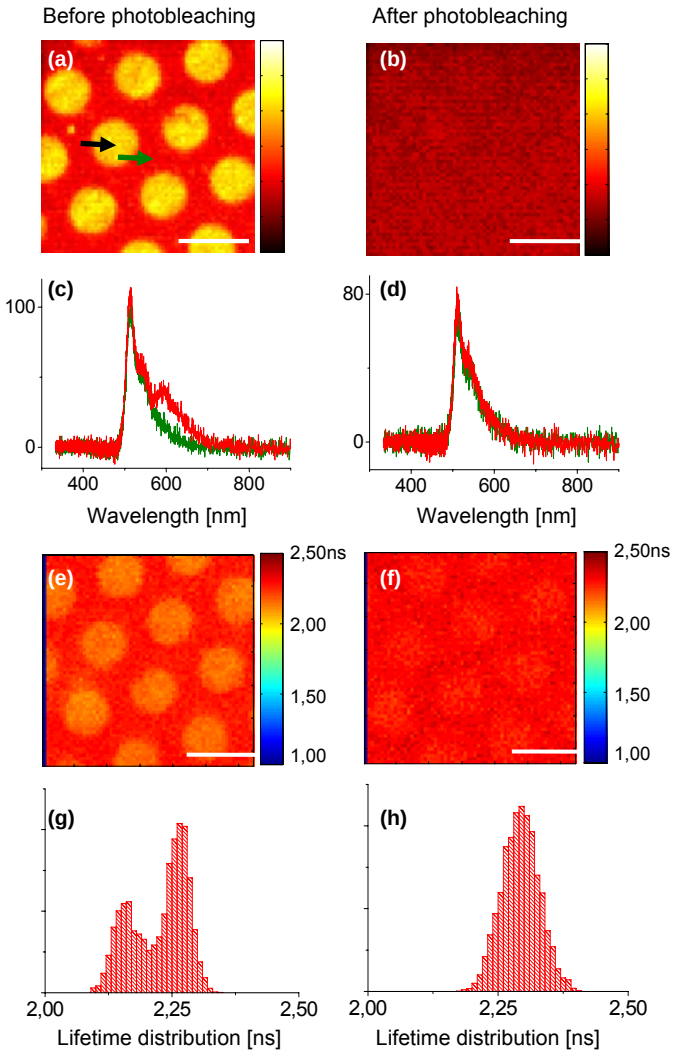

Figure 5.3. *Spectral and lifetime imaging of micrometer arrays of DsRed-FT onto EGFP functionalized substrates, scale bar 15 μm. After initial characterization (left column), the sample was exposed to intense green light (510-560 nm) to selectively bleach the red emitting DsRed-FT chromospheres and characterized again (right column). (a), (b) Spectral images of the spectral range of the DsRed-FT emission maximum. (c), (d) Spectra on the regions indicated by the arrows, after bleaching the peak at ~ 590 nm (characteristic of the DsRed-FT) disappears. Lifetime images of the emission of the donor EGFP, the lifetime of the areas in contact with the DsRed-FT is reduced due to FRET (e), after bleaching the image looks homogeneous (f). Lifetime histograms, on panel (g) the two distinctive distributions can be observed and correlated with the patterned areas, on (h) the lifetime of the donor has recovered upon photobleaching of the acceptor molecule.*

Lifetime imaging in the emission band of the EGFP was performed in order to compare the fluorescence lifetime of the EGFP in close proximity with the acceptor DsRed-FT and in absence of DsRed-FT, Figure 5.3e. In the lifetime image of the EGFP emission, the dot pattern of DsRed-FT can be observed. The histogram of the EGFP lifetimes shows a clear bimodal distribution. The distribution at lower lifetimes (~2.15 ns) is spatially attributed to areas where DsRed-FT was printed on top of EGFP, the longer lifetimes (2.27 ns) are attributed to areas where there is no DsRed-FT printed. The decreased lifetime of EGFP in areas where there is close contact to DsRed-FT is a clear sign for FRET between the molecules.

As a further test to prove FRET between patterned EGFP/DsRed-FT and to rule out possible artifacts, for example, from the printing process, that could influence the lifetime of the base protein (EGFP), we performed a photobleaching experiment of the FRET acceptor. In such an experiment the FRET acceptor is selectively destroyed. By removing the FRET acceptor the donor lifetime in absence of the acceptor is restored.

The mercury lamp was used to expose the sample for several minutes through a standard green cube (510 - 560 nm), in order to photobleach the DsRed-FT acceptor chromophore while the FRET donor chromophores are unaffected since they do not absorb at this wavelength. The bleaching process was followed by widefield microscopy until no more red emission was observed by the camera nor registered in the spectral signal. The spectral image of the red-bleached area integrated on the emission band of the DsRed-FT is depicted in Figure 5.3b. The former dots array in the spectral image has clearly disappeared, instead the sample surface looks spectrally uniform; this confirms the photodestruction of the DsRed-FT acceptor chromophore. The spectra along the whole area do not show signs of the DsRed-FT emission anymore but only emission of the EGFP (Figure 5.3d). Lifetime imaging of the EGFP was performed over the same red-bleached area, resulting in a homogenous distribution over the surface (Figure 5.3f). The decay curves characteristics fitted well to a monoexponential decay function. This shows that the characteristic donor lifetime shortening on the patterned areas has disappeared upon bleaching of the acceptor and that indeed the chromophores were coupled via FRET before bleaching and proves that FRET systems that exhibit energy transfer in the axial direction can be formed by printing techniques.

For the former FRET structures we estimated an energy transfer efficiency, *E*, of around 5% (based on equation 1). Since the Förster distance (R_o) for the GFP/DsRed pair is known,[27] this efficiency can be translated to a separation r = 8 nm, assuming an ensemble of identical FRET pairs with fixed donor-acceptor distance. However, a donor-acceptor distance of 8 nm is unlikely for the case presented here, because of the intrinsic characteristics of the fabrication process where the VFP pair is expected to be in close contact, resulting in a distance between donor and acceptor of about 3-5 nm. Hence we interpret the observed energy transfer efficiency as an average value from efficient transfer from EGFP with DsRed-FT in close contact and less efficient transfer from EGFP with DsRed-FT which is further away (> 10 nm). This suggests a low number of acceptor molecules with respect to donor molecules, which can be expected considering the unspecific nature of the binding between both proteins. The FRET efficiency can be controlled by tuning different fabrication parameters such as concentration, immobilization interactions, or by engineering specific binding sites between the biological emitters.

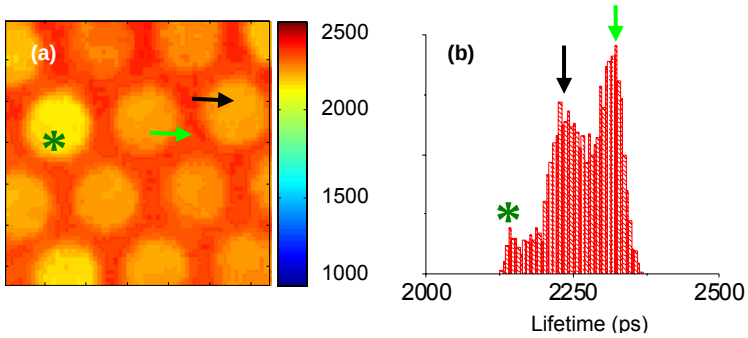

Figure 5.4. *(a) Lifetime imaging of the emission of the donor on micrometer arrays of mRFP onto EGFP functionalized substrates, 45 x 45 μm. (b) Lifetime histograms from panel a. The histogram shows a multimodal distribution. Right peak: Only EGFP areas, green arrow. Middle peak: areas where EGFP is in contact with mRFP. Left peak: Lifetime of the EGFP is reduced in a bigger proportion in this specific dot with respect to the other patterned areas (indicated by the green asterisk).*

To show that this FRET pair printing approach is applicable to different FRET pairs, we also used the variant mRFP as FRET acceptor. mRFP is an engineered monomeric DsRed, showing pure red emission. We used mRFP as an acceptor patterned on top of an EGFP modified glass substrate (Figure 5.4). In the same way,

the lifetime of the EGFP in contact with the mRFP patterned areas is reduced with respect to the areas where the EGFP is not in contact with the mRFP.

5.4 CONCLUSIONS

We have created for the first time printed FRET pairs at the interfaces between microcontact printed donor and acceptor molecules in the lateral and axial directions of the patterned structures. We used the VFPs EGFP/DsRed-FT (and mRFP) as donor/acceptor pairs, and characterized the structures using multiparameter optical microscopy. Energy transfer was shown to occur at the interfaces where the donor and the acceptor molecules meet. With different patterning techniques such as high resolution microcontact printing, multistep nanoimprint lithography or AFM assisted dip-pen nanolithography this work can be expanded to the fabrication of FRET pairs in nanometer dimensions; for the lateral FRET pair approach this will directly enhance the reported averaged efficiencies because of the increase of interfaces at the confocal spot of the laser beam.

Furthermore, this work can be used to address directly the interaction between different proteins on structured surfaces and/or the interaction of the same protein with different substrates, due to the sensitivity of lifetime to environmental changes. Hence, lifetime imaging could provide invaluable information for hybrid bioelectronics systems where the fluorescence decay times of the fluorophores is an important parameter for the design of functional devices.

5.5 ACKNOWLEDGEMENTS:

We thank the Nanotechnology Network in The Netherlands (NANONED), for financial support, project number 7124. We also acknowledge ¨Stichting voor Fundamenteel Onderzoek der Materie" (FOM), which is supported by the "Nederlandse Organisatie voor Wetenschappelijk Onderzoek" (NWO). We thank Prof. Dr. J. Huskens for continued support.

5.6 REFERENCES

1. Ramanujan, C. S.; Sumitomo, K.; de Planque, M. R. R.; Hibino, H.; Torimitsu, K.; Ryan, J. F., *Applied Physics Letters* **2007,** 90, 033901.
2. Chirico, G.; Cannone, F.; Diaspro, A.; Bologna, S.; Pellegrini, V.; Nifosì, R.; Beltram, F., Multiphoton switching dynamics of single green fluorescent proteins. *Physical*

Review E - Statistical, Nonlinear, and Soft Matter Physics **2004,** 70, (3 1), 030901-1-030901-4.
3. Cinelli, R. A. G.; Pellegrini, V.; Ferrari, A.; Faraci, P.; Nifosì, R.; Tyagi, M.; Giacca, M.; Beltram, F., Green fluorescent proteins as optically controllable elements in bioelectronics. *Applied Physics Letters* **2001,** 79, (20), 3353-3355.
4. Chalfie, M.; Tu, Y.; Euskirchen, G.; Ward, W. W.; Prasher, D. C., Green fluorescent protein as a marker for gene expression. *Science* **1994,** 263, (5148), 802-805.
5. Yang, F.; Moss, L. G.; Phillips Jr, G. N., The molecular structure of green fluorescent protein. *Nature Biotechnology* **1996,** 14, (10), 1246-1251.
6. Ormö, M.; Cubitt, A. B.; Kallio, K.; Gross, L. A.; Tsien, R. Y.; Remington, S. J., Crystal structure of the Aequorea victoria green fluorescent protein. *Science* **1996,** 273, (5280), 1392-1395.
7. Alonso, J. M.; Reichel, A.; Piehler, J.; Del Campo, A., Photopatterned surfaces for site-specific and functional immobilization of proteins. *Langmuir* **2008,** 24, (2), 448-457.
8. Verkhusha, V. V.; Lukyanov, K. A., The molecular properties and applications of Anthozoa fluorescent proteins and chromoproteins. *Nature Biotechnology* **2004,** 22, (3), 289-296.
9. Ward, W. W.; Bokman, S. H., Reversible denaturation of Aequorea green-fluorescent protein: Physical separation and characterization of the renatured protein. *Biochemistry* **1982,** 21, (19), 4535-4540.
10. Shaner, N. C.; Campbell, R. E.; Steinbach, P. A.; Giepmans, B. N. G.; Palmer, A. E.; Tsien, R. Y., Improved monomeric red, orange and yellow fluorescent proteins derived from Discosoma sp. red fluorescent protein. *Nature Biotechnology* **2004,** 22, (12), 1567-1572.
11. Creemers, T. M. H.; Lock, A. J.; Subramaniam, V.; Jovin, T. M.; Völker, S., Photophysics and optical switching in green fluorescent protein mutants. *Proceedings of the National Academy of Sciences of the United States of America* **2000,** 97, (7), 2974-2978.
12. Di Benedetto, F.; Biasco, A.; Bizzarri, R.; Arosio, D.; Ricci, F.; Beltram, F.; Cingolani, R.; Pisignano, D., Two dimensional patterning of fluorescent proteins in hydrogels. *Langmuir* **2006,** 22, (1), 29-31.
13. Renault, J. P.; Bernard, A.; Bietsch, A.; Michel, B.; Bosshard, H. R.; Delamarche, E.; Kreiter, M.; Hecht, B.; Wild, U. P., Fabricating arrays of single protein molecules on glass using microcontact printing. *Journal of Physical Chemistry B* **2003,** 107, (3), 703-711.
14. Maury, P.; Escalante, M.; Péter, M.; Reinhoudt, D. N.; Subramaniam, V.; Huskens, J., Creating nanopatterns of his-tagged proteins on surfaces by nanoimprint lithography using specific NiNTA-histidine interactions. *Small* **2007,** 3, (9), 1584-1592.
15. Ludden, M. J. W.; Mulder, A.; Schulze, K.; Subramaniam, V.; Tampé, R.; Huskens, J., Anchoring of histidine-tagged proteins to molecular printboards: Self-assembly, thermodynamic modeling, and patterning. *Chemistry - A European Journal* **2008,** 14, (7), 2044-2051.
16. Ludden, M. J. W.; Péter, M.; Reinhoudt, D. N.; Huskens, J., Attachment of streptavidin to β-cyclodextrin molecular printboards via orthogonal host-guest and protein-ligand interactions. *Small* **2006,** 2, (10), 1192-1202.
17. Li, L.; Hitchcock, A. P.; Cornelius, R.; Brash, J. L.; Scholl, A.; Doran, A., X-ray microscopy studies of protein adsorption on a phase segregated polystyrene/ polymethylmethacrylate surface. 2. Effect of pH on site preference. *Journal of Physical Chemistry B* **2008,** 112, (7), 2150-2158.
18. Vallières, K.; Chevallier, P.; Sarra-Bournet, C.; Turgeon, S.; Laroche, G., AFM imaging of immobilized fibronectin: Does the surface conjugation scheme affect the protein orientation/conformation? *Langmuir* **2007,** 23, (19), 9745-9751.
19. Busby, M.; Blum, C.; Tibben, M.; Fibikar, S.; Calzaferri, G.; Subramaniam, V.; De Cola, L., Time, space, and spectrally resolved studies on J-aggregate interactions in zeolite L nanochannels. *Journal of the American Chemical Society* **2008,** 130, (33), 10970-10976.
20. Jain, A.; Blum, C.; Subramaniam, V., *Advances in Biomedical Engineering*. Elsevier Science & Technology Books: Amsterdam, 2009.

21. Blum, C.; Mosk, A. P.; Nikolaev, I. S.; Subramaniam, V.; Vos, W. L., Color control of natural fluorescent proteins by photonic crystals. *Small* **2008,** 4, (4), 492-496.
22. Wall, M. A.; Socolich, M.; Ranganathan, R., The structural basis for red fluorescence in the tetrameric GFP homolog DsRed. *Nature Structural Biology* **2000,** 7, (12), 1133-1138.
23. Tinazli, A.; Tang, J.; Valiokas, R.; Picuric, S.; Lata, S.; Piehler, J.; Liedberg, B.; Tampé, R., High-affinity chelator thiols for switchable and oriented immobilization of histidine-tagged proteins: A generic platform for protein chip technologies. *Chemistry - A European Journal* **2005,** 11, (18), 5249-5259.
24. Suhling, K.; Siegel, J.; Phillips, D.; French, P. M. W.; Lévêque-Fort, S.; Webb, S. E. D.; Davis, D. M., Imaging the environment of green fluorescent protein. *Biophysical Journal* **2002,** 83, (6), 3589-3595.
25. Borst, J. W.; Hink, M. A.; Van Hoek, A.; Visser, A. J. W. G., Effects of refractive index and viscosity on fluorescence and anisotropy decays of enhanced cyan and yellow fluorescent proteins. *Journal of Fluorescence* **2005,** 15, (2), 153-160.
26. Van Manen, H. J.; Verkuijlen, P.; Wittendorp, P.; Subramaniam, V.; Van Den Berg, T. K.; Roos, D.; Otto, C., Refractive index sensing of green fluorescent proteins in living cells using fluorescence lifetime imaging microscopy. *Biophysical Journal* **2008,** 94, (8), L67-L69.
27. Erickson, M. G.; Moon, D. L.; Yue, D. T., DsRed as a potential FRET partner with CFP and GFP. *Biophysical Journal* **2003,** 85, (1), 599-611.

Chapter 6

2D and 3D Assembly of Core-Dimers from *Rhodobacter Sphaeroides* into Micro- and Nanostructures

This chapter reports the fabrication and characterization of 3D and 2D assemblies of core dimer complexes. Fluorescence spectral microscopy is used to study the optical properties of the complexes in the different assemblies. AFM topographies of 3D crystals of core dimers indicate that the crystals are formed by stacking of sheet like layers. The surfaces of the crystals were very rough with cracks up to 1µm in depth. Fluorescence emission from the 3D crystals is red-shifted with respect to the fluorescence from core dimers in solution. Nanometer arrays of core dimers (~ 80 nm in width and several micrometers in length) were fabricated by a combination of top-down and bottom-up nanofabrication approaches. NiNTA monolayers were used as chemical templates for the controlled immobilization of His_6 tagged core dimers. Fluorescence time trace data hint at long-range energy transport.

6.1 INTRODUCTION

Photosynthetic bacteria provide an excellent natural system to study the conversion of light energy into chemical energy. Energy conversion is possible as a result of an exquisitely ordered and interconnected supramolecular arrangement of membrane-bound pigments that has recently been characterized by AFM.[1-2] This supramolecular assembly is usually comprised of the "core" complex composed of light harvesting complex 1 (LH1) and the reaction center (RC). The energy absorbed by LH1 is transferred to the RC, where photochemical charge separation takes place.[3] Kinetics calculations show that excitation is trapped within 200 ps or less at the RC for a large variety of photosynthetic units (PSU).[4]

In native conditions, the RC from *Rhodobacter (Rb.) sphaeroides* is embedded in the bacterial cytoplasmic membrane and is composed of three subunits labeled L, M and H. The L and M subunits, each forming five transmembrane α-helices, are related by an axis of approximate two-fold symmetry.[5-7] The H subunit is located at the cytoplasmic surface and binds to both the L and M subunits. Multiple pigment molecules (cofactors) are bound to the L and M subunits and are arranged in two symmetric branches, commonly referred to as the A branch and B branch respectively. Except for a single carotenoid molecule, cofactors are symmetrically arranged in the L and M subunits and include a bacteriochlorophyll (BChl) dimer (termed as P, P_L, P_M) known as the primary donor, two monomer bacteriochlorophylls (B_M and B_L), two bacteriopheophytins (H_M and H_L), two quinones (Q_M and Q_L) and one non-heme iron. It is by now well established that most of the photo-induced electron transfer (ET) in RC appears to occur along the A branch (L) under normal conditions.

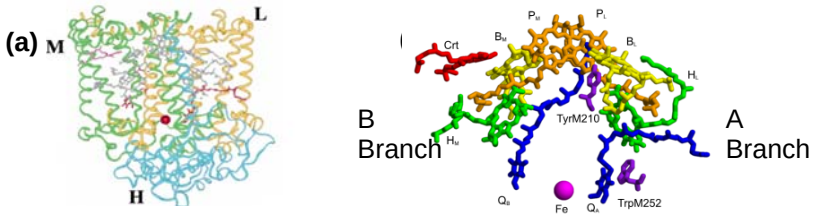

Figure 6.1. *(a) Three-dimensional structure of RC from Rb. sphaeroides. The L, M and H subunits are shown as yellow, green and blue ribbons. (b) Chromophores RC special pair (P_L, P_M, orange), accessory BChls (B_L, B_M, yellow), bacteriopheophytins (H_L, H_M, green), quinones (Q_A, Q_B, blue) and a carotenoid molecule (red).*[8]

The RC exists in two spectral forms. In the *open* form, the RC special pair is neutral and can be optically excited to generate an electron transfer.[9] After electron transfer, the RC is in the *closed* form with the active special pair BChl oxidized and unable to be further excited until it is reduced by the uptake of an electron. An excitation that encounters a closed RC will be back-transferred towards the LH1 rather than being dissipated in the RC, which might result in overheating of the RC. This excitation can then be transferred to another unit with an open RC. Several studies have been focused on the route for ultrafast electron transfer within photosynthetic reaction centers, including pump-probe experiments performed in solution.[6, 10] Experimental information of energy transfer among different core dimer complexes (LH1-LH1) is at this moment scarce. High resolution AFM images of the native architecture of membranes of *Rb. sphaeroides*[2] have shown that they are composed in part of linear arrays of dimeric complexes, typically forming rows of up to 6 dimers of RC-LH1-PufX complexes. It has been proposed that the linear arrays of dimers cooperate in the overall process of energy trapping. If any particular RC is already undertaking photochemical charge separation rendering it unavailable for receiving excitation energy from its corresponding LH1 ring, the LH1 excitation can migrate along a succession of such dimers until an *open* RC is reached. Moreover, it has been observed that mutants lacking the LH2 complexes that normally separate rows of core dimers form tubular membranes containing linear rows of dimers aligned in parallel.[11-12]

Recent efforts have turned towards the fabrication of functional assemblies of purified components of the PSU with defined size and shape by means of self-assembly and/or nanopatterning techniques.[13-15] In the following sections we assemble 3D and 2D structures from natural core dimer complexes with the objective to investigate properties of LH1-RC in close-packed structures. These artificial assembled structures range in sizes from micrometer-sized crystals to nanometer arrays of sub-100 nm width and several microns in length, clearly differing from the domain sizes encountered in the natural bacteria. We use fluorescence microscopy to investigate the spectral behavior and to qualitatively probe energy transfer properties of these assemblies.

6.2 MATERIALS AND METHODS

***Compounds*:** All chemicals were used as received. N- 3-(trimethoxysilyl)propyl ethylenediamine (Aldrich), 1H,1H,2H,2H perfluorodecyltrichloro silane (ABCR), 1,4-phenylene diisothiocyanate (Acros), N,N-bis(carboxymethyl)-lysine (Aldrich), NiCl2 (Aldrich), PMMA (molecular weight 350 kD, Aldrich)

Protein purification and 3D crystallization: Following the protocol of Qian *et al*,[16] cells were cultured, membrane was prepared and solubilised, and the dimer complex was purified. Crystallization trials were set up as reported.[17] Thin, plate-like crystals from one trial were selected for analysis by fluorescence microscopy and AFM.

Core dimers his-mutants: A His_6 tag was added to the carboxy terminus of the RC-H subunit,[18] resulting in one His_6 tag per RC, i.e. two per dimer. The interaction between the His_6 tags and a NiNTA SAM results in the directed, specifically oriented, adsorption of the core dimer complexes (i.e. RC-H side down).

Substrate preparation for 3D core crystals: Substrates (microscope coverslips, Menzel-glaser # 1,5) were cleaned by immersion in piranha solution (3:1 concentrated H_2SO_4 / 33% aqueous H_2O_2) for 15 min, rinsed copiously with water and dried with a stream of N_2. *Warning: Piranha solution should be handled with care*. An amino terminated self-assembled monolayer was formed by gas-phase evaporation of *N*-3-(trimethoxysilyl)propyl-ethylenediamine in a desiccator under vacuum.[19]

***Substrate preparation for 2D nanometer arrays of core dimers*:** Nanoimprint Lithography (NIL) was performed using stamps with silicon ridges as small as 40 nm with a 4 μm period.[20] Substrates (microscope coverslips, Menzel-glaser # 1.5) were cleaned as described above. The substrates were then coated with a 90 nm thick layer of PMMA (20 g/L) by spin coating. The stamp and the substrate were put in contact and a pressure of 40 bars was applied at a temperature of 180 °C using a hydraulic press (Specac). Demolding was performed at 110 °C. After imprinting, the residual layer was removed by physical etching during approximately 20 seconds in oxygen plasma (RIE-Elektrotech, 20 W, 10 mT, 10 sccm O_2). In this step, the lateral dimension of the polymer-free area increased in width relative to that of the NIL stamp, since, during etching, the side walls of the polymer barrier are also slightly etched away. Activation of the surface

subsequently took place by deposition of the aminoalkyl SAM from the gas phase. The remaining PMMA was stripped by sonication in acetone and the complementary areas were passivated with 2-Methoxy(polyethyleneoxy)propyl trimethoxysilane (referred to as PEG silane) in distilled toluene for 2 hours. The substrates were later copiously rinsed with toluene followed with ethanol and dried with a stream of N_2. NiNTA monolayers were obtained as described elsewhere.[21] Transformation of the amine-terminated monolayer to isothiocyanate-terminated layers was accomplished by exposure to a 0.1 M solution of 1,4-phenylenediisothiocyanate in toluene at 50 °C for 2 h under N_2, followed by rinsing with toluene and drying with N_2. NTA monolayers were obtained by reaction of the isothiocyanate-terminated monolayers with a 2.5 mM aqueous solution of N,N-bis(carboxymethyl)-l-lysine solution (10 mM TRIS buffer, pH 8) at 50 °C for 4 h. The substrates were rinsed with Millipore water and gently dried in a stream of N_2. Samples were immersed in a 0.1M solution of $NiCl_2$ (10mM TRIS buffer, pH 8), to allow absorption of Ni^{2+} on the NTA SAM, during 10 min, rinsed with buffer and dried in a N_2 flow.

Atomic force microscopy (AFM): AFM characterization was performed with a Bioscope II, NanoScope 7.30 (R2Sr1), mainly because of its large z-range (~20 μm). The AFM part from the AFFM was not suitable for these measurements because of its limited z-range, 1 μm maximum.

Standard silicon nitride cantilevers (Mikromasch), force constant of 0.6 N/m, and operating frequencies of 50–105 kHz (in air) were used. AFM images were obtained using tapping mode in liquid. Images contained either 256x256 or 512x512 pixels and were recorded at a line scanning frequency of 2–4 Hz. Topographical images were quantitatively analyzed using the Scanning Probe Image Processor (SPIP) software (Image Metrology ApS, Lyngby, Denmark).

Optical characterization: Fluorescence spectral microscopy was performed using 800 nm excitation by a diode laser (Roithner Laser Technik, RLT80010MG). The laser beam is reflected via a dichroic beam splitter (Chroma, Q850LPXXR) towards an oil-immersion objective (Nikon, Plan Fluor 100 ×NA 1.3), which focuses the light onto the sample. The fluorescence light is collected by the same objective and passes through the dichroic beam splitter. By switching a foldable mirror, the fluorescence light can be directed either towards a single photon counting avalanche

photodiode (APD) (SPCM-AQR-14, Perkin Elmer Optoelectronics) or towards a custom designed prism-based spectrograph with single molecule sensitivity equipped with a liquid nitrogen-cooled CCD camera (Spec-10:100B, Princeton Instruments). The spectrograph–CCD camera combination is used for conventional spectral imaging where a complete spectrum is recorded for each image pixel.[22]

6.3 RESULTS AND DISCUSSION

6.3.1 Core-dimers 3D Crystals

6.3.1.1 AFM topography

A solution containing 3D core dimer crystals was incubated on an amino-terminated functionalized glass substrate, followed by 100 μL of buffer (20 mM Hepes, pH 8). For AFM characterization, the crystals needed to be incubated overnight at 4 °C. Shorter incubation times resulted in the detachment of the crystals from the surface while imaging with the AFM. Incubation on untreated clean glass substrates resulted in the removal of the crystals from the substrate upon gently washing with buffer. Figure 6.2a shows a white light image of the AFM cantilever resting on top of a 3D crystal of core dimer. The crystals showed a large heterogeneity in size ranging from sub-micrometer dimensions up to more than 200 micrometers, as can be observed in the areas marked 1-4. Figure 6.2b shows an AFM topography of a 20 x 20 μm area of a 3D crystal. The surface is clearly rough with eroded lesions on the surface of the crystal on the order of 1μm in depth and few micrometers in width as is shown in the height profile measured along the dotted line in panel a (Figure 6.2c). Some sharp triangular-shape features can be observed at the bottom of panel b. These features (indicated by the arrow in the figure) are attributed to an artifact due to imaging of the AFM tip because of the height of the crystals. To acquire information about individual complexes at the surface of the crystal, AFM imaging was performed on a smaller relatively flat area, of dimensions 2 x 2 μm (Figure 6.2d). From the image, it can be observed a disordered arrangement of units that exhibit an average height of approximately 9 nm.

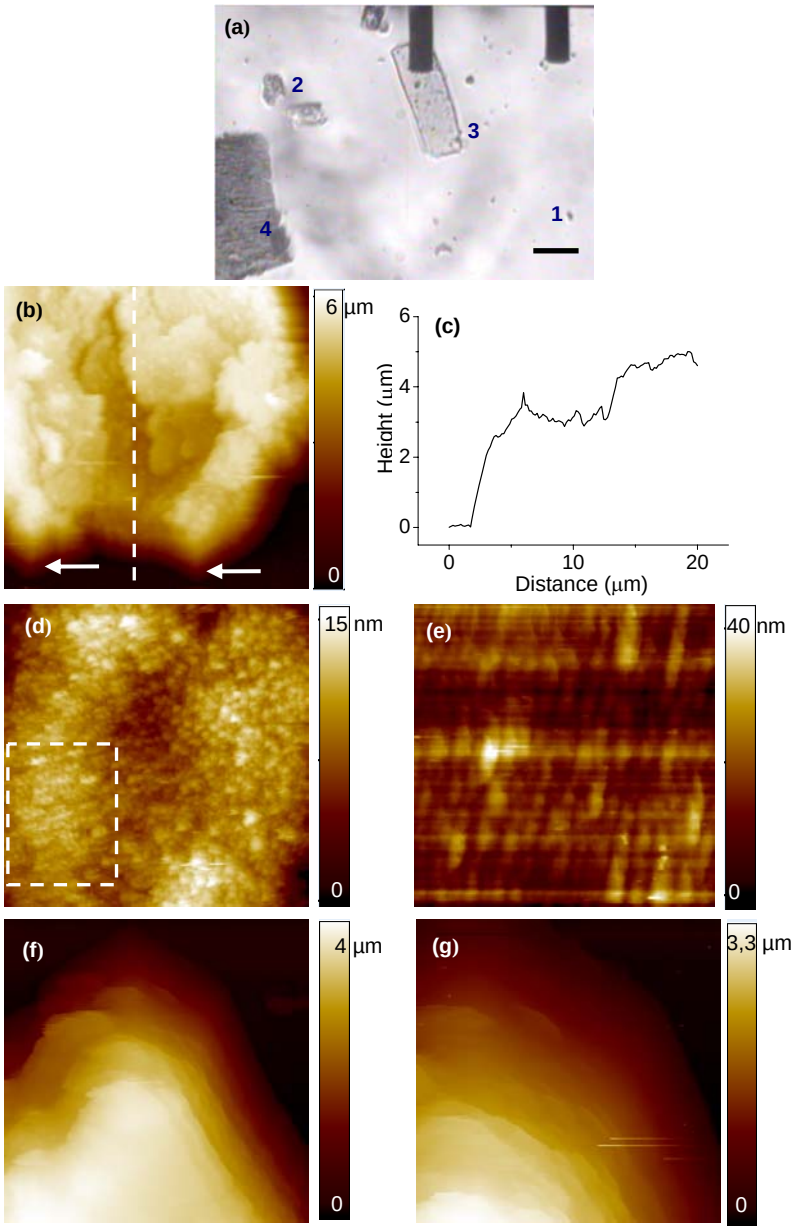

Figure 6.2. *(a) White light image of 3D core dimmer crystal resting on the substrate, scale bar 70 µm. Different crystals are indicated with number from 1 to 4. AFM height images of 3D core dimer crystals. (b) 20 x 20 µm, (c) Line profile from panel (b), (d) 2 x 2 µm, (e) 1 x 1 µm, (f) 5 x 5 µm, (g) 2.5 x 2.5 µm*

Some regular packing can be distinguished in the area marked by the white square in panel d. Upon further inspection of the 3D crystals, only scarcely periodic

regions (panel e) could be observed. Imaging at the edges of the 3D crystals revealed that some crystals appeared to be formed by a stacked arrangement of layers. To the best of our knowledge these are the first AFM measurements of 3D crystals of a membrane protein. AFM characterization of 3D crystals can provide information about gradual erosion of the 3D assemblies in different buffers.

6.3.1.2 Fluorescence

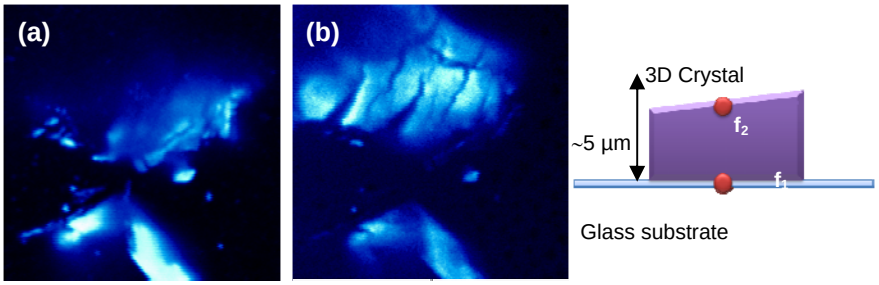

Figure 6.3. *Fluorescence images (false color) of several fragments of 3D core dimer crystals, 32 x 32 µm. (a) Laser focused on the surface of the glass coverslip, bottom part of the crystals, as indicated in the schematic by f_1. (b) Laser spot focused ~ 5 µm above the substrate surface (f_2). It is important to highlight that we do not have the possibility to perform automated 3D confocal images of the samples, which makes it difficult to determine the geometry of the crystal.*

For optical characterization of the 3D assemblies, a solution with 3D core dimer crystals was incubated on an amino terminated functionalized glass substrate for two hours. For shorter incubation times it was not possible to observe the crystals bound to the surface. We speculate that because of their dimensions (several micrometers) a long incubation time was necessary in order to allow the crystals to reach the surface of the substrate. The incubation time for the fluorescence characterization of the 3D crystals is shorter than the incubation time for AFM imaging. This is due to the fact that optical characterization is a noncontact technique and therefore does not induce detachment of the sample by mechanical forces and unintentional contact with the crystals, as is the case by approaching the AFM tip to inspect the topography of the crystal. The 3D core dimer crystals were kept in a closed chamber in liquid (20 mM Hepes, pH 8, deoxygenated by flushing with nitrogen) for the whole duration of the measurements. Fluorescence and spectral images were acquired upon excitation with 800 nm laser light. Figure 6.3a shows a fluorescence image of various 3D crystal fragments when the imaging laser is focused on the

substrate that supports the crystals (indicated by f_1 in the schematic in Figure 6.3). By changing the position of the focus, it was also possible to inspect the exposed surface of the crystals. Similar to the AFM data, the crystals showed a large heterogeneity in size. Also, the bigger crystals exhibit cracks along the surface as can be observed in Figure 6.3b. Spectral images were also acquired in order to compare the spectral response of the 3D crystal assemblies with the protein complexes in solution.

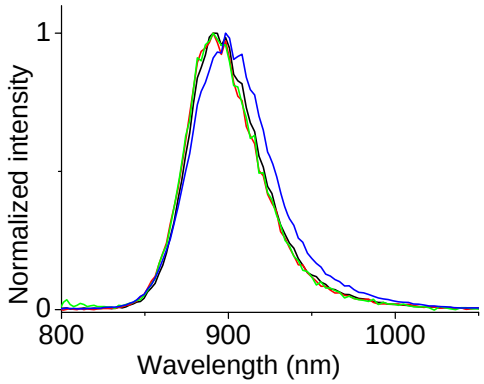

Figure 6.4. *Normalized emission of 3D core crystals (blue) and LH1 only (black), core monomers (red) and core dimer (green) in solution.*

Figure 6.4 shows a comparison between LH1-only (black), core dimers (green), core monomer (red) complexes in solution and the spectral response upon 800 nm excitation of the core dimers assembled in a 3D crystal (dark blue). No significant differences are observed between the emission spectra from LH1, core dimers and core monomers. The fluorescence emission spectra of the complexes within the 3D crystal show a clear red shift with respect to the other species. The red shift is attributed to the highly packed chromophores within the crystal. As a control experiment, fluorescence spectra were acquired from small fragments of crystals (subconfocal dimensions) directly on the glass substrate. These fragments could be, for example, either potential aggregates of dimer complexes which have broken apart from the main crystal, or those that did not crystallize in the first instance. The spectra from the small fragments showed no difference with respect to the spectra from the core dimer solution measured earlier. This observation further supports the fact that the observed fluorescence red shift is due to a strong coupling between the

dimers in the closely packed 3D crystals. Red shift of the fluorescence emission in crystals of photosynthetic protein has been recently reported from crystals of plant light-harvesting complexes LHC-II measured at 100 K.[23]

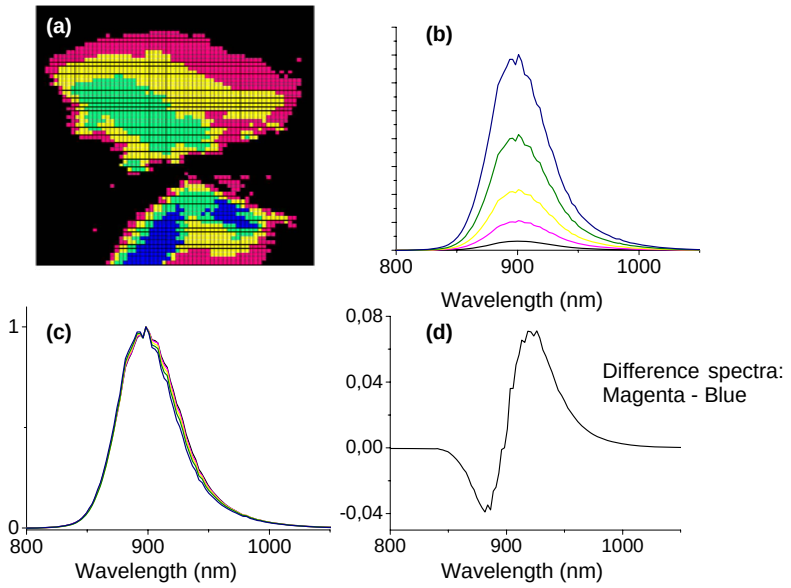

Figure 6.5. *Cluster analysis of the spectral image corresponding to Figure 6.3. (a) Clustered image, note that the image is mirrored in the horizontal direction with respect to Figure 6.3. (b) Spectra associated to the clusters. (c) Superposition of the normalized spectra. (d) Difference spectra between the magenta and the blue clusters.*

Spectral images of 3D core dimer crystals were acquired to investigate spectral differences in emission over the crystal. For the analysis of the data we first applied singular value decomposition (SVD)[24-25] in order to reduce noise of the individual spectra, followed by clustering using principal component analysis (PCA) and hierarchical cluster analysis (HCA). With the last procedure it is possible to identify major components present in each spectrum and to group them into similar spectral clusters. SVD and HCA were performed on the data corresponding to the spectral images of 3D core dimer crystals. A full spectrum was recorded at each pixel and SVD-HCA performed on the whole data matrix. Areas within the crystal were identified which present different spectral properties. Figure 6.5a shows the spectral image grouped in clusters. The spectra associated with each cluster and the corresponding relative intensity is displayed in panel b. The superposition of all the

clusters is shown in Figure 6.5c. The maximum emission does not exhibit a significant shift among the spectra but a slight broadening of the spectra can be distinguished for the magenta (less intense) areas with respect to the blue areas. Figure 6.5d shows the difference spectra between the clusters with the highest (blue) and the lowest (magenta) intensity where the broadening towards higher wavelengths can be observed. This behavior is consistently reproduced in measurements on different crystals. Spectral imaging at different confocal planes could be used to address whether the differences in spectra are observed due to reabsorption of fluorescence in the crystal areas of different thickness and/or positioning of the incident beam within the crystal.

6.3.1.3 Energy transfer

Figure 6.6 shows a schematic representation of a possible scenario of energy transfer in the core dimer assemblies. Initially all the RC are open (Figure 6.6a). Upon excitation with laser light, first the RCs directly within the area of the confocal spot are occupied due to energy transfer from the LH1 complex (Figure 6.6b). It has been proposed for natural systems that the linear arrays of dimers cooperate in the overall process of energy trapping,[2] because if any particular RC is already closed and unavailable for receiving excitation energy from its respective LH1 ring, the LH1 excitation can migrate along a succession of such dimers until an open RC is reached. This process is further depicted in panel c where the extent of the excitation reaches beyond the area initially excited by the laser beam. Figure 6.6d shows the possible pathways that can be undertaken upon irradiation of a core dimer assembly: excitation from the LH1 can be transferred to the RC. Upon occupation of the RC, the excitation can be back-transferred to the LH1 ring. Subsequently, energy can be transferred to the next empty RC. Also, energy can be lost as fluorescence, dissipated as heat, or can be quenched due to, for example, irregular molecular contacts at domain boundaries, occasional free pigments, impurities, singlet-singlet annihilation, or reaction with oxygen.

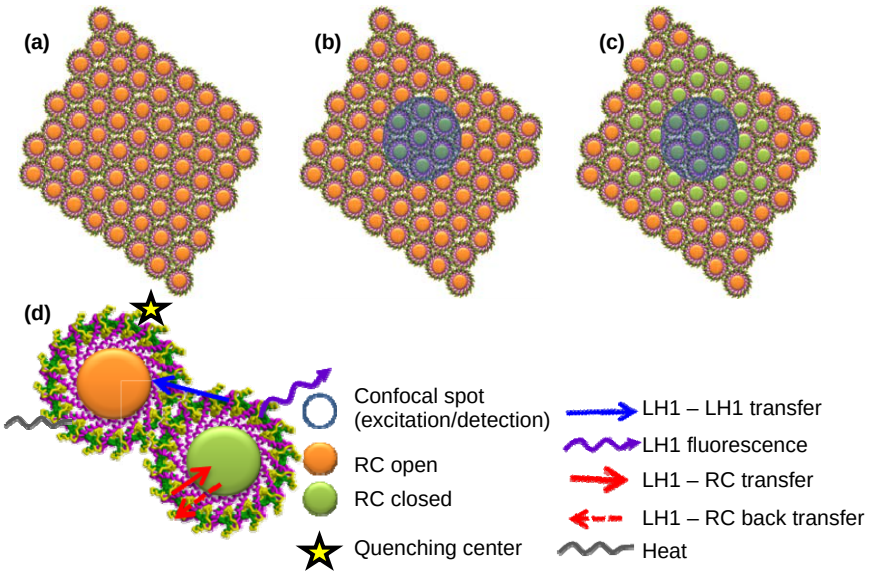

Figure 6.6. *Schematic representation of energy transfer and dissipation in LH1-RC assemblies. (a) Initially all RCs are open, (b) upon excitation of the LH1 antennas, energy transfer occurs and RCs in the area of excitation are photo-oxidized (RC closed) and unable to accept more energy. (c) When all RCs in the confocal spot are occupied, energy migration occurs to the neighboring LH1-RCs indicated in green. (d) Schematic representation of the different processes involved: LH1 fluorescence emission, LH1-RC energy transfer, LH1-LH1 energy transfer, dissipation by heat, and quenching of fluorescence by several factors.*

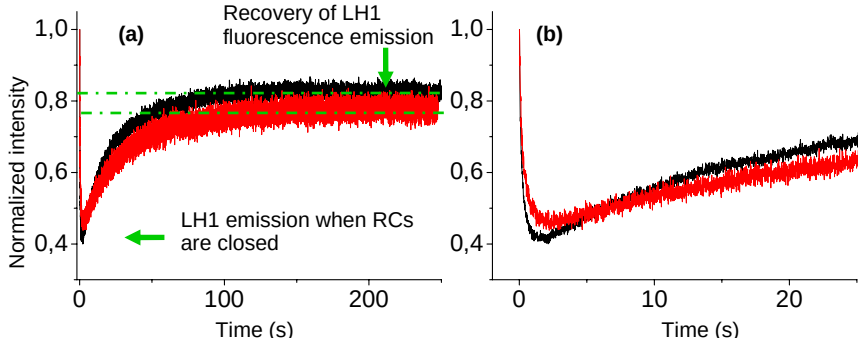

Figure 6.7*. (a) Fluorescence time traces from 3D core dimer crystals at different excitation powers. Black curve, 370 nW, red curve 80 nW measured at the back aperture of the objective. Two asymptotes are indicated by the dashed green line. Time constants (τ) are derived from a first order exponential fit. (b) First 25 seconds from the time traces in panel (a). At higher power the RC in the crystals get occupied faster with a* τ_d *= 0.20 seconds. At lower power* τ_d *= 0.32 seconds. The recovery of the LH1 emission in such a macro-structure is* τ_r *= 25.25 seconds at higher power and* τ_r *= 34.40 seconds at lower power.*

250 s long fluorescence time traces were acquired with a sampling time of 1 ms, using different excitation powers on large crystals (with x-y dimensions over 10 micrometers). The fluorescence time traces were acquired in a confocal configuration, recording only the LH1 fluorescence emission in the confocal volume. Fluorescence emitted in areas outside the confocal volume due to energy transfer or light scattering (due to the bulky 3D crystal) is not recorded in the confocal configuration. Figure 6.7 shows two fluorescence time traces acquired in similar crystals at different excitation powers. The time traces showed first a pronounced decrease followed by an increase of the LH1 fluorescence intensity. The black curve was acquired at an excitation power, measured at the back aperture of the objective, of ~ 370 nW, and the red curve was acquired with an excitation power of 80 nW. Details of the curve can be observed during the first 25 seconds of the fluorescent time traces (Figure 6.7b). The curves have been fitted with an exponential function $y_0 + A_1 e^{-x/t_1} + A_2 e^{x/t_2}$, yielding fits in all cases with $\chi^2 \sim 1$ and $R^2 > 0.94$. At higher powers the reduction of the intensity is faster than at lower power, with a respective decay time constant, τ_d, of $\tau_{d\text{-}370} = 0.20$ s, and $\tau_{d\text{-}80} = 0.32$ s. Also the recovery of the fluorescence is faster at higher excitation powers, with a time constant for recovery, τ_r, of $\tau_{r\text{-}370} = 25.25$s, and $\tau_{r\text{-}80} = 34.40$s. The curves show that the photo-oxidation of the primary donor (P) caused an increase in LH1 fluorescence by a factor between 1.8 and 2.1. This factor is calculated by dividing the LH1 fluorescence emission after recovery (asymptotes Figure 6.7a) by the LH1 emission when all the RCs in reach are closed (minimum value from the curves Figure 6.7a). The magnitude of these factors are in agreement with values extracted by a comparison of the fluorescence spectra of different membranes of *Rb. sphaeroides* with maximum emission at the LH1 band.[26] These authors report a ratio of LH1 emission with oxidized RC and open RC to be between 1.7 and 2.3.[26]

At higher excitation powers (~20x), with the current time resolution it was still possible to observe the transient behavior in the fluorescence emission, with a $\tau_{d\text{-}7800}$ = 0.02 s. This can be attributed to rapid occupation of all RCs and to non-linear processes such as singlet-singlet annihilation which play an important role as quenchers of excess excitation at high excitation densities.[27-28] At lower excitation powers occupation of the RCs was reached after ~23 s ($\tau_{d\text{-}2.4}$ 15,32 s), Figure 6.8.

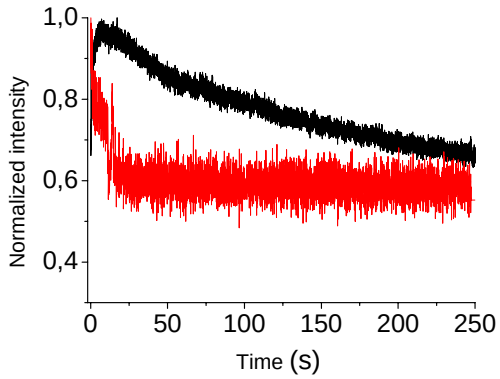

Figure 6.8. *Fluorescence time traces from 3D core dimer crystals at different excitation powers. Red curve, 2.4 nW, Black curve 7.8 µW measured at the back aperture of the objective.*

The time constants associated with the fluorescence time traces from 3D crystal assemblies can be thought to be a function of the number of available acceptor units (RCs) and the excitation power. Energy transfer from B870 to the RC has been reported to be between 20 – 50 ps.[4] A simple model is proposed to explain the fluorescence time traces.

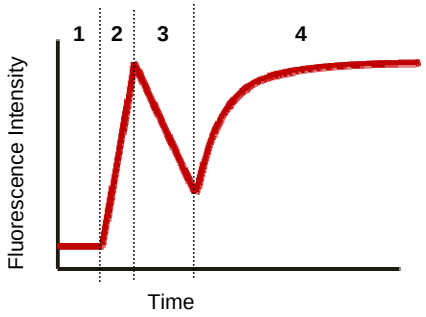

Figure 6.9. *Representation of a fluorescence time trace from a 3D core dimer crystal. Different regimes are depicted in the figure:* ***1*** *Excitation energy is transferred from LH1 to RC,* ***2*** *RC within the confocal volume are closed, LH1 fluorescence emission recovers. The first two processes are faster than the current timeresolution of 1ms , therefore it was not possible to observe these transients in Figure 6.7 and Figure 6.8.* ***3****, Because all the RC within the confocal volume are closed, energy transfer occurs between adjacent LH1-RC until all RCs in reach are occupied* ***4*** *Equilibrium between the different processes.*

At t=0, the transfer rate out of the excited confocal spot (k_{out}) equals the transfer rate into (k_{in}) the confocal spot, $t = 0 \rightarrow k_{in} = k_{out}$. At t=0 all RC are in the "open" state. For $t > 0$, $k_{in} < k_{out}$. The transfer rate into the excitation volume decreases

possibly due to occupation of the RCs, charge accumulation and heating. This model also assumes competition between the forward transfer to an open RC and the emission of LH1 fluorescence once the RC is closed. This gives rise to the decay of the LH1 fluorescence emission in the confocal volume, because the excitation moves outwards (Figure 6.6 panels b,c). The subsequent rise in LH1 fluorescence is ascribed to equalization of the transfer rates, t >> 0, $k_{in} = k_{out}$. At this stage all the RCs within reach are occupied, and the LH1 fluorescence gradually recovers in time. A process that determines this time-scale could be a dissipation process, for example, due to heat.

The particular shape of the previous fluorescence time traces (Figures. 6.7 and 6.8) was not observed in crystals of pure LH2 and LH1. The fluorescence time traces of crystals of LH2 and LH1 showed a continuous decrease in intensity. This supports the notion that the presence of the RC gives rise to the dynamic processes presented in Figures 6.7 and 6.8. In order to test whether energy transfer between adjacent units of LH1-RC in the crystal could cause the transient behavior, time traces were acquired from solutions of core dimers. The transient behavior was also absent from solutions of core dimers. As an additional control experiment, fluorescence time traces were measured on small aggregates of either core dimers or LH1 only complexes. The aggregates were formed by incubation for a prolonged time of a solution of the molecule on an amino-functionalized glass coverslip. In spite of the fact that such surfaces cannot be expected to give rise to a crystalline contiguous assembly of core complexes the fluorescence time traces, recorded at two different excitation powers, namely 370 and 80 nW, (Figure 6.9) revealed similar transient behavior.

The black traces in Figure 6.10 show the fluorescence time traces recorded on the LH1 aggregates. The LH1 traces show a typical photobleaching curve of a fluorophore. However, the red traces, which correspond to the core dimer aggregates on the surface, show a transient decrease in LH1 fluorescence with a subsequent rise in the fluorescence similar to that observed in the 3D crystals. The time traces were acquired with a laser power of 370 nW and 80 nW, resulting in decay times of $\tau_{d\text{-}370} = 0.07$ s, and $\tau_{d\text{-}80} = 0.64$ respectively.

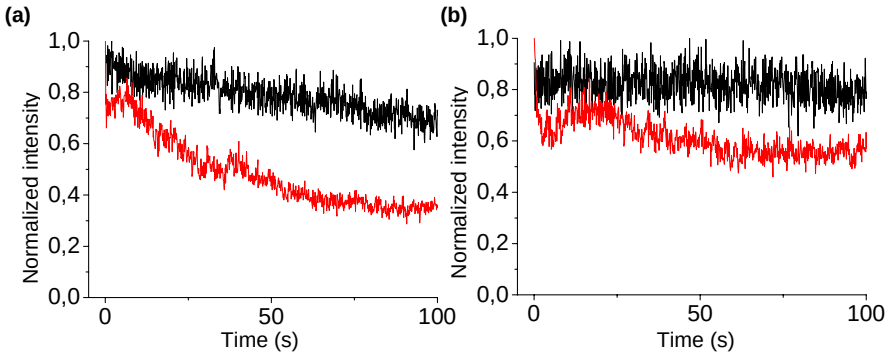

Figure 6.10. *Fluorescence time traces of aggregates of core dimers (red curve) and LH1 complexes (black curve) measured at different excitation powers (a) 370 nW, (b) 80 nW. Measurements were performed in an oxygen reduced environment.*

Spectral time traces were recorded to address whether there are differences in spectral response in the different regimes of the time trace curves. A fluorescence spectral time trace is shown in Figure 6.11a. This time trace was recorded in a small fragment of a 3D core dimer crystal (~ 1-2 μm). Different regimes can be observed in this curve. First a decrease in intensity is observed and attributed to progressive saturation of the RCs followed by an increase in LH1 fluorescence. At longer timescales a slower decrease in intensity is observed. This decrease in intensity is attributed to photobleaching of the LH1 after all the RCs are in the closed form. SVD and HCA was performed on the data set, and grouped into 5 clusters displayed in Figure 6.11c. The time traces were composed of 4096 spectra, with 100 ms integration time. These data were built into a matrix which was used to construct a square image (64 x 64 pixels) in a zigzag pattern (Figure 6.11b) color coded with the respective cluster information, the clusters appear in the following order (black, magenta, yellow, green and blue). However, after superposition of all the clusters (panel d) no apparent difference could be observed among the separated clusters. Higher level of clusters did not produce different results to the ones already presented based only on differences in intensity. Ultrafast time resolved measurements would be necessary to give quantitative information regarding energy transfer in these structures. One can conceive that with picosecond time resolution the initial rise in intensity of the LH1 fluorescence in the time traces, corresponding to regions 1 and 2 of the plot in Figure 6.9, could be resolved. In these experiments, the 1 ms integration time is the limit of our time resolution.

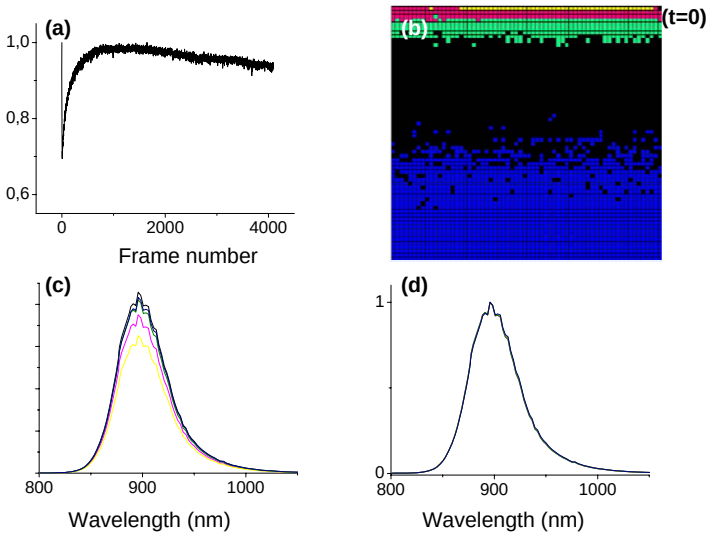

Figure 6.11. *(a) Spectral time trace on a 3D core dimer crystal. 370 nW, 100 ms integration time per frame. (b) Spatial representation of the different clusters in function of time (t = 0 at top right corner, in a zig-zag pattern), (c) Different clusters (n = 5), the appearance order is: black, magenta, yellow, green and blue. A higher number of clusters did not generate different results to the ones reported. (d) Superposition of the different clusters.*

Global imaging, a concept introduced in Chapter 4 was performed on the 3D core dimer crystals. The point spread function observed (PSF_{obs}) of the excitation beam (Figure 6.12a) was compared with the PSF_{obs} of the fluorescence emission after excitation of the crystal structure. Two different images are shown in Figure 6.12. Panel b shows the PSF_{obs} in a thick section of the crystals and panel c in a thinner section of the crystal. The exact height dimensions are unknown because in the AFFM we did not have the possibility to measure the height profile over these bulky assemblies in situ. By comparison of the images and the respective intensity profiles of the PSF_{obs}, it can be observed that the propagation length is larger in the thinner sections of the crystal. This could be due to fewer energy traps (RCs), fewer irregular domains and fractures in the thinner regions than in the thicker ones. More detailed interpretation of the data is hindered by several facts: (i) scattering because of the irregular crystal surface and structure, (ii) difficulty in assessing in which plane it is focused (at the moment the set-up does not present the possibility of

stacked imaging in the z-direction), (iii) out of focus contribution cannot be ruled out because of the inherent 3D characteristics of the sample.

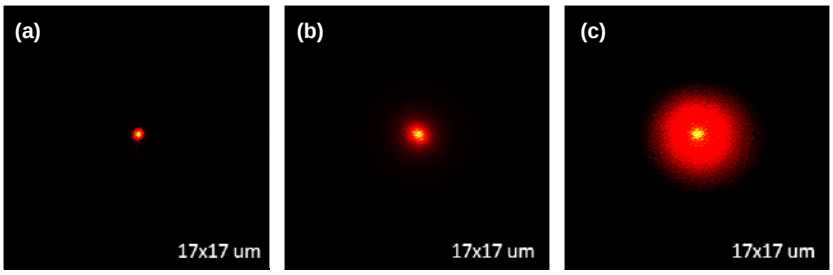

Figure 6.12. *(a) PSF_{obs} observed from the reflection of the excitation on glass substrates. PSF_{obs} of the emission upon local excitation with 800 nm excitation of a 3D core dimer crystal (b) thicker section (c) thinner section.*

6.3.2 Nanometer arrays of core-dimer complexes

In the previous section we discussed that complex 3D crystals are not optimal structures to address energy migration using the global imaging configuration of the AFFM. We tried to simplify the problem by creating 2D arrangements of core dimers with one dimension in the sub-100 nm scale. Global imaging of a 2D array does not suffer from contributions from scattered light nor from out of focus contribution since the thickness of the array is one monolayer ~10nm (<< confocal spot). Natural occurring core dimer arrays have been observed in native membranes[2] and mutants where the peripheral antenna (LH2) has been removed. Here we fabricate arrays of natural core dimers that might prove useful for elucidating the extent of excitonic energy transfer within these structures.

His_6 groups incorporated to the carboxy terminus of the RC-H subunit[18] served as anchor points for the directed assembly of core dimers on a NiNTA template surface. Chemically patterned substrates with active (NiNTA monolayers) and passivated (PEG monolayer) surfaces were created by the combination of nano-imprint lithography and a multistep covalent process for the formation of the NiNTA monolayer.[21] Upon incubation in a solution of His_6-core dimers the protein complexes selectively bound to the active areas. Figure 6.13a shows a fluorescent image of nanometer arrays of core dimer complexes. Panel b shows the comparison of the relative spectral responses, which indicated a good contrast on the different regions of the sample. Spectral time traces were acquired on lines that presented

different domains of core dimers. For example line 2 appeared to be continuous and uniform with a standard deviation of 4% in intensity. Line 3, on the contrary, was interrupted in several areas and had a standard deviation of 22 % in intensity, which is indicative of non-uniform distribution of the complexes within the assembled nanoarray. These defects can be attributed to several factors during the processing of this specific set of samples: non-uniform coating of the initial polymer layer in the NIL process, the etching time for the removal of the polymer residual layer was not enough, wearing of the silicon stamp after multiple usages (> 100), non uniform distribution of the pressure while hot embossing.

The results of SVD and HCA (4 clusters) of the spectral time traces on the lines are displayed as the clusters, superposition of clusters and a graphical representation of their occurrence in time, for line 2 panels (e), (f), (d, top) and for line 3 in panels (g), (h), (d, bottom). On line 2, an increase of the fluorescence emission form the LH1 is observed, also the signal becomes more dynamic with the increase of intensity, attributed to on/off states of the LH1 antenna (Figure 6.13c, black curve). Clusters representative of different positions on the fluorescence spectra time trace are shown in panel e. The clustering has been performed based on intensity differences, as is observed by the superposition of the normalized clusters in Figure 6.13f. For line 3, the fluorescence emission is monotonically decreasing (photobleaching). It can be speculated that this is related to the packing density in the array as similar behavior was observed with smaller fragments (sub-micron) from core dimer crystals. Global images of the arrays of core dimer are depicted in Figure 6.13 (line 2, panel i; line 3 panel j). By inspection of the images, it can be indicated that because of the close-packing of the core dimer complexes on line 2, energy propagation events can be observed at more extended locations from the excitation spot than on line 3. More experiments are necessary to quantify the extent of the energy transfer in nanometer arrays of core dimers.

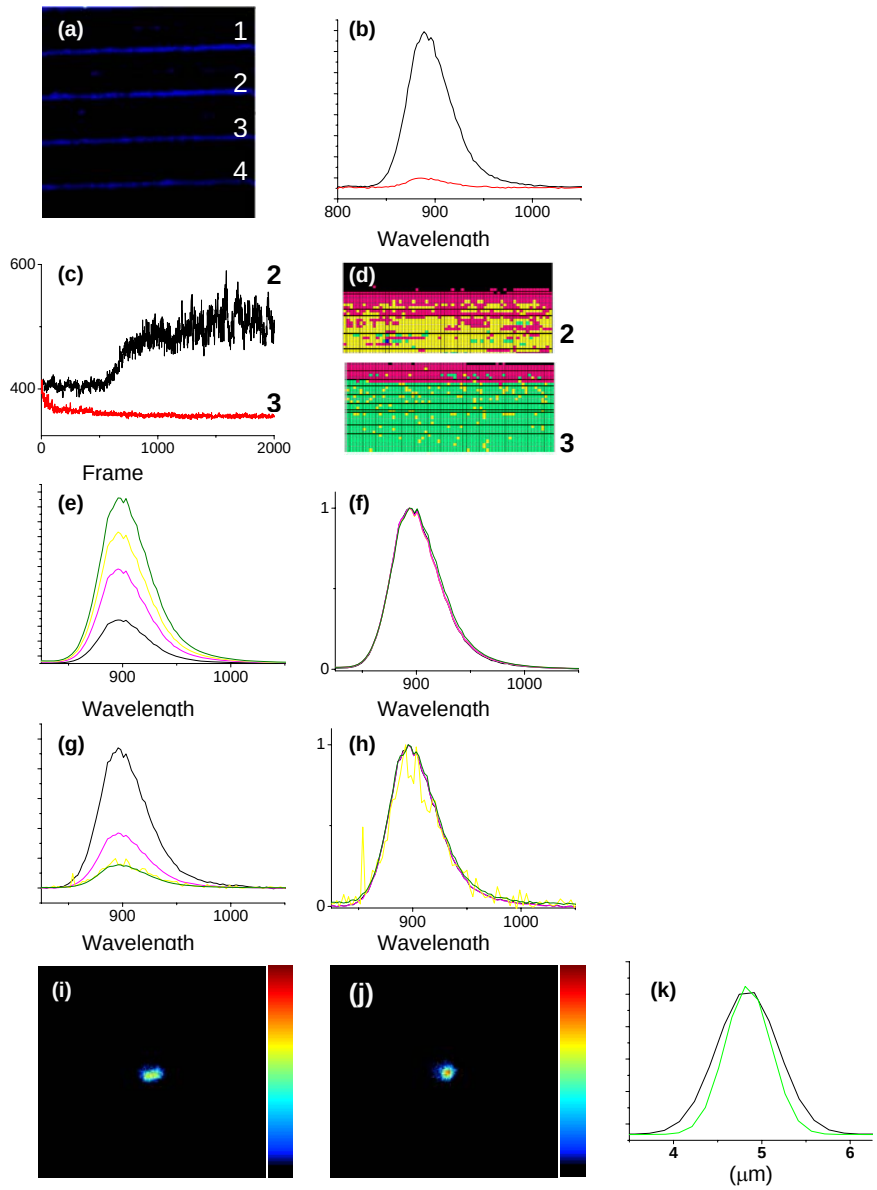

Figure 6.13*. (a) False color fluorescent image of core dimer complexes assembled onto chemically patterned substrates (NiNTA / PEG monolayer). (b) Comparison emission spectrum on active (black) and passivated (red) areas. (c) Spectra time traces acquired on lines 2 and line 3, 100 ms integration time. Results of SVD and HCA on the time traces divided in clusters, clusters normalized for comparison, and image representation, line 2 ((e), (f), (d) top) and line 3 ((g), (h), (d) bottom). PSF_{obs} of the fluorescent emission upon local excitation of patterned 2D core dimers (i) line 2, (j) line 3, 200 x 200 pixels. (k) PSF_{obs} profile, FWHM line 2 (860 nm), line 3 (650 nm)*

6.3.3 Alternative approach

At this stage we have shown we can fabricate patterns of LH complexes and that the complexes remain functional upon patterning. For structures and patterns of core complexes, the fluorescence time traces have shown a decrease and subsequent increase in the fluorescence intensity of the LH1 emission. A systematic characterization of this behavior will allow the acquisition of decay and rise times as function of excitation power and array dimensions.

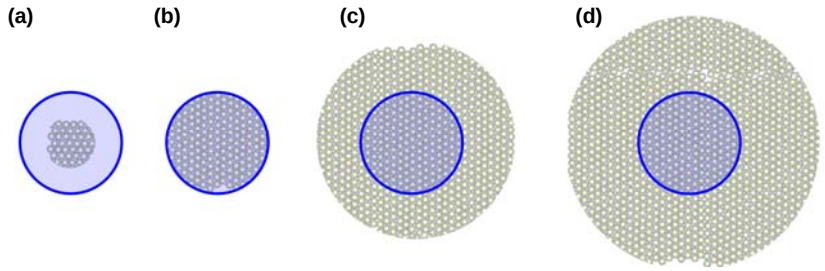

Figure 6.14*. Proposed experiment to use fluorescence time trace information as indicator for energy transfer. Arrays of core complexes of different diameters from sub-confocal dimensions up to several micrometers, for example (a) 200 nm, (b) 500 nm, (c) 1 μm, (d) 2.5 μm. The confocal laser spot is represented by the blue circle.*

An experiment is proposed in order to use the time constants associated with the fluorescence time trace plots as an indicator/evidence of the putative energy propagation in artificial arrays, but requires time resolution in the ps regime. The experiment makes use of arrays of core-dimers of different dimensions ranging from sub-confocal spot diameter up to several micrometers (~ 5 μm) as displayed in Figure 6.14. The arrays should fulfill the following requirements: (i) protein complexes should be absorbed in a consistent manner (all complexes with the same orientation on the substrate), (ii) uniform coverage (a monolayer), because aggregates and multilayer assemblies will influence the optical response of the assembly, (iii) closely packed arrangement.

Based on the previous experiments performed on core complex assemblies, it can be hypothesized that t_d will increase as the diameter of the structure increases until it reaches a plateau. For example in Figure 6.14a, b, all the complexes of the structure are directly excited by the laser beam, and a decrease in LH1 fluorescence emission at the beginning of the curve will be due to energy transfer from the LH1 to the RC, which then will recover after occupation of the RC acceptors available. If no energy

transfer occurs beyond the excited area by the laser beam, then the t_d and t_r will remain the same for the structures with diameter equal to or bigger that the excitation beam. However, if energy transfer occurs beyond the excitation area, then t_d will continue to increase in order to fill all the RCs within reach. At some moment a plateau will be reached which is associated with the maximum propagation length for a given excitation power and later it might progressively photobleach. It is worth highlighting that the fluorescent time trace is acquired always on areas of equal diameter (excitation area). The contribution to the total fluorescence signal is restricted to the area actually excited by the laser beam, neglecting the contribution to the fluorescence from the outer areas, and it is only when all the RC at reach are filled that the LH1 fluorescence emission in the sampled area starts to increase.

6.4 CONCLUSIONS

We have fabricated and characterized 3D and 2D assemblies of core dimer complexes. Crystals formed of stacked layer of core dimers are heterogeneous in size, and with a highly eroded surface. Fluorescence time traces acquired on 3D crystals indicate different regimes which can be thought to be associated with energy transfer from the complexes within the excitation confocal volume to the core complexes outside the excitation confocal volume. Similar fluorescence time traces curve were acquired on aggregates and nanopatterned core dimers arrays. Although the experiments described in the previous sections hint towards long range energy transfer between core dimers, fluorescence time resolved measurements will generate complementary information about lifetimes, excitonic coupling and quenching sites in this structures. Prospective studies include similar experiments, in the presence of a reducing agent (ascorbate or sodium dithionite[29]), it will reduce the back transfer from the RC to the LH1, increasing the time constant for the recovery of the LH1 fluorescence. It can be speculated that time traces acquired on core-dimer arrangements in the presence of an oxidative agent will lack the first deep in intensity of the fluorescence time trace.

6.5 REFERENCES

1. Scheuring, S.; Sturgis, J. N.; Prima, V.; Bernadac, A.; Levy, D.; Rigaud, J. L., Watching the photosynthetic apparatus in native membranes. *Proceedings of the National Academy of Sciences of the United States of America* **2004,** 101, (31), 11293-11297.
2. Bahatyrova, S.; Frese, R. N.; Siebert, C. A.; Olsen, J. D.; van der Werf, K. O.; van Grondelle, R.; Niederman, R. A.; Bullough, P. A.; Otto, C.; Hunter, C. N., The native architecture of a photosynthetic membrane. *Nature* **2004,** 430, (7003), 1058-1062.
3. Olsen, J. D.; Tucker, J. D.; Timney, J. A.; Qian, P.; Vassilev, C.; Hunter, C. N., The Organization of LH2 Complexes in Membranes from Rhodobacter sphaeroides. *Journal of Biological Chemistry* **2008,** 283, (45), 30772-30779.
4. Hu, X. C.; Ritz, T.; Damjanovic, A.; Autenrieth, F.; Schulten, K., Photosynthetic apparatus of purple bacteria. *Quarterly Reviews of Biophysics* **2002,** 35, (1), 1-62.
5. Allen, J. P.; Feher, G.; Yeates, T. O., Structural homology of reaction centers from Rhodopseudomonas sphaeroides and Rhodopseudomonas viridis as determined by x-ray diffraction. *Proceedings of the National Academy of Sciences of the United States of America* **1986,** 83, (22), 8589.
6. Van Brederode, M. E.; Van Grondelle, R., New and unexpected routes for ultrafast electron transfer in photosynthetic reaction centers. *FEBS Letters* **1999,** 455, (1-2), 1.
7. Van Brederode, M. E.; Van Mourik, F.; Van Stokkum, I. H. M.; Jones, M. R.; Van Grondelle, R., Multiple pathways for ultrafast transduction of light energy in the photosynthetic reaction center of Rhodobacter sphaeroides. *Proceedings of the National Academy of Sciences of the United States of America* **1999,** 96, (5), 2054.
8. Tucker, J. D. University of Sheffield, Sheffield, 2005.
9. Cogdell, R. J.; Gall, A.; KoÌˆhler, J., The architecture and function of the light-harvesting apparatus of purple bacteria: From single molecules to in vivo membranes. *Quarterly Reviews of Biophysics* **2006,** 39, (3), 227.
10. Cohen Stuart, T. A.; van Grondelle, R., Multipulse spectroscopy on the wild-type and YM210W Bacterial Reaction Centre uncovers a new intermediate state in the special pair excited state. *Chemical Physics Letters* **2009,** 474, (4-6), 352.
11. Siebert, C. A.; Qian, P.; Fotiadis, D.; Engel, A.; Hunter, C. N.; Bullough, P. A., Molecular architecture of photosynthetic membranes in Rhodobacter sphaeroides: The role of PufX. *Embo Journal* **2004,** 23, (4), 690-700.
12. Frese, R. N.; Olsen, J. D.; Branvall, R.; Westerhuis, W. H. J.; Hunter, C. N.; Van Grondelle, R., The long-range supraorganization of the bacterial photosynthetic unit: A key role for PufX. *Proceedings of the National Academy of Sciences of the United States of America* **2000,** 97, (10), 5197-5202.
13. Escalante, M.; Maury, P.; Bruinink, C. M.; van der Werf, K.; Olsen, J. D.; Timney, J. A.; Huskens, J.; Hunter, C. N.; Subramaniam, V.; Otto, C., Directed assembly of functional light harvesting antenna complexes onto chemically patterned surfaces. *Nanotechnology* **2008,** 19, (2), -.
14. Escalante, M.; Zhao, Y. P.; Ludden, M. J. W.; Vermeij, R.; Olsen, J. D.; Berenschot, E.; Hunter, C. N.; Huskens, J.; Subramaniam, V.; Otto, C., Nanometer arrays of functional light harvesting antenna complexes by nanoimprint lithography and host-guest interactions. *Journal of the American Chemical Society* **2008,** 130, (28), 8892-+.
15. Reynolds, N. P.; Janusz, S.; Escalante-Marun, M.; Timney, J.; Ducker, R. E.; Olsen, J. D.; Otto, C.; Subramaniam, V.; Leggett, G. J.; Hunter, C. N., Directed formation of micro- and nanoscale patterns of functional light-harvesting LH2 complexes. *Journal of the American Chemical Society* **2007,** 129, (47), 14625-14631.
16. Qian, P.; Bullough, P. A.; Hunter, C. N., Three-dimensional reconstruction of a membrane-bending complex - The RC-LH1-PufX core dimer of Rhodobacter sphaeroides. *Journal of Biological Chemistry* **2008,** 283, (20), 14002-14011.
17. Ng, I. University of Sheffield, Sheffield, 2009.

18. Abresch, E. C.; Axelrod, H. L. A.; Beatty, J. T.; Johnson, J. A.; Nechushtai, R.; Paddock, M. L., Characterization of a highly purified, fully active, crystallizable RC-LH1-PufX core complex from Rhodobacter sphaeroides. *Photosynthesis Research* **2005,** 86, (1-2), 61-70.
19. Maury, P.; Peter, M.; Mahalingam, V.; Reinhoudt, D. N.; Huskens, J., Patterned self-assembled monolayers on silicon oxide prepared by nanoimprint lithography and their applications in nanofabrication. *Advanced Functional Materials* **2005,** 15, (3), 451-457.
20. Zhao, Y.; Berenschot, E.; Jansen, H.; Tas, N.; Huskens, J.; Elwenspoek, M., Sub-10 nm silicon ridge nanofabrication by advanced edge lithography for NIL applications. *Microelectronic Engineering* **2009,** 86, (4-6), 832.
21. Maury, P.; Escalante, M.; Peter, M.; Reinhoudt, D. N.; Subramaniam, V.; Huskens, J., Creating nanopatterns of his-tagged proteins on surfaces by nanoimprint lithography using specific NiNTA-Histidine interactions. *Small* **2007,** 3, (9), 1584-1592.
22. Kassies, R.; Van der Werf, K. O.; Lenferink, A.; Hunter, C. N.; Olsen, J. D.; Subramaniam, V.; Otto, C., Combined AFM and confocal fluorescence microscope for applications in bio-nanotechnology. *Journal of Microscopy-Oxford* **2005,** 217, 109-116.
23. Barros, T.; Royant, A.; Standfuss, J.; Dreuw, A.; Kuhlbrandt, W., Crystal structure of plant light-harvesting complex shows the active, energy-transmitting state. *Embo Journal* **2009,** 28, (3), 298-306.
24. Golub, G. H.; van Loan, C. F., *Matrix computations*. North Oxford Academic Publishing: Oxford, 1983.
25. Uzunbajakava, N.; Lenferink, A.; Kraan, Y.; Volokhina, E.; Vrensen, G.; Greve, J.; Otto, C., Nonresonant confocal Raman imaging of DNA and protein distribution in apoptotic cells. *Biophysical Journal* **2003,** 84, (6), 3968-3981.
26. Kramer, H.; Jones, M. R.; Fowler, G. J. S.; Francke, C.; Aartsma, T. J.; Hunter, C. N.; Amesz, J., Energy Migration in Rhodobacter-Sphaeroides Mutants Altered by Mutagenesis of the Peripheral Lh2 Complex or by Removal of the Core Lh1 Complex. *Biochimica Et Biophysica Acta-Bioenergetics* **1995,** 1231, (1), 89-97.
27. Paillotin, G.; Swenberg, C. E.; Breton, J.; Geacintov, N. E., Analysis of Picosecond Laser-Induced Fluorescence Phenomena in Photosynthetic Membranes Utilizing a Master Equation Approach. *Biophysical Journal* **1979,** 25, (3), 513-533.
28. Den Hollander, W. T. F.; Bakker, J. G. C.; Van Grondelle, R., Trapping, loss and annihilation of excitations in a photosynthetic system. I. Theoretical aspects. *BBA - Bioenergetics* **1983,** 725, (3), 492.
29. Lu, Y.; Xu, J.; Liu, B.; Kong, J., Photosynthetic reaction center functionalized nano-composite films: Effective strategies for probing and exploiting the photo-induced electron transfer of photosensitive membrane protein. *Biosensors and Bioelectronics* **2007,** 22, (7), 1173.

Chapter 7

Assembly of LH2 complexes on glass-gold substrates

In this chapter we describe the fabrication of micro- and nanostructured substrates that combine gold and SiO_2 (glass) or CaF_2 and their subsequent chemical functionalization by means of self-assembled monolayers for the adsorption of light harvesting complexes. We use fluorescence and Raman microscopy to examine the optical properties of the LHCs immobilized on the different surfaces. Increased photostability of LH2 complexes on the patterned gold regions is reported. Also, we present hybrid micro- and nanostructures that combine photosynthetic protein complexes and metal nanoparticles. We report the observation of metal enhanced fluorescence and surface enhanced Raman signals on the gold nanoparticle patterns.

7.1 INTRODUCTION

Functional devices combining conductive and insulating materials, or organic and inorganic layers, are essential for creating novel platforms for optoelectronics and sensing. Such complex platforms with smart interfaces are usually based on micro- and nanoengineered substrates together with self-assembly of molecules or nanoscopic objects with tailored physical and chemical properties. Biomicroelectromechanical systems (BioMEMS) are mainly constructed of two types of materials: silicon and metal-patterned silicon. The metal usually acts as a sensing layer that interacts directly with the analyte while the substrate usually remains passive to the analyte in order to ensure high signal-to-noise ratio. Surface properties of the substrates are modified by physical or chemical means to control the assembly on the surfaces of the target molecules. The most extensively studied systems are self-assembled monolayers (SAMs) on gold and silicon(oxide) substrates[1-5] To date these SAMs have been applied to study the adsorption of a wide range of biomolecules.

The photosynthetic unit (PSU) of purple bacteria has been envisioned as a candidate for the fabrication of hybrid organic-inorganic devices. The PSU is composed of a macromolecular network, which behaves as a molecular optical and electronic circuit organized by a protein scaffold.[6] Photosynthetic membrane proteins have previously been adsorbed on different substrates such as gold,[7-8] SiO_2 (glass),[9-10] and ITO.[11] In these studies the authors reported that the optical properties of the light harvesting complexes (LHC) were preserved. However, no comparative study has been presented of LHC integrity and functionality in microstructured gold-glass substrates.

Here we describe the fabrication of micro- and nanostructured substrates that combine gold and SiO_2 (glass) or CaF_2 and their chemical functionalization by means of SAMs. The substrates serve as a platform for the immobilization of the photosynthetic membrane protein light harvesting complexes LH1 and LH2 from *Rhodobacter sphaeroides.* We use fluorescence and Raman microscopy to examine the optical properties of the LHCs adsorbed on the different surfaces. Furthermore, we fabricate micro- and nanometer patterns of gold nanoparticles. Metal substrates with controlled nanoscale roughness, which allow for a strong electromagnetic enhancement, are commonly used to exploit surface-enhanced effects.[12] Here we use

nanoparticle patterned substrates to: (i) evaluate the possibility of metal enhanced fluorescence of the photosynthetic proteins and (ii) as substrates for surface-enhanced Raman spectroscopy (SERS).

In the last section of this chapter we demonstrate the use of convective assembly for the fabrication of substrates coated with gold nanoparticles for SERS characterization of LHCs. The results are compared with the observations on non-structured micrometer gold patterns where, in contrast to the assemblies on gold nanoparticle arrays, the fluorescence is quenched and the Raman signal is very low.

7.2 MATERIALS AND METHODS

Compounds: All chemicals were used as received. *N*-3-(trimethoxysilyl)propyl-ethylenediamine (Aldrich), 1H,1H,2H,2H perfluorodecyltrichlorosilane (ABCR), octadecanethiol (ODT) 98% purity Sigma-Aldrich.

Protein purification: The LH2 complex was solubilized from membranes from photosynthetically grown *Rhodobacter sphaeroides* using 4% *N*,*N*-Dimethyldodecylamine-*N*-oxide (LDAO), and purified on DEAE (Sigma) and Resource Q (GE Healthcare) columns, then size fractionated on a Superdex 200 gel filtration column (GE Healthcare). The mutagenesis protocol has been described before.[13]

Preparation of PDMS stamps: PDMS stamps were prepared by casting a manually mixed 10:1 solution (v/v) of poly(dimethylsiloxane) and curing agent (Sylgard 184, Dow Corning) against a patterned silicon master. The stamps were cured overnight at 60 °C. Silicon masters fabricated by photolithography contained micrometer-sized features (hexagonally oriented 5 μm circular features separated by 3 μm) and treated with 1H,1H,2H,2H perfluorodecyltrichlorosilane to facilitate separation of the PDMS from the master.

Planar gold–glass (or CaF_2) substrate preparation: glass substrates (microscope coverslips, Menzel-glaser # 1,5) were cleaned by immersion in piranha solution (3:1 concentrated H_2SO_4 / 33% aqueous H_2O_2) for 15 min, rinsed copiously with water and dried with a stream of N_2. *Warning: Piranha solution should be handled with care.* CaF_2 windows for Raman, 20mm diameter x 2mm thick (Crystran Ltd., UK) were cleaned by immersion into ethanol for 10 minutes in an ultrasonic bath and dried with a stream of N_2. Deposition of a 2 nm chromium layer (adhesion

promoter) and a 20 nm gold layer was performed in a sputtering system, in an Argon atmosphere at 6.6 x 10^{-3} mbar. Cleaning of fresh gold coated substrates was performed by immersion into ethanol for 10 min. The ink was applied to the PDMS stamps by exposing the stamps to a drop of ODT (0.3 mM) solution in ethanol for 1 min. The gold substrates and stamps were dried with a continuous stream of nitrogen prior to printing. All the printing experiments were carried out manually with a printing duration of one minute.

Wet-chemical etching of gold: Etching of the unprotected gold was achieved by immersing the gold substrates in an aqueous solution of 1.0 M NaOH, 0.1 M $Na_2S_2O_3$, 0.01 M $K_3Fe(CN)_6$, and 0.001 M $K_4Fe(CN)_6$ at room temperature for 7 min. *Warning: potassium ferricyanide is light sensitive. Photodecomposition releases products that can contain free cyanide. Potassium ferricyanide is also incompatible with acids and liberates HCN.*

***Attachment of gold nanoparticles*:** Particle attachment was performed using a suspension of 40 nm diameter gold nanoparticles (BBInternational, 10^6 particles/ml). The vertical deposition setup[14] consisted of a stepper motor (RS instruments, Code 191-8334) driven by a control card (RS instruments, GSM2 unipolar stepper motor driver). A gear box attached to the motor decreased the number of revolutions per minute (RS instruments 641:1). The withdrawal speed was 0.1 μm/s. The PMMA template was removed by immersion in acetone in an ultrasonic bath for 1 hour.

Chemical functionalization: Substrates were cleaned in O_2 plasma (300 W, 0,3 mbar, 1 min) and then submerged in ethanol prior to chemical functionalization. Mercaptoundecanoic acid (MUA) self-assembled monolayers were selectively formed on the gold areas following well-established procedures,[8, 15-17] by the immersion of the substrates in 1 mM solution of MUA in ethanol for 18 h and then rinsed with ethanol. *N*-3-(trimethoxysilyl)propylethylenediamine (TPEDA) monolayer formation on the glass (or CaF_2) substrates was performed by gas-phase evaporation in a desiccator under vacuum for two hours. Functionalized substrates were rinsed and sonicated in ethanol and dried in a stream of N_2. To achieve a covalent bond between the carboxylic acid terminated SAM and the LH2 complexes, the MUA SAM was first activated to form surface-bound N-hydroxysuccinimidyl esters by exposure of the sample to an aqueous solution of N-

hydroxysuccinimide (Sigma) (20 mM) and 1-ethyl-3,3-dimethyl carbodiimide (Sigma) (20 mM) for 30 minutes.[8, 18-19]

Sample characterization:

Fluorescence spectral microscopy: Fluorescence spectral microscopy was performed using 800 nm excitation from a diode laser (Roithner Laser Technik, RLT80010MG). The laser beam is reflected via a dichroic beam splitter (Chroma, Q850LPXXR) towards an oil-immersion objective (Nikon, Plan Fluor 100 ×NA 1.3), which focuses the light onto the sample. The fluorescence light is collected by the same objective and passes through the dichroic beam splitter. By switching a flip mirror, the fluorescence light can be directed either towards a single photon counting avalanche photodiode (APD) (SPCM-AQR-14, Perkin Elmer Optoelectronics) or towards a custom designed prism-based spectrograph equipped with a liquid nitrogen-cooled CCD camera (Spec-10:100B, Princeton Instruments) with single molecule sensitivity.[20]

AFM imaging: A custom-built stand-alone AFM combined with a confocal fluorescent (spectral) microscope was used for morphological and optical characterization.[20] For AFM imaging, standard silicon nitride cantilevers with a length of 85 μm, force constant of 0.5 N/m, and operating frequencies of 85–155 kHz (in air) (ThermoMicroscopes, Sunnyvale, CA) were used. AFM images were obtained using tapping mode. Images contained either 256x256 or 512x512 pixels and were recorded at a line scanning frequency of 2–4 Hz. Topographical images were quantitatively analyzed using the Scanning Probe Image Processor (SPIP) software (Image Metrology ApS, Lyngby, Denmark).

Contact angles: were measured on a Krüss G10 contact angle setup equipped with a CCD camera. Advancing and receding contact angles were determined automatically during growth and reduction of a clean water droplet by the droplet shape analysis routine.

XPS measurements: were performed on a Quantera SXM (Scanning XPS microprobe) from Physical Electronics, equipped with a monochromatic Al KR X-ray source producing approximately 25 W of X-ray power. XPS data were collected from a surface area of 600 x 300 μm with pass energy of 224 eV and a step energy of 0.8 eV for survey scans and 0.25 eV for element scans with an equal number of sweeps for all elements.

Confocal Raman microscopy: Raman microspectroscopy and imaging were performed using an custom-built confocal Raman microscope.[21] A Krypton ion laser (Coherent, Innova 90K, Santa Clara, CA) emitting at 647.1 nm was used as an excitation source. A water immersion objective with 63x magnification and 1.2 NA (Zeiss Plan Neofluar, Carl Zeiss. Thornwood, NY) is used for focusing the laser light on the sample. The microscope in epi-illumination detection mode uses the same objective for collecting the Raman scattered photons. A custom built spectrograph disperses the Raman scattered photons on an air-cooled EMCCD (Newton DU-970N, Andor Technology, Belfast, Northern Ireland) which provided a spectral resolution of 1.85 to 2.85 cm^{-1}/pixel. A 15 μm pinhole in front of the spectrograph determined the confocality of the detector. Raman imaging is accomplished by recording the full spectra (-20 to 3670 cm^{-1}) from each excited position. A scanning beam was used for illumination. Raman images were acquired over an area of 20 × 20 μm^2 with 64 × 64 pixels, 125 μW laser power and an accumulation time of 100 ms/pixel resulting in a hyperspectral data cube.

7.3 RESULTS AND DISCUSSION

7.3.1 Micrometer Patterning of LH2 complexes onto Au-glass substrates

The different environment around the fluorophore can influence the radiative decay rate. For example, interactions with metal surfaces can have a number of effects including increase of the photostability, increased distances for resonance energy transfer, and fluorescence quenching.[22] Here we fabricated substrates of glass and non-structured gold patterns in order to compare the optical response of the LHC on both surfaces. This approach allowed us to (i) quantify average quenching by the metal substrate underneath, (ii) to compare the photostability of the LHC immobilized on both materials, and (iii) have a reference sample with non-roughened gold (no gold nanoparticles) and glass where we could compare spectral response.

Microcontact printing (μCP) was used to pattern micrometer circular patterns of octadecanothiol (ODT) on a freshly deposited gold surface. The fabrication process is shown in Figure 7.1. Poly-(dimethylsiloxane) (PDMS) is a soft, chemically

crosslinked rubber that establishes conformal contact with a substrate and exhibits excellent printing characteristics with apolar inks such as alkanethiols.[23-24]

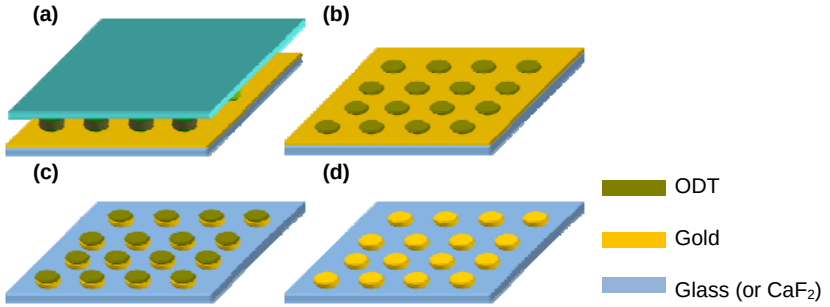

Figure 7.1. *Schematic representation of μCP process used for the fabrication of gold patterns onto glass (or CaF_2) substrates. (a) The PDMS stamp is incubated with an ODT solution and placed in contact with the gold substrate. (b) The printed contact areas are protected by the ODT SAM, which acts as an etch-resistant layer. (c) Selective wet-chemical etching of the gold results in a hexagonal array of gold patterns. (d) The substrate is treated in an oxygen plasma environment for the removal of the protective ODT monolayer, leaving the gold area available for further functionalization.*

A PDMS stamp was immersed in an ODT solution (0.3 mM in ethanol) for 1 minute. The stamp was dried and printed on a gold substrate for 1 minute (Figure 7.1a) resulting in the formation of an ODT SAM on the areas in contact with the substrate (Figure 7.1b). The etch-resistant properties of alkanethiols, such as ODT, are based on steric hindrance and wettability properties. The alkyl chain is hydrophobic, and given the dense packing, the SAM shields the underlying substrate from aqueous solutions.[25] The gold substrates were etched in a solution that comprises a basic solution containing $K_2S_2O_3/K_3Fe(CN)_6/K_4Fe(CN)_6$ at pH 14.[26] This aqueous etch solution is known to be superior to the conventional gold etch solution (aqueous KCN at pH 14) in terms of etch rate and selectivity.[26] This approach resulted in substrates with defined gold and glass (or CaF_2) areas. In order to render the patterned gold areas suitable for selective and independent functionalization by using self-assembly techniques, a cleaning step is necessary to remove the ODT monolayer from the gold areas, and is achieved by mild exposure to O_2 plasma, and further immersion in ethanol for 30 minutes. An alternative procedure for the substitution of the ODT SAM for a different thiol SAM is the exposure of the sample to UV light. Upon exposure to UV light the thiol adsorbates are converted to sulfonate species which, unlike the thiols, are only weakly adsorbed

to the gold surface.[27] These sulfonates could be easily displaced and substituted on the surface upon immersion in a solution of a contrasting thiol adsorbate, (in this case, mercaptoundecanoic acid, MUA, a carboxylic acid terminated thiol). Selective functionalization of the heterogeneous substrates has been performed using standard procedures.[17, 28] The gold regions were modified by immersion of the sample in a MUA solution (1 mM in ethanol) for 18 h. Subsequently the complementary areas were modified with an amino-terminated silane deposited from the gas phase. The substrates were briefly sonicated in ethanol to remove any physisorbed material on the surface.[29] Carboxyl groups of the MUA surfaces were activated using *N*-hydroxysuccinimide and 1-ethyl-3,3-dimethyl carbodiimide.[18-19] The result of the activation process is the formation of active ester intermediates at the monolayer surface which react with free amine groups (from lysine residues on the protein, e.g. LH2) to form amide linkages.

A dilute solution of LH2 complexes (0.2 μM in buffer pH 8, 20mM Hepes, 0.3% βDDM) was incubated for 20 minutes on the substrates and then gently washed with buffer solution. On the gold patterned regions, the high number of lysine residues, solely found on the cytoplasmic face of LH2, ensures adequate attachment and probably directs a consistent topology for bound complexes.[8] On the amino-terminated regions, previous work has shown that the LH2 complexes bind due to electrostatic interactions,[9] but this time towards the periplasmic face due to the presence of glutamic and aspartic residues on this side. The fluorescence emission properties of micron-scale patterns of LH2 on the different materials were examined using a confocal fluorescence microscope[20] equipped with an avalanche photodiode (APD) and a CCD camera with a monochromator wavelength selector.

The sample was illuminated with monochromatic light of 800 nm; this coincides with one of the two major near infrared absorbance bands of LH2. Excitation energy is transferred from the B800 to the B850 molecules within the LH2 complex, from which the energy is eventually lost as fluorescence. For fluorescence characterization, the sample had to be placed with the patterned side facing the objective protected by a thin layer of buffer and a clean glass coverslip (Figure 7.2); otherwise the fluorescence signal emitted from the gold regions could not go through the 20 nm thick gold layer and be detected by the objective.

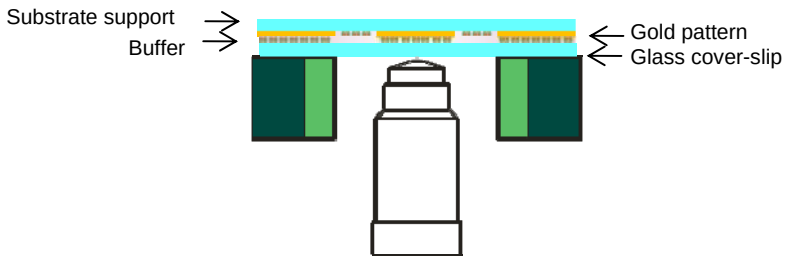

Figure 7.2. *Schematic of the placement of the gold-patterned substrates for the characterization of the protein complexes assemblies on the different areas. The patterned side faces the objective and is protected by a buffer solution and a glass coverslip.*

Figure 7.3a shows the fluorescence image of LH2 complexes immobilized onto the patterned Au-glass substrate. The darker circular features correspond to the areas where the LH2 complexes have been adsorbed on the gold patterns. The surrounding light blue areas correspond to areas with LH2 complexes adsorbed on glass. The fluorescence emission spectra on each area (average over 15 pixels) can be observed in Figure 7.3b. The curves have been normalized with respect to the LH2 maximum emission on glass regions (black curve). The LH2 fluorescence emission on the gold regions is decreased by approximately 70 % with respect to the LH2 fluorescence intensity immobilized on the glass regions. Figure 7.3c shows the LH2 emission spectra on each area (gold, glass) normalized to their respective emission maxima. The LH2 emission on the gold areas is slightly shifted (1.6 nm) towards the red, the difference spectra is shown in the inset in panel c. A comparison of the photostability of the fluorophore on the different substrates has been acquired by measuring the emission intensity with continuous excitation over time. Figure 7.3d shows photostability curves (fluorescence time traces) measured on the different areas with the same incident light intensity. When the curves are normalized at time zero, it is evident that the LH2 complexes on the gold regions photobleach slower than those on the glass regions. The difference in bleaching decay times reflect that LH2 adsorbed on gold has different dynamic parameters than LH2 on glass. Fluorophores in close proximity with planar metal surfaces display a decrease in fluorescence lifetime.[22] Photochemical reactions occur while the fluorophore is in the excited state. If the lifetime is shorter, it is more probable that the fluorophore emits before it undergoes decomposition; therefore it can

undergo more excitation-relaxation cycles before it permanently photobleaches, increasing the photostability of the fluorophore.[22] The increased photostability of core complexes on gold substrates has been reported before.[30]

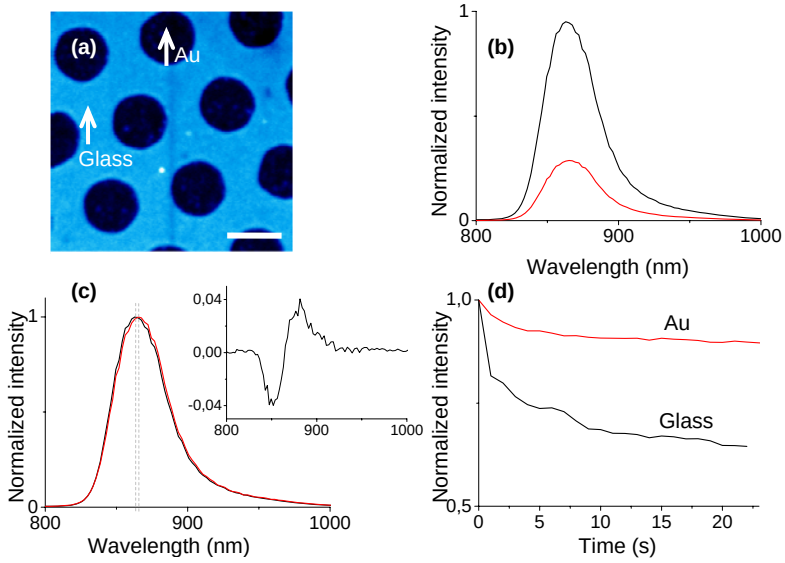

Figure 7.3. *(a) Fluorescence image (false color) of LH2 complexes on an Au / glass substrate, scale bar 5 µm. Fluorescence emission spectra of LH2 complexes on each area, Au islands red curve, glass areas black curve (b) normalized with respect to the maximum emission on the Au patterned areas. (c) each spectrum normalized with respect to their respective maximum emission, difference spectra (red-black) shown in the inset. (d) Fluorescence timetraces normalized at t = 0 s. The measurements were performed in ambient oxygen condition because the sample has to be sandwiched with a glass coverslip underneath.*

The fluorescence time traces information could also be used to rule out that the difference in LH2 emission intensity (displayed in Figure 7.3a) is due only to differences in concentration of protein complexes on the different surfaces (i.e. less LH2 adsorbed on the gold patterns). Because the bleaching rate is independent of the concentration of the fluorophore (at the same excitation power)[31] if the difference in LH2 emission intensity would be solely an effect different concentrations on the gold and glass patterns, the fluorescence time traces should be superimposable after normalization at t = 0 s. Since this is clearly not the case (Figure 7.3d), the decrease in fluorescence intensity emission on the gold pattern is attributed to interaction with the gold substrate, for example fluorescence quenching due to the underlying metal.

Selective assembly of LH2 complexes exclusively on the gold pattern could also be achieved. For this purpose, after functionalization of the Au areas with MUA as described before, the glass regions were functionalized with a polyethylene glycol derivative (PEG) silane.[28] Oligo(ethyleneglycol) derivatives have been found to exhibit good resistance to the adsorption of plasma and membrane proteins.[8] When proteins approach a PEG modified surface, the highly hydrated PEG chains minimize the hydrophobic interaction of the proteins with the surfaces, and the space available for the polymer chains to occupy is decreased, leading to a decrease in the chain conformational entropy.[32] The substrates with the MUA self-assembled monolayers (SAMs) on gold and PEG on glass substrate were then immersed in aqueous solution EDC/NHS for 30 min to attach the NHS group to the –COOH termini of SAMs prior to the incubation with the protein solution.

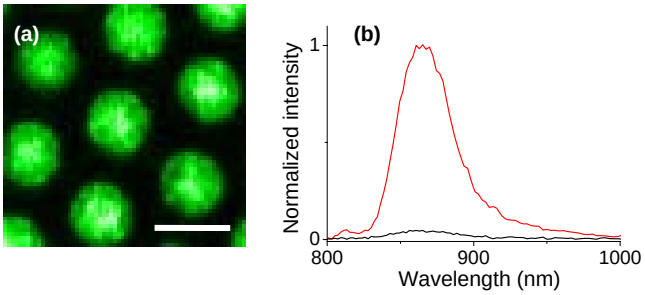

Figure 7.4. *Spectral image of the directed assembly of LH2 complexes onto gold islands, scale bar 5 µm. The surrounding glass substrate has been passivated with PEG-silane.*

Figure 7.4a shows a spectral image of the LH2 complexes immobilized onto the gold patterned areas shown as green dots. The PEG passivated areas correspond to the darker regions. The intensity of the emission spectra intensity on the gold and the passivated areas the emission spectra have been normalized with respect to the LH2 maximum emission on the gold pattern (Figure 7.4b). The fluorescence intensity on the passivated areas is reduced by 94%. Since the fluorescence intensity on the gold areas is quenched by the metal as shown in Figure 7.3b, the reduction of unspecific protein binding on the passivated areas is most likely even better than the value derived from Figure 7.4b because it has to be corrected by the quenching ratio.

7.3.2 Nanometer Patterning of LH2 complexes onto Au-glass substrates

Glass-gold substrates could also be prepared with structures of gold in the nanometer regime. Nanoimprint lithography (NIL) was carried out on a gold-covered substrate to create nanometer chemical patterns of ODT. The schematic of the fabrication procedure is displayed in Figure 7.5.

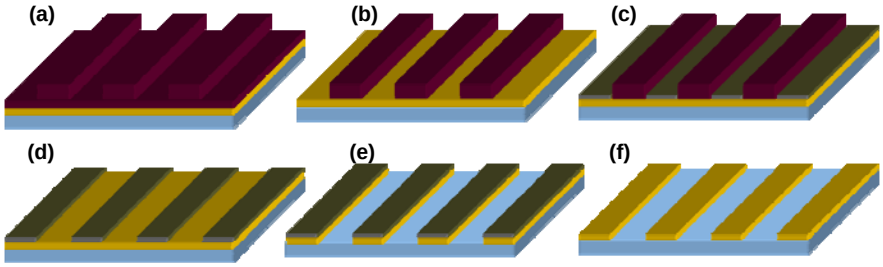

Figure 7.5. *(a) Nanoimprint lithography is performed on a 20 nm thick gold-coated glass coverslip substrate. (b) Removal of the polymer residual layer by O_2 RIE and subsequent immersion in ethanol. (c) Functionalization of the exposed gold areas with ODT. (d) Removal of the polymer mask by immersion in acetone. (e) Selective wet-chemical etching of the gold results in trenches in the gold. (f) The protective ODT monolayer is removed in a mild oxygen plasma environment.*

A silicon stamp with nanoridges (40 nm wide, 100 nm height, 4 µm period), fabricated by the combination of edge lithography and wet chemical etching, was used. [33] PMMA nanogrooves with a 4 µm period were created on the gold substrate. After NIL the residual layer was removed in O_2 RIE in order to expose the underlying gold. The substrate was immersed in ethanol for 30 min and subsequently immersed in an ODT solution (0.3 mM in ethanol) for 1 min. The ODT will assemble inside the small trenches in the PMMA layer and later the ODT SAM serves as a mask for wet-chemical etching of the gold. The polymer template was removed in acetone for 10 minutes in order to expose the unprotected gold to the gold-etching solution.

A SEM microscopy image of the nanometer gold arrays is displayed in Figure 7.6a. Parallel lines of gold with a width of 80 ± 5 nm could be reproducibly fabricated. LH2 complexes were assembled on the glass nanopatterned gold substrates following the same chemical functionalization used for the micrometer size gold features. Upon binding of the LH2 complexes on the substrates, quenching of the fluorescence on the planar nanoarrays could be observed, although not very clearly because the width of the lines are smaller that the optical resolution of the

microscope, resulting in contributions from LH2 bound to the glass surface around the Au lines also being detected during imaging. The fluorescence image is shown in Figure 7.6b. The areas where the LH2 complexes are adsorbed on the gold patterns are indicated by the white arrows at the bottom of the image.

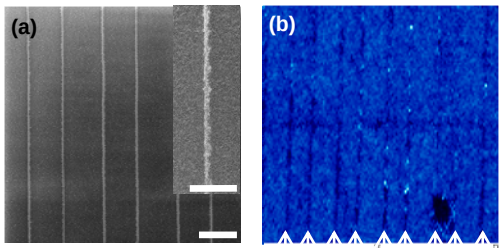

Figure 7.6. *(a) Scanning electron microscope image (SEM) of Au nanometer lines on a glass substrate prepared by the combination of NIL and the selective wet-chemical etching of Au, scale bar 4µm, inset scale bar 500 nm. (b) Fluorescence image (false color) of LH2 complexes on the substrate from panel a. The fluorescence intensity in the gold nanolines is reduced due to quenching because of the close proximity with the metal substrate.*

7.3.3 Patterning of LH2 complexes onto colloidal gold assemblies

Highly ordered structures of nanoparticles exhibit attractive properties for future nanoelectronics. One novel type of hybrid structure incorporates photosynthetic molecules and metallic substrates.[34-36] Experiments with these structures are aimed at the construction of sensitive sensors and efficient photocells and utilize the photosynthetic molecules as an active medium due to their high quantum yield and energy conversion efficiency. In this section we present hybrid micro- and nanostructures that combine photosynthetic protein complexes and metal nanoparticles. Effects such as metal enhanced fluorescence and enhanced Raman microscopy of LH2 complexes on the gold nanoparticle patterns have been observed. The electromagnetic field arising from the excitation of localized surface plasmon (LSPs) resonances from the roughness features (gold nanoparticles) is responsible for fluorescence enhancement due to an increase in the local electric field.

7.3.3.1 *Preparation of colloidal gold assemblies on patterned surfaces and attachment of LH2 complexes*

Spherical gold nanoparticles of 40 nm in diameter were used as building blocks for the fabrication of multiparticle patterns. We created micro- and nanometer arrays of gold nanoparticles by the combination of nanoimprint lithography and convective assembly. The general scheme for the fabrication of the nanoparticle arrays is depicted in Figure 7.7.

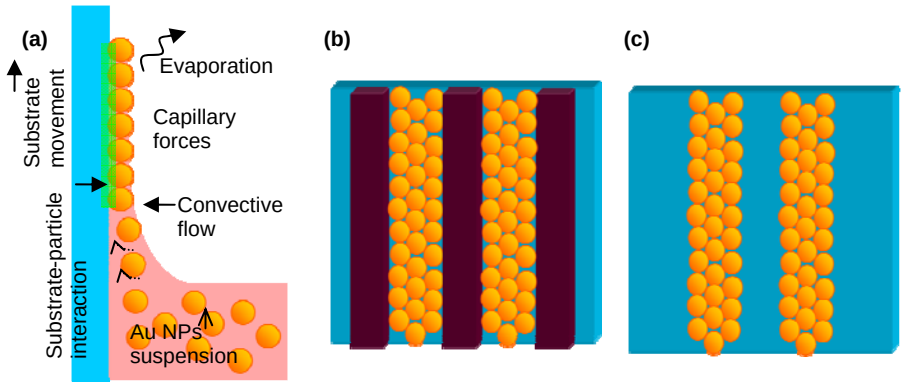

Figure 7.7. *(a)Schematic representation of the convective assembly process of gold nanoparticles onto polymer templated substrates prepared by NIL. The polymer features act as a physical barrier on a glass substrate while the sample is withdrawn from the particle suspension at constant speed. (b) Representation of the particle assembly on the patterned substrate and (c) after removing the polymer template.*

Convective assembly assisted by capillary forces was performed by dragging the meniscus of an aqueous colloidal suspension over a substrate at constant velocity (Figure 7.7a). This approach has been previously examined by others for the assembly of various types of particles.[14, 37-40] The polymer template is used to define the x-y dimensions of the particle assemblies. Here, we also make use of electrostatic interactions between an amino-terminated monolayer on a glass (or CaF_2) substrate and citrate-coated gold colloids. The confinement effect induced by the meniscus coupled to the capillary forces appearing between particles during the drying process leads to the formation of a continuous 2D lattice. The layer of particles grows while the substrate is withdrawn from solution together with the already formed layer as is indicated in Figure 7.7a. If the withdrawal rate is equal to the rate of layer formation, a homogeneous layer grows continuously. The 40 nm

gold particles are assembled on the polymer free areas (Figure 7.7b) and subsequently the polymer template can be removed (Figure 7.7c). Three major process parameters can be used to control the coating thickness and structure: (i) the substrate velocity, (ii) the particle volume fraction, and (iii) the solvent evaporation rate.[41] A systematic variation of all parameters has not been attempted in these experiments.

Figure 7.8 a-c shows different examples of 40 nm gold nanoparticle arrays. NIL has been used for the fabrication of the polymer patterns of PMMA. After NIL and removal of the polymer residual layer by O_2 RIE, the substrate was functionalized with an amino-terminated silane in the gas phase. The substrate was immersed in the nanoparticle suspension and withdrawn at constant speed (0.1 μm/s, 20 ºC). After assembly, the polymer template was removed by sonication in acetone for 1 hour. After this prolonged treatment in the ultrasonic bath, the particles remained bound to the surface which reflects the stability of the assembly. Figure 7.8a shows a SEM image of an array of two particles width in a zigzag arrangement. Wider arrays, 1.5 μm in width, constituting a single layer of particles, can be observed in panel b. The particles are closely arranged, although only small domains exhibit a perfect hexagonal packing. Panel c shows arrays of 160 nm in width (4 gold nanoparticles). In the inset it can be observed that the particles are closely packed. This last arrangement (4 particles) is used as a substrate for the assembly of LH2 complexes.

Prior to the adsorption of the protein complexes, the substrates were exposed to O_2 plasma to remove any surfactant remaining on the surface of the gold nanoparticles and immersed in absolute ethanol to render the surfaces suitable for further functionalization as in the previous sections. A (false color) fluorescence image of LH2 complexes adsorbed on nanometer arrays of gold nanoparticles (~160 nm in width) and on the surrounding glass is presented in Figure 7.8d. Metallic particles can cause quenching, can concentrate the incident light field, and can also increase the radiative decay rate.[42] In this case, in contrast to the assembly of the LH2 complexes onto the flat-Au substrates shown in Figure 7.3 and Figure 7.6, the fluorescence emission of the LH2 complexes on the Au nanoparticles is enhanced by a factor of ~5.5 instead of being quenched as revealed by the intensity profile along the patterned substrate (Figure 7.8e). Aggregates of gold colloids with very

short interparticle separation have shown a broad absorption band through the red and near-infrared region because of the strong particle-particle interaction.[43-48]

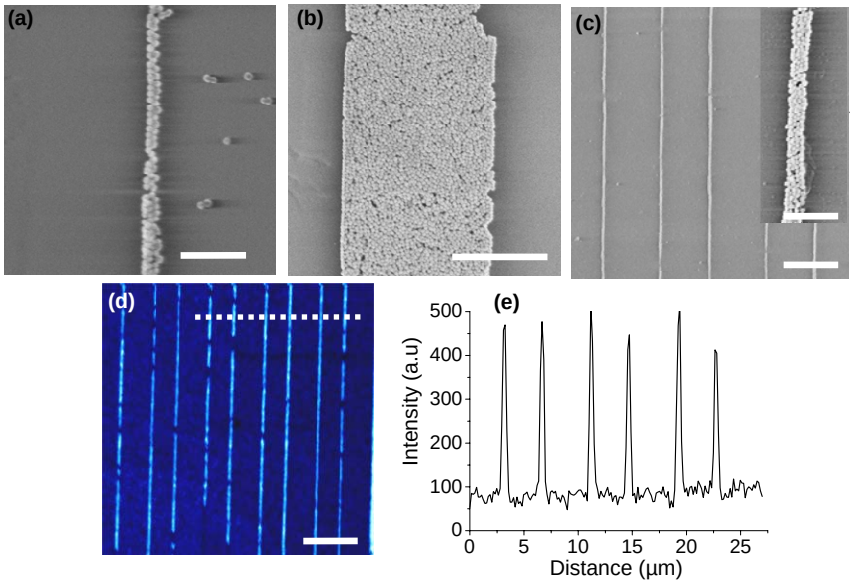

Figure 7.8. *SEM image of 40 nm diameter gold nanoparticles arrays on a glass substrate (a) scale bar 400 nm. (b) scale bar 1µm. (c) Scale bar 4µm, inset scale bar 400 nm. (d) Fluorescence image (false color) of LH2 complexes deposited on the Au NPs arrays and on the glass regions, 2 µW, 0.5 ms integration time. (e) Fluorescence intensity profile along the dotted line (panel d)*

Characterization of the enhancement and spectral response on the LH2 complexes is carried out on surfaces patterned with gold nanoparticles arrays of micrometer dimensions, and the corresponding fluorescence image is shown in Figure 7.9a. The gold nanoparticles and glass regions are indicated by the arrows in Figure 7.9a. The fluorescence intensity on the glass regions is uniform, with an intensity variation of ± 4%. The variation in the intensity of the emission of LH2 on Au NPs arrays is approximately 30%. The non-uniformity of the spatial distribution of the fluorescence emission is possibly due to significant variations in the local field around the nanoparticles. Interactions between nanoparticles may also affect the variation. Figure 7.9b shows an averaged intensity profile along the patterned areas as is indicated by the white box in the figure. The intensity on the Au NPs is on average approximately 4 to 7 fold higher than the intensity on the glass regions and is slightly red-shifted (panel c). We have assumed that the density of LH2

complexes (number LH2 complexes per gold surface unit) is the same for the assemblies on the gold micrometer patterns and on the gold nanoparticle patterns. A small emission band is observed at 975 nm. This band is absent in the particles patterned alone on the surface and also in the solution of the gold particles. The origin of this band in the emission for the LH2 on the particle arrays is at this moment unknown.

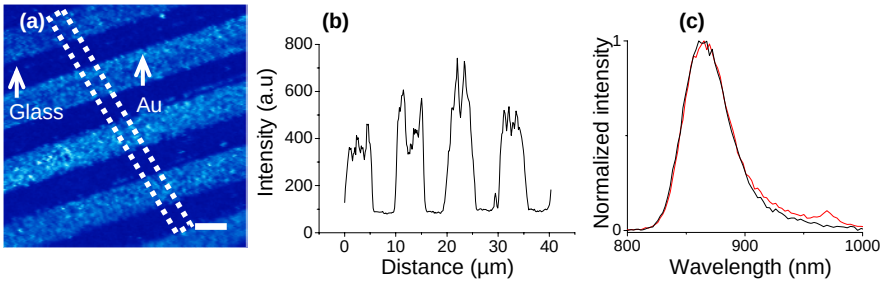

Figure 7.9. *(a) Fluorescence microscopy image of LH2 complexes patterned on Au-NPs/Glass areas. (b) Fluorescence intensity profile along the dotted area in panel (a). (c) Fluorescence emission spectra of LH2 complexes on each area, Au NPs red curve, glass areas black curve each spectrum normalized with respect to the value at their respective maximum emission.*

7.3.3.2 Raman and surface-enhanced Raman Spectroscopy of LH2 complexes.

Glass substrates are not suitable for Raman microscopy due to the large background signal in the fingerprint region (500 – 2000 cm^{-1}). A common substrate used for Raman microscopy is CaF_2 because of its very flat baseline with low noise in both fingerprint and high frequency regions and only one very sharp peak at 322 cm^{-1}.[49] Preliminary attempts were performed in order to render the CaF_2 substrates suitable for protein adsorption, (i) either by the deposition of a self-assembled monolayer or (ii) by the deposition of a thin silicon oxide (SiOx) layer and subsequent use of conventional silane chemistry. X-ray photoelectron spectroscopy (XPS) and water contact angle (CA) measurements were performed on references substrates to evaluate the chemical surface modification procedure. Surface-enhanced Raman spectroscopy (SERS) makes use of metal substrates with controlled nanoscale roughness which allows a strong electromagnetic enhancement. In this section we assembled gold colloids from solution on a CaF_2

solid support for use as a SERS substrate. Raman spectra of LH complexes monolayers were acquired either from CaF_2/Au or CaF_2/Au nanoparticles substrates.

Direct chemical functionalization of CaF_2 substrates.

Self-assembled monolayers were deposited from the gas phase onto CaF_2 substrates which were previously treated in O_2 plasma. To study whether the monolayer was deposited on the substrates, XPS and CA measurements were performed on four different substrates. (i) CaF_2 (after 10 minutes sonication in ethanol), (ii) CaF_2 cleaned in a O_2 plasma, (iii) CaF_2 cleaned in a O_2 plasma and amino-terminated silane, and (iv) CaF_2 cleaned in a O_2 plasma and fluorosilane. The XPS spectra (3 times 600 x 300 μm^2) areas of the four samples are shown in Figure 7.10. Panel (a), (b) show the XPS spectra from the CaF_2 and CaF_2 + O_2 plasma respectively. This is basically a cleaning step where the adsorbed fluorocarbon from the environment is removed. The most significant difference between these spectra is the absence of the C(1s) peak (289 eV) in the O_2 plasma-treated substrate. Also, there is a slight increase in the O_2 content of 8% with respect to the non-treated CaF_2 slide. CA measurements also show marked difference between both samples; the advancing CA of the bare CaF_2 changed from $\theta = 60$ to $\theta \leq 5$ degrees after O_2 plasma treatment. Amino-terminated and perfluorinated silane was adsorbed from the gas phase onto O_2 plasma treated CaF_2 slides. Most silane monolayers are formed on oxide substrates to which they can covalently bind. Their stability on other substrates depends on lateral crosslinking and polymerization and not on direct binding to the substrates.[50] Surprisingly, after sonication in acetone both monolayers remained bound to the substrates. Figure 7.10c,d shows the survey XPS spectra, in panel c, the N(1s)-peak (401.87 eV) confirms the formation of the amino-terminated SAM. This peak is absent on the other 3 samples. The Si(2p)-peak (102.92 eV) present in panels (c) and (d) further support the adsorption of the monolayers on the CaF_2 substrates. High resolution XPS data are in reasonable agreement with full layers of the respective silanes. However, water contact angle measurements show a large hysteresis between the advancing and the receding contact angle (difference ~ 25 - 35°) for both SAMs which indicate non uniform coverage of the surface. This might be attributed to the roughness of the CaF_2 substrates which has been investigated by AFM microscopy (Figure 7.11).

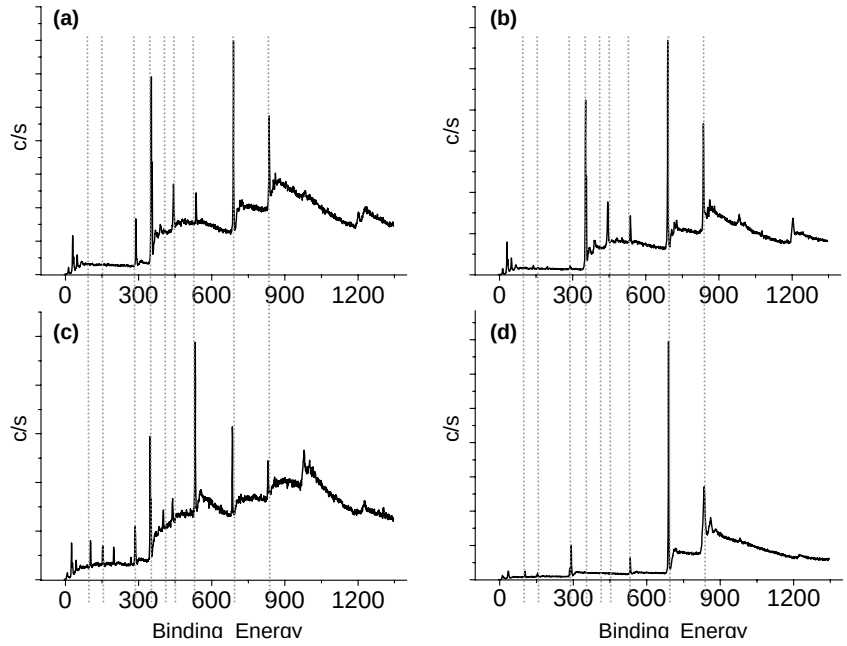

Figure 7.10. *(a) CaF_2, (b) CaF_2 + O_2 plasma treatment, (c) CaF_2 + O_2 plasma treatment + aminosilane, (d) CaF_2 + O_2 plasma treatment + fluorosilane.*

Table 1. XPS analysis of the CaF_2 substrates after different treatments

CaF_2 substrate	XPS (%)					
	C(1s)	N(1s)	O(1s)	F(1s)	Si(2p)	Ca(2p)
Bare	29.31	0.00	11.75	35.99	0.00	22.94
$O_{2\text{-plasma}}$	4.35	0.00	12.79	53.77	0.00	29.09
$O_{2\text{-plasma- aminosilane}}$	21.74	6.22	25.62	23.45	6.46	16.51
$O_{2\text{-plasma- fluorosilane}}$	32.54	0.00	5.32	58.74	3.37	-

An AFM topography of bare CaF_2 substrates is shown in Figure 7.11a. The AFM image reveals fractures at the surface of the substrate, which has a mean roughness of ~ 5 nm over an area of 1 μm^2. It is anticipated that patterns formed on these substrates will have the same irregularities in their structure.

As an alternative for the deposition of monolayers directly onto CaF_2, first a deposition of a layer of SiO_x can be performed on the substrates and then conventional silane chemistry can be used to modify the properties of the surface.

Figure 7.11b shows an AFM topograph of a CaF_2 substrate after deposition of SiO_x. The mean roughness over an area of 1 μm^2 is ~ 5.5 nm; this value indicates that there is not a significant variation in roughness due to the deposition of the SiO_x layer. The deposition of SiO_x was confirmed by water contact angle measurements and XPS. The layer proved to be firmly adsorbed to the substrate since it withstood prolonged immersion in an ultrasonic bath in ethanol and the "scotch tape" test. Direct measurement on the SiO_x layer on the CaF_2 by ellipsometry was not possible because the refractive indexes of both materials at the wavelength used (632 nm) are very close in range. The 30 nm thickness of the layer was measured by ellipsometry on a reference sample deposited on a Si substrate.

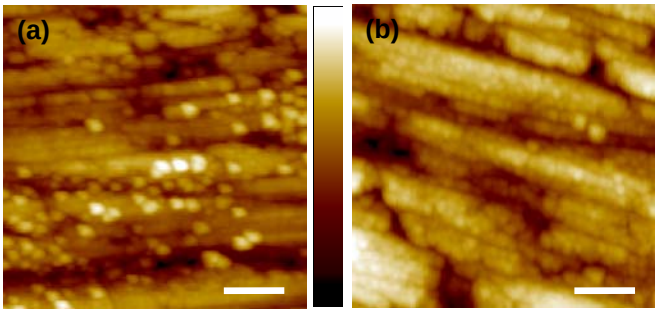

Figure 7.11. *AFM height image of CaF_2 substrates before, scale bar 200 nm, z-scale 0-20 nm, 512 x 512 pixels (a) before (b) and after deposition of 30 nm thick SiO_x.*

LH complexes assemblies on gold–CaF_2 substrates.

Micrometer size gold patterns were fabricated on top of CaF_2 substrates following the same procedure described in section 7.3.1. Despite the nanoscale irregularities of the substrate, the μCP process turned out to be successful due to the flexibility of the stamp and the possibility of conformational contact with the gold layer underneath. The sample was incubated in a solution of LH1 or LH2 complexes and subsequently gently washed with buffer. The sample was kept in liquid (20 mM Hepes, 0.03% βDDM. pH 8) at ambient conditions for the duration of the measurements. Raman imaging was performed with 647.1 nm light which is non-resonant with the absorption bands of the LH2 complex. Images of 64 x 64 pixels were acquired from the substrates with an excitation power of 5 mW (measured at the back aperture of the objective) with 100 ms integration time.

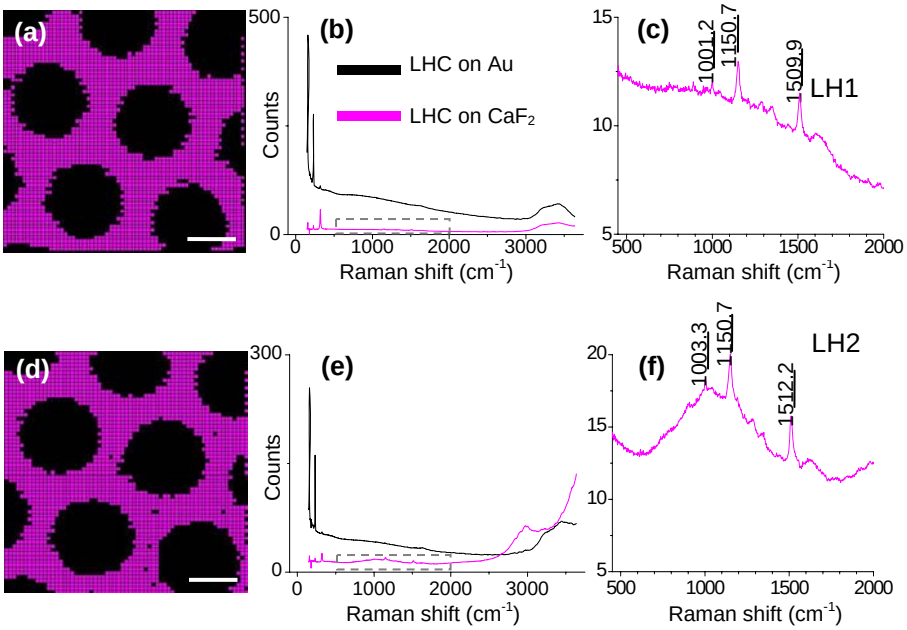

Figure 7.12. *Raman Spectral image after SVD and HCA, scale bar 4 µm. LH complexes were immobilized onto CaF_2 substrates patterned with 5µm diameter gold islands. Raman spectra were acquired at 5 mW excitation power measured at the back aperture of the objective. Full range Raman spectra and inset in the fingerprint region are shown: (a, b, c) LH1, (d, e, f) LH2 complexes*

For the analysis of the data first singular value decomposition (SVD)[51-52] was applied in order to reduce the noise of the individual spectra followed by hierarchical cluster analysis (HCA). HCA enables to identify major components present in each spectrum and to group them into similar spectral clusters. Figure 7.12 shows typical Raman spectral images and representative spectra of LH complexes onto the gold-CaF_2 substrates. Figure 7.12 (a), (d) shows the two-level cluster image reconstructed from the Raman spectra acquired in the regions of interest for substrates coated with LH1 and LH2 respectively. The black colored circles are the areas corresponding to the gold pattern. The pink colored areas correspond to the CaF_2 regions. Figure 7.12 (b), and (e) show the average Raman spectra of pixels corresponding to magenta and black in the low, middle and high frequency regions, also an inset from the fingerprint region is shown in panels (c), (f) for LH1 and LH2 respectively. The curves recorded on the gold pattern showed two distinctive bands in the Raman spectra at 160 and 232 cm^{-1}. Further inspection

of the Raman spectra by expanding the view in the fingerprint region of the LH2 assemblies on gold did not show significant Raman bands of the analyte. Poor Raman signal on planar gold substrates has been reported before.[53] Although the CaF_2 substrate showed a considerable roughness before any treatment, which will result in gold patterns with similar topography, this roughness was not enough to induce any surface enhancement of the signal. The band at 321.8 cm^{-1} is the Raman band of the CaF_2 which is higher on the non-gold coated regions, magenta spectra (after removal of the baseline). At the high frequency region, in particular in the LH2 spectra, the signal from 3000 cm^{-1} onwards is result of the fluorescence from the sample. The fact that the protein complex is still fluorescent in the near infrared region indicates that the complex is still intact under these imaging conditions.

The expanded view in the fingerprint region of the LHC assemblies on the CaF_2 shows distinctive Raman bands (Figure 7.12 panel c for LH1, and panel f for LH2). In the LH1 and LH2 spectra strong bands (indicated on the curves) can be observed at 1001.2-1003 due to ring breathing of the molecule, 1150.7 due to C-C bonds and 1509.9 cm^{-1} due to C=C bonds. These bands are attributed to spheroidene/spheroidenone, the most abundant carotenoid present in this bacterial strain. To the best of our knowledge this is the first time Raman microscopy of light harvesting complexes from *Rb. sphaeroides* monolayers at RT is carried out without surface enhanced aid. Previous reports are in solution[54 55] or on roughened silver substrates at 77 K.[54]

Gold nanoparticle assemblies were formed as described in section 7.3.3.1 on CaF_2 slides in order to use these substrates for SERS. The excitation power used for the SERS measurements was reduced to 125 μW, 40 times smaller than the power used on bare CaF_2 and non-structured gold. Higher powers were not necessary and moreover could compromise the integrity of the LHC because of the enhancement of the electromagnetic field which could damage the complexes affecting their integrity and the photophysical response of the fluorophores. Figure 7.13 a,b shows the SERS spectra for LH1 and LH2 respectively. From these curves, it can be observed that the overall signal-to-noise level in the SERS spectra was substantially better than in the Raman measurements (Figure 7.12), for both the LH1 complexes where similar intensity was obtained with 40 times less power and in particular for the LH2 where the intensity was increased 30-fold. Also, several differences are

observed from the comparison of the SERS and RS spectra. In the SERS signal the carotenoid bands are enhanced, and the spectra is much richer in bands than in RS. These bands are assumed to be due to the Bchl a.[54] We have shown that these substrates yield increases in the Raman cross-section that are large enough to compensate for both the inherently low intensity of the Raman effect and the limited signals expected for a monolayer.

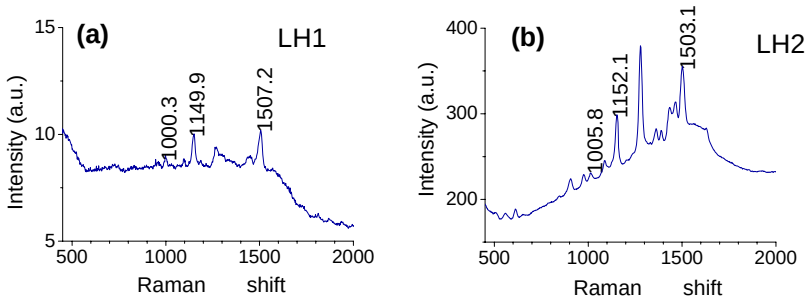

***Figure 7.13**. SERS spectroscopy of light harvesting complexes bound onto 40 nm diameter Au NPs assembled on a CaF_2 substrate (similar to Figure 7.8), excitation power at back aperture of the objective 125µW, 100 ms integration time. (a) LH1, (b) LH2.*

This experimental approach can be further improved by performing Surface Enhanced Resonance Raman spectroscopy (SERRS) exciting directly the Q_x and Q_y transition of the bacteriochlorophylls. Alternative substrates can be used which offer the possibility of a more controlled surface modification method and that are suitable for Raman microscopy such as quartz (which only has bands in the low wavenumber range < 500 cm^{-1})[49] or silicon substrates. However, the latter has very prominent bands at 520 and 940-980 cm^{-1} and a significant increase in baseline from 1200 cm^{-1} onwards.

7.4 CONCLUSIONS

Micro- and nanometer arrays of LH complexes have been fabricated on gold-patterned glass (or CaF_2) substrates. LH2 complexes assembled on gold patterns showed longer photostability. This is presumably due to the excited state quenching by the metal. Arrays of gold nanoparticles were fabricated on glass and CaF_2 slides. Due to the enhancement of the electric field and strong coupling of the particles, metal-particle fluorescence enhancement effects were observed when the LH2

proteins complexes were adsorbed on those structures. Also, these assemblies proved to be suitable as substrates for SERS measurements.

Substrates with nanometer gold features can be used to study the effect of the metal substrate in energy transfer experiments which include energy propagation along the arrays and modulation of energy transfer between donor-acceptor pairs such as LH2 and LH1 complexes. As a prospective application, hybrid photosynthetic nanoparticle assemblies could be used to generate plasmon-enhanced photocurrent. Different gold nanoparticles can be used, for example gold nanorods can provide a higher enhancement factor because of the higher Q extinction in the near-infrared region.[56]

7.5 REFERENCES

1. Wen, K.; Maoz, R.; Cohen, H.; Sagiv, J.; Gibaud, A.; Desert, A.; Ockos, B. M., Postassembly chemical modification of a highly ordered organosilane multilayer: New insights into the structure, bonding, and dynamics of self-assembling silane monolayers. *ACS Nano* **2008,** 2, (3), 579.
2. Ulman, A., Formation and structure of self-assembled monolayers. *Chemical Reviews* **1996,** 96, (4), 1533.
3. Nuzzo, R. G.; Allara, D. L., Adsorption of bifunctional organic disulfides on gold surfaces. *Journal of the American Chemical Society* **1983,** 105, (13), 4481.
4. Delamarche, E.; Michel, B.; Biebuyck, H. A.; Gerber, C., Golden interfaces: The surface of self-assembled monolayers. *Advanced Materials* **1996,** 8, (9), 719.
5. Sagiv, J., Organized monolayers by adsorption. 1. Formation and structure of oleophobic mixed monolayers on solid surfaces. *Journal of the American Chemical Society* **1980,** 102, (1), 92.
6. Das, R.; Kiley, P. J.; Segal, M.; Norville, J.; Yu, A. A.; Wang, L. Y.; Trammell, S. A.; Reddick, L. E.; Kumar, R.; Stellacci, F.; Lebedev, N.; Schnur, J.; Bruce, B. D.; Zhang, S. G.; Baldo, M., Integration of photosynthetic protein molecular complexes in solid-state electronic devices. *Nano Letters* **2004,** 4, (6), 1079-1083.
7. Kondo, M.; Nakamura, Y.; Fujii, K.; Nagata, M.; Suemori, Y.; Dewa, T.; Iida, K.; Gardiner, A. T.; Cogdell, R. J.; Nango, M., Self-assembled monolayer of light-harvesting core complexes from photosynthetic bacteria on a gold electrode modified with alkanethiols. *Biomacromolecules* **2007,** 8, (8), 2457.
8. Reynolds, N. P.; Janusz, S.; Escalante-Marun, M.; Timney, J.; Ducker, R. E.; Olsen, J. D.; Otto, C.; Subramaniam, V.; Leggett, G. J.; Hunter, C. N., Directed formation of micro- and nanoscale patterns of functional light-harvesting LH2 complexes. *Journal of the American Chemical Society* **2007,** 129, (47), 14625.
9. Escalante, M.; Maury, P.; Bruinink, C. M.; Van Der Werf, K.; Olsen, J. D.; Timney, J. A.; Huskens, J.; Neil Hunter, C.; Subramaniam, V.; Otto, C., Directed assembly of functional light harvesting antenna complexes onto chemically patterned surfaces. *Nanotechnology* **2008,** 19, (2).
10. Escalante, M.; Zhao, Y. P.; Ludden, M. J. W.; Vermeij, R.; Olsen, J. D.; Berenschot, E.; Hunter, C. N.; Huskens, J.; Subramaniam, V.; Otto, C., Nanometer arrays of functional light harvesting antenna complexes by nanoimprint lithography and host-guest interactions. *Journal of the American Chemical Society* **2008,** 130, (28), 8892-+.

11. Suemori, Y.; Nagata, M.; Nakamura, Y.; Nakagawa, K.; Okuda, A.; Inagaki, J. I.; Shinohara, K.; Ogawa, M.; Iida, K.; Dewa, T.; Yamashita, K.; Gardiner, A.; Cogdell, R. J.; Nango, M., Self-assembled monolayer of light-harvesting core complexes of photosynthetic bacteria on an amino-terminated ITO electrode. *Photosynthesis Research* **2006,** 90, (1), 17-21.
12. Garrell, R. L., Surface-enhanced Raman spectroscopy. *Analytical Chemistry* **1989,** 61, (6), 401 A.
13. Olsen, J. D.; Robert, B.; Siebert, A.; Bullough, P. A.; Hunter, C. N., Role of the c-terminal extrinsic region of the alpha polypeptide of the light-harvesting 2 complex of Rhodobacter sphaeroides: A domain swap study. *Biochemistry* **2003,** 42, (51), 15114-15123.
14. Maury, P.; Escalante, M.; Reinhoudt, D. N.; Huskens, J., Directed assembly of nanoparticles onto polymer-imprinted or chemically patterned templates fabricated by nanoimprint lithography. *Advanced Materials* **2005,** 17, (22), 2718-+.
15. Bain, C. D.; Troughton, E. B.; Tao, Y. T.; Evall, J.; Whitesides, G. M.; Nuzzo, R. G., Formation of monolayer films by the spontaneous assembly of organic thiols from solution onto gold. *Journal of the American Chemical Society* **1989,** 111, (1), 321.
16. Nuzzo, R. G.; Fusco, F. A.; Allara, D. L., Spontaneously organized molecular assemblies. 3. Preparation and properties of solution adsorbed monolayers of organic disulfides on gold surfaces. *Journal of the American Chemical Society* **1987,** 109, (8), 2358.
17. Vogel, N.; Jung, M.; Retsch, M.; Knoll, W.; Jonas, U.; Köper, I., Laterally patterned ultraflat surfaces. *Small* **2009,** 5, (7), 821.
18. Patel, N.; Davies, M. C.; Hartshorne, M.; Heaton, R. J.; Roberts, C. J.; Tendler, S. J. B.; Williams, P. M., Immobilization of protein molecules onto homogeneous and mixed carboxylate-terminated self-assembled monolayers. *Langmuir* **1997,** 13, (24), 6485.
19. Montague, M.; Ducker, R. E.; Chong, K. S. L.; Manning, R. J.; Rutten, F. J. M.; Davies, M. C.; Leggett, G. J., Fabrication of biomolecular nanostructures by scanning near-field photolithography of oligo(ethylene glycol)-terminated self-assembled monolayers. *Langmuir* **2007,** 23, (13), 7328.
20. Kassies, R.; Van der Werf, K. O.; Lenferink, A.; Hunter, C. N.; Olsen, J. D.; Subramaniam, V.; Otto, C., Combined AFM and confocal fluorescence microscope for applications in bio-nanotechnology. *Journal of Microscopy-Oxford* **2005,** 217, 109-116.
21. Pully, V. V.; Lenferink, A.; Otto, C., Hybrid Rayleigh-, Raman and TPE fluorescence spectral confocal microscopy of living cells. *Journal of Raman spectroscopy* **2009**. In press
22. Lakowicz, J. R., *Principles of Fluorescence Spectroscopy*. 3rd ed ed.; Springer: 2006.
23. Love, J. C.; Estroff, L. A.; Kriebel, J. K.; Nuzzo, R. G.; Whitesides, G. M., Self-assembled monolayers of thiolates on metals as a form of nanotechnology. *Chemical Reviews* **2005,** 105, (4), 1103-1169.
24. Gates, B. D.; Xu, Q. B.; Stewart, M.; Ryan, D.; Willson, C. G.; Whitesides, G. M., New approaches to nanofabrication: Molding, printing, and other techniques. *Chemical Reviews* **2005,** 105, (4), 1171-1196.
25. Sharpe, R. B. A.; Burdinski, D.; Huskens, J.; Zandvliet, H. J. W.; Reinhoudt, D. N.; Poelsema, B., Oxidized gold as an ultrathin etch resist applied in microcontact printing. *Journal of the American Chemical Society* **2006,** 128, (49), 15560-15561.
26. Xia, Y. N.; Mrksich, M.; Kim, E.; Whitesides, G. M., Microcontact Printing of Octadecylsiloxane on the Surface of Silicon Dioxide and Its Application in Microfabrication. *Journal of the American Chemical Society* **1995,** 117, (37), 9576-9577.
27. Leggett, G. J., Scanning near-field photolithography-surface photochemistry with nanoscale spatial resolution. *Chemical Society Reviews* **2006,** 35, (11), 1150-1161.
28. Lan, S.; Veiseh, M.; Zhang, M., Surface modification of silicon and gold-patterned silicon surfaces for improved biocompatibility and cell patterning selectivity. *Biosensors and Bioelectronics* **2005,** 20, (9), 1697.

29. Aminuzzaman, M.; Kado, Y.; Mitsuishi, M.; Miyashita, T., Immobilization of a fluorinated polymer Langmuir-Blodgett monolayer on a solid substrate for surface nanocoating. *Journal of Materials Chemistry* **2004,** 14, (20), 3014-3018.
30. Aartsma, T. J.; Hunter, C. N.; Olsen, J. D.; Magis, G.; Frese, R.; Leggett, G. J.; Reynolds, N. P.; Jones, M. In *Stability and activity of light-harvesting complexes assembled on a gold electrode*, Light Harvesting Processes LHP 2009, Kloster Banz, Staffelstein, Germany, 2009; Kloster Banz, Staffelstein, Germany, 2009; p 208.
31. Benson, D. M.; Bryan, J.; Plant, A. L., Digital imaging fluorescence microscopy: Spatial heterogeneity of photobleaching rate constants in individual cells. *Journal of Cell Biology* **1985,** 100, (4), 1309-1323.
32. Sharma, S.; Johnson, R. W.; Desai, T. A., Ultrathin poly(ethylene glycol) films for silicon-based microdevices. *Applied Surface Science* **2003,** 206, (1-4), 218-229.
33. Zhao, Y.; Berenschot, E.; Jansen, H.; Tas, N.; Huskens, J.; Elwenspoek, M., Sub-10 nm silicon ridge nanofabrication by advanced edge lithography for NIL applications. *Microelectronic Engineering* **2009,** 86, (4-6), 832.
34. Das, R.; Kiley, P. J.; Segal, M.; Norville, J.; Yu, A. A.; Wang, L.; Trammell, S. A.; Reddick, L. E.; Kumar, R.; Stellacci, F.; Lebedev, N.; Schnur, J.; Bruce, B. D.; Zhang, S.; Baldo, M., Integration of photosynthetic protein molecular complexes in solid-state electronic devices. *Nano Letters* **2004,** 4, (6), 1079-1083.
35. Frolov, L.; Rosenwaks, Y.; Carmeli, C.; Carmeli, I., Fabrication of a photoelectronic device by direct chemical binding of the photosynthetic reaction center protein to metal surfaces. *Advanced Materials* **2005,** 17, (20), 2434-2437.
36. Govorov, A. O.; Carmeli, I., Hybrid structures composed of photosynthetic system and metal nanoparticles: Plasmon enhancement effect. *Nano Letters* **2007,** 7, (3), 620.
37. Maya, L.; Stevenson, K. A.; Muralidharan, G.; Thundat, T. G.; Kenik, E. A., Assembly of gold nanoclusters on silicon surfaces. *Langmuir* **2002,** 18, (6), 2392.
38. Wybourne, M. N.; Hutchison, J. E.; Clarke, L.; Brown, L. O.; Mooster, J. L., Fabrication and electrical transport characteristics of low-dimensional nanoparticle arrays organized by biomolecular scaffolds. *Microelectronic Engineering* **1999,** 47, (1-4), 55-57.
39. Chi, L. F.; Hartig, M.; Drechsler, T.; Schwaack, T.; Seidel, C.; Fuchs, H.; Schmid, G., Single-electron tunneling in Au-55 cluster monolayers. *Applied Physics a-Materials Science & Processing* **1998,** 66, S187-S190.
40. Schmid, G.; Baumle, M.; Beyer, N., Ordered two-dimensional monolayers of Au-55 clusters. *Angewandte Chemie-International Edition* **2000,** 39, (1), 181-+.
41. Malaquin, L.; Kraus, T.; Schmid, H.; Delamarche, E.; Wolf, H., Controlled particle placement through convective and capillary assembly. *Langmuir* **2007,** 23, (23), 11513-11521.
42. Lakowicz, J. R., Radiative decay engineering: Biophysical and biomedical applications. *Analytical Biochemistry* **2001,** 298, (1), 1-24.
43. Grant, C. D.; Schwartzberg, A. M.; Norman, T. J.; Zhang, J. Z., Ultrafast electronic relaxation and coherent vibrational oscillation of strongly coupled gold nanoparticle aggregates. *Journal of the American Chemical Society* **2003,** 125, (2), 549-553.
44. Khlebtsov, N. G.; Dykman, L. A.; Krasnov, Y. M.; Mel'nikov, A. G., Light absorption by the clusters of colloidal gold and silver particles formed during slow and fast aggregation. *Colloid Journal* **2000,** 62, (6), 765-779.
45. Quinten, M.; Kreibig, U.; Schonauer, D.; Genzel, L., Optical-Absorption Spectra of Pairs of Small Metal Particles. *Surface Science* **1985,** 156, (Jun), 741-750.
46. Westcott, S. L.; Oldenburg, S. J.; Lee, T. R.; Halas, N. J., Construction of simple gold nanoparticle aggregates with controlled plasmon-plasmon interactions. *Chemical Physics Letters* **1999,** 300, (5-6), 651-655.
47. Xu, H.; Tseng, C. H.; Vickers, T. J.; Mann, C. K.; Schlenoff, J. B., Near-Infrared Surface-Enhanced Raman-Spectroscopy of Chemisorbed Compounds on Gold Colloids. *Surface Science* **1994,** 311, (3), L707-L711.

48. Zhang, F.; Skoda, M. W. A.; Jacobs, R. M. J.; Dressen, D. G.; Martin, R. A.; Martin, C. M.; Clark, G. F.; Lamkemeyer, T.; Schreiber, F., Gold Nanoparticles Decorated with Oligo(ethylene glycol) Thiols: Enhanced Hofmeister Effects in Colloid-Protein Mixtures. *Journal of Physical Chemistry C* **2009,** 113, (12), 4839-4847.
49. Schuster, K. C.; Reese, I.; Urlaub, E.; Gapes, J. R.; Lendl, B., Multidimensional information on the chemical composition of single bacterial cells by confocal Raman microspectroscopy. *Analytical Chemistry* **2000,** 72, (22), 5529-5534.
50. Olson, L. G.; Lo, Y. S.; Beebe T.P, Jr.; Harris, J. M., Characterization of silane-modified immobilized gold colloids as a substrate for surface-enhanced Raman spectroscopy. *Analytical Chemistry* **2001,** 73, (17), 4268.
51. Golub, G. H.; van Loan, C. F., *Matrix computations*. North Oxford Academic Publishing: Oxford, 1983.
52. Uzunbajakava, N.; Lenferink, A.; Kraan, Y.; Volokhina, E.; Vrensen, G.; Greve, J.; Otto, C., Nonresonant confocal Raman imaging of DNA and protein distribution in apoptotic cells. *Biophysical Journal* **2003,** 84, (6), 3968-3981.
53. Chen, H.; Wang, Y.; Dong, S.; Wang, E., An approach for fabricating self-assembled monolayer of Ag nanoparticles on gold as the SERS-active substrate. *Spectrochimica Acta - Part A: Molecular and Biomolecular Spectroscopy* **2006,** 64, (2), 343.
54. Chumanov, G.; Picorel, R.; De Zarate, I. O.; Cotton, T. M.; Seibert, M., Resonance Raman and surface-enhanced resonance Raman spectra of LH2 antenna complex from Rhodobacter sphaeroides and Ectothiorhodospira sp. Excited in the Qx and Qy transitions. *Photochemistry and Photobiology* **2000,** 71, (5), 589.
55. Sturgis, J. N.; Robert, B., Pigment binding-site and electronic properties in light-harvesting proteins of purple bacteria. *Journal of Physical Chemistry B* **1997,** 101, (37), 7227.
56. Vial, S.; Pastoriza-Santos, I.; Pérez-Juste, J.; Liz-Marzán, L. M., Plasmon coupling in layer-by-layer assembled gold nanorod films. *Langmuir* **2007,** 23, (8), 4606-4611.

Chapter 8

Outlook

This chapter provides a perspective on potential directions and describes preliminary experiments for the fabrication of protein arrays with different nanofabrication techniques that could complement the approaches discussed in the previous chapters. We use "swelling microcontact printing" and dip pen nanolithography for the fabrication of sub-micrometer arrays of LH complexes. These techniques have the capability to fabricate interconnected patterns of different (bio)molecules which might prove to be a useful approach for explorative studies to address energy transfer between custom-made donor-acceptor pairs such as LH2 and LH1. We further introduce an unconventional approach for the assembly of macromolecular structures from monomers of α-Synuclein, which results in aggregated super-fibrils. Finally, we briefly discuss future developments to manipulate optical properties of the LH complexes in artificial assemblies.

8.1 Sub-micrometer arrays of LH complexes fabricated by swelling μCP (s-μCP)

We have investigated the feasibility of "swelling micro-contact printing" to prepare nanoscale patterns of LH2. We have used micrometer-sized patterned oxidized stamps of PDMS, which were immersed in water for prolonged times. Immersion of the oxidized PDMS material in water leads to swelling of the PDMS as a result of the uptake of water in the polymer matrix. Three different experiments are shown in Figure 8.1. Panel a shows an example of conventional μCP with an oxidized PDMS stamp to print micrometer size features of LH2 complexes. The protein solution was initially incubated on the stamp and gently dried in a stream of N_2. Subsequently the stamp was manually placed on the substrate. After removal of the stamp and rinsing with buffer the protein pattern remained adsorbed on the surface.

Figure 8.1b shows submicrometer patterns of LH2 complexes fabricated by μCP with a swollen PDMS stamp. The PDMS stamp was oxidized and then immersed in water for > 24 h. After removal of the stamp from the water, the PDMS stamp appeared opaque due to the infiltration of water into the outer polymer matrix. The depth to which water had penetrated was not investigated. The stamp was incubated with the protein solution and gently dried in a stream of N_2. Because the PDMS bulk is hydrophobic the water infiltrated into the matrix will tend to flow outwards to the surface. This will cause accumulation of liquid (water and protein) into the trenches in the pattern of the stamp. After bringing the swollen stamp in contact with the substrate, water is released from the stamp and a micro droplet is formed on the glass substrate at the edges in the pattern. The "ink" in the micro-droplets gives rise to the production of sub-micrometer patterns of "ink" molecules. Although a small fraction of material is printed from the faces of the stamp in contact with the substrate, this amount is not significantly higher than the unspecific binding on passivated areas reported by other methods.[1]

A control experiment was performed to show that water intake into the PDMS is necessary for the fabrication of sub-micrometer patterns with swelling μCP. The swollen PDMS stamp was placed onto a hot plate (60 ºC) to help the release of water from the polymer. With this stamp, micrometer features of LH2 complexes were fabricated (Figure 8.1c). From the intensity profile, the PDMS stamp after

evaporation of the water seemed to hold more protein on the surface. This could be attributed to small deformations or corrugations on the PDMS surface that served to hold more ink. More detailed characterization of the PDMS surface before and after heat treatment for the removal of the liquid, for example, by AFM imaging or electron microscopy, will be necessary to understand the detailed surface morphology.

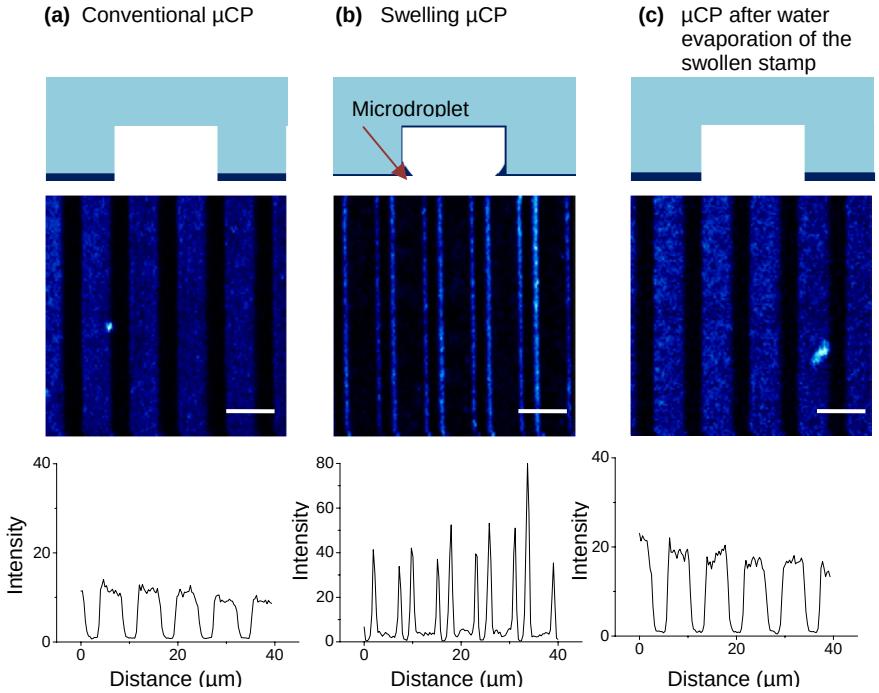

Figure 8.1. *Micro and sub-micrometer arrays of LH2 complexes by microcontact printing using the same pattern on the PDMS stamp. PDMS stamps have been mildly oxidized. The size of the images is 40 x 40 µm. (a) µCP with PDMS right after oxidation. (b) µCP after swelling of the PDMS stamp by immersion in water for 24 h. (c) µCP after evaporation of the water in the initially swollen PDMS stamp. All fluorescence measurements were performed in liquid.*

The combination of µCP and swelling-µCP has been used to fabricate different patterns. Figure 8.2a shows a grid of crossing submicrometer and micrometer LH2 arrays. Grid fabrication was realized by two consecutive printing steps, first by swelling-µCP to achieve sub-micrometer features, followed by conventional µCP with the pattern rotated 90 degrees. Panel b shows islands of LH1 complexes. Two consecutive printing steps were also used to fabricate this pattern. First

submicrometer parallel lines were fabricated by swelling-μCP. Subsequently a recently oxidized PDMS, microstructured with parallel lines was placed with the pattern orthogonal to the original pattern. When the stamp was separated from the substrate, the LH1 complexes in contact with the naked stamp were removed from the surface. The sample could later be backfilled with a LH2 solution, Figure 8.2c.

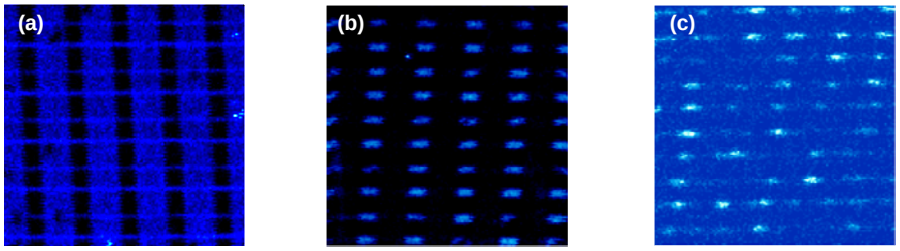

Figure 8.2. *Different architectures fabricated by swelling and conventional μCP. (a) Micro and nanometer LH2 patterns created by sequential μCP (broad lines vertical) and swelling-μCP (narrow lines horizontal). (b) Submicron LH1 islands fabricated by swelling-μCP followed by the removal of the protein by contact with a naked oxidized PDMS stamp with micrometer features. (c) Submicron LH1 islands surrounded by LH2 antennas.*

This approach constitutes a promising step towards the facile fabrication of nanometer patterns with a conventional microstructured PDMS stamp. Optimization of parameters such as: concentration, humidity and evaporation rate, pressure on the stamp during μCP, surface functionality, pattern aspect ratio, morphology and density and edge geometry will help to further develop this approach for the fabrication of arrays of different molecules.

8.2 Sub-micrometer arrays of LH2 complex fabricated by DPN

The modularity and flexibility of the AFFM make the instrument suitable for dip-pen nanolithography (DPN). The combination of direct writing with simultaneous single molecule optical detection enables in situ observation and spectral analysis of the nano-scale patterns. This is a significant added value to conventional DPN approaches.[2] For applications for photosynthetic systems, this technique can be used to fabricate biomolecular photonic wires. Figure 8.3 shows a proof-of-principle experiment where DPN nanolithography has been used for the fabrication of arrays of LH2 complexes.

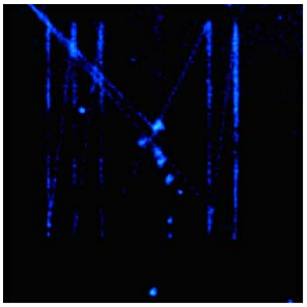

Figure 8.3. *Sub-micrometer arrays of LH2 complexes fabricated by DPN. Image size 38 x 38 µm. A bare AFM tip has been incubated in a 0.2 µm solution of LH2. The tip was gently dried and DPN was performed in ambient humidity (45%).*

Different designs can be produced by DPN. One could conceive patterning mixed arrays of LH2 (donor) and LH1-RC (acceptor) even with instruments that sequentially use different tips. First the AFM tip could be inked with LH2 molecules for the creation of nanoarrays. Subsequently, the AFM tip could be replaced and inked with LH1-RC molecules. Patterns such as LH1-RC/LH2 grids could serve as test structures for energy transport experiments in which the LH2 assembly is excited and the emission is detected from a co-assembled LH1. Also LH1-RC islands, similar to the core dimer row encountered in the natural membrane from *Rhodobacter Sphaeroides* could be patterned in such a manner.

8.3 Template assisted growth of super fibrils: test platforms and novel nanomaterials.

Amyloid fibrils are common in a diverse group of diseases of unrelated origin, including Parkinson's disease, Alzheimer's disease, and type II diabetes.[3-7] Amyloid fibrils share similar biophysical and structural properties, forming well-defined morphologies with a diameter of ~10 nm and lengths of several micrometers. Fibrils have a predominantly cross β-sheet secondary structure, as concluded from birefringence measurements upon staining with Congo red dye, and are insoluble in aqueous solutions.[8]

α-Synuclein is a 140 amino acid intrinsically disordered cytoplasmic protein.[9] Because of the lack of static secondary and tertiary structure, α-synuclein can adopt a multitude of conformations in response to its environment, earning the nickname of 'protein-chameleon'.[9] The propensity of α-synuclein to aggregate depends

strongly on its environment (pH, salt concentration,[10] addition of polyamines,[11] enzymes involved in protein folding[12]). It has been reported that the interaction of soluble amyloid monomers with a solid surface is important for amyloid formation in vivo.[8, 13] Based on this premise, synthetic amyloid templates have been prepared by the covalent attachment of amyloid seeds distributed uniformly on a surface.[8] Also, miniaturized microfluidic systems have been developed for the formation of insulin amyloids, and have enabled the investigation of changes as a function of aggregation conditions.

From the biotechnological point of view, the regular elongated features of the amyloid fibrils have been explored as structural elements because of their potential to serve as nanowires and nanoscaffolds.[14 3, 15-17] For example, peptide nanotubes have been used as nanoscale molds for the casting of silver nanowires. Also conducting nanowires have been prepared by a hierarchical assembly of amyloid fibrils and the subsequent attachment of gold nanoparticles.[18]

We present proof of concept experiments where a chemical template is used to direct the assembly and growth of a "super-fibril" with sub-micron dimensions in width and several millimetres in length. The concept of amyloid self-assembly onto chemically patterned substrates is described in Figure 8.4.

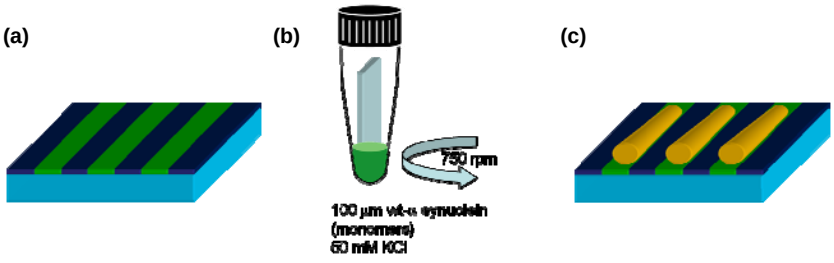

Figure 8.4. *Nanometer arrays of wt α-synuclein super fibrils. (a) Amino-terminated/PEG chemically patterned Si-SiO_2 substrate. (b) Aggregation of the fibrils by immersion of the substrates in a container with α-synuclein monomers. (c) Substrates result in the aggregation of fibrils on the amino terminated regions.*

Chemical templates on a Si/SiO_2 substrate with amine/PEG regions were fabricated as described in Chapter 2, Figure 8.4a. The substrates were immersed in small glass vials containing the monomeric protein solution (100 µM wt α-synuclein). Aggregation of the monomers into fibrils was induced by incubating the substrates at 37 ºC in 10 mM HEPES, 50 mM KCl, pH 7.4 under constant stirring at

750 rpm inside the glass vials. Aliquots of 5 µl were withdrawn at 24 h intervals to follow, by measuring Thioflavin T (ThioT) fluorescence, the kinetics of aggregation in the solution containing the substrates. ThioT is a fluorescent dye that specifically binds to cross-β structures characteristic of amyloid fibrils.[19] The ThioT intensity curve is displayed in Figure 8.5. Initially, there is hardly any fibrillar material as indicated by the low value of the intensity, but the ThioT signal progressively increases, indicating the formation of β-sheet folded protein.

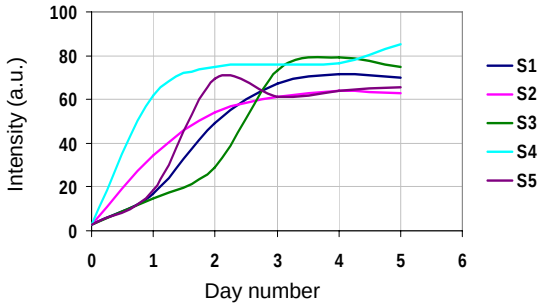

Figure 8.5. *Kinetics of wt-α synuclein aggregation in solution measured by Thioflavin T fluorescence emission.*

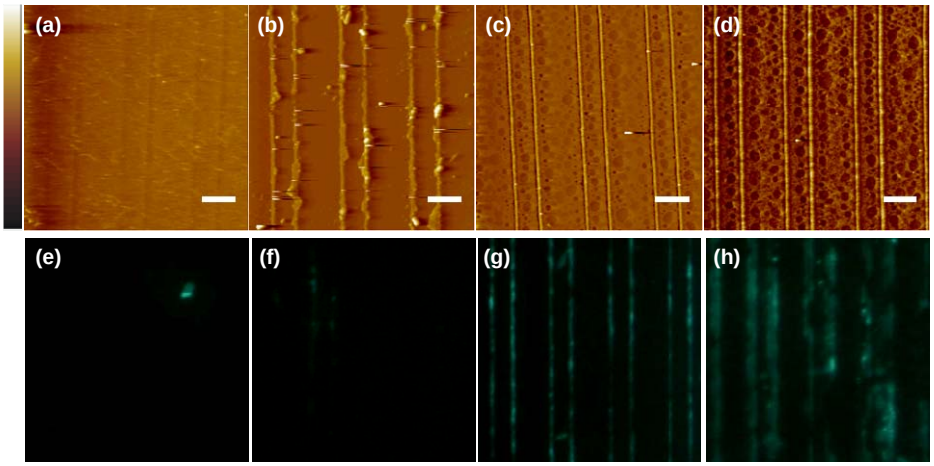

Figure 8.6. *AFM (top) and fluorescence microscopy (after addition of Thioflavin T, ThioT) characterization of wt-α synuclein assemblies onto chemically patterned substrates. (a-e) 24 h, (b-f) 48 h, (c-g) 96 h, (d-h) 120 h.*

AFM imaging was performed to follow the aggregation of the protein on the nanopatterned substrates (Figure 8.6, top row). The AFM images reveal that the amount of protein aggregates increased on the nanopatterned regions as time

progresses. Parallel lines of aggregates become more prominent after 96 h and 120 h. Irregular deposition of material can be observed in between the patterned lines, possibly due to either degradation of the PEG layer or to imperfections in the initial polymer template pattern. To confirm whether the aggregates have amyloid properties, the substrates were treated with ThioT, which shows increased fluorescence only after binding to amyloid aggregates. Figure 8.6 (bottom row) shows the increase of fluorescence intensity along the nanopatterned structures with longer incubation time.

Raman microscopy on the patterned substrates shows the typical amide I and amide III bands. The contribution at ~1672 cm^{-1} corresponds to β-sheet conformation, and the contribution at ~ 1683 cm^{-1} can be due to short β-strand fragments and random conformations.[20] Moreover, these aggregates prove to be extremely physically stable. The samples could not be easily scratched with the AFM tip. Further, the patterned aggregates were tested for mechanical and chemical stability by prolonged sonication in aqueous and organic solvents and showed no difference with the initial images (AFM and fluorescence).

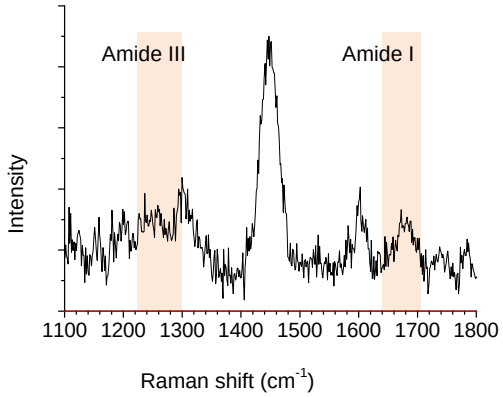

Figure 8.7. *Raman spectra on patterned wt-α synuclein after 96 h aggregation.*

These experiments constitute the first example of induced aggregation of amyloid fibrils onto chemically confined patterns. Plaque deposition has been associated with surfaces for different neurodegenerative disorders.[13] The approach presented here could serve as a platform for analysis of amyloid aggregate formation, inhibition and dissociation under different conditions on surfaces. From the technological approach, such aggregates might prove useful as scaffold materials for

the absorption of optically active components such as light harvesting molecules or quantum dots.

8.4 Outlook

The growing understanding of the molecular aspects of natural processes has reached a level that is inspiring many scientists around the world to implement concepts and materials from nature in synthetic man-made structures. A motivation for such explorations is to benefit from interesting material properties and to understand the underlying associated processes.

This research has contributed combinations of state-of-the-art nanofabrication technologies and self-assembly for the fabrication of functional structures of light harvesting proteins. Long-range energy transport has been shown in the artificial nanoarrays of LH2 protein complexes. This constitutes an elegant example in which the nanopatterned structure illustrates the perspective that we can implement materials from nature, use their properties, and even observe that these properties (in our case the extent of propagation) are beyond what is expected from the natural system. This property is not immediately revealed from the natural photosynthetic membrane where high-resolution AFM images[21] indicate energy propagation distances of ~50 nm. The precise nature of the mechanism behind the long-range energy transfer deserves further investigation.

Creative design of natural light harvesting arrays (different shapes, mixed arrays, FRET pairs) and manipulation of the optical properties of the light harvesting complexes on nanostructured surfaces could be useful to discover new properties of photosynthetic proteins in an unnatural environment. For example, emission lifetime control of biological emitters[22] can be achieved by assembling the LHC arrays on a planar silver mirror. The distance-dependent modification of the local density of states results in a characteristic oscillation in the fluorescence decay rate.[23-27] It could be conceivable that with this approach the energy propagation distances can be modulated.

Complementary research could be envisioned which incorporates photosynthetic proteins as model molecules into functional devices. Earlier studies in this line of research include the assembly of individual RC on surfaces targeting their behavior as natural supramolecular photoelectric devices that are unique for the light energy

conversion in biosystems, and for the potential of using and enhancing their natural properties on tailored hybrid surfaces. Conducting Atomic Force Microscopy (CAFM) has been used[28] to measure electron transfer mediated by RC (from *Rb. sphaeroides*) between two gold surfaces modified with different SAMs. In different experiments core complexes from different species were assembled onto amino-terminated ITO surfaces.[29] The authors observed efficient energy transfer and photocurrent response of the core complexes on ITO electrodes upon illumination. By tuning the RC/LH1 ratio of mixed assemblies of LH1 and RC units on planar surfaces the photocurrent response could be varied.[30] An interesting suggestion is the assembly of core complexes onto heterostructures of correlated perovskite oxide films,[31-32] for the development of oxide-based electronic devices.

8.5 REFERENCES

1. Reynolds, N. P.; Janusz, S.; Escalante-Marun, M.; Timney, J.; Ducker, R. E.; Olsen, J. D.; Otto, C.; Subramaniam, V.; Leggett, G. J.; Hunter, C. N., Directed formation of micro- and nanoscale patterns of functional light-harvesting LH2 complexes. *Journal of the American Chemical Society* **2007,** 129, (47), 14625.
2. Kassies, R.; Van Der Werf, K. O.; Lenferink, A.; Hunter, C. N.; Olsen, J. D.; Subramaniam, V.; Otto, C., Combined AFM and confocal fluorescence microscope for applications in bio-nanotechnology. *Journal of Microscopy* **2005,** 217, (1), 109-116.
3. Bong, D. T.; Clark, T. D.; Granja, J. R.; Reza Ghadiri, M., Self-assembling organic nanotubes. *Angewandte Chemie - International Edition* **2001,** 40, (6), 988-1011.
4. Dobson, C. M., Protein misfolding, evolution and disease. *Trends in Biochemical Sciences* **1999,** 24, (9), 329-332.
5. Gazit, E., The "correctly folded" state of proteins: Is it a metastable state? *Angewandte Chemie - International Edition* **2002,** 41, (2), 257-259.
6. Harper, J. D.; Lansbury Jr, P. T., In 1997; Vol. 66, pp 385-407.
7. Wickner, R. B.; Taylor, K. L.; Edskes, H. K.; Maddelein, M. L.; Moriyama, H.; Roberts, B. T., Prions of yeast as heritable amyloidoses. *Journal of Structural Biology* **2000,** 130, (2-3), 310-322.
8. Kip, S. N.; Hunter, L. W.; Ren, Q.; Harris, P. C.; Somlo, S.; Torres, V. E.; Sieck, G. C.; Qian, Q., [Ca2+](i) reduction increases cellular proliferation and apoptosis in vascular smooth muscle cells - Relevance to the ADPKD phenotype. *Circulation Research* **2005,** 96, (8), 873-880.
9. Uversky, V. N., Neuropathology, biochemistry, and biophysics of α-synuclein aggregation. *Journal of Neurochemistry* **2007,** 103, (1), 17-37.
10. Hoyer, W.; Antony, T.; Cherny, D.; Heim, G.; Jovin, T. M.; Subramaniam, V., Dependence of α-synuclein aggregate morphology on solution conditions. *Journal of Molecular Biology* **2002,** 322, (2), 383-393.
11. Antony, T.; Hoyer, W.; Cherny, D.; Heim, G.; Jovin, T. M.; Subramaniam, V., Cellular polyamines promote the aggregation of α-synuclein. *Journal of Biological Chemistry* **2003,** 278, (5), 3235-3240.
12. Gerard, M.; Debyser, Z.; Desender, L.; Baert, J.; Brandt, I.; Baekelandt, V.; Engelborghs, Y., FK506 binding protein 12 differentially accelerates fibril formation of wild type alpha-synuclein and its clinical mutants A30P or A53T. *Journal of Neurochemistry* **2008,** 106, (1), 121-133.

13. Esler, W. P.; Stimson, E. R.; Jennings, J. M.; Vinters, H. V.; Ghilardi, J. R.; Lee, J. P.; Mantyh, P. W.; Maggio, J. E., Alzheimer's disease amyloid propagation by a template-dependent dock- lock mechanism. *Biochemistry* **2000,** 39, (21), 6288-6295.
14. Reches, M.; Gazit, E., Casting metal nanowires within discrete self-assembled peptide nanotubes. *Science* **2003,** 300, (5619), 625-627.
15. Ghadiri, M. R.; Granja, J. R.; Milligan, R. A.; McRee, D. E.; Khazanovich, N., Self-assembling organic nanotubes based on a cyclic peptide architecture. *Nature* **1993,** 366, (6453), 324-327.
16. Vauthey, S.; Santoso, S.; Gong, H.; Watson, N.; Zhang, S., Molecular self-assembly of surfactant-like peptides to form nanotubes and nanovesicles. *Proceedings of the National Academy of Sciences of the United States of America* **2002,** 99, (8), 5355-5360.
17. Zhang, S.; Marini, D. M.; Hwang, W.; Santoso, S., Design of nanostructured biological materials through self-assembly of peptides and proteins. *Current Opinion in Chemical Biology* **2002,** 6, (6), 865-871.
18. Scheibel, T.; Parthasarathy, R.; Sawicki, G.; Lin, X. M.; Jaeger, H.; Lindquist, S. L., Conducting nanowires built by controlled self-assembly of amyloid fibers and selective metal deposition. *Proceedings of the National Academy of Sciences of the United States of America* **2003,** 100, (8), 4527-4532.
19. Ban, T.; Hamada, D.; Hasegawall, K.; Naiki, H.; Goto, Y., Direct observation of amyloid fibril growth monitored by thioflavin T fluorescence. *Journal of Biological Chemistry* **2003,** 278, (19), 16462-16465.
20. Van Raaij, M. E. Biophysical characterization of alpha-synuclein aggregates: Parkinson's diseace at the nanoscale
University of Twente, Enschede, 2008.
21. Bahatyrova, S.; Frese, R. N.; Siebert, C. A.; Olsen, J. D.; van der Werf, K. O.; van Grondelle, R.; Niederman, R. A.; Bullough, P. A.; Otto, C.; Hunter, C. N., The native architecture of a photosynthetic membrane. *Nature* **2004,** 430, (7003), 1058-1062.
22. Cesa, Y.; Blum, C.; Van Den Broek, J. M.; Mosk, A. P.; Vos, W. L.; Subramaniam, V., Manipulation of the local density of photonic states to elucidate fluorescent protein emission rates. *Physical Chemistry Chemical Physics* **2009,** 11, (14), 2525-2531.
23. Amos, R. M.; Barnes, W. L., Modification of the spontaneous emission rate of Eu3+ ions close to a thin metal mirror. *Physical Review B - Condensed Matter and Materials Physics* **1997,** 55, (11), 7249-7254.
24. Astilean, S.; Garrett, S.; Andrew, P.; Barnes, W. L., Controlling the fluorescence lifetime of dyes in nanostructured geometries. *Journal of Molecular Structure* **2003,** 651-653, 277-283.
25. Chance, R. R.; Prock, A.; Silbey, R., *J. Chem. Phys.* **1974,** 60, 2184.
26. Chance, R. R.; Prock, A.; Silbey, R., *Wiley & Sons* **1978**.
27. Lakowicz, J. R., *Principles of Fluorescence Spectroscopy*. 3rd ed ed.; Springer: 2006.
28. Mikayama, T.; Miyashita, T.; Iida, K.; Suemori, Y.; Nango, M., Electron transfer mediated by photosynthetic reaction center proteins between two chemical-modified metal electrodes. *Molecular Crystals and Liquid Crystals* **2006,** 445, 291-296.
29. Suemori, Y.; Nagata, M.; Nakamura, Y.; Nakagawa, K.; Okuda, A.; Inagaki, J. I.; Shinohara, K.; Ogawa, M.; Iida, K.; Dewa, T.; Yamashita, K.; Gardiner, A.; Cogdell, R. J.; Nango, M., Self-assembled monolayer of light-harvesting core complexes of photosynthetic bacteria on an amino-terminated ITO electrode. *Photosynthesis Research* **2006,** 90, (1), 17.
30. Suemori, Y.; Fujii, K.; Ogawa, M.; Nakamura, Y.; Shinohara, K.; Nakagawa, K.; Nagata, M.; Iida, K.; Dewa, T.; Yamashita, K.; Nango, M., Molecular assembly of artificial photosynthetic antenna core complex on an amino-terminated ITO electrode. *Colloids and Surfaces B: Biointerfaces* **2007,** 56, (1-2), 182.
31. Huijben, M.; Brinkman, A.; Koster, G.; Rijnders, G.; Hilgenkamp, H.; Blank, D. H. A., Structure-Property Relation of SrTiO3/LaAlO3 Interfaces. *Advanced Materials* **2009,** 21, (17), 1665-1677.

32. Huijben, M.; Rijnders, G.; Blank, D. H. A.; Bals, S.; Aert, S. V.; Verbeeck, J.; Tendeloo, G. V.; Brinkman, A.; Hilgenkamp, H., Electronically coupled complementary interfaces between perovskite band insulators. *Nature Materials* **2006,** 5, (7), 556-560.

Summary

In this research we used diverse nanofabrication techniques in order to direct the assembly on micro- and nanostructured surfaces of purified units from the photosynthetic unit of purple bacteria. This allowed us to explore the unique energy transfer properties of light harvesting complexes by producing biomolecular photonic wires. Other biological systems used were visible fluorescent proteins and α-synuclein, an intrinsically unfolded protein associated with Parkinson's disease. In order to characterize the biological assemblies on the surfaces AFM imaging in combination with optical imaging (spectral fluorescence microscopy and lifetime measurements) were performed in liquid conditions.

Chapter 1 introduces the concepts associated with bionanofabrication in general. The overview includes the most common chemical approaches for the adsorption of biomolecules on surfaces. Also a survey of unconventional nanofabrication for low cost and fast prototyping of bionanostructures at the micro- and nanometer scale is presented and their respective advantages and open challenges of each technique are discussed. The survey includes: microcontact printing (μCP), nanoimprint lithography (NIL), optical lithography and dip-pen nanolithography. Furthermore, we introduce the photosynthetic unit (PSU) from purple bacteria. In **Chapter 2** we report the directed assembly of the photosynthetic membrane proteins LH1 and LH2 isolated from *Rhodobacter Sphaeroides* onto chemically patterned substrates. Nanoimprint lithography was used to pattern discrete regions of amino- and fluoro-terminated or poly(ethylene glycol) self-assembled monolayers onto a glass substrate. Densely packed layers of assembled protein complexes were observed with atomic force microscopy. The protein complexes attached selectively to the amino-terminated regions by electrostatic interactions. Spectral images generated with a hybrid scanning probe and fluorescence microscope confirmed that the patterned proteins retained their native optical signatures. **Chapter 3** show an approach based on the combination of site-directed mutagenesis, nanoimprint lithography and multivalent host-guest interactions for the realization of engineered

ordered functional arrays of purified components of the photosynthetic system, the membrane-bound LH2 complex. In addition to micrometer-scale patterned structures, we demonstrated the use of nanometer-scale hard NIL stamps to generate functional protein arrays approaching molecular dimensions.

In **Chapter 4** we report the first observation of long-range transport of excitation energy within a bio-mimetic molecular light-guide constructed from LH2 antenna complexes organized vectorially into functional nanoarrays. Fluorescence microscopy of the emission of light after local excitation with a diffraction-limited light beam reveals long-range transport of excitation energy over micrometer distances, which is much larger than required in the parent bacterial system. The transport was established from the influence of active energy-guiding layers on the observed Point Spread Function (PSF) of the fluorescence emission. We speculate that such an extent of energy migration occurs as a result of efficient coupling between many hundreds of LH2 molecules. These results demonstrate the potential for long-range energy propagation in hybrid systems composed of natural light harvesting antenna molecules from photosynthetic organisms.

Chapter 5 reports for the first time the directed assembly and characterization of FRET pairs on micrometer dimension patterned surfaces. We used visible fluorescent proteins expressing a hexahistidine affinity tag as component molecules for the construction of the FRET constructs, where His_6-EGFP served as donor fluorophore and His6-DsRed-FT as the acceptor. We created 2D and 3D structures that exhibit Fluorescence Resonance Energy Transfer at the interfaces between the donor and acceptor patterns in the lateral or axial directions respectively. We quantitatively visualized the energy transfer by multiparameter optical microscopy.

Chapter 6 reports the fabrication and characterization of 3D and 2D assemblies of core dimer complexes. Fluorescence spectral microscopy is used to study the optical properties of the complexes in the different assemblies. AFM topographies of 3D crystals of core dimers indicate that the crystals are formed by stacking of sheet like layers. The surfaces of the crystals were very rough with cracks up to 1μm in depth. Fluorescence emission from the 3D crystals is red-shifted with respect to the fluorescence from core dimers in solution. Nanometer arrays of core dimers (~80 nm in width and several micrometers in length) were fabricated by a combination of top-down and bottom-up nanofabrication approaches. NiNTA

monolayers were used as chemical templates for the controlled immobilization of His_6 tagged core dimers. Fluorescence time trace data hint at long-range energy transport.

Chapter 7 describes the fabrication of micro- and nanostructured substrates that combine gold and SiO_2 (glass) or CaF_2 and their subsequent chemical functionalization by means of self-assembled monolayers for the adsorption of light harvesting complexes. We use fluorescence and Raman microscopy to examine the optical properties of the LHCs immobilized on the different surfaces. Increased photostability of LH2 complexes on the patterned gold regions is reported. Also, we present hybrid micro- and nanostructures that combine photosynthetic protein complexes and metal nanoparticles. We report the observation of metal enhanced fluorescence and surface enhanced Raman signals on the gold nanoparticle patterns. **Chapter 8** provides a perspective on potential directions and describes preliminary experiments for the fabrication of protein arrays with different nanofabrication techniques that could complement the approaches discussed in the previous chapters. We use "swelling microcontact printing" and dip pen nanolithography for the fabrication of sub-micrometer arrays of LH complexes. These techniques have the capability to fabricate interconnected patterns of different (bio)molecules which might prove to be a useful approach for explorative studies to address energy transfer between custom-made donor-acceptor pairs such as LH2 and LH1. We further introduce an unconventional approach for the assembly of macromolecular structures from monomers of α-Synuclein, resulting in aggregated super-fibrils. Finally, we briefly discuss further developments to manipulate optical properties of the LH complexes in artificial assemblies.

Samenvatting

Het onderzoek beschreven in dit proefschrift presenteert verscheidene nanofabricage technieken, die de mogelijkheid bieden om de ordening van geïsoleerde componenten van fotosynthetische paarse bacteriën op micro- en nanogestructureerde oppervlakken te controleren. De preparatie van "biomolecular photonic wires" maakt het mogelijk om met bovengenoemde technieken unieke eigenschappen van "light harvestign complexes" te onderzoeken, zoals de energie-overdracht. Andere biologische moleculen die gepatroneerd zijn, zijn "visible fluorescent proteins" en "α-synuclein". Dit laatste eiwit is een intrinsiek ongevouwen eiwit dat wordt geassocieerd met de ziekte van Parkinson. Ten einde de biologische ordening te karakteriseren zijn verschillende microscopie technieken toegepast, zoals atomaire kracht microscopie in combinatie met optische beeldvorming (spectrale fluorescentie microscopie) en fluorescentie levensduur microscopie.

Hoofdstuk 1 geeft een introductie in de concepten die geassocieerd worden met "bionanofabricage" in het algemeen. Dit overzicht beschrijft de meest gangbare chemische technieken voor de adsorptie van biomoleculen op oppervlaktes. Tevens wordt er een studie beschreven naar onconventionele nanofabricage voor kosten effectieve en snelle prototypes van bionanostructuren met afmetingen op micro- en nanometer schaal waarvan de respectievelijke voordelen en uitdagingen worden bediscussieerd. Deze studie omvat: "microcontact printing" (μCP), "nanoimprint lithography" (NIL), "optical lithography" en "dip-pen nanolithography". Verder wordt de "photosynthetic unit" (PSU) voor paarse bacteriën geïntroduceerd. In **hoofdstuk 2** wordt beschreven hoe de ordening van de fotosynthetische membraan eiwitten LH1 en LH2, afkomstig van de paarse bacterie Rhodobacter Sphaeroides op chemische gepatroneerde oppervlakten verkregen zijn. Om specifieke plaatsen met amino- en fluoro-eindgroepen of poly(ethylene)glycol zelfrangschikkende monolagen op een glas substraat te patroneren is "Nanoimprint lithography" toegepast. Dicht gepakte lagen van gerangschikte eiwit complexen zijn geobserveerd met AFM. De eiwit complexen hechten selectief aan plaatsen met

amino-eindgroepen vanwege elektrostatische wisselwerking. Spectrale beelden die met een “hybrid scanning probe” en een fluorescentie microscopie zijn gemaakt, bevestigen dat de gepatroneerde eiwitten hun oorspronkelijke optische kenmerken behouden. **Hoofdstuk 3** toont een methode gebaseerd op een combinatie van “site-directed mutagenesis”, “nanoimprint lithography” en “multivalent host-guest interactions” om kunstmatig geordende functionele reeksen te verkrijgen van geïsoleerde componenten van het fotosynthetische systeem; het membraan gebonden LH2 complex. Naast de op micrometer schaal gepatroneerde structuren laten we eveneens het gebruik van harde NIL stempels met nanometer resolutie zien ten einde functionele eiwit reeksen te verkrijgen die qua grootte moleculaire afmetingen benaderen.

In **hoofdstuk 4** wordt beschreven dat gepatroneerde systemen van licht transporterende eiwitten excitatie-energie over lange afstand kan transporteren in een “bio-mimetic molecular light-guide” opgebouwd uit geordende LH2 antenne complexen van Rhodobacter Sphaeroides. Fluorescentie microscopie van het uittredende licht, na lokale excitatie met een diffractie gelimiteerde laser bundel, toont lange afstand transport van geëxciteerde energie aan over afstanden ter grootte van micrometers. Hetgeen veel langer is dan nodig binnen het oorspronkelijke bacteriële organisme. Het transport was vastgesteld door middel van de invloed van de actieve energie geleidende lagen op de geobserveerde “Point Spread Function” (PSF) van de fluorescerende emissie. Er wordt gespeculeerd dat een dergelijk transport van energie migratie als gevolg van efficiënte koppeling tussen vele honderden LH2 moleculen plaatsvindt. Deze resultaten laten het potentieel zien van lange afstands propagatie in hybride systemen samengesteld uit “natural light harvesting” antenne moleculen uit fotosynthetische organismen.

In **hoofdstuk 5** wordt het werk beschreven aan ordening van potentiele FRET-paren in gepatroneerde oppervlakken op micrometer schaal. Als FRET paren is gebruik gemaakt van “visible fluorescent proteins”, die een hexahistidine functioinaliteit hebben voor de affiniteit met het oppervlak. His_6-EGFP fungeert als donor en His6-DsRed-FT fungeert als acceptor in het FRET paar.. Er zijn 2D en 3D structuren gemaakt die “Fluorescence Resonance Energy Transfer” vertonen aan het grensvlak tussen donor en acceptor patronen in respectievelijk de laterale of de

axiale richting. We hebben de energie overdracht kwantitatief gevisualiseerd door middel van “multiparameter optical microscopy”.

Hoofdstuk 6 gaat over de fabricage en karakterisering van 2D en 3D samenstellingen van “core” dimeer complexen. Om de optische eigenschappen van de complexen in de verschillende samenstellingen te bestuderen is gebruik gemaakt van “fluorescence spectral microscopy”. AFM topografie van 3D kristallen van “core” dimeren suggereren aan dat de kristallen worden gevormd door stapeling van dunne laagjes. De oppervlakten van de kristallen waren erg ruw met defecten tot 1 μm diep. De fluorescentie emissie van de 3D kristallen vertoond roodverschuiving in vergelijking met de fluorescentie van de “core” dimeren in oplossing. Nanometer reeksen van “core” dimeren (~ 80 nm breed en enkele micrometers lang) waren gefabriceerd door middel van een combinatie van top-down en bottom-up nanofabricage. Er is gebruik gemaakt van NiNTA monolagen als chemische nucleatie plaatsen om His_6 gelabelde “core” dimeren gecontroleerd te binden. Op basis van het traceren van fluorescentie emissie, wordt energie transport over lange afstand vermoed.

Hoofdstuk 7 beschrijft de fabricage en opvolgende chemische functionalisatie met zelf rangschikkende monolagen van micro en nano gestructureerde substraten waarbij goud en SiO_2 (glas) of CaF_2 gecombineerd worden voor de absorptie van “light harvesting complexes”. Er is gebruikgemaakt van fluorescentie en Raman microscopie om de optische eigenschappen van de op verscheidene oppervlakten gebonden LHCs te onderzoeken. Er is een toename van de fotostabiliteit van LH2 complexen op de gepatroneerde goud oppervlakken vastgesteld. Tevens worden hybride micro en nano structuren gepresenteerd waarbij fotosynthetische eiwit complexen en metalen nanodeeltjes gecombineerd zijn. Aansluitend wordt de waarneming van “metal enhanced fluorescence” en “Surface Enhanced Raman” signalen op de goud nanodeeltjes patronen beschreven.

In **hoofdstuk 8** wordt een vooruitblik gegeven op potentiële richtingen en voorlopige experimenten voor het fabriceren van eiwit structurn met andere nanofabricage technieken die de in de voorgaande hoofdstukken beschreven aanpak kunnen aanvullen. We maken gebruik van “swelling microcontact printing” en “dip pen nanolithography” om sub-micrometer structuren van LH complexen te fabriceren. Deze technieken leveren de mogelijkheid om verbindingspatronen van

verschillende (bio)moleculen te fabriceren die het mogelijk maken om verder onderzoek te doen naar energie overdracht tussen kunstmatig gemaakte donor-acceptor paren zoals LH2 en LH1. Verder wordt een onconventionele aanpak geïntroduceerd voor de rangschikking van macromoleculaire structuren die zijn samengesteld uit monomeren van α-Synuclein. Dit resulteert in gegroepeerde super fibrillen. Ter afsluiting worden verdere ontwikkelingen besproken om optische eigenschappen van de LH complexen in kunstmatige samenstellingen te manipuleren.

Acknowledgemets

Every period comes to an end. With these words I would like to express my gratitude to all the people who have contributed to this research and my enjoyable time in Enschede.

Vinod, I still remember with pleasure when I first went to BPE to inquire regarding a PhD position. Thanks for the opportunity to be part of this group. Thanks for the continued support during good and rush times. I very much enjoyed the freedom to collaborate, take our own decisions, the responsibility you grant your students, and the way you encourage that we become independent with a vision beyond the borders of the lab. You are incredibly busy, yet always available to attend to anybody who knocked on your door (or mailbox) with a usually long list of questions.

Cees, I would like to express my gratitude for driving this project and giving me the opportunity to work with such an interesting system. Thanks for the scientific stimulus not only in our weekly group meetings, but also during the several occasions I interrupted you in your office or during attendances to conferences and meetings. You were proactively demanding and always pushed to get the best out of ourselves.

Prof. Jurriaan Huskens, this thesis would not have been possible without the collaboration with your group. Thanks for such interesting discussions and input during these past years. I am also infinitely grateful for allowing me to work in your lab and use all the facilities as another member of MnF.

Prof. Neil Hunter and Dr. John Olsen, thanks for providing us with most of the biological material we used in this research and for the constructive discussions, prompt replies to the last-minute e-mails sent to Sheffield and the kind attention during our visit to your lab. Jaimey, Nick, Cvetelin, Peter (thanks for the pleasant time during your visit to Twente and the contribution to chapter 6) and Pu Qian (thanks for the 3D crystals). It was nice to work with you at different stages of my PhD project and to host most of you in Twente.

Furthermore, I thank the generous financial support from NanoNed, which made possible the utilization and acquisition of state-of-the-art technologies and the attendances to different seminars and conferences. I also thank Dr. Leon Gielgens and the participants of the Nanofabrication Flagship users' committee meetings that kept our feet on the ground with the valorization perspective of our research.

BPE colleagues and friends, you were important contributors and supporters during my time as an AIO. Aufried, thanks for the immense support and time invested in the set-up. Kees van der Werf, thanks for all the AFM training and fruitful discussion about experiments in the AFM group meetings. Christian Blum and Yanina, my paranymph, thanks for all the knowledge you shared with me, your patience with all the questions and your friendship. Guys, I enjoyed the FRET pair work, chapter 5, it was a nice team effort. Dodo, thanks for your enthusiasm and support during the last months, I strongly regret that we did not have more opportunities to work together. Sylvia, thanks for all the arrangements, paper work and organization of the group's social activities, you managed to keep all things on track! Kirsten and Ivonne, thanks for all the chemicals and critical orders on such a short notice. Frans thanks for all the kind attention to the entire group. Vishnu, I really admire your energy (you should share the secret with us someday ☺…), thanks for the Raman measurements for chapters 7 and 8. Chien-Ching, thanks for the chats, meeting, coffees and dinners, I am glad we both made it. To all the colleagues from BPE, thanks for making this time enjoyable:

Cicerone, Cynthia (we miss you at the girls dinners), my roommates in Hogekamp: Jurgen, Chandra, Tomasz and Bart (thanks for all the help, especially at the end ☺), and in the Zuidhorst: Roy, Chandra, Tycho and Markus; you were very pleasant company. Martijn vR (a very patient Dutch teacher), Marieke, Kim (thanks for the help with the Bioscope), Raja, Constantine (thanks for the simulations), Felicia, Alex, Shashank, Yujie, Christian, Dirk-Roelof, Martijn S., Tom, Mireille, Martin, Ine, Tomasz, Henk-Jan, Erwin, Srirang, Liesbeth, Remco (thanks for the particles), Dianwen (thanks for your help with Matlab), Rolf (thanks for the support and contribution to chapter 3), and to Roel and Sveta who shared their knowledge at the initial stage of this project.

Within MESA+ opportunities are unlimited, especially if you do not mind walking from building to building (sometimes through the rain…) to do experiments and to meet people, which I quite enjoyed. Besides BPE; MnF, SMCT, TST and the cleanroom were the other groups/locations where I spent most of my time during my PhD.

From MnF, Manon, thanks for the synthesis of the adamantane derivatives, the fruitful discussions about surface functionalization and the pleasant talks concerning many topics. Pascale, thanks for your help and support at the beginning of the PhD, although I was not your *student* anymore you were willing to share the tips and experience accumulated during your PhD. Christiaan Bruinink, thanks for the NIL stamps I used in chapter 2 and also for sharing your knowledge and the pleasant talks while waiting for equipment in the cleanroom. There were periods when I spent whole weeks in the MnF/SMCT labs, where I even had a small bench for the experiments. Was a real pleasure to spend these long hours with the 2719 lab mates: Andras (thanks for the CD), Francesca, Huaping, Jordi, Lanti, Veera, Oktay, Pieter, Xuexin. Form the bigger labs: Alberto, Arancha (nice talks), Denis, Francesca, Henk, Janet (always willing to help with a big smile), Jealemy (se va! se va!), Kim, Mirko (chevere!), Shu-Han (laughing all the time, very nice roommate in Israel), Xing Yi (never stopping, thanks for all the tips). Marcel and Richard, thanks for the support at emergency moments. And of course the unforgettable previous SMCT/MnF generation: María Péter, Lourdes, Fernando, Olga, Alessio, Soco, Marta, Becky, Mercedes, Mathijs and Francesca.

TST (a.k.a. MICMEC), you guys are simply the best in technology, I was lucky to start my journey at the UT with you. Yiping, it was a huge pleasure to work with you, I enjoyed your commitment to perfection! (Maybe because we were both Henri's students at some stage!). Thanks to you and Erwin for the generous contribution of the silicon nanoridges that made possible chapters 3 and 4. Niels and Joost, it was nice and productive to continue the nanochannel work over this time. As Deladi would say: "once a MicMecer always a MicMecer", I never felt I left the group. Thanks guys for the good memories, international dinners, uitjes and the sailing trip (where I realized that sailing was also possible in the middle of a storm…). In particular Jeroen (my first boss and now my paranymph), Henri and Niels (thanks for your friendship and lessons), Pino (thanks for hosting us during my only New Year in The Netherlands), microscope Henk, Duy and Laura for organizing the MICMEC events, Boudewijn, Srinivas, Deladi, Miko, Marcel, Marcus, Imran, Dannis, Erwin, Rik, Meint, Doekle, Sandeep, Roald and John.

To the cleanroom staff, thanks for all the discussions, introductions and maintenance, particularly to Dominique, Huib, Hans, Peter, Ite-Jan, Marion, Samantha, Eddy and Rene. Mark, thanks for the HR-SEM images and the chats during the measurements, and to Gerard Kip, thanks for XPS measurements.

I would like to express my gratitude to Prof. David Reinhoudt, Prof. Niek van Hulst, Prof. María García-Parajó and Dr. Martin Bennink for making the transition for all the students from the Master in Nanotechnology to PhD candidate within MESA+ as smooth as possible; and to the colleagues and participants from the Master in Nanotechnology that served as a starting point for the interaction and collaborations during this research. In this paragraph I also thank the former Optical Techniques Group (now Optical Sciences). Herman (the PSTM

quite an experience, thanks for your trust), Robert (thanks for your patience & so nice concert!), Maria and Niek (thanks for all the care), Frans & Jeroen (thanks for the technical support), Erik, Jacob, Gert Jan, Martin and of course Nancy!

To the "*dinner club*" thanks for the delicious evening, taste-and-company wise.

All guys from P-NUT, PhD Network of the University of Twente, Anika, Marije, Michel, Nicolas, Sergio. Good luck to the new generation: Aimee, Björn, Giovane, Josine, Shashank, I enjoyed being part of all the discussions and activities dedicated to the development of the working and social atmosphere for PhDs candidates in Twente.

Ivan, after bachelor, master and PhD at the same University, I think this is the end of our academic career together; you were a great company and support all time long, success with the next step!

A mis amigos de Valencia, Caracas y primos y tíos en Venezuela y otros países, cada vez que iba de regreso a casa era como si el tiempo no hubiese pasado, la diversión es igual que siempre solo que ahora con más gente ☺!!!

A mis mama, papa y a mi hermano, muchas gracias por el amor y el permanente apoyo que me han brindado toda la vida. El amor de familia es lo que nos ha llevado siempre hacia adelante. Son lo más maravilloso que tengo.

Boudewijn, mijn lieve man, ik ben van ver gekomen en heb je hier ontmoet, sindsdien zijn we samen gelukkig en ik weet zeker dat we dat nog vele jaren blijven. Dank je voor je onvoorwaardelijke liefde, zorg en steun. Ook dank aan je familie die mij als één van de hare heeft verwelkomd.

Maryana

Enschede, December 2009

About the Author

Maryana Escalante Marun was born on August 11th, 1980 in Barcelona, Venezuela. After graduating from high school in Valencia in 1997 she went to study Electronics Engineering at the University Simón Bolívar (USB) in Caracas. During this period she was scholar from Petróleos de Venezuela (PDVSA). Her graduation project was entitled “Tele-monitoring Electrocardiogram (ECG) System via Internet for PC and PDA”. She obtained her undergraduate degree cum-laude in November 2002. She joined the International Nanotechnology Master Program in 2003 at the University of Twente, the program was funded by MESA+ Institute for Nanotechnology and the Twente Scholarship Program (TSP). During the master program she had the opportunity to work in four different projects and rotate between three different groups from MESA+, Transducers Science and Technology, under the supervision of Dr. Henri Jansen and Dr. Niels Tas, Supramolecular Chemistry and Technology under the supervision of Prof. dr. Jurriaan Huskens and Optical Techniques under the supervision of Dr. Herman Offerhaus.

In 2005 she joined the Biophysical Engineering Group (BPE) as a PhD candidate under the supervision of Dr. Cees Otto and Prof. Vinod Subramaniam on the subject of nanofabrication of bioinspired architectures with light harvesting proteins. The results of this research are described in this thesis.

List of Publications

Published articles

Escalante, M.; Blum, C.; Cesa, Y.; Otto, C.; Subramaniam, V. FRET pair printing of fluorescent proteins. *Langmuir* **2009**, 25, (12), 7019

Blum, C.; Cesa, Y.; Escalante, M.; Subramaniam, V., Multimode microscopy: spectral and lifetime imaging. *Journal of the Royal Society Interface* **2009**, 6, S35-S43.

van Honschoten, J. W.; Escalante, M.; Tas, N. R.; Elwenspoek, M., Formation of liquid menisci in flexible nanochannels. *Journal of Colloid and Interface Science* **2009**, 329, (1), 133-139.

Escalante, M.; Zhao, Y. P.; Ludden, M. J. W.; Vermeij, R.; Olsen, J. D.; Berenschot, E.; Hunter, C. N.; Huskens, J.; Subramaniam, V.; Otto, C., Nanometer arrays of functional light harvesting antenna complexes by nanoimprint lithography and host-guest interactions. *Journal of the American Chemical Society* **2008**, 130, (28), 8892.

Ludden, M. J. W.; Li, X.; Greve, J.; van Amerongen, A.; Escalante, M.; Subramaniam, V.; Reinhoudt, D. N.; Huskens, J., Assembly of bionanostructures onto beta-cyclodextrin molecular printboards for antibody recognition and lymphocyte cell counting. *Journal of the American Chemical Society* **2008**, 130, (22), 6964-6973.

Escalante, M.; Maury, P.; Bruinink, C. M.; van der Werf, K.; Olsen, J. D.; Timney, J. A.; Huskens, J.; Hunter, C. N.; Subramaniam, V.; Otto, C., Directed assembly of functional light harvesting antenna complexes onto chemically patterned surfaces. *Nanotechnology* **2008**, 19, (2), 025101.

Reynolds, N. P.; Janusz, S.; Escalante-Marun, M.; Timney, J.; Ducker, R. E.; Olsen, J. D.; Otto, C.; Subramaniam, V.; Leggett, G. J.; Hunter, C. N., Directed formation of micro- and nanoscale patterns of functional light-harvesting LH2 complexes. *Journal of the American Chemical Society* **2007**, 129, (47), 14625-14631.

van Honschoten, J. W.; Escalante, M.; Tas, N. R.; Jansen, H. V.; Elwenspoek, M., Elastocapillary filling of deformable nanochannels. *Journal of Applied Physics* **2007**, 101, (9), 094310.

Maury, P.; Escalante, M.; Peter, M.; Reinhoudt, D. N.; Subramaniam, V.; Huskens, J., Creating nanopatterns of his-tagged proteins on surfaces by nanoimprint lithography using specific NiNTA-Histidine interactions. *Small* **2007**, 3, (9), 1584-1592.

Offerhaus, H. L.; van den Bergen, B.; Escalante, M.; Segerink, F. B.; Korterik, J. P.; van Hulst, N. F., Creating focused plasmons by non collinear phase matching on functional gratings. *Nano Letters* **2005**, 5, (11), 2144-2148.

Maury, P.; Escalante, M.; Reinhoudt, D. N.; Huskens, J., Directed assembly of nanoparticles onto polymer-imprinted or chemically patterned templates fabricated by nanoimprint lithography. *Advanced Materials* **2005**, 17, (22), 2718

Manuscripts in preparation

Maryana Escalante, Aufried Lenferink, Yiping Zhao, Niels R. Tas, Jurriaan Huskens. C. Neil Hunter, Vinod Subramaniam and Cees Otto. *Long range energy transfer in nanometer arrays of light harvesting antenna complexes.* (submitted)

Niels R. Tas, Maryana Escalante, Joost W. van Honschoten, Henri V. Jansen, and Miko Elwenspoek. *Capillary negative pressure measured by nanochannels collapse*. (submitted)

Maryana Escalante, Vishnu Pully, Ine Segers-Nolten, Cees Otto, Vinod Subramaniam. *Template assisted growth of superfibrils.*

Roman Truckenmüller, Stefan Giselbrecht, Maryana Escalante, Max Groenendijk, Bernke Papenburg, Nicolas Rivron, Hemant Unadkat, Volker Saile, Vinod Subramaniam, Clemens van Blitterswijk, Matthias Wessling and Dimitrios Stamatialis. *A new approach for tailoring the topographical factors of cells' 3D microenvironments in chip sized TE scaffolds.*

Gustavo Higuera, Roman Truckenmueller, Lorenzo Moroni, Maryana Escalante, Vinod Subramaniam, van Boxtel A., Marcel Karperien and Clemens van Blitterswijk. *Three-Dimensional Tissue Patterns formed by Human Mesenchymal Stem Cells are Controlled by Contact Inhibition.*

Jaimey Tucker, Alistair Siebert, Hilary Lewis, Maryana Escalante, Nicholas Reynolds, John Timney, Graham Leggett, Cees Otto, Mark Dickman, David Stokes, C. Neil Hunter. *Assembly of a bacterial membrane organelle.*

Contributions to conferences

MicroNano Conference. (Oral presentation), November **2009**, Delft, The Netherlands

Annual Dutch meeting on Molecular and Cellular Biophysics. (Poster) September **2009,** Veldhoven, The Netherlands

MESA+ Institute for Nanotechnology Annual meeting. (Oral presentation), September **2009**, Enschede, The Netherlands

Light Harvesting Processes. (Poster), March **2009**, Kloster Banz, Germany

MicroNano Conference. (Poster), November, **2008**, Ede, The Netherlands

7th International Conference on Nanoimprint and Nanoprint Technologies (NNT'08). (Poster), October **2008**, Kyoto, Japan

Annual Dutch meeting on Molecular and Cellular Biophysics. (Oral presentation) September **2008**, Veldhoven, The Netherlands

MESA+ Institute for Nanotechnology Annual meeting. (Poster), September **2008**, Enschede, The Netherlands

Workshop Advanced Macromolecular Systems Across the Length Scales III. (Poster) May **2008**, Enschede, The Netherlands

International PhD Workshop “Global Challenges – How Nanotechnology can Help”. (Workshop), April **2008**, Venice, Italy

Meeting on Molecular Materials. (Poster), November **2007**, Rehovot, Israel

NanoMicroNed Symposium II. (Poster), November **2007**, Eindhoven, The Netherlands

Annual Dutch meeting on Molecular and Cellular Biophysics. (Poster) , September **2007**, Veldhoven, The Netherlands.

Advanced Macromolecular Systems Across the Length Scales (Poster). April **2007**, Enschede, The Netherlands

AFM Biomade Conference. (Oral presentation), April **2007**. Barcelona, Spain

Annual Dutch meeting on Molecular and Cellular Biophysics. (Poster), October **2006**, Lunteren, The Netherlands

MESA+ Institute for Nanotechnology Annual meeting. (Oral presentation), September **2006**, Enschede, The Netherlands

9th International Summer School on Biophysics Supramolecular Structure and Function. (Poster), September **2006**, Rovinj, Croatia